Morphological Development of Meandering Rivers Due to Changing Discharge Regimes

Von der

Fakultät Architektur, Bauingenieurwesen und Umweltwissenschaften

der Technischen Universität Carolo-Wilhelmina

zu Braunschweig

zur Erlangung des Grades eines

Doktor-Ingenieurs (Dr.-Ing.)

genehmigte

Dissertation

von

Mohd. Sarfaraz Banda
geboren am 05. Januar 1981
aus Kushtia, Bangladesh

Eingereicht am: 19. Januar 2018
Disputation am: 16. April 2018

Berichterstatter: Prof. Dr.-Ing. Jochen Aberle
Prof. Dr.-Ing. Günter Meon

(2018)

Acknowledgment

I would like to pay special thanks, warmth, and appreciation to the persons below who made my research successful and assisted me throughout the process to cherish my goal:

This thesis would not exist at all without my prior supervisor Prof. Dr.-Ing. habil. Andreas Dittrich, who accepted me as a doctoral student. I would like to express my sincere gratitude to him for his supervision and encouragement, and providing me with an excellent atmosphere for doing research at the Leichtweiß-Institute for Hydraulic Engineering and Water Resources (LWI) at the Technische Universität Braunschweig (Germany). I thank him for also being my thesis examiner.

I would like to gratefully acknowledge the enthusiastic supervision of Prof. Dr.-Ing. Jochen Aberle. It has been an honor to be a PhD student under his supervision. The writing of this dissertation would not have been possible without his assistance and guidance. His scholarly advice and constant motivation encouraged me to meet the deadlines.

I gratefully acknowledge the German Academic Exchange Service (DAAD - Deutscher Akademischer Austauschdienst) for providing the EXCEED-SWINDON PhD scholarship throughout the period of this research.

My special thanks are extended to Prof. Dr. Andreas Haarstrick (the chairman of my committee and the scientific coordinator of the EXCEED-SWINDON project). He has shown me, by his example, what a good scientist (and person) should be.

I also thank Prof. Dr.-Ing. Günter Meon for being the second reviewer of my thesis. I thank Prof. Dr.-Ing. Reinhard Hinkelmann for being my thesis examiner and giving the valuable suggestions and corrections to this work.

I would like to especially acknowldge the valuable input of Dr.-Ing. Katinka Koll, who contributed to many discussions that helped to shape this project. Special thanks are reserved for Stephan Niewerth. My research would not have been possible without his Matlab scripts. The thesis has also benefited from comments and suggestions made by Dr. Francisco Núñez-González, Ronald Möws, Paride Nardone, Bahaeldeen Zaid, Till Branß, Ralph Eikenberg, Manuela König and Birgit Schnick. My special thanks are extended to Jakaria Pervez for helping me collect survey data from the field.

Finally, I am grateful to my mother Firoza Begum, who has provided me with moral and emotional support in my life. I am indebted to my elder brother Md. Imtiaz Banda, who has given me the opportunity of an education from the best institutions and support throughout my life. I also would like to thank my younger brother Md. Niaz Banda, who has always encouraged me and believed that I could do it. This thesis is dedicated to the memory of my father Banda Fattah, whose role in my life was, and remains, immense.

Abstract

This PhD thesis investigates the effects of changing discharge regimes on the morphological development of meandering rivers. The reduction of discharge causes bed morphology and planform changes in alluvial rivers with erodible banks, and restoring the discharge may alter the existing morphology, leading to a new (so far unpredictable) river course. A promising tool to investigate the morphological development of natural meandering rivers is the use of numerical models, and the present thesis explores the capability of the open-source software Delft3D to simulate the adaption of both planform dynamics and bed topography to changed discharge regimes. A specific reach in the Dhaleshwari River (Bangladesh) is taken as a case study as it provides relevant data for model validation.

Both two-dimensional (2D) and three-dimensional (3D) modelling approaches were applied. The 3D model, which was calibrated against measured three-dimensional flow data, was used for predicting bed level changes over a one-year period. The simulated morphological changes showed a certain degree of resemblance with the available field data, but the required computational time prevented further analyses. Therefore, a 2D model, which takes into account the three-dimensional flow phenomena in a parameterized way, was used for the further simulations to achieve acceptable computational times, and to enlarge the spectrum of investigated scenarios. This 2D model, in which the parameterization of the 3D flow effect was validated against curved flume data, was used to simulate the morphological development for different discharge scenarios over a 10-year period.

The results of the simulations revealed that the 2D model could predict scour depth, bank erosion, and riffle-pool sequences under both constant and varying discharge scenarios. However, the prediction of channel bankfull width showed some deficiencies. The simulations with varying discharge demonstrated a more realistic prediction of the meander planform than the simulations with constant discharge. The conclusion from this research is that a two-dimensional (2D) modelling approach, in combination with a time-varying discharge (i.e., hydrograph), can be used to simulate the natural dynamics of meandering rivers, both in terms of the development of bed topography and channel planform. The morphological development of a river reach operates at a different temporal scale than the hydrodynamic flow features, and the results of the study showed also that a morphological scale factor can be used as a speed-up factor for morphological development without the need to change the order of hydrographs.

The results further revealed that a discharge magnitude of about 90% of the bankfull discharge best represents the dominant discharge, and that the meander wavelength increases with the discharge magnitude. The results of the simulation for time-varying discharge records reveal that larger floods favor enlargement of meander wavelength and smaller floods favor shortening of meander wavelength during the first 50% of the simulation period. However, after the first 5-year period, the meander wavelength becomes nearly unresponsive to altered high- and low- floods. A particular application of the model can be Monte-Carlo simulations to predict the potential location of the future river channel as morphological changes in the Dhaleshwari River may endanger the local infrastructure in the study reach.

Table of Contents

List of Symbols

Variable	Meaning	Unit
a	Van Rijn's reference height	[m]
A	Secondary flow direction coefficient	[-]
B	Channel bankfull width	[m]
c	Sediment concentration	[kg m^{-3}]
c_a	Sediment concentration at the van Rijn's reference height	[kg m^{-3}]
C	Chézy coefficient	[$m^{1/2}$ s^{-1}]
C_{3D}	3D Chézy coefficient	[$m^{1/2}$ s^{-1}]
C_{kmx}	Concentration of sediment in the reference layer	[kg m^{-3}]
$D_{x,}$ $D_{y,}$ D_z	Sediment diffusivity coefficients in x, y, z direction	[m^2 s^{-1}]
D_v	Vertical sediment mixing coefficient	[m^2 s^{-1}]
D_*	Dimensionless particle diameter	[-]
D_{50}	Median sediment diameter	[m]
$E_{h,}$ E_u	Migration coefficients	[-]
E_s	Calibration coefficient to control the spiral flow effect on the bed-load transport direction	[-]
E_{NS}	Nash-Sutcliffe efficiency index	[-]
f	Coriolis coefficient	[s^{-1}]
f_{bed}	Calibration factor for bed-load transport	[-]
f_{sus}	Calibration factor for supended load transport	[-]
g	Gravitational acceleration	[m s^{-2}]
h	Water depth	[m]
H'_B	Near-bank excess flow depth	[m]
I	Spiral flow intensity	[m s^{-2}]
k_s	Effective bed roughness height of Nikuradse	[m]
L	Meander length	[m]
M	Fraction of silt-clay in the channel perimeter	[-]
M_B	Meander belt width	[m]
$MORFAC$	User-specified morphological scale factor	[-]

n	Mannings roughness coefficient	[s $m^{-1/3}$]
n_B	Transverse coordinate	[m]
p	Atmospheric pressure	[N m^{-2}]
P	Hydrostatic pressure	[N m^{-2}]
Q	Discharge	[m^3 s^{-1}]
Q_{bf}	Bankfull discharge	[m^3 s^{-1}]
Q_{ma}	Mean annual discharge	[m^3 s^{-1}]
Q_{mm}	Mean monthly maximum discharge	[m^3 s^{-1}]
Q_{maf}	Mean annual flood	[m^3 s^{-1}]
r	Correlation coefficient	[-]
R	Radius of curvature	[m]
R_s	Effective radius of streamline curvature	[m]
s	Relative density of sediment	[kg m^{-3}]
S_b	Bed load transport rate per unit width	[m^2 s^{-1}]
$S_{b,x}$	Adjusted bed load transport rate in the x direction per unit width	[m^2 s^{-1}]
$S_{b,y}$	Adjusted bed load transport rate in the y direction per unit width	[m^2 s^{-1}]
$S'_{b,x}$	Un-adjusted bed load transport rate in the x direction per unit width	[m^2 s^{-1}]
$S'_{b,y}$	Un-adjusted bed load transport rate in the y direction per unit width	[m^2 s^{-1}]
S_0	Bed slope	[-]
t	Time	[s]
T	Dimensionless bed shear stress	[-]
$ThetSD$	Factor for erosion of adjacent dry cells	[-]
u_b	Local near-bed flow velocity	[m s^{-1}]
$u_{b,u}$	Local near-bed flow velocity component in the x direction	[m s^{-1}]
$u_{b,v}$	Local near-bed flow velocity component in the y direction	[m s^{-1}]
u_*	Shear velocity	[m s^{-1}]
u'_*	Effective bed shear velocity	[m s^{-1}]
U	Flow velocity in the x direction	[m s^{-1}]
$\bar{U}$	Depth-averaged velocity component in the x direction	[m s^{-1}]

U'_B	Near-bank excess flow velocity	[m s^{-1}]
V	Flow velocity in the y direction	[m s^{-1}]
$\bar{V}$	Depth-averaged velocity component in the y direction	[m s^{-1}]
w_s	Settling velocity of suspended sediment	[m s^{-1}]
W	Flow velocity in the z direction	[m s^{-1}]
X	Computed bed level	[m]
Y	Measured bed level	[m]
z_b	Bed level	[m]
z_0	Bed roughness length	[m]
Z_i	Initial bed level	[m]
α	Calibration factor for sediment transport rate	[-]
α_e	Measure of bedform phase error	[-]
α_n	Transverse bed slope correction factor	[-]
α_s	Longitudinal bed slope correction factor	[-]
α_{bn}	Calibration factor for transverse bed slope correction	[-]
α_{bs}	Calibration factor for longitudinal bed slope correction	[-]
β_c	Secondary flow correction factor	[-]
β_e	Measure of bedform amplitude error	[-]
γ	Transverse bed slope	[-]
γ_e	Measure of an average bed level error	[-]
Δ	Relative mass density of sediment under water	[-]
Δt_{hydro}	Hydrodynamic time step	[s]
Δt_{mor}	Morphodynamic time step	[s]
Δz_b	Distance to the computational grid point closest to the bed	[m]
ε_e	Normalization term for measurement error	[-]
ζ	Water surface elevation	[m]
η	Relative availability of the sediment fraction in the mixing layer	[-]
θ	Shields parameter	[-]

λ	Meander wavelength	[m]
ν_k	Kinematic viscosity coefficient of water	[m^2 s^{-1}]
ν_H	Horizontal eddy viscosity	[m^2 s^{-1}]
ν_v	Vertical eddy viscosity	[m^2 s^{-1}]
ρ	Density of water	[kg m^{-3}]
ρ_s	Density of sediment particles	[kg m^{-3}]
ρ_0	Reference density of water	[kg m^{-3}]
τ_b	Bed shear stress	[N m^{-2}]
$\tau_{b,cr}$	Critical bed shear stress	[N m^{-2}]
ϕ	Angle of repose	[°]
ϕ_τ	Angle between downstream and sediment transport direction	[°]
ψ	Longitudinal bed slope	[-]
ω	Vertical flow velocity relative to the σ-plane	[m s^{-1}]

List of Figures

List of Tables

1 Introduction

1.1 Motivation

Meandering rivers tend to have a low gradient and thus slow flow. Their river bed is typically composed of fine sediments, and most of the sediment is transported in suspension. These features are typical of lowland rivers, although low-gradient rivers are found also in upland areas. Large seasonal variations in river flow result in fluctuating sediment transport capacities, which causes river bank erosion, excessive scour of fine bed material, sedimentation and formation of bars, and development of meandering channels.

Discharge is one of the most important boundary conditions for a river. Reduction of the discharge can be due to climate changes (droughts), morphological changes, as for instance the obstruction of an intake, but also due to human interventions, such as damming and water extraction, and management strategies. Due to reduced discharge, rivers are subject to morphological changes, such as channel aggradation (silting up of rivers). This is a major problem for the people living along the river, since this means gradual reduction of the water resource for household, agriculture, industry and it restricts the use of the river channel as navigation route. In addition to the morphological alteration of the river bed, the discharge variation causes also different trends in the river planimetric evolution. In order to manage these systems suitably, it is important to know how the decrease in discharge causes planimetric changes of rivers.

The need for the prediction of river planimetric changes arises from the fact that channel migration creates an important problem for water supply, hydraulic structures such as bridges and intakes. In rivers which are silting up, the main channel narrows and vegetation grows on river banks. The decrease in discharge changes the river planimetric trends leading to a new, so far hardly predictable, river course. In particular, the silting up of meandering rivers results in the formation and development of smaller meanders (Crosato 2008). This may occur in regulated rivers, in which a dam, barrage or simply water extraction reduces the water discharge. Restoring the discharge, if this is possible, does not mean that the river returns to its original state and course. Instead, the discharge increase may induce new trends in planimetric changes, i.e. there is a risk that the river will follow a new undesirable course, far from where water is needed. This means that water resources management approaches need to address the morphological response of a river to reduction or increase of discharge.

1.2 Approaches for morphological studies

Successful river management requires thorough understanding and prediction methods of river dynamics. Tools for the prediction and evaluation of river planimetric changes, which are available, are satellite image analysis, physical modelling and numerical models.

1.2.1 Satellite image analysis

Time-series of satellite images are generally used to study the planimetric changes of rivers, and dry season satellite images are commonly used for such an analysis. There are two rea-

sons for using dry season images – (i) cloud free optical images are available and (ii) these images show the alignment of the main flow path of the river system. Superimposing the bank lines of consecutive years, it is possible to obtain information on cumulative erosion along the banks of a river reach. Figure 1.1 is an example of such an approach, in which superimposing techniques have been applied to the Dhaleshwari River in Bangladesh (CEGIS 2013). This river will be introduced in more detail in this thesis (see Figure 3.1).

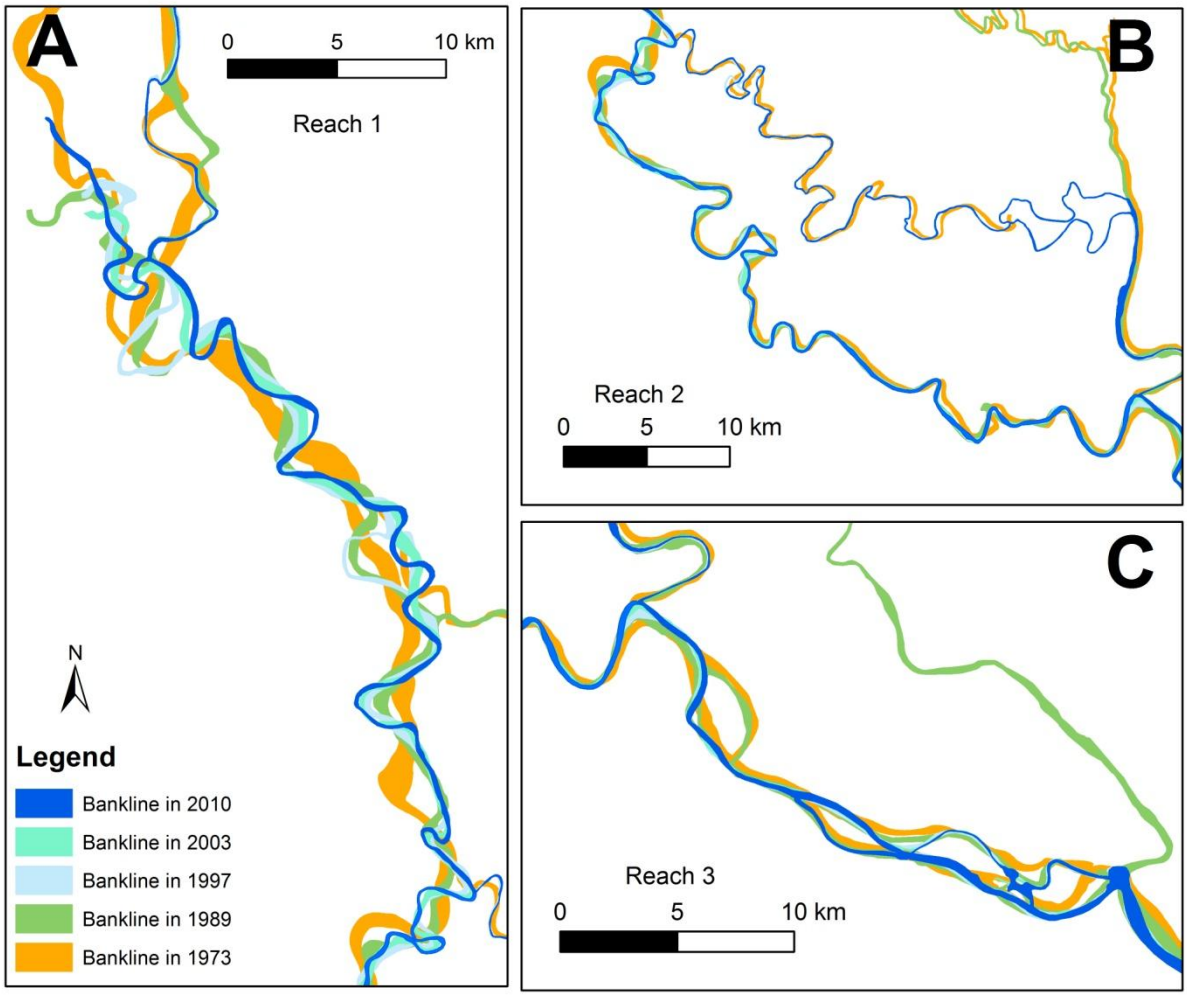

Fig. 1.1 *Channel migration in the Dhaleshwari River in Bangladesh (A) upper reach, (B) middle reach and (C) lower reach (CEGIS 2013).*

The results of such an analysis can be presented in a graphical form showing the dominant direction of bank line migration and its magnitude (see Figure 1.1). Thus satellite image analysis can be a powerful tool for the derivation of approaches to predict bank erosion. However, this method has some limitations. Firstly, spatial and temporal resolutions of images are important factors. For example, if the spatial resolution of an image is 30 m and the rate of lateral shifting is within the range of 20 m/year, the occurrence of erosion using image based analyses of consecutive years may not be captured. Secondly, data extracted from satellite images do not allow the extraction of all the information required for a complete analysis of morphological processes. In fact, such data provide two-dimensional information, whereas the extent of the morphological processes is three-dimensional. In this context, it is difficult if not impossible to derive essential information such as flow depth, velocity and sediment concentration from satellite images.

1.2.2 Physical modelling

Physical modelling is an important tool in environmental hydraulics and has been extensively used for the analysis of sediment transport processes and the morphological development of rivers (Frostick et al. 2011, Muste et al. 2017). Friedkin's (1945) mobile-bed experiments with erodible banks (see Figure 1.2) are a classical example of physical modelling applied to fluvial hydraulics. Physical modelling can provide specific results but it is expensive and time consuming. Moreover, the flow, sediment transport, and bed change processes in rivers are complicated. Correspondingly, it is difficult to attain the similarity with respect to sediment transport and flow resistance (Yalin 1971, Peakall et al. 1996, Peakall & Warburton 1996). Furthermore, scale effects may hamper the upscaling of the model results to prototype conditions (Hydralab+ 2016).

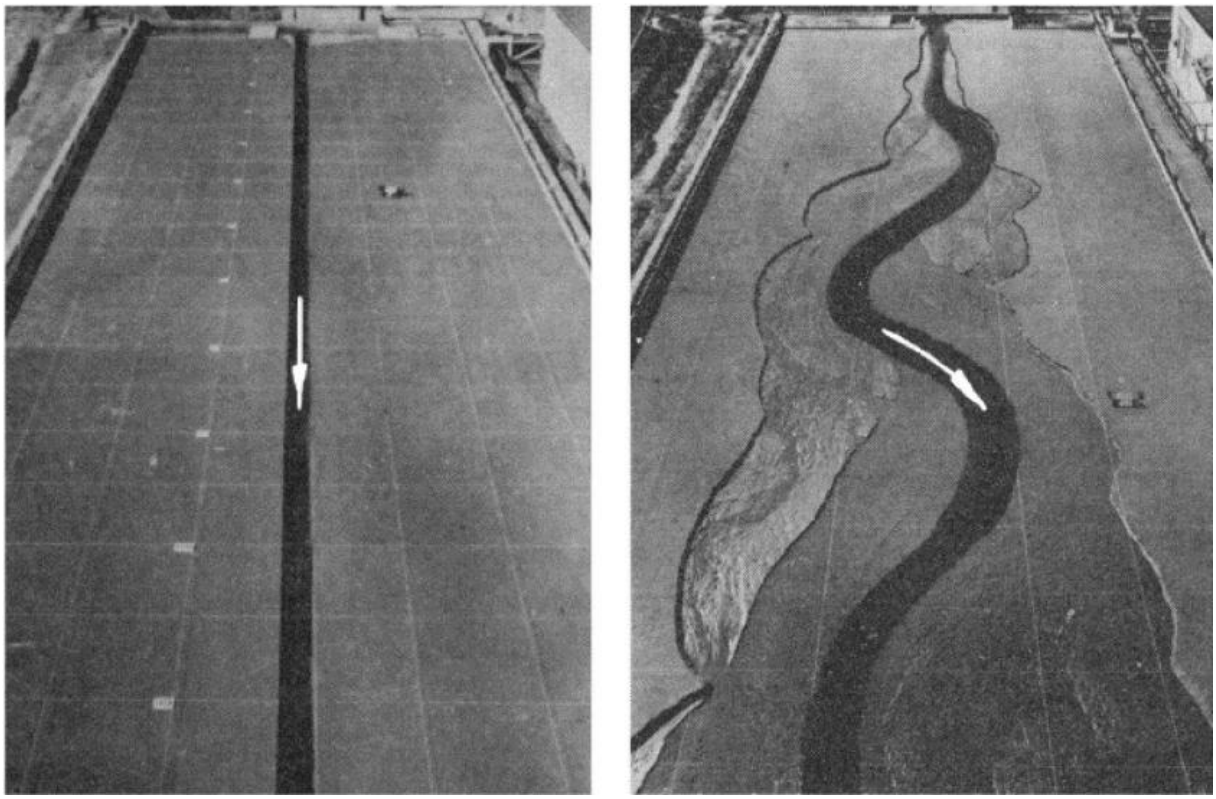

Fig. 1.2 Mobile-bed experiments with erodible banks (Friedkin 1945).

1.2.3 Numerical modelling

Numerical models simulate the physical phenomena and can contribute considerably to the understanding of the governing physical processes dominating river morphological changes. They can provide direct, real-scale predictions without scale distortion which can be validated if field data are available. Moreover, numerical models can provide data for areas where no measurements are available and they offer the possibility to extend analyses to flow conditions beyond those measured directly in the field, respectively (Sukhodolov et al. 2015). An additional benefit of numerical modelling is that it can be used to isolate the effects of a change in a single boundary condition, model schematization, or model parameter settings by comparison of scenarios (van de Wiel & Darby 2004, Schuurman et al. 2016). In addition, prediction of long-term and large-scale evolution processes is feasible by means of simplified and parameterized descriptions of the flow and bank erosion processes. Furthermore, nu-

merical models can be customized for a particular river system or condition, or to address specific questions in river management.

In this study, the last approach of the abovementioned three is adopted. Attention has been paid to channel behavior at management time (years to decades) and space (kilometers) scales.

1.3 Objectives and outline of the thesis

The main objective of the present thesis is to explore the capability of a process-based numerical model to simulate the adaption of both planform dynamics and bed topography to changed discharge regimes. A specific reach in the Dhaleshwari River (Bangladesh) is taken as a case study as it provides relevant data for model validation.

The thesis is organized in seven chapters. Following this introduction, Chapter 2 presents a literature review on the morphodynamics of meandering rivers providing the basis for the subsequent detailed description of the aim of this study and the formulation of specific research questions.

Chapter 3 describes the morphological characteristics of the Dhaleshwari River (Bangladesh), which is used as a study reach in this thesis as available morphological data could be used for validation of the modelling results. However, a complete continuous time-series of daily discharges had to be estimated from statistical moment-based analysis of hydrologic data, because the available data had a few gaps or periods of missing data. Characteristic flow discharges and trends in discharge time-series (Mann–Kendall and Sen's tests) are estimated based on the continuous time-series of daily discharges. This chapter is concluded by the presentation of the possible evolutionary scenario of the Dhaleshwari River in the study reach.

Chapter 4 describes the process-based numerical model Delft3D which was used in this thesis to investigate the morphodynamic processes in meandering rivers. Following this description, the application of the 3D numerical model Delft3D to the case study area (the Dhaleshwari River, Bangladesh) is presented. The considerations include the suitability of the depth-averaged 2D approach, which is implemented in Delft3D, to model flow in curved river sections. For this purpose, the Delft3D bend-flow sub-model is validated against experimental data acquired in a curved flume. The validated model is then used to simulate bed morphology and meander planform in the study area, on a decadal time scale, under bankfull discharge condition. The numerical results are presented and discussed at the end of this chapter.

In Chapter 5, the depth-averaged 2D morphodynamic model is used for additional numerical experiments to investigate the effects of different discharge magnitudes on channel morphology and planform adjustment in the study area.

Chapter 6 provides a comparison of model predictions and observed data for a yearly river discharge hydrograph and a schematized (i.e., simplified) discharge hydrograph in the long-term morphodynamic simulations. An evaluation of compressed and non-compressed simplified hydrographs, in combined usage with the morphological scale factor approach, is pre-

sented. Finally, the model is used to predict future channel planimetric evolution taking into account different hydrologic scenarios. The numerical results are presented and discussed.

Chapter 7 presents a summary of conclusions drawn from the present work and provides avenues for future research.

2 Meandering rivers in lowlands

2.1 River patterns

Rivers exhibit different types of planforms which depend on bank and bed material, riparian vegetation, as well as sediment and water discharge regimes. The planform of alluvial river patterns are in general categorized as (1) straight, (2) meandering, and (3) braided rivers (Leopold & Wolman 1957):

1. When the river is straight, sinuosity (i.e., the ratio of the river thalweg-length to the down-valley length, see Section 2.2.6) has a minimum value of one. Such rivers exist only over short reaches and long straight rivers occur seldom in nature. Therefore, rivers with a sinuosity of less than 1.1 are commonly described as straight (see Figure 2.1(a)), and those between 1.1 and 1.5 are sinuous.
2. Meandering rivers have a sinuosity of greater than 1.5. Meandering rivers wander back and forth over their floodplains (see Figure 2.1(b)), and hence, sinuosity tends to increase but it reverts close to unity when braiding (i.e., multiple-thread channels separated by mid channel bars) occurs.
3. In large rivers, the river splits often into several channels as a single channel cannot convey all the discharge. The separate channels are called anabranches (or anastomoses) as shown in Figure 2.1(c). Each anabranch is a distinct and rather permanent channel with banklines. However, Leopold & Wolman's (1957) classification scheme does not explicitly recognize the anabranched channel pattern (Knighton & Nanson 1993). Braided rivers (see Figure 2.1(d)) are relatively unstable compared to anabranching channels. Braided rivers are characterized by multiple channels and braid bars within the banklines of a single broad channel.

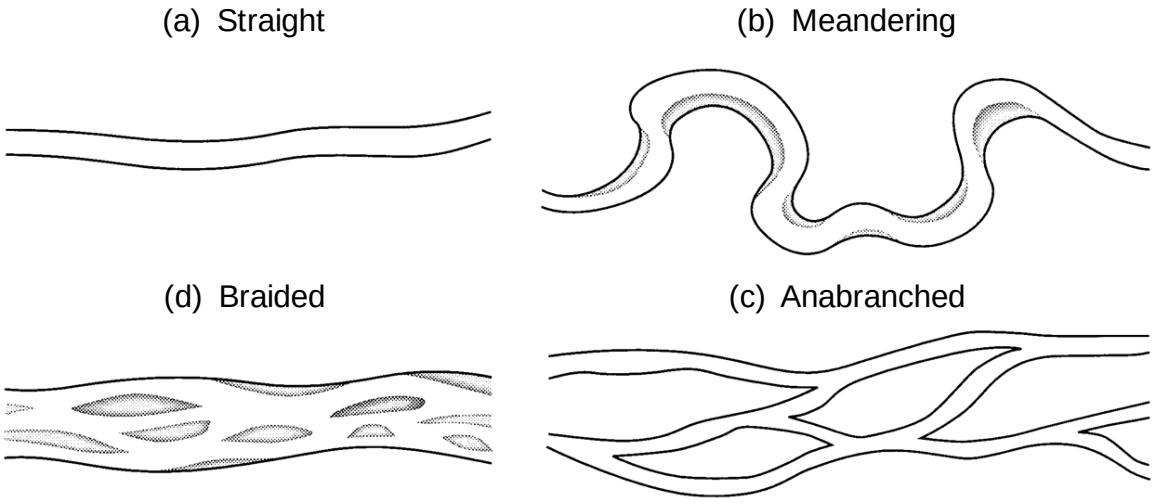

Fig. 2.1 Classification of river channel patterns: (a) straight, (b) meandering, (c) anabranched and (d) braided. Available at: http://www.seddepseq.co.uk/DEPOSITIONAL_ENV/Fluvial/Fluvial.htm [accessed 7 January 2018].

The sequence of straight, meandering, and braided rivers corresponds to an increase in valley slope or stream power magnitude. Lowland rivers are characterized by meandering channels; piedmont rivers by braiding channels. Leopold & Wolman (1957) and subsequently Bridge (2003) found that if data for average channel slope (S_0) is plotted as a function of bankfull discharge (Q_{bf}), braided rivers plot above the position of meandering rivers (see Figure 2.2). This means that braided systems might also be found in flat planes and meandering streams in mountain valleys, if they fulfill certain conditions.

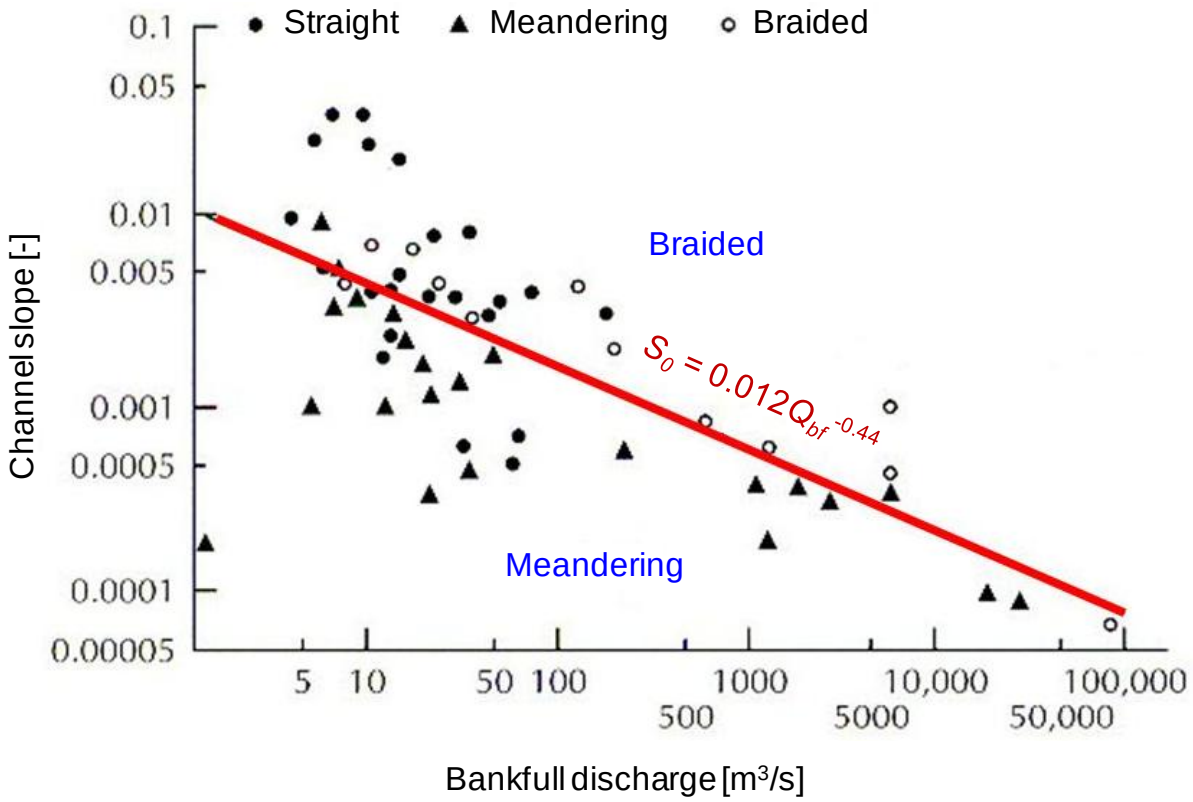

Fig. 2.2 *Channel pattern (meandering, straight, and braided) as a function of channel slope (S_0) and bankfull discharge (Q_{bf}). Leopold & Wolman (1957) provided a threshold between meandering and braided rivers as shown by the red line (adapted from Bridge 2003).*

2.2 Morphological characteristics and morphodynamics of meandering rivers

Meandering is the most common river planform in nature (Darby et al. 2002, Crosato 2008). In a meandering river, bends with different amplitudes and radii of curvature constitute a continuous sinuous channel. Figure 2.3 shows zones of erosion and deposition in a meandering river. A meander bend usually consists of a gently sloped point bar attached to the convex side (inner bank) and a deep pool on the concave side (outer bank). Meander bends are connected at the points of inflection or by short straight crossings. The flow depth at crossings (section A_1 - A_2 in Figure 2.3) is relatively shallow compared to the flow depth at pools in bend (section C_1 - C_2 in Figure 2.3). The thalweg (i.e., the line of maximum depth) wanders from the deep pool at the outer side of a bend over a shallow crossover to the next deep pool at the outer side of the next bend.

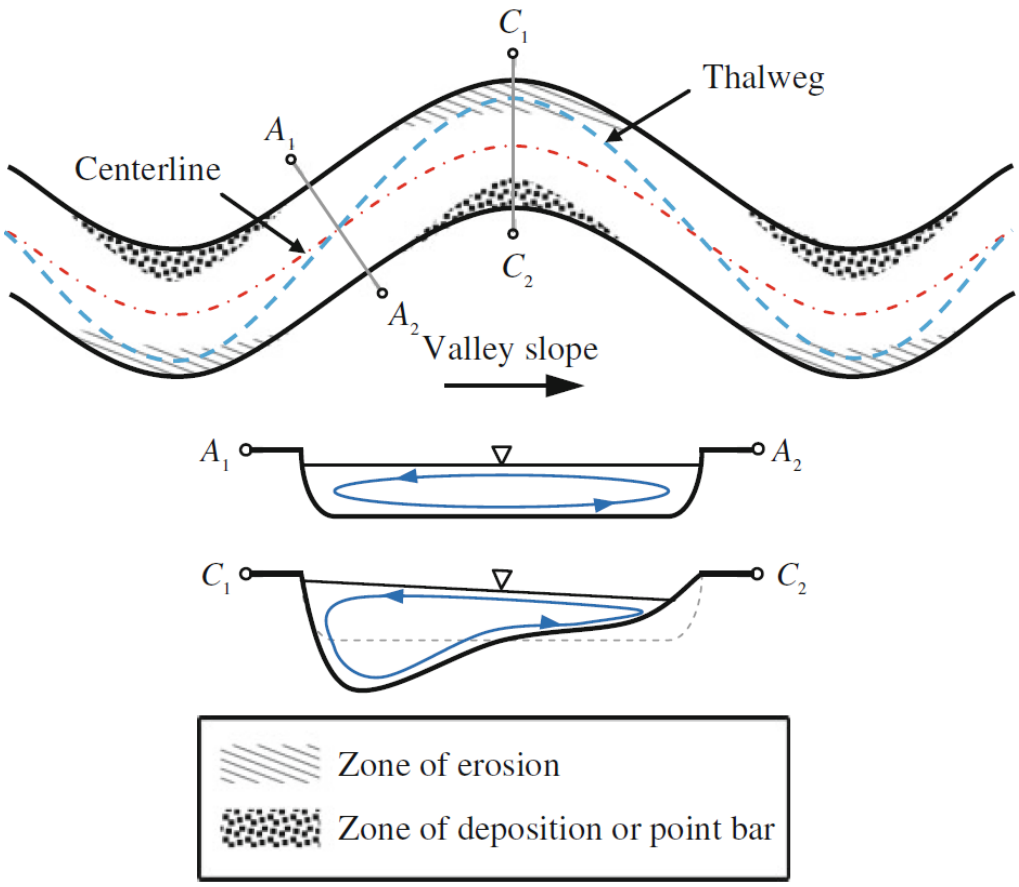

Fig. 2.3 Sketch showing zones of erosion and deposition in a meandering river (adapted from Dey 2014).

The morphology of a river channel is a function of a number of processes. A comprehensive literature review on river meanders is given by Julien (1985). In the following sections, a short literature review about the important processes is presented.

2.2.1 Sediment transport

The knowledge of the processes of sediment transport is fundamental for evaluating channel morphological changes. The river sediment load originates from two sources. The first is the river bed material that is displaced by the bed shear stress and the second is the material resulting from the basin erosion. The size fractions which are found in large quantities in the bed are referred to as bed material load. Wash load is carried by the flow such that it always remains in suspension without deposition. In general, all size fractions that are finer than 0.063 mm are considered as wash load. A further definition of wash load was given by Einstein (1950), who defined wash load as the smallest 10% of the bed material size distribution. Wang & Dittrich (1992) used the non-dimensional Rouse number (Z) to differentiate wash load and bed material load, in which the Rouse number (Z) is defined as

$$Z = \frac{w_s}{\kappa u_*} \tag{2.1}$$

where w_s is the settling velocity of suspended sediment (m s^{-1}), κ is the von Karman constant (= 0.4), and u_* is the shear velocity (m s^{-1}). According to Wang & Dittrich (1992), the Rouse number (Z) is less than 0.06 for wash load and greater than 0.1 for bed material load.

Sediment transport is often decomposed into bed load and suspended load. Bed material is transported in suspension if the turbulence of the flow is large enough to lift particles from the bed into the water column. Suspended sediment travels at a velocity similar to that of the flow while bed load progresses with a lower speed. Suspended load combines thus both bed material and wash load. Bed load transport takes place near the bottom of the river where the sediments are transported by sliding or rolling on the bed or by saltation.

Morphological change is caused by spatial and temporal gradients in sediment transport. More sediment entering into a reach than going out of the reach results in aggradation. On the other hand, less sediment entering into a reach than going out of the reach results in degradation. Previous studies have reported that outer bank erosion is the leading process in meander migration, followed by point-bar growth and bar-floodplain conversion (Kasvi et al. 2017). Generally, bank erosion occurs at the outer bank of a meander bend during flood flows. The eroded material is transported as bed load and suspended load and is deposited more downstream near the inner banks where the flow velocities are low. As a result, inner banks advance with the build-up of point bars, leading to bank accretion. At large spatial and temporal scales, the bank erosion rate near the outer bank is counterbalanced by the bank accretion rate near the inner bank (Ikeda et al. 1981, Crosato 2008).

2.2.2 Spiral flow in a meander bend

Flow in a meander bend has been studied in detail by Shukry (1950), Rozovskii (1957), Bathurst et al. (1979), Kalkwijk & De Vriend (1980) and others. In curved open channels, centrifugal force caused by channel curvature creates stronger momentum in the upper layer of water and weaker momentum in the lower layer of water, leading to a super-elevation of the water on the concave side. Due to the local imbalance between the centrifugal force and the cross-stream pressure gradient, a cross-stream circulation (secondary flow) is generated (see Figure 2.4). The combination of the secondary flow and the stream-wise flow produces a screw like path of streamline around a bend (spiral flow). In the literature, however, the term ‘spiral flow’ has often been used interchangeably with the terms ‘secondary flow’ and ‘helicoidal flow’ (Kleinhans et al. 2008). In the outer bank region sediment particles near the bed are driven towards the inner bank region by the spiral flow. Thus the spiral flow induces deposition along the inner bank and scouring along the outer bank in curved channel bends. The tendency to erode the outer bank and deposit sediment along the inner bank causes the channel to migrate laterally (see Figure 2.3).

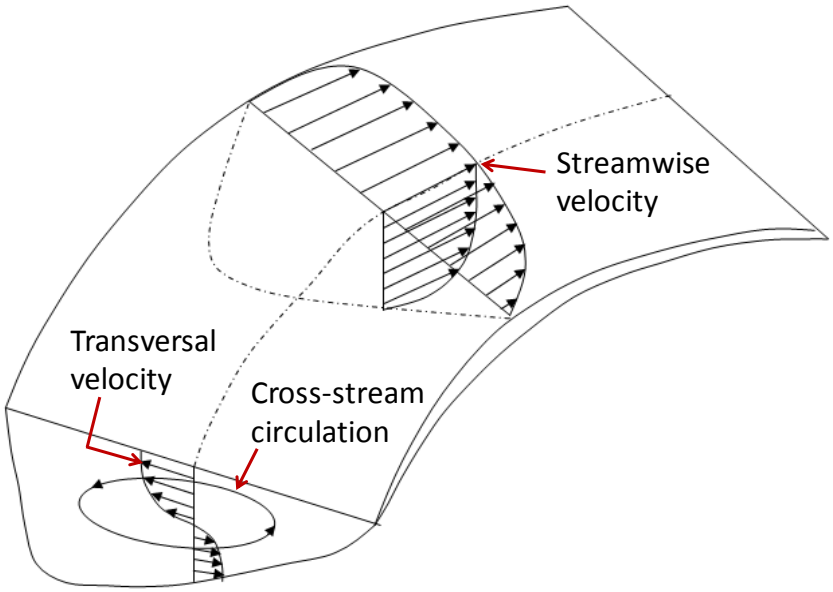

Fig. 2.4 Flow in meander bends.

2.2.3 Effects of the transverse bed slope

River bends are characterized by a transversely sloped bed profile (deeper near the outer bank and shallower on the inner bank). On a transverse sloping bed, the migrating particles are continuously subjected to a downward gravitational force and hence they tend to move downslope deviating from the near bed flow direction. In the presence of secondary flow, downslope sediment transport due to gravity is balanced by spiral flow dragging the sediment upslope, which in turn controls the sediment transport, and thereby the shape of transverse bed slope of the point bar (Weisscher et al. 2017).

The quantitative knowledge of the direct effect of gravity on sediment moving on a transverse sloping river bed is based on experiments in curved flume channels with simple bed configuration (Ikeda 1982, Struiksma et al. 1985, Talmon et al. 1995, Wiesemann et al. 2006). Struiskma et al. (1985) derived an analytical model based on experiments in a curved flume, in which the vertical sidewalls were fixed and the flume bed was initially transversely flat. The analytical model is:

$$\frac{\partial z_b}{\partial y} = f(\theta) A \frac{h}{R_s} \tag{2.2}$$

in which z_b is the bed level (m), y is the transverse distance (m), A is the secondary flow direction coefficient (-), $f(\theta)$ is a weight-function of the Shields-parameter θ which describes the ratio of drag force to resistance force, h is the water depth (m) and R_s is the radius of streamline curvature (m). The lateral bed slope is determined by local parameters such as water depth, bed shear stress, radius of curvature of a bend and sediment properties. The secondary flow direction coefficient is defined as:

$$A = \frac{2}{\kappa^2} E_s \left(1 - \frac{1}{2} \frac{\sqrt{g}}{\kappa C} \right) \tag{2.3}$$

in which C is the Chézy coefficient ($m^{1/2}\ s^{-1}$), g is the gravitational acceleration ($m\ s^{-2}$), and E_s is a coefficient to control the spiral flow effect on the bed load transport direction (-).

The weight-function has been calibrated for laboratory experiments by Talmon et al. (1995):

$$f(\theta) = 9\left(\frac{D_{50}}{h}\right)^{0.3}\sqrt{\theta} \tag{2.4}$$

in which D_{50} is the median sediment diameter (m).

2.2.4 Bank erosion

For the process of lateral migration of the river channel, bank erosion plays the most important role. Bank erosion is a combination of fluvial erosion (i.e., the removal of bank material by the action of hydraulic forces) and gravitational mass failure processes. The secondary flow is considered to be the dominant factor for the erosion of the outer bank as explained by Johannesson & Parker (1987): “It can, however, by no means be concluded that this is the one and only, or even the dominant, process driving bank erosion in meandering rivers”.

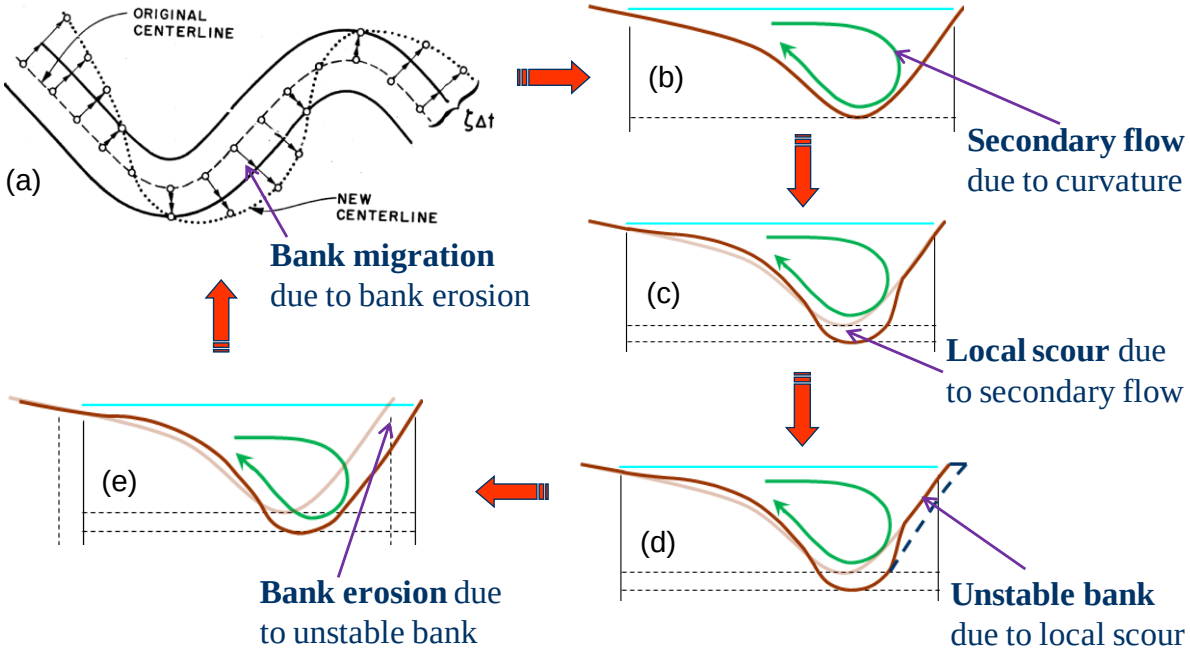

Fig. 2.5 Bank migration process (adapted from Banda & Egashira 2016).

The meandering channel migration process is shown in Figure 2.5 where sub-plot 2.5(a) demonstrates the planform of a meandering channel (Johannesson & Parker 1985), sub-plot 2.5(b) shows that secondary flow is generated due to channel planform curvature, sub-plot 2.5(c) exhibits that secondary flow carries the near bottom sediments from the outer bank to the inner bank region in the downstream, sub-plot 2.5(d) illustrates that the outer bank is undermined and becomes unstable and the last sub-plot 2.5(e) shows that unstable bank collapses and induces bank erosion resulting in a new planform.

2.2.5 Bank accretion

Bank accretion is a fundamental process leading to the advance of banklines and to the formation of channel width. The alternation of high and low flows, the nature of sediment forming the river bed and banks, and the presence of riparian vegetation are keys to the advance of banklines. Using field data over a period of 20 years, Hooke (2008) investigated the morphological responsiveness to discharge variations on a 10 km gravel-bed meandering reach (Dane River, England) and stated that during high flow periods erosion exceeds deposition resulting in the widening of the channel, but during lower peak flow periods deposition catches up and results in narrowing of the channel. Kasvi et al. (2013) employed an acoustic Doppler current profiler (aDcp) at three flow stages in a sand-bed meandering river (Pulmanki River, Finland) and examined how the 3D flow structure changes over the flow regimes. They found that secondary circulation is responsible for scroll bar formation on the point bar. The strength of the spiral flow increases as discharge rises, and large floods produce deposition on the point bar, leading to bank advance. This indicates that meandering rivers exhibit width fluctuations both in time and space, varying with the river discharge, but over long time periods, meandering rivers exhibit a more or less constant width (Zolezzi et al. 2012, Vargas-Luna 2016, Bogoni et al. 2017).

2.2.6 Planform characteristics of meandering rivers

The mutual interaction between hydraulics and sediment transport processes controls the shape of meander planform. This section describes the characteristics of meander planform geometry.

2.2.6.1 Planform parameters

Meandering river bends occur in natural river channels at all scales, and all around the world meander planforms have been intensively studied (Fargue 1868, Jefferson 1902, Leopold & Wolman 1957, 1960, O'Boyle 1981, Williams 1986, Magdaleno & Fernández-Yusti 2011, Howett 2017). Fargue (1868), who made one of the first attempts to describe meander planform, argued that meandering rivers have one essential property, namely 'the continuity of the change in curvature'. From observations at the Garonne River (France), he correlated river planform geometry with flow depth, however, his findings stayed largely unknown (Hager 2003, Dittrich & Huppmann 2013).

Generally, meander planform, which can be described best when viewed from above, is described based on a range of parameters (Leopold & Wolman 1957, 1960). Figure 2.6 illustrates the most commonly used parameters to describe the geometry of bends: The meander belt width (M_B) is the shortest distance between tangents drawn at the outside of the meanders; the meander wavelength (λ) is defined as the distance between two subsequent inflection points of the wave pattern; the radius of curvature (R) is the radius of a circular arc that best fits a meander loop and the channel widths (B) are measured from topographic maps based on the assumption that these are not significantly different from bankfull widths (Williams 1986).

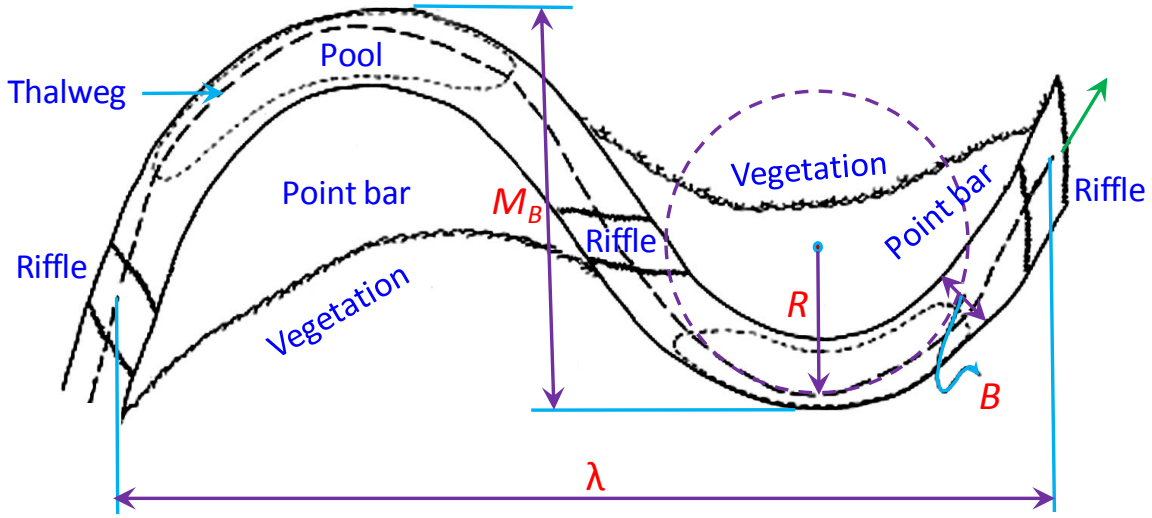

Fig. 2.6 *Definition of key planform parameters: M_B is the meander belt width which is defined as the distance between tangents drawn at the outside of the meanders; λ is the meander wavelength which is defined as the distance between two subsequent inflection points of the wave pattern; R is the radius of curvature which is defined as the radius of a circular arc that best fits a meander loop and B is the channel width which denotes bankfull width (modified after Leopold & Wolman 1957).*

2.2.6.2 Interrelations between meander parameters

Planform studies using maps and aerial photographs have been used to derive empirical equations for reach-scale meander geometry by relating meander belt width (M_B), meander wavelength (λ) and radius of curvature (R) to each other as well as to characteristics of the cross-section such as bankfull width (B) (Williams 1986). Such empirical relationships are considered to be applicable to all meandering streams as the plans of river bends look alike regardless of scale (Leopold & Wolman 1960, Shahjahan 1970, O'Boyle 1981). The underlying assumption is that the parameters change over time dependent on the processes affecting the development of the floodplains, but that, at the same time, they maintain their average values when the entire reach is considered.

Correlations between meander parameters were first developed by Jefferson (1902), who examined 23 streams with floodplains and found that M_B is equivalent to 1.43 times λ. Furthermore, Jefferson (1902) established an empirical relationship between M_B and B, and showed that M_B is equal to about 17.6 B. Later, Bates (1939) found that M_B is equivalent to 14.32 times B. Williams (1986), using data collected from 153 rivers around the world, found that M_B is equal to about 6 times B. The apparent lack of agreement with prior studies can mainly be associated with the meander belt width (M_B) delineation. Jefferson (1902) and Bates (1939) defined M_B as the distance between lines drawn tangentially to the outside bends of the laterally extreme meander bends in a series of meanders, whereas Williams (1986) used lateral distance between tangential lines of two successive meander bends.

Leopold & Wolman (1960) found that the empirical relationship describing the link between λ and B showed the best-fit for all empirical relationships used to describe meander geome-

try. A few years later, Leopold et al. (1964) suggested that λ is most commonly in the range of 10 - 14 times B. Later, other researchers have further investigated this relationship and also found that λ is linearly related to B and the λ/B ratio lies in between 10 to 14 (see Table 2.1).

Leopold & Wolman (1960), in their investigation of 50 rivers, found that most meanders tend to develop a radius of curvature to channel width ratio (R/B) between 2 and 3, regardless of the size of the river. For R/B values of 2 to 3, Bagnold (1960) showed that the energy losses caused by the flow in a bend are minimized. Hickin & Nanson (1984), based on a study of several sand-bed rivers in Canada, found that the bank erosion rate is a function of the R/B ratio, with a maximum value at R/B = 2.5. The meander migration rate decreases on either side of the range (2< R/B <3). Other authors have confirmed a similar role for the R/B ratio in controlling channel migration (see Table 2.1).

Tab. 2.1 Relation between planform parameters and channel width

Source	M_B/B	λ/B	R/B
Jefferson (1902)	17.6	12.6	-
Bates (1939)	14.32	-	-
Leopold & Wolman (1960)	7.9	11.6	2.3
Zeller (1967)	4.5	10	-
Young (1974)	-	10.8	2.3
Dury (1976)	-	11	-
O'Boyle (1981)	9.1	11.6	2.96
Williams (1986)	6	10.47	2.43
Chang (1988)	-	10.23	3
Soar & Thorne (2001)	-	10.23	-
Julien (2002)	4.5	12.34	-
Howett (2017)	6.89	-	-

From Table 2.1 it can be seen that, up to the 1960s, several investigators attempted to discover relationships between planform parameters and channel width (B), and newer studies basically confirmed those relationships. Leopold & Wolman (1960), O'Boyle (1981) and Williams (1986) considered meander belt width (M_B), meander wavelength (λ) and mean radius of curvature (R), whereas others focused on either one or two of these parameters depending on the aim of their investigations. It should be noted that M_B is 0.5 to 1.5 times λ which is rarely outside the range of 10 to 14 times B, and R is generally 2 to 3 times B. However, sediment load and channel forming sediments can distort this generalized rule (Leopold & Wolman 1960, Soar & Thorne 2001).

2.2.6.3 Relation between discharge and channel cross-sectional parameters

The idea of representing a river regime with a single discharge has attracted the attention of the scientific community, both in the fields of fluvial geomorphology and hydraulic engineering, since the beginning of the previous century. Hydraulic engineers developed a variety of empirical relationships known as "regime theory" to aid in the design of stable drainage, irrigation or navigation channels in order to reduce the costs associated with maintenance of such channels (Lindley 1919, Lacey 1930, Leopold & Maddock 1953). Relationships have been developed for both at-a-station geometry and downstream geometry by relating a target variable to the discharge in the form of an exponential equation (for example, $B = aQ^b$, where a and b are constants). Downstream hydraulic geometry relationships describe the shape of alluvial channels in terms of bankfull width, mean depth, mean velocity, and channel slope. On the other hand, at-a-station hydraulic geometry describes the relationship between water-surface width, mean depth, and mean velocity with changing discharge at a cross-section in the channel (Singh 2003). Using data from stable canals in India and Pakistan, Lacey (1930) remarked that irrigation canals remain stable when their width scales as the square root of their discharge ($B \propto Q^{0.5}$), even if the bed and banks are subject to erosion and deposition. Recently, field observations revealed that Lacey's law is applicable to natural rivers as well (Gaurav et al. 2017, Métivier et al. 2017).

2.2.6.4 Relation between discharge and meander wavelength

Jefferson (1902) first demonstrated that meander belt width (M_B) varies with the volume of water discharged by a river. On the basis of Jefferson's (1902) and own data, Inglis (1949) found that the meander wavelength (λ) is proportional to the square root of "dominant" discharge:

$$\lambda = 36\sqrt{Q_{bf}} \tag{2.5}$$

where λ and Q_{bf} are in meters and cubic meters per second, respectively.

The dominant discharge is a hypothetical term which is defined as the steady flow rate that will shape the bankfull channel over moderate time scales in the same way as the natural hydrologic regime does. The dominant discharge has been used interchangeably with the bankfull discharge, channel-forming discharge and effective discharge in the literature (Ferro & Porto 2012). Classical explanations of dominant discharge (Inglis 1949) use the bankfull discharge (Q_{bf}). Later, several authors correlated λ with a range of discharge indices (see Table 2.2).

Inglis (1949), Leopold & Wolman (1957) suggested that λ varies with the square root of Q_{bf}. Dury (1964) adopted the mean annual flood discharge (Q_{maf}) as a typical value of dominant discharge, and found a similar type of relationship. Carlston (1965) stated that the dominant discharge is associated with a range of flows between the mean discharge for the month where the maximum discharge occurs (Q_{mm}) and the mean annual discharge (Q_{ma}). Ackers & Charlton (1970) related λ with Q_{bf} using both laboratory and field data. Schumm (1967) found that λ is dependent not only on flow discharge, but also on the type of sediment load trans-

ported through the channel. Later, he showed that λ correlates with Q_{bf} and the fraction of silt-clay in the channel perimeter (M) (Schumm 1977). Thus, a question that needs to be discussed is which discharge should be used in finding the relationship between discharge and channel characteristics such as meander wavelength (λ).

Tab. 2.2 Meander wavelength-discharge relationships (λ in [m], Q in [m^3 s^{-1}])

Source	Relationship	Discharge
Inglis (1949)	$\lambda = 36\sqrt{Q_{bf}}$	Bankfull discharge (Q_{bf})
Leopold & Wolman (1957)	$\lambda = 65.2\sqrt{Q_{bf}}$	Bankfull discharge (Q_{bf})
Dury (1964)	$\lambda = 54.3\sqrt{Q_{maf}}$	Mean annual flood (Q_{maf})
Carlston (1965)	$\lambda = 166Q_{ma}^{0.46}$	Mean annual discharge (Q_{ma})
	$\lambda = 126Q_{mm}^{0.46}$	Mean monthly maximum discharge (Q_{mm})
Ackers & Charlton (1970)	$\lambda = 61.2Q_{bf}^{0.47}$	Bankfull discharge (Q_{bf})
Schumm (1977)	$\lambda = 1936Q_{ma}^{0.34}M^{-0.74}$	Mean annual discharge (Q_{ma})
Mackey (1993)	$\lambda = 72.16Q_{bf}^{0.49}$	Bankfull discharge (Q_{bf})

M = Fraction of silt-clay in the channel perimeter (-)

2.2.6.5 Estimation of dominant discharge

Classical explanations of dominant discharge use the bankfull discharge (Q_{bf}) as it represents the flow that fills the channel from bank to bank before spilling into the floodplain (Inglis 1949, Leopold & Wolman 1960). Williams (1978) presented a detailed review on the identification of bankfull stage ranging from vegetation boundaries to morphological breaks in bank profiles and outlined 16 methods to depict bankfull elevation. However, considerable expertise is required to apply these methods in practice as the field identification of bankfull stage can be difficult and subjective (Radecki-Pawlik 2015).

The second deterministic discharge concerns the channels that are at or near dynamic equilibrium (i.e., neither aggrading nor degrading). The channel forming discharge governing the cross-sectional and planform characteristics can be based on a chosen recurrence interval of flooding. Channel-forming discharges have often been associated with a fixed recurrence interval which is seldom outside the 1 to 3 year range (Soar & Thorne 2001, Biedenharn et al. 2001). Recently, Bolla Pittaluga et al. (2014), Lanzoni et al. (2014), Frascati & Lanzoni (2013) have approached this problem by means of numerical modelling. Bolla Pittaluga et al. (2014) and Lanzoni et al. (2014) applied one-dimensional models to the Magra River (Italy) and to the Po River (Italy) respectively, and suggested that the river bed morphology is controlled by moderate discharges in the presence of fixed (non-erodible) wall. They further suggested that the dominant (or channel-forming) discharge lies between mean annual dis-

charge and bankfull discharge. Similar results were obtained by Frascati & Lanzoni (2013), who used a two-dimensional analytical linearized model to simulate the Po River in Italy. It should be noted that these numerical experiments were conducted in natural rivers with fixed (non-erodible) walls where the river banks were artificially protected. As the flow regime not only influences channel cross-sectional shape, but also affects meander geometry, it is unclear whether previous assessments of channel-forming discharges apply to meandering rivers with erodible floodplains (i.e., freely meandering rivers). The application of numerical models to estimate channel-forming discharges in freely meandering rivers is still in its infancy.

The third deterministic discharge is the effective discharge. The effective discharge is the discharge which, over time, transports the largest quantity of sediment. A method for determining the effective discharge is the Wolman & Miller (1960) method which states that the effective discharge is a function of both the magnitude of a flood-event and its frequency of occurrence. In this method, the effective discharge is computed by finding the maximum of the curve resulting from multiplying the flow frequency curve with the sediment discharge rating curve (Doyle et al. 2007). The maximum of the curve indicates the flow that does the most geomorphic work. Goodwin (2004) developed analytical solutions for predicting effective discharge using sediment discharge rating equation and theoretical flow frequency distributions (i.e., normal, lognormal, and gamma). Soar & Thorne (2001) noted that bankfull and mean annual discharges, respectively, formed the upper and lower bounds for a range of effective discharges for sand-bed meandering rivers in the USA. It should be noted that the effective discharge method is founded on sediment transport rating curves, in which measurement uncertainty is inherent. Although the meander movement is essentially accompanied by sediment-transport, a sediment transport rating curve gives no insight into the changing geometries of a meandering channel, because the influence of changing geometries is already included in the rating equation (Goodwin 2004).

Although the bankfull, channel-forming and effective discharges are each considered to be dominant discharges, they may not be identical, because their values are determined from calculations following a designated procedure. There is no universally agreed method, and therefore, all three methods should be used and cross-checked against each other (Soar & Thorne 2001).

2.3 Modelling of meandering rivers

2.3.1 Physical modelling

Morphodynamics of rivers can be studied through physical modelling or numerical modelling (see Section 1.2.2 and Figure 2.7). A physical model is a scaled representation of the prototype where the model results are obtained by measurements (De Vries 1993). The basic requirements to achieve similitude are geometric similarity, kinematic similarity, and dynamic similarity (Yalin 1971, Peakall et al. 1996, Peakall & Warburton 1996). A particular advantage of physical modelling is that it can provide specific results and direct visual feedback.

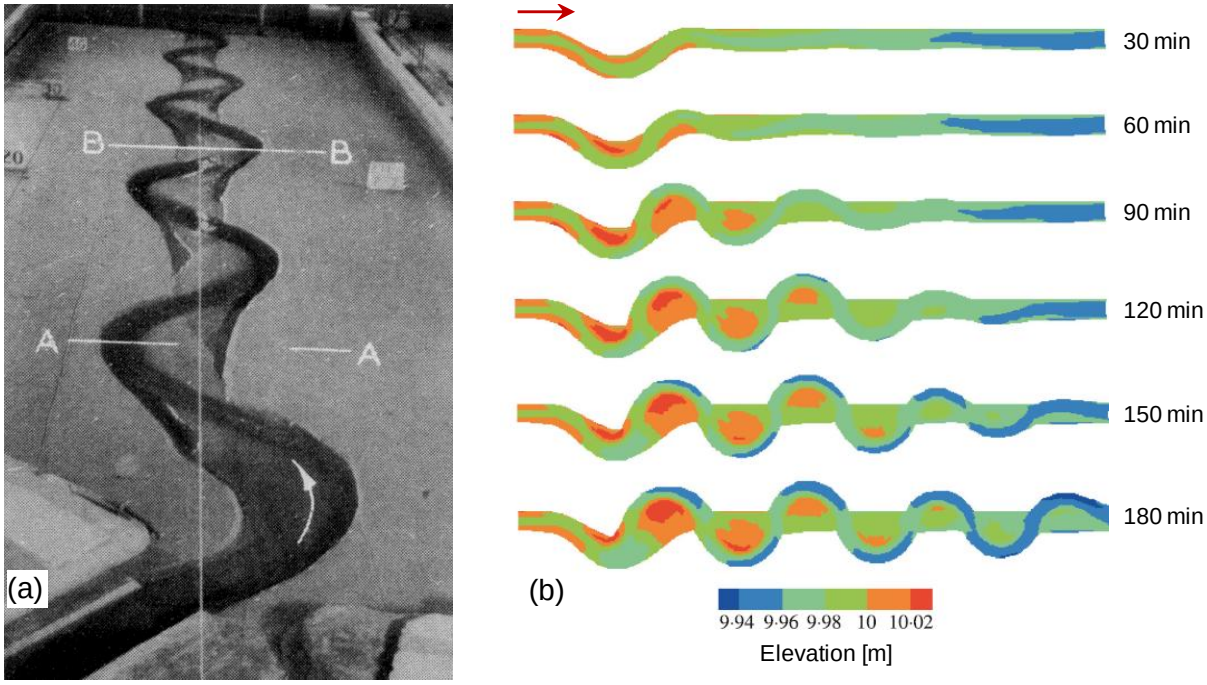

Fig. 2.7 *(a) Meandering channel evolution from an initially straight channel (see the left plot in Figure 1.2) after 3 hours in a physical model study (Friedkin 1945) and (b) Numerical simulation of Friedkin' (1945) laboratory channel (Duan & Julien 2010).*

Friedkin (1945) pioneered the physical experiments to study the meander evolution from an initially straight channel (see Figure 1.2) and investigated the effect of discharge, slope, initial cross-section, bed material, skewed inlet angle of the flow and sediment supply. The results of the investigations are valuable although only qualitative descriptions were reported. Friedkin (1945) found that, over time, amplitude of the meanders tends to increase and that the meanders gradually migrate downstream. Later, several researchers investigated how meanders are initiated and how they develop in laboratory channels (Ackers & Charlton 1970, Schumm & Khan 1972, Schumm et al. 1987, Braudrick et al. 2009, Visconti et al. 2010, van Dijk 2013). Visconti et al. (2010) found that the temporal variation of discharge influences the development of sand bar and meandering channel pattern. Van Dijk (2013) found that meander dynamics are controlled by bankfull discharge conditions, but overbank flow is highly important in modifying the floodplain. By means of scaling analysis, Braudrick et al. (2009) suggested that the experimental meander migration was faster as compared to most natural channels. This pointed out indirectly the so-called "scale effects" that hamper the upscaling of physical model results to prototype conditions (e.g., Hydralab+ 2016). The use of physical models can provide useful predictions of meander evolution, but time and cost constraints prevent the use of physical models. Furthermore, for extensive sets of investigated scenarios, the physical modelling approach requires more schedule time and more cost than numerical modelling. In contrast, numerical modelling can provide direct, real-scale predictions without scale distortion, and multiple numerical experiments are feasible within acceptable times. Since numerical modelling is the main approach in the present study, different types of numerical models used by the river engineers are described briefly in the following section.

2.3.2 Numerical modelling

Numerical models can be used to simulate the physical phenomena involved in river morphology changes and can contribute considerably to the understanding of the governing physical processes. They provide direct, real-scale predictions without scale distortion, but include uncertainties due to simplifications, computational errors and schematizations. Numerical models are based on mathematical equations adapted for numerical computations by means of numerical methodologies. The governing equations for water flow are the mass conservation equation (continuity equation) and the momentum conservation equation. Similarly, the governing equations for sediment transport are mass conservation and either a sediment transport capacity equation (bed material load only) or entrainment/deposition equations coupled to advection diffusion equations for suspended transport.

For an acceptable quality of model results, a model needs to be calibrated and validated. Calibration is basically the adaptation of the model to a specific case and is obtained by the comparison between calculated results and physical measurements, for instance water level series. Calibration is based on the optimization of calibration parameters to minimize the difference between computed and measured variables. Validation is another important step in modelling. In this case, the calibrated model is run to simulate another condition and then the results are again compared to measured data which has not been used for calibration. Validation is carried out to assess the model performances, which makes the analysis of model results possible also in case the model simulates future scenarios.

Different types of numerical models used by river engineers are described briefly in the following sections.

2.3.2.1 3D models

The Navier-Stokes equations are the fundamental governing equations that describe the instantaneous motions of turbulent flow for incompressible fluid (Navier 1823, Stokes 1845). The continuity equation is

$$\frac{\partial u_i}{\partial x_i} = 0 \tag{2.6}$$

The general equation for conservation of momentum is

$$\frac{\partial u_i}{\partial t} + u_j \frac{\partial u_i}{\partial x_j} = g_i - \frac{1}{\rho}\frac{\partial p}{\partial x_i} + \frac{\partial}{\partial x_j}\left(\nu \frac{\partial u_i}{\partial x_j}\right) \tag{2.7}$$

where u_i is the velocity, t is the time, g_i is the acceleration due to gravity, p is the pressure, and ν is the viscosity. A short-hand notation is used where x_i = (x, y, z) and u_i = (u, v, w) for u = 1, 2, 3.

There are four unknown variables u, v, w and p in the Navier-Stokes equations. Four equations (continuity and momentum) are sufficient to solve the problem when the boundary conditions are specified. Three different methods are generally used for the simulation of turbulent flows: direct numerical simulation (DNS), large eddy simulation (LES) and Reynolds-averaged Navier-Stokes (RANS) simulation.

DNS and LES use the governing equations directly without time averaging. DNS is the most accurate numerical method for simulating turbulent flows. However, DNS is computationally expensive as sufficiently refined mesh and time steps are required to capture all relevant scales of turbulence. LES uses spatial filters to remove the scales of turbulence that are smaller than the grid spacing, and then the effect of the large scales is directly computed. The effects of the smaller-scale eddies are modeled either empirically or by sub-grid scale turbulence modelling. Reynolds-averaged Navier-Stokes (RANS) method is based on the time averaging of the flow field where an instantaneous quantity is decomposed into its time-averaged and fluctuating quantities. For instance, $u_i = U_i + u_i'$ and $p = P + p'$ with U_i the mean velocity, P the mean pressure and u_i' and p' the fluctuating turbulent quantities, respectively. However, the averaging procedure introduces the so-called Reynolds stress terms (the last term in equation 2.8) which represent the influence of the turbulence on the mean flow field (Rodi 1980)

$$\frac{\partial U_i}{\partial t} + U_j \frac{\partial U_i}{\partial x_j} = g_i - \frac{1}{\rho}\frac{\partial P}{\partial x_i} + \frac{\partial}{\partial x_j}\left(\nu \frac{\partial U_i}{\partial x_j}\right) - \frac{\partial \overline{u_i' u_j'}}{\partial x_j} . \tag{2.8}$$

As the RANS equations are not a closed set of equations due to the presence of non-linear Reynolds stress terms, various closure models have been developed over the years. The best known of these models is perhaps the standard k-ε model, in which k is the turbulent kinetic energy and ε is the turbulent dissipation (e.g., Rüther et al. 2010). A standard model includes five closure coefficients and three closure functions (Rüther et al. 2010). An in-depth analysis of the computational algorithms, turbulence closures, as well as other assumptions and simplifications is beyond the scope of this study. For details on the turbulence modelling and simulation in hydraulics, reference is made to Wu (2007) and Rodi (2017).

River engineers are mainly interested in averaged flow characteristics. For this purpose, Reynolds Averaged Navier-Stokes (RANS) equations are commonly used in 3D models, which can be further subdivided into non-hydrostatic and hydrostatic models. Non-hydrostatic models use the momentum equations in three directions and the continuity equation, whereas hydrostatic models use a hydrostatic pressure relation for the vertical momentum equation, and thus vertical velocities are solved using only the continuity equation (Parsapour-Moghaddam & Rennie 2014, 2015, 2017).

Based on the RANS equations, various numerical models have been developed in the past three decades. Examples for 3D-programs are Delft3D (Deltares, the Netherlands), MIKE 3 (Danish Hydraulic Institute, Denmark), TELEMAC 3D (National Hydraulics and Environment Laboratory, France), FLOW 3D (Flow Science Inc., USA), CCHE3D (National Center for Computational Hydroscience and Engineering, University of Mississippi) and SSIIM (Norwegian University of Science and Technology).

2.3.2.2 2D models

Two-dimensional (2D) models deal with spatial variations of flow properties in the lateral and longitudinal directions (in the horizontal plane) or in vertical and longitudinal directions (in

the vertical plane). The term 2D model will always refer to two-dimensional models in the horizontal plane (i.e., depth-averaged 2D models) in the context of the present thesis.

Depth-averaged 2D models consider the fluid domain as a thin layer of fluid. Two assumptions are sufficient to describe a thin layer of fluid: the horizontal length scale is considerably larger than the vertical scale and the velocity field is homogeneous over the water depth. Under these conditions, the 3D RANS equations can be simplified to the 2D RANS equations, also called shallow water equations (equations 2.9 and 2.10). Different derivations of 2D shallow water equations can be found in the literature depending on the author's preference (Cea & Vázquez-Cendón 2007).

$$\frac{\partial h}{\partial t}+\frac{\partial h\overline{U}_i}{\partial x_i}=0 \tag{2.9}$$

$$\frac{\partial \overline{U}_i}{\partial t}+\frac{\partial h\overline{U}_i\overline{U}_j}{\partial x_j}=-gh\frac{\partial \zeta}{\partial x_i}-\frac{\tau_{b,i}}{\rho}+\frac{\partial}{\partial x_j}\left(\nu h\frac{\partial \overline{U}_i}{\partial x_j}\right)-\frac{\partial h\overline{u_i'u_j'}}{\partial x_j}+F_{\mathrm{sec},i} \tag{2.10}$$

where $\overline{U}_i$ are the depth-averaged velocity components, ζ is the water surface elevation, $\tau_{b,i}$ are the friction shear stress terms at the bed surface, $F_{sec,i}$ are the correction terms in order to account the effect of secondary flow on the depth-averaged momentum equations. A short-hand notation is used where i = 1, 2.

The depth-averaged horizontal Reynolds stresses $\overline{u'^2}$, $\overline{u'v'}$, $\overline{v'^2}$ appearing in the 2D shallow water equations need to be computed by a depth-averaged turbulence model (Cea & Vázquez-Cendón 2007). The depth-averaging of the 3D RANS equations introduces an additional dispersion term ($F_{sec,i}$) in the depth-averaged momentum equations. The effect of spiral flow, which represents the discrepancy between depth-averaged velocity and actual velocity, is expressed as the dispersion stress terms (Yu & Duan 2013). For that reason, several secondary flow correction models have been proposed in the literature to account for the 3D flow characteristics of secondary flow (Bernard 1993, Lien et al. 1999, Hsieh & Yang 2003, Wu & Wang 2004, Guan et al. 2016). Examples of depth-averaged 2D codes with secondary flow parameterization are Delft3D (Deltares, the Netherlands), MIKE 21C (Danish Hydraulic Institute, Denmark), TELEMAC 2D (National Hydraulics and Environment Laboratory, France), HSTAR (University of Exeter, UK), River2D (University of Alberta, Canada), mRIPA (Coventry University, England), and Nays2D (Hokkaido University, Japan). The present thesis is based on the application of the Delft3D code for which a detailed explanation of the 2D hydrodynamics with secondary flow parameterization is shown in Section 4.1.2.2.

2.3.2.3 1D models of meandering rivers

Ikeda et al. (1981) pioneered the theoretical study and numerical simulation of meander migration processes. They developed a linear meander migration model based on a shallow water (St. Venant) flow model coupled with the assumption that bank erosion rate is proportional to the near-bank "excess" flow velocity (U_B') which is defined as the difference between the near-bank and cross-sectional average velocity. In Ikeda et al.'s (1981) model, the proportionality constant between the bank erosion rate and U_B' is often termed as "erosion"

coefficient. Erosion coefficients are calibrated empirically based on field observations, historical maps, aerial photographs and remote sensing imagery. Hasegawa (1989) proposed a formula to compute the erosion coefficient derived from integration of sediment continuity equation.

Crosato (1989) extended the approach of Ikeda et al. (1981) and developed the meander migration model 'MIANDRAS'. By including the sediment balance equation, Crosato's (1989) model includes the longitudinal adaptation of bed topography. This model computes the longitudinal profiles of the near-bank excesses of flow velocity (U'_B) and water depth (H'_B), assuming perfectly point-symmetrical cross-stream profiles of water velocity and depth with respect to the channel centerline. The local bank erosion rate is assumed to be a function of both U'_B and H'_B. The general equation that is used to compute the rate of lateral shift of the channel centerline is:

$$\frac{\partial n_B}{\partial t} = E_u U'_B + E_h H'_B \tag{2.11}$$

where n_B denotes the transverse coordinate, which is equal to zero at the channel centreline, t is time, and E_u and E_h are migration coefficients.

Ever since the pioneering work of Ikeda et al. (1981), different 1D meander migration models (e.g., Crosato 1989, Johannesson & Parker 1989, Sun et al. 1996, Zolezzi & Seminara 2001, Larsen et al. 2006, Motta et al. 2012a) have been developed to simulate the planform evolution of meandering rivers at large spatial and temporal scales. In 1D meander migration models, the general characteristics of a river reach is represented by a single (reach-averaged) value, such as the reach-averaged channel width, the sediment median diameter, the bankfull discharge and the roughness coefficient. Larsen et al. (2006) showed that the variable flow algorithm can also be used in meander migration simulations.

2.4 Morphodynamic modelling of meandering rivers

Morphodynamic processes operate at different spatial (ranging from millimeter to kilometers) and temporal (ranging from minute to millennium) scales (see Figure 2.8). This thesis examines the morphological development of meandering rivers at the spatial scale of several meanders. That is also the typical scale of engineering works (10^{-1}-10^{1} km in length and year to decades in time).

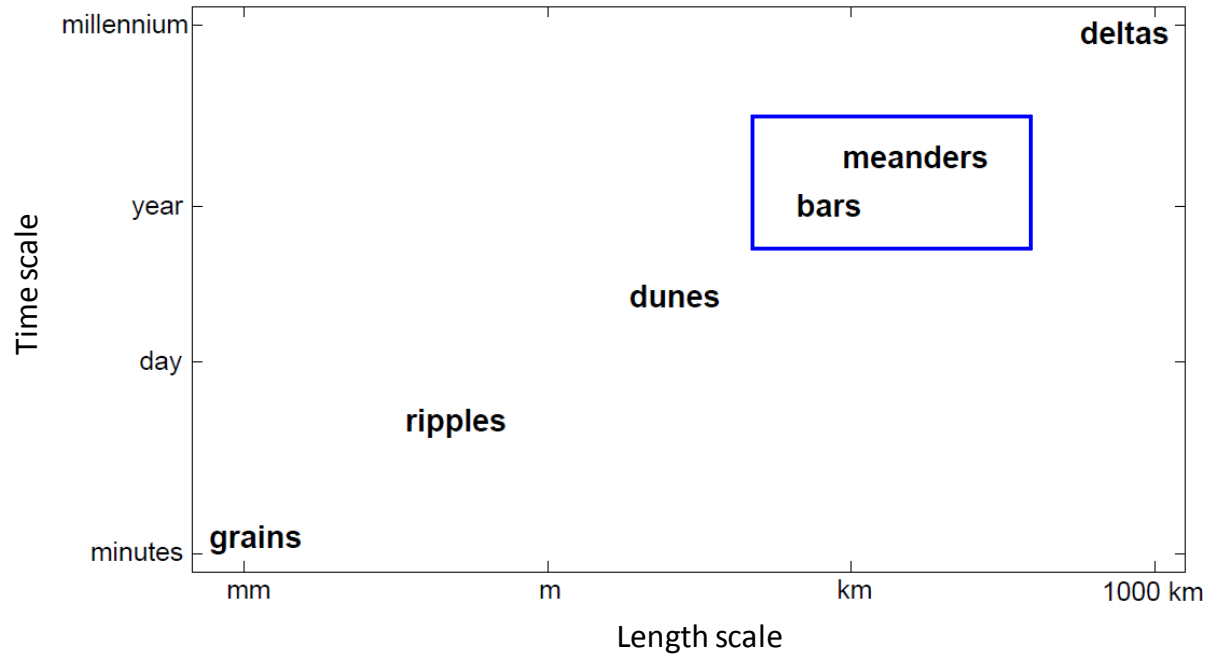

Fig. 2.8 *Typical spatial and temporal scales of morphological units in rivers (adapted from Schuurman 2015). This thesis focuses on the scale of bars and meander bends (indicated by the blue box). That is also the typical scale of engineering works.*

Engineers and scientists are frequently asked to make predictions of water-surface elevation, flow patterns, sediment transport and morphologic evolution in rivers. Because of this demand, a great deal of time and effort has been invested in developing sophisticated computational models that predict these quantities. One-dimensional (1D) linear modelling has expanded to become multi-dimensional (2D or 3D) morphological models.

As stated above, it is well known that meander bends migrate through bank erosion in the outer bends and deposition in the inner bends, under the influence of curvature induced secondary flow. Both the secondary flow and transverse bed slope in river bends deflect the sediment transport from the main flow direction. In a 3D model, the secondary flow is resolved on the vertical grid. The transverse bed slope predictor calculates the sediment transport deflection by the direct effect of gravity on particles moving on the transverse slope. It should be noted that the transverse bed slope effect is implemented in all process-based morphological models (e.g., Delft3D, Mike 3/21C, TELEMAC 3D/2D, CCHE 3D/2D, HSTAR, mRIPA, Nays2D) and even in 1D meander migration models (e.g., Ikeda et al. 1981, MIANDRAS). However, at the moment an exact parameterization of the transverse bed slope effect can only be achieved by calibration (Villaret et al. 2013, Kasvi et al. 2015, Schuurman et al. 2016). Model input further requires a range of parameterizations for bed roughness, and bed material composition (i.e., sediment heterogeneity and porosity). The bed level change is the result of sediment transport, transverse bed slope effects, bank erosion, and mass conservation in the bed.

There exist only few morphodynamic studies considering model calibration with secondary flow in meander bends (e.g., Parsapour-Moghaddam & Rennie 2014, Banda et al. 2016). In many verification studies of morphodynamic models there is a tendency to focus on the bed evolution only, without providing information on the reliability of secondary flow, mainly because secondary flow data are often lacking. It is usually pre-assumed that the model gener-

ates necessary secondary flow in meander bends to control sediment transport. This is probably true for the bed level changes in meandering rivers with fixed (non-erodible) wall, for which process understanding is better due to empirical functions obtained from laboratory experiments (Ikeda 1982, Struiksma et al. 1985, Talmon et al. 1995, Wiesemann et al. 2006). However, this may not be true in some situations, for example, meandering rivers with erodible floodplains where the morphology is determined by a complex mutual interaction among flow, sediment transport, and both bed and bank morphodynamics. In a 2D model, the effect of the spiral flow needs to be parameterized due to the nature of the modelling approach (see Section 2.4.2.2). Due to curvature induced secondary flow, surface water moves towards the outer bank while near-bed water moves towards the inner bank. The direction of near-bed velocity (and corresponding bed shear stress) deviates from the direction of primary flow. The deviation of the direction of bed shear stress from the primary flow direction is one of the more important effects of curvature on sediment transport. The angle between bed shear stress and depth-averaged shear stress (or flow) plays an important role in a bed topography model in river bends (Vasquez et al. 2006, Nabi et al. 2016). In depth-averaged 2D models the inclusion of the secondary flow effect and sediment transport model parameters (e.g. transverse bed slope, bed roughness, sediment grain size) have yielded variable results (see Table 2.3). Kasvi et al. (2015) argued that a depth-averaged 2D morphodynamic model can predict the feature of erosion and deposition reasonably well in a natural meandering bend without the inclusion of a secondary flow parameterization due to the major role of main flows. On the other hand, Guan et al. (2016), Nicholas (2013) and Mosselman (1998) reported the relevance of secondary flow parameterization in morphological simulations.

Tab. 2.3 Example applications of depth-averaged 2D model

Source	River	Model type	Time span	Key issues
Guan et al. (2016)	Greta River (England)	Depth-averaged 2D model	1 year	Secondary flow effect and grain size parameterization should be given a first priority among other parameters.
Kasvi et al. (2015)	Pulmanki River (Finland)	Delft3D, depth-averaged 2D model	1 flood event	Secondary flow effect parameterization can be neglected but spatially varying grain size parameterization is necessary to simulate the flow field and morphological changes on a meander point bar.
Nicholas (2013)	Hypothetical straight channel with an oscillating inlet	HSTAR, depth-averaged 2D model	240 years	Secondary flow effect parameterization leads to high sinuosity meanders. In the absence of this parameterization, bend evolution is dominated by translation.
Mosselman (1998)	Ohre River (Czechoslovakia)	Depth-averaged 2D model	10 years	It is not possible to accurately capture river channel migration in a model that allows bank erosion alone. Adequate description of the depth-averaged flow field and grain size is necessary.

Regarding morphological predictions over a long period of time (for example, years to decades), the computational effort and the simulation time are relevant factors. One of the challenges in long-term, process-based morphological modelling is the integration of hydrodynamic and morphodynamic timescales, as the bed morphology evolves much more slowly than the hydrodynamic variables (Nicholas et al. 2013). Since river discharge is rarely constant and it generally varies rapidly, several studies have focused on the flood events greater than a threshold to save computational time (e.g., Ziliani et al. 2013, Guan et al. 2016). Lesser et al. (2004) and Roelvink (2006) have recommended the morphological acceleration technique to bridge the gap between hydrodynamic and morphological timescales. This technique consists of multiplying the calculated depth changes over a hydrodynamic time step (Δt_{hydro}) by a constant factor ($MORFAC$), effectively predicting morphological changes over a time-period of:

$$\Delta t_{mor} = \Delta t_{hydro} \times MORFAC \tag{2.12}$$

Thus the $MORFAC$ is an erosion and sedimentation acceleration factor. Through the use of this method, hydrodynamic timescales are adapted to much longer timescales of morphological evolution. As an illustration, 1 year hydrodynamic simulation with a $MORFAC$ = 10 represents 10 years of morphodynamic evolution. The morphological acceleration technique, which is implemented in all process-based morphological models (e.g., Delft3D, Mike 3/21C, HSTAR, Nays2D), has been validated in numerous coastal and estuarine applications (Dissanayake 2011, Deltares 2014), in which the boundary conditions are dominated by tidal cycles. In river applications, however, there is no such periodicity as a tidal cycle. Recently, Williams et al. (2016) simulated a gravel-bed braided river (the Waimakariri River in New Zeland) using a depth-averaged 2D model (Delft3D) and suggested that, in case of cyclic flow (i.e., repeated annual hydrograph), flow inputs can easily be reduced by reducing the number of cycles. Kikillus et al. (2016) simulated the Iller River (Germany) using a 2D numerical model and found that the order of the occurence of the flood events has a relevant influence on the results of the morphological bed change predictions.

In numerical models, both constant discharge and variable discharge have been applied with variable results (see Table 2.4). Most numerical studies on river meandering can be grouped according to their focus on boundary conditions. A group of studies addressed the significance of high and low flows on the hydrodynamics, but without placing them in a wider context of morphology (Sukhodolov et al. 2015, Legleiter et al. 2011, Rinaldi et al. 2008). The second group of studies focused on small spatial scales such as laboratory settings (Asahi et al. 2013, Duan & Julien 2010, 2005, Rüther & Olsen 2007, Olsen 2003). In a laboratory channel, the planform evolution attains a state of dynamic equilibrium just after a short period of time, for example, 32 hours in Friedkin's (1945) experiments. When calibrating numerical models to the 32-hour planform, those calibration parameter values cannot be used to predict future planforms (Posner & Duan 2012), which in turn, limits their applicability at the field scale. The third group of studies focused on hypothetical rivers with either uniform rectangular or trapezoidal cross-sections. An important reason is that bathymetric data to define initial and boundary conditions for the model were lacking. Models were initialized using a straight channel with a constant bed slope and a small perturbation at the inlet in order to study the physical mechanisms by which a straight channel evolves into a freely meandering planform.

Schuurman et al. (2016) and van de Lageweg et al. (2016) found that constant discharge is sufficient to attain sinuous planform, whereas Nicholas et al. (2013) and Crosato & Saleh (2010) showed that planform using a steady discharge is different from the planform obtained with a variable discharge. The fourth group of studies dealt with real-world meandering rivers and has reached different conclusions regarding the role of discharge on the planform changes. Banda & Egashira (2016), Motta et al. (2012b), van de Wiel & Darby (2004) applied the bankfull (or channel-forming) flow, which made it impossible to correlate meander migration to discharge. In contrast, Schwendel et al. (2015), van Dijk et al. (2014), Gautier et al. (2007), and Larsen et al. (2006) used variable flow and found that the meander migration rate is a function of variable flow rates. Further investigations are necessary to understand whether bankfull (or channel-forming) discharge or variable discharge is significant for simulating meander planform and bed topography adjustment.

Tab. 2.4 Applications of numerical models in meandering channels

Source	Simulated channel	Model type	Time span	Results of the investigations
Hydraulics - Reach scale				
Sukhodolov et al. (2015)	Spree River (Germany)	3D hydrodynamic model	-	Flow velocities vary spatially between pools and riffles in a bend over a range of discharge conditions.
Legleiter et al. (2011)	Merced River (USA)	Depth-averaged 2D model	-	Point bar growth drives the evolution of both the magnitude and spatial pattern of flow complexity.
Rinaldi et al. (2008)	Cecina River (Italy)	Delft3D, depth-averaged 2D model	-	Bank erosion processes are very sensitive to the sequence of high and low flows.
Morphodynamics - Laboratory channels				
Asahi et al. (2013)	Straight channel with a sine-generated bend set at the inlet	Nays2D, depth-averaged 2D model	8 minutes	Discharge variation, even in the form of a simple hydrograph corresponding to two cycled discharges, promotes the development of high-amplitude meander planform than constant discharge.
Duan & Julien (2010)	Sine-generated meandering channel of da Silva (1995)	Depth-averaged 2D model	32 hours	A meandering channel can evolve from a mildly curved channel to a highly sinuous channel under constant discharge conditions.
Rüther & Olsen (2007), Olsen (2003)	Laboratory channel of Friedkin (1945)	SSIIM, 3D model	3 days	Formation of meandering thalweg can occur from an initially straight channel under steady flow conditions.

Duan & Julien (2005)	Laboratory channel of Friedkin (1945)	Depth-averaged 2D model	3 hours	A 2D model can simulate the initiation of channel meandering, gradual increase of meander wavelength and amplitude under constant discharge.
Morphodynamics - Hypothetical rivers				
Schuurman et al. (2016)	Straight channel with a transversely moving inlet	Nays2D, Delft3D, depth-averaged 2D model	50 years	A highly sinuous channel can be developed from a straight channel under constant discharge.
Lageweg et al. (2016)	Straight channel with a transversely moving inlet	Nays2D, depth-averaged 2D model	28 days	The width of the meander belt along with a highly sinuous channel can be formed during constant bankfull discharge.
Nicholas et al. (2013)	Paraná (Argentina), Japurá (Brazil) Jamuna (Bangladesh), Orinoco (Venezuela)	HSTAR, depth-averaged 2D model	530 years	Variable discharge favors bar emergence to the height of the largest floods, whereas steady flow does not allow bars to emerge above the corresponding water level.
Crosato & Saleh (2010)	Allier River (France)	Delft3D, depth-averaged 2D model	10 years	The river planform using a constant discharge below bankfull is different from the planform obtained with a variable discharge that includes overbank flow.
Morphodynamics - Natural meandering rivers				
Banda & Egashira (2016)	Madhumati River (Bangladesh)	1D meander migration model	5 years	Meander bend migration can be simulated with bankfull discharge if the spatially constant bankfull width is specified reasonably in the model.
Schwendel et al. (2015) & Gautier et al. (2007)	Rio Beni River (Bolivia)	1D meander migration model	50 and 25 years, respectively	Mean annual bend migration rates are correlated with a number of discharge metrics such as accumulated discharge during wet seasons, maximum annual discharge and the number of days with discharge in excess of bankfull.
van Dijk et al. (2014)	Allier River (France)	Delft3D, depth-averaged 2D model	10 years	Bankfull discharge is sufficient to initiate channel migration, but floods promote high lateral migration rate and increased bend amplitude.
Motta et al. (2012b)	Mackinaw River (USA)	1D meander migration model	40 years	Constant discharge is able to simulate migration of meander bends in the lateral and downstream directions.

Larsen et al. (2006)	Sacramento River (USA)	1D meander migration model	19 years	Meander migration in yearly time steps is a function of annual flow rates, whereas a constant flow rate does not reveal differences in migration patterns.
van de Wiel & Darby (2004)	Goodwin Creek (USA)	mRIPA, depth-averaged 2D model	5.5 years	Steady discharge can reproduce channel bed morphology and planform adjustment to some extent in a meandering stream with erodible cohesive banks.

2.5 Synthesis

In meandering rivers, morphological development (i.e., changes in channel morphology and planform) is a consequence of complex interactions among flow, sediment transport, and both bed and bank morphodynamics. The most commonly used parameters to describe the meander planform are meander belt width (M_B), meander wavelength (λ), radius of curvature (R) and channel bankfull width (B) (see Figure 2.6). Several empirical relationships were derived based on field observations in different meandering rivers to define the geometry of meander planform (see Table 2.1), however, predicting the future planform remains a challenging task, and the validity of these equations should be tested before applying them for the simulation of a particular river. The difficulties arise from the fact that meander evolution occurs over longer time and space scales that render traditional field-based measurements impractical or impossible.

A potential alternative to field-based observation is numerical modelling. One-dimensional (1D) approaches are able to capture the shifting of the channel centerline (Larsen et al. 2006, Schwendel et al. 2015, Banda & Egashira 2016), however it is not possible to simulate bed topography changes across the width due to lack of information with regard to the transverse flow field. Multi-dimensional (2D or 3D) models can be useful to overcome this limitation. The proper reproduction of the meanders behavior requires 3D models (Olsen 2003). Nevertheless, depth-averaged 2D models are often adopted in practice because the computational time is at least an order of magnitude shorter than for a fully 3D model (Guan et al. 2015, 2016). In the literature, the simulated pattern of channel migration showed many similarities with field observations, although they were not directly compared with field data (Duran et al. 2009, van Dijk et al. 2014). An important reason is that field datasets for model validation covering typical morphological time-scales of years to decades are scarce. The present thesis addresses this gap by modelling the co-evolution of bed topography and meander planform geometry, and comparing the model results with field observations.

Morphodynamic models are based on various assumptions and simplifications, and therefore, have uncertainty in their parameterizations. The sediment transport predictor is an important parameter when calculating bed elevation changes. Bed roughness parameterization determines the water level, flow velocity and the bed shear stress for sediment transport. Grain-size parameterization has a direct impact on a number of factors, such as settling velocity of a sediment particle in motion, incipient motion of sediment particles, dimensionless bed shear stress, and sediment transport capacity. Furthermore, the bed load transport direction is influenced by the secondary flow and the transverse bed slope. In a depth-

averaged 2D model, the effect of spiral flow is parameterized. Apart from this, sediment-related parameterizations (such as the spiral flow and transverse bed slope effects on bed load transport direction, bed roughness, and sediment grain size) should be treated properly in the model and the model should have the capacity of simulating the morphological changes. Recent studies (e.g., Villaret et al. 2013, Kasvi et al. 2015, Guan et al. 2016) reported that the change in each factor can lead to a modification of erosion and deposition on the river bed. However the understanding of the influence of these factors on the long-term morphological development is limited by the lack of field data, and the degree to which an input parameter affects the model predictions needs to be addressed.

To predict morphological evolution over longer time-scales, the morphological scale factor ($MORFAC$) is implemented in all process-based morphological models. Although $MORFAC$ can keep the computations within practical time limits, it introduces additional source of uncertainty (Roelvink 2006). The $MORFAC$ approach works well for boundary conditions with regular periodicity (e.g., tidal cycles) (Dissanayake 2011). However, river discharge generally varies rapidly and does not exhibit regular periodicity. To date, only a few published studies have focused on the implementation of $MORFAC$ under the river discharge hydrograph. Kleinhans et al. (2008), Nicholas et al. (2013) and Schuurman et al. (2015) pointed out that flow inputs can be reduced by compressing the discharge hydrograph using $MORFAC$. Williams et al. (2016) suggested to reduce the cycles of annual hydrograph, although this needs to be supported by further research as the order of the occurence of the flood events can influence the bed change predictions (Kikillus et al. 2016).

Meander wavelength (λ), which is the most widely used geometric property of meanders, is controlled by discharge. The well-known empirical relations between λ and "dominant" discharge (see Table 2.2) are based on data from different reaches in the same river or different streams. It is believed that the only complete model of a river is the river itself as it takes into account site-specifc hydro-morphological and sediment characteristics (Lagasse et al. 2004). To date, it has not been reported how river discharge affects λ in a specific meandering reach. It is also important to understand whether or not λ undergoes cyclic elongation or shortening due to natural variability in river discharges.

Dominant discharge is the most important parameter for river restoration or engineering design. Dominant discharge is a concept, and consequently, it has been given several names by different researchers, including bankfull, channel forming (or specified recurrence interval), and effective discharge. Such interchangeable names raise the question as to what is the meaning of the term "dominant discharge". Recent numerical studies for natural rivers with fixed (non-erodible) wall suggest that the channel forming discharge, which controls the river bed morphology, lies between mean annual discharge and bankfull discharge (Frascati & Lanzoni 2013, Bolla Pittaluga et al. 2014, Lanzoni et al. 2014). However, such findings remain untested in the case of freely meandering rivers. It should be noted that none of the above mentioned methods addresses links between hydrologic functioning and river planform adjustment (e.g. meander migration). Planform responses to discharge variation have been studied by means of flume experiments (e.g., Friedkin 1945, Visconti et al. 2010), numerical modelling (e.g., Larsen et al. 2006, Crosato & Saleh 2010, Asahi et al. 2013), and field observations (e.g., Inglis 1949, Leopold & Wolman 1957, Dury 1964, Schumm 1977). As

the dominant discharge indicates maximum morphological activities for a channel, the linkage between planform parameters (such as meander wavelength) and discharge needs to be put forward in estimating dominant discharge.

The alteration of natural flow regimes may occur due to climate change or management strategies, such as augmentation of dry season flows. Restoring the discharge will not lead to the restoration of the old river course, but the river will change path again. This means that restoring the discharge should be done with knowledge on how the river alignment will change. Understanding how the river will respond to climate change or river restoration can have implications such as being able to predict or prevent a meander cut-off. A comprehensive literature review on the morphodynamic simulation of channel response to future climate change is given by Lotsari et al. (2015). They pointed out that, to predict future channel changes over multiple decades or centuries, one-dimensional models have been used so far as they are computationally efficient. The process-based 2D numerical model can be a promising tool to assess the impact of hydrologic scenarios on the future river morphology.

2.6 Aim of the study

The aim of this research is to investigate the effects of changing discharge regimes on the morphological development of meandering rivers. A promising tool to explore the morphological development of natural meandering rivers is the use of numerical models. The main objective of the present thesis is to explore the capacity of a process-based numerical model to simulate the adaption of both planform dynamics and bed topography to changed discharge regimes.

Based on the preceding literature review and in order to achieve the main objective, six specific research questions are formulated.

1. Which morphological features of meandering rivers can be simulated using a process-based numerical model?

Planform responses to discharge variation have been studied by means of 2D numerical modelling (e.g., Crosato & Saleh 2010, Asahi et al. 2013). The present study employs a process-based 2D numerical model (Delft3D) as a tool to reproduce bed topography and planform adjustment, and compare the model predictions with field observations.

2. How does the input of sediment-related parameters affect the modeled morphodynamics?

Uncertainties in model predictions arise from sediment-related parameterizations such as the spiral flow and transverse bed slope effects on bed load transport direction, bed roughness, and sediment grain size (Guan et al. 2016). The question is which processes are relevant and which processes are of second order in describing morphodynamic evolution. Such analysis is important to guide future model applications.

3. How can the morphological scale factor ($MORFAC$) approach be used under an imposed cyclic hydrograph?

Lesser et al. (2004) and Roelvink (2006) have recommended morphological acceleration techniques (i.e., $MORFAC$) for long-term morphodynamics. Several studies (e.g., Nicholas et al. 2013, Williams et al. 2016) have shown efficacy of $MORFAC$ for river applications; however, the applicability of the $MORFAC$ approach under an imposed cyclic hydrograph has not been fully investigated to date.

4. How does river discharge influence the meander wavelength in a meandering reach?

The well-known empirical relations between meander wavelength and “dominant” discharge (e.g., Leopold & Wolman 1957, Dury 1964) are based on data from different reaches in the same river or different streams. It is important to have an understanding on how river discharge affects meander wavelength in a specific meandering reach.

5. How to estimate the dominant discharge in a freely meandering river?

Frascati & Lanzoni (2013), Lanzoni et al. (2014) and Bolla Pittaluga et al. (2014) described the application of numerical models to predict dominant (or channel-forming) discharge for a natural river with fixed (non-erodible) walls. However, to date, the results of these approaches have not been compared with model predictions for a meandering river with erodible floodplains.

6. Can a process-based numerical model be used to assess the impact of hydrologic scenarios on the future river planform?

The alteration of natural flow regimes may occur due to climate change or human modification (e.g., river restoration), which can cause shifting of the river in other locations. To manage such situations it is necessary to predict the effects of different hydrologic scenarios on the future river morphodynamics.

3 Case study: the Dhaleshwari River

The focus of the present thesis is on the Dhaleshwari River in Bangladesh, which is a typical example of a single-thread sand-bed meandering river as it is free to migrate in the alluvial floodplain. A decrease in streamflow over time has been documented in previous studies and in response to the declining flow volume, the river has adjusted its bed morphology and planform characteristics (CEGIS 2003, 2013). A specific reach is taken as a case study in order to investigate the effects of changing discharge regimes on morphological changes endangering the stability of structures located in the area. However, lack of adequate field data is often considered a limitation when undertaking morphological studies. This can be counteracted by using numerical simulations of the morphological processes, and a numerical model has been applied in this thesis. Before the model is described, this chapter describes the Dhaleshwari River system (see Figure 3.1), analyses of hydrological data, the study area, available morphological data and a summary of previous researches in the study area. A general perspective of the possible evolutionary scenario of the Dhaleshwari River in the study area concludes this chapter.

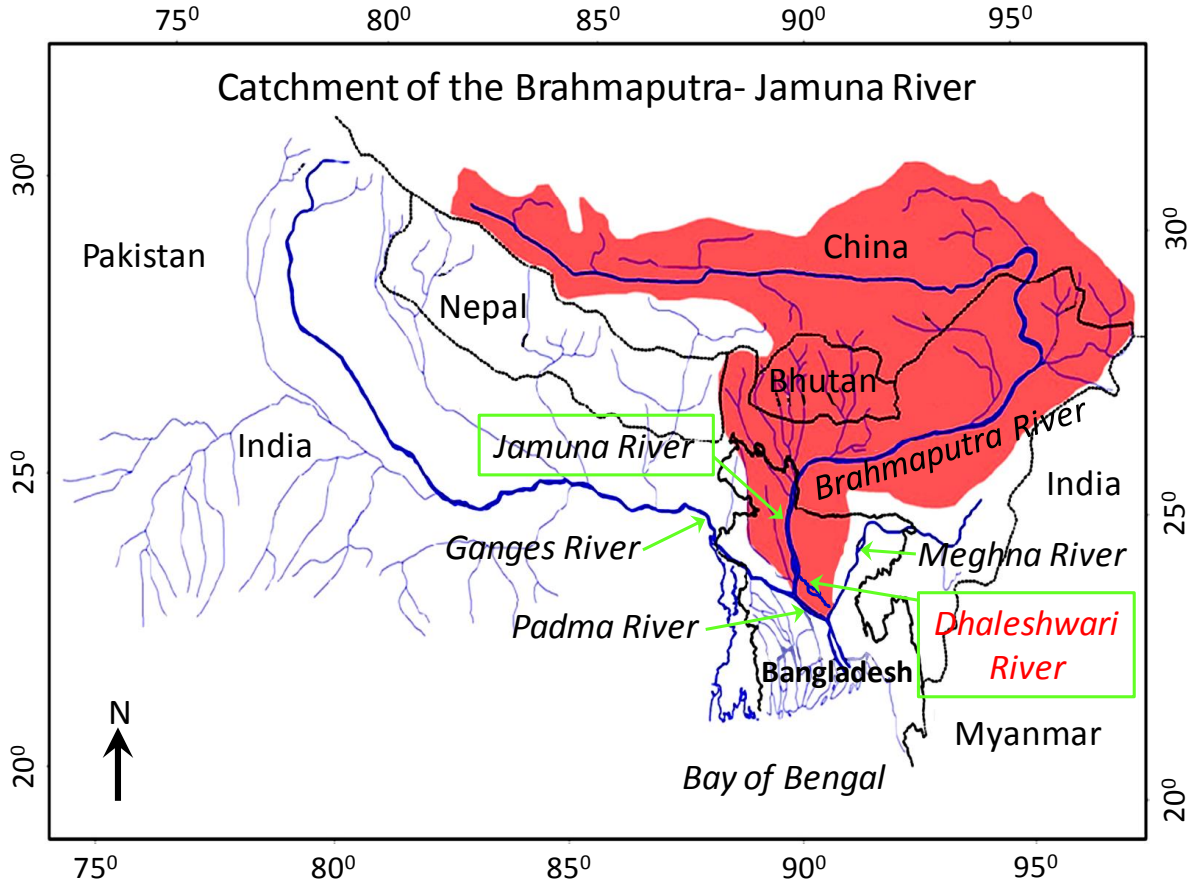

Fig. 3.1 Catchment area of the Brahmaputra - Jamuna River (modified after Sarker et al. 2011).

3.1 The Dhaleshwari River system

The Dhaleshwari River is one of the main distributaries of the Jamuna River in Bangladesh. The Jamuna River (also known as the Brahmaputra- Jamuna River) is 2900 km long and drains water from the northern and eastern slopes of the Himalayas (see Figure 3.1). The total catchment area of the Jamuna River is about 573,500 km^2, of which 46,644 km^2 are located in Bangladesh, with the remainder in China and India (Rahman et al. 2012). The length of the Jamuna River inside Bangladesh is 240 km. The Jamuna River is a large sand-bed braided river of 5 - 17 km width (Jagers 2003).

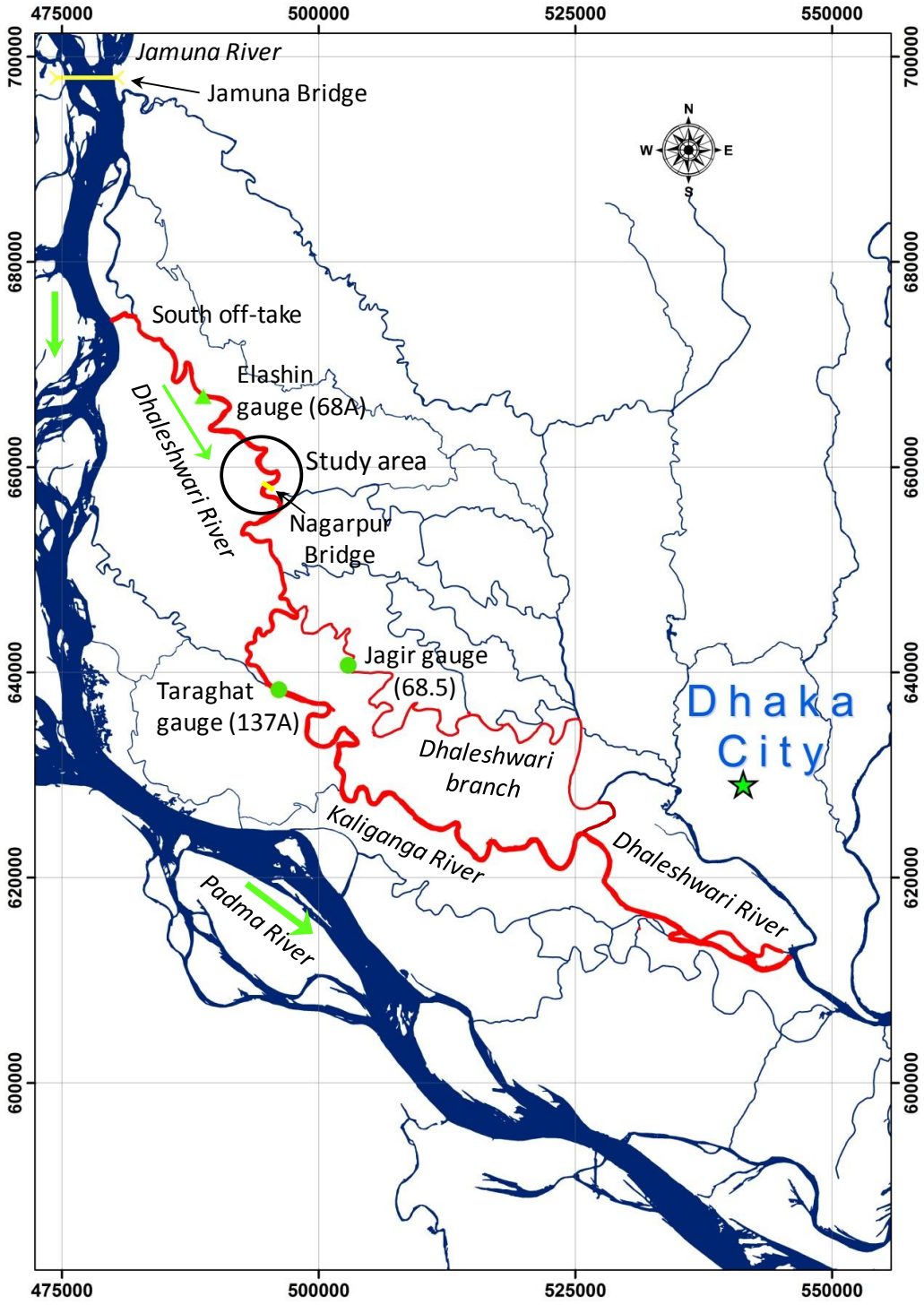

Fig. 3.2 The Dhaleshwari River system

The Dhaleshwari River is about 162 km long and has a (local) drainage basin of 7,253 km^2 (BWDB 2011). In the middle reach, the river bifurcates into two courses: the Kaliganga River and the Dhaleshwari branch. As the Dhaleshwari branch is merely a flood spill channel, the main flow of the Dhaleshwari River runs into the Kaliganga River (CEGIS 2003, 2013, NHC 2016). The Kaliganga River again joins with the Dhaleshwari branch further downstream. These two rivers continue as the Dhaleswhari River until merging with the Meghna River, which finally flows into the Bay of Bengal.

3.2 Hydrological data

3.2.1 General description of the catchment hydrology

Flow through the Dhaleshwari River mainly depends on the flow of the Jamuna River. The discharge in the Jamuna River results from snow melt in the Himalayas, but rainfall in the state of Assam (India) and the north-eastern part of Bangladesh also contributes significantly. Most of the rainfall takes place during the monsoon season and the rest of the year remains dry. The tropical monsoon climate constitutes four hydrological seasons: pre-monsoon (April - May), monsoon (June - September), post-monsoon (October - December), and dry season (January - March). Due to the seasonality of flows, discharge in the Jamuna River varies from a minimum of 3,000 $m^3 s^{-1}$ to a maximum of 100,000 $m^3 s^{-1}$, with a bankfull discharge of approximately 48,000 $m^3 s^{-1}$ (Rahman et al. 2012).

Morphology around the off-take in the Jamuna River plays a major role in diverting flow through the Dhaleshwari River. Before mid 1995, there were two off-takes of the Dhaleshwari River: north off-take and south off-take. The braiding nature of the Jamuna River has led to a regular shifting of the off-takes. Figure 3.3(a) and Figure 3.3(b) show the locations of the off-takes in 1973 and 1989, respectively. The north off-take was just downstream of the Jamuna Bridge and was closed in 1995 during the construction of the Jamuna Bridge (see Figure 3.2). Presently the river is mainly fed by the south off-take. Further downstream of the south off-take, a new off-take has been developing, as shown in Figure 3.3(c) (CEGIS 2013).

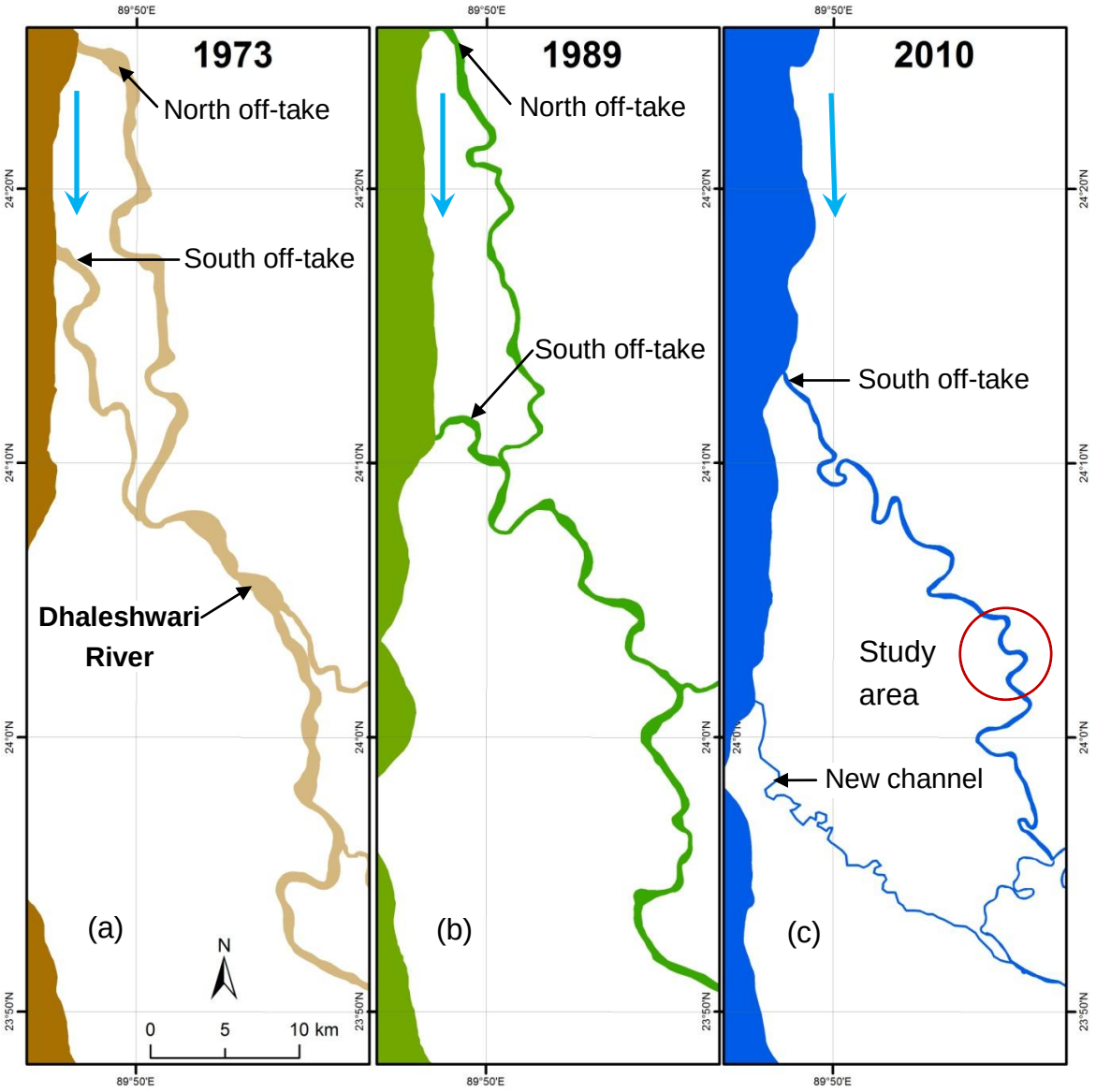

Fig. 3.3 *Off-takes of the Dhaleshwari River at three different times (a) 1973, (b) 1989 and (c) 2010 (adapted from CEGIS 2013).*

Hydrological data are recorded at the Bangladesh Water Development Board (BWDB) gauging stations. Locations of the gauging stations are shown in Figure 3.2. Elashin gauging station (68A) records water level only. Discharge measurements are recorded via gauging station Taraghat (137A) on the Kaliganga River and gauging station Jagir (68.5) on the Dhaleshwari branch. The Center for Environmental and Geographic Information Services (CEGIS) studied the combined flow at Taraghat and Jagir gauging stations and found that a gradual decline in the percentage of flow volume to the Dhaleshwari River from the Jamuna River has taken place from 1967 to 2008 (CEGIS 2013). This is due to the formation of a large sand bar at the intake (south off-take) that deteriorated the flood discharging capacity into the Dhaleshwari River. Presently, the discharge of the Dhaleshwari River is only about 1% of the discharge of the Jamuna River (NHC 2016). In contrast to rivers with a natural hydrologic regime with large discharges and relatively short durations of high-water events, floods in this river can last periods from 4 to 6 months because of continuous water inflow from the Jamuna River. The characteristic discharge hydrograph begins with a low

discharge, monotonically increasing to a peak discharge and fluctuating around the peak discharge during the whole monsoon season, and then monotonically decreasing to a low “end” discharge.

3.2.2 Discharge time series data

For simplicity, the discharge of the Dhaleshwari River in the study area (described in the next section) can safely be assumed equal to that of the Kaliganga River as the Dhaleshwari branch is merely a flood spill channel. Discharge measurements via Taraghat gauging station (137A) on the Kaliganga River are available from the Bangladesh Water Development Board (BWDB) for the period from 1979 to 2016, with the monitoring frequency mostly bi-weekly but varying from weekly to monthly at various times. The data appear to be of generally good quality, but there are a few gaps or periods of missing data (NHC 2016). Incomplete datasets pose a challenge for river morphological studies as the hydrological data constitute the boundary conditions. Simply replacing missing data with a statistical technique (such as the mean of all other observations) has statistical shortcomings (Gao 2017), as hydrological data consist generally of time-series data in which statistical patterns such as autocorrelation or seasonality emerge over time. A complete continuous time-series of daily discharges deemed necessary prior to the practical use of hydrological time series.

3.2.3 Generation of continuous time-series of daily discharge

Available data on river discharge were not continuous. In order to estimate daily discharges, a statistical moment-based Matlab script (Hydro Fit Curve, developed by S. Niewerth in the Leichtweiß-Institute for Hydraulic Engineering and Water Resources) was applied to 37 years of streamflow data. The script is based on a statistical mean standard curve, which is the average of each yearly standard curve which in turn is calculated by normalizing the observed data with the observed maximum discharge of that year. The observed data are then replaced by the product of the mean standard curve and the maximum discharges. In case of missing data, the maximum discharges are predicted through fitting a cubic spline function over all available maximum discharges. The record of synthetic daily flows is shown in Figure 3.4 and is compared with the observed data.

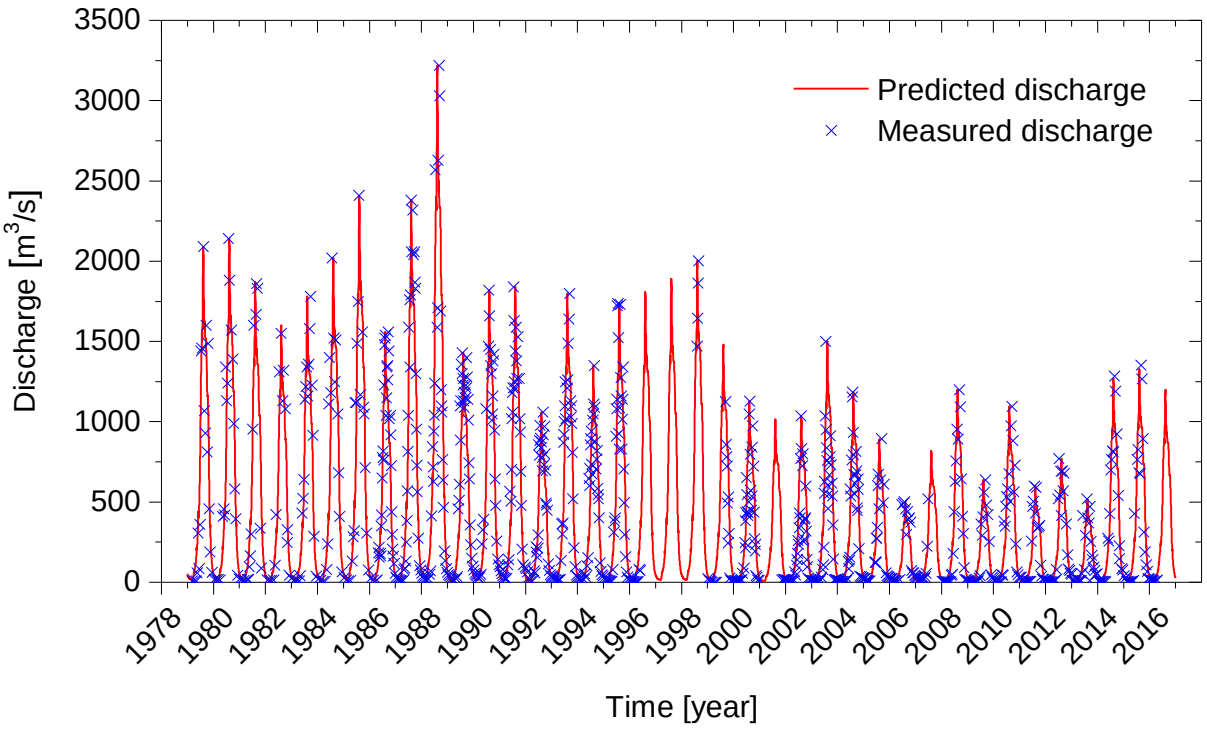

Fig. 3.4 Continuous time-series of daily discharge in the period 1979 - 2016.

The goodness of the results presented in Figure 3.4 can be evaluated by mathematical parameters. The Nash-Sutcliffe efficiency index (Nash & Sutcliffe 1970) was applied to the simulated results for evaluating the ability of reproducing the time evolution of stream flows. The equation reads:

$$E_{NS} = 1 - \frac{\sum (o_i - p_i)^2}{\sum (o_i - \bar{o})^2} \tag{3.1}$$

where o_i is the i th value of observed values, $\bar{o}$ is the mean value of all observations, and p_i is the i th value of predicted values.

The Nash-Sutcliffe efficiency index (E_{NS}) can range from $-\infty$ to 1. Unlike with a statistical model (for instance, coefficient of determination), the sum of squares of the prediction error $\sum (o_i - p_i)^2$, may be greater than $\sum (o_i - \bar{o})^2$, and the coefficient can therefore be negative. An efficiency of 1 corresponds to a perfect match of predicted and observed discharge. For the present case, the Nash-Sutcliffe efficiency index (E_{NS}) was 0.85, which is reasonable as it is close to 1.

3.2.4 Inter-annual variability in river discharge

Figure 3.5 shows yearly maximum, mean and minimum discharges that were computed based on the continuous time-series of daily discharges for the period 1979 – 2016. In addition, Table 3.1 shows characteristic discharge values of the river at Taraghat gauging station (137A).

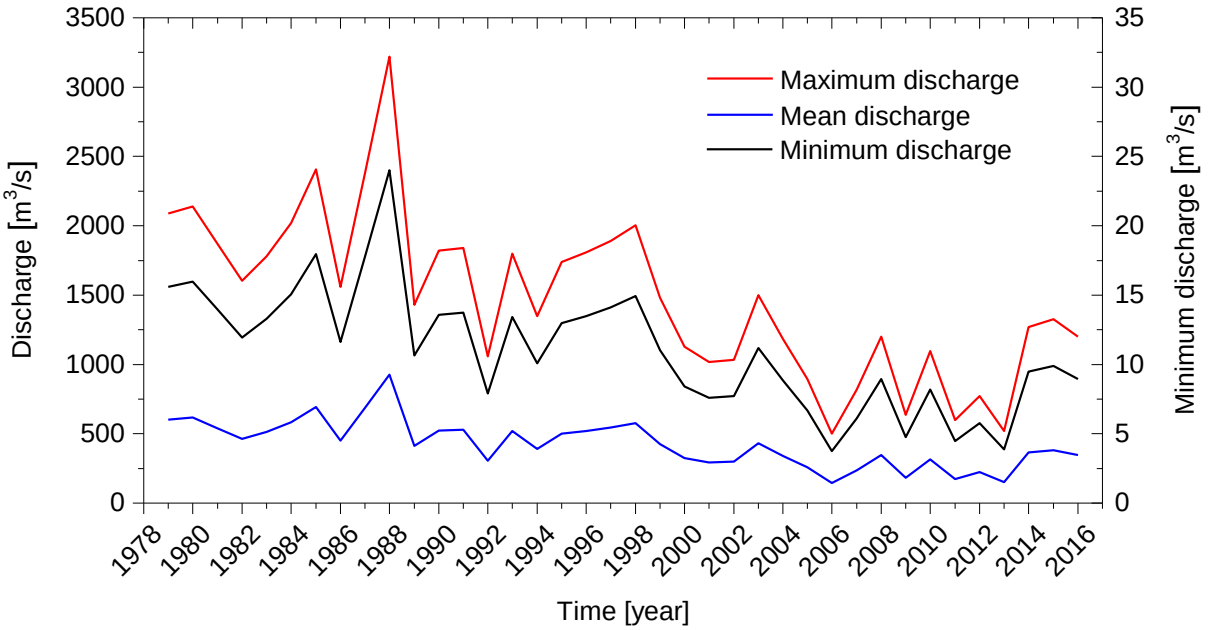

Fig. 3.5 *Yearly maximum, minimum and mean discharges at Taraghat gauging station (137A) in the period 1979 - 2016.*

Tab. 3.1 *Characteristic discharge values of the Dhaleshwari River at Taraghat gauging station*

	Discharge (m^3 s^{-1})
Maximum	3,218
Mean	424
Minimum	5
Mean annual peak flow	1,473
Bankfull discharge	700
Effective discharge (1979 – 1995)	1,005
Effective discharge (1996 – 2016)	628

The bankfull discharge, characterized by a stage corresponding to the elevation of the flood plains at the downstream end of the study area (described in the next section), was found to be about 700 m^3 s^{-1} (described in Section 4.3.2.3), and has a statistical return interval of 1.06 years. Figure 3.5 indicates that the annual peak flow discharge has rarely exceeded the mean annual peak discharge (1,473 m^3 s^{-1}) after the closing of the north off-take in 1995. Since then, the river has experienced several flood-free years (i.e., annual peak discharge less than bankfull). Similarly, the annual low flows have been falling from a typical value of about 12 m^3 s^{-1} in the early 1990s to about 5 m^3 s^{-1} at the present time. The reduced discharge during the low flow season indicates that the south off-take may even be fully closed by sediment deposits. A general decrease in streamflow has also been documented in similar studies (Crosato 2008, CEGIS 2003, 2013, NHC 2016). Following the methodology of Goodwin (2004), the characteristic effective discharge, also termed as channel-forming discharge by Wolman & Miller (1960), was computed for two distinct periods. The effective dis-

charge for the period 1979 – 1995 is 1005 m^3 s^{-1}, whereas for the period 1996 – 2016 is 628 m^3 s^{-1}.

3.2.5 Trends in discharge time-series

An important task in hydrological modelling is to determine if significant trends exist in time series which can be achieved by a number of statistical tests. One of the commonly used tests is the Mann-Kendall trend test (Kendall 1938, Mann 1945). It is a non-parametric test, and therefore, the data need not conform to any particular distribution (for instance, normal distribution). Furthermore, it does not depend upon the magnitude of data, missing data or irregularly spaced monitoring periods. In the classical Mann-Kendall trend test (Kendall 1938, Mann 1945), each value is compared to all subsequent time period values, which gives a total of $n(n-1)/2$ pairs of data, where n is the number of observations. If the subsequent value is greater than the former, a "$+1$" score is assigned. If it is lower than the former value, then a "-1" score is assigned. All scores are finally summed up to calculate the test statistic. A positive test statistic means that the trend is increasing, and a negative test statistic means that the trend is decreasing. It should be noted that the Mann-Kendall test (Kendall 1938, Mann 1945) does not provide an estimate of the magnitude of the trend. For this purpose, Sen's slope estimator (Sen 1968) has been widely used (Kahyaa & Kalayci 2004). It computes the slope as the median of all slopes between paired values.

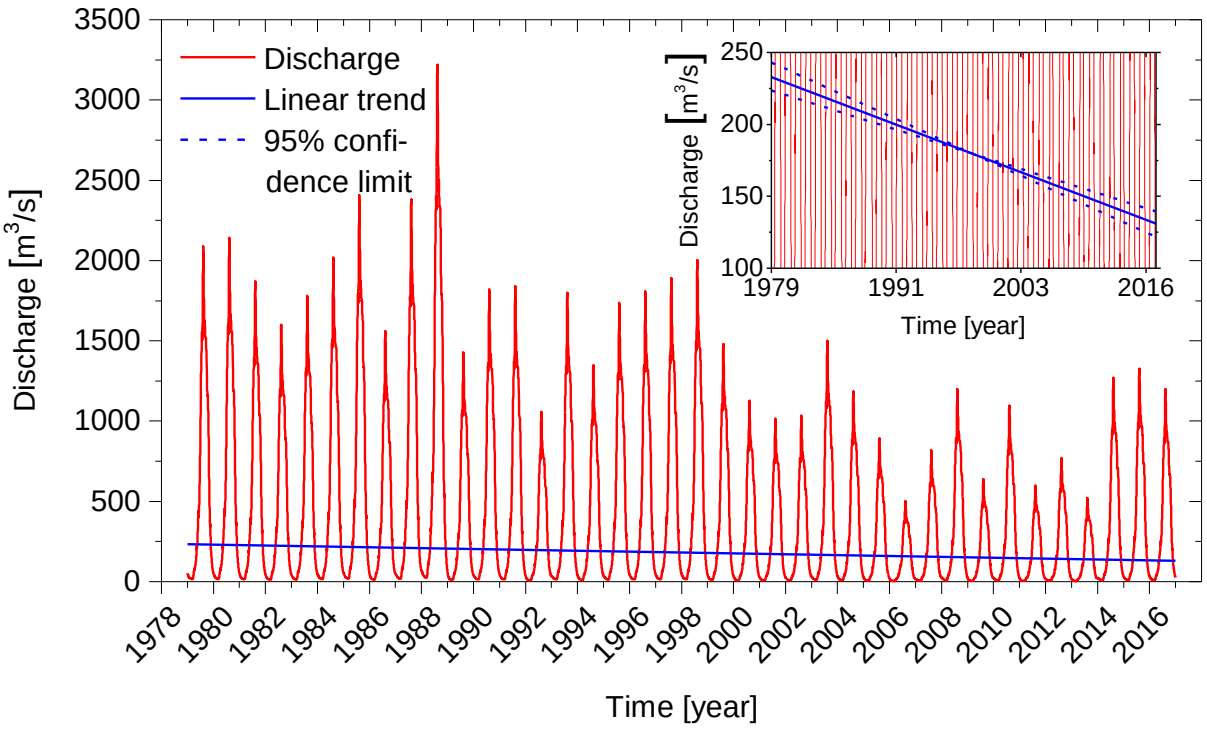

Fig. 3.6 The Sen estimate of linear trend associated with the Mann-Kendall trend test.

The Mann-Kendall trend test and Sen's slope estimator were applied to the continuous time-series of daily discharges for the period 1979 – 2016 using a Matlab script (Fatichi 2011). Trends were considered statistically significant at the 0.05 level when identified by the two statistical methods. The Sen estimate of linear trend associated with the Mann-Kendall trend test is shown in Figure 3.6. The Sen estimate of linear trend is shown as a solid line and dashed lines are the 95% confidence limits. The solid line indicates that the daily dis-

charge series are characterized by a negative (downward) trend, suggesting a possible future water resources scarcity.

3.3 Study area

3.3.1 Location of the study area

The study area is located in the upper reach of the Dhaleshwari River between Latitude 24°20' - 25°10'N and Longitude 89°30' - 89°50'E. The starting point of the study area is about 10 km downstream of Elashin gauging station (68A) and the end point is about 40 km upstream of Taraghat gauging station (137A) (see Figure 3.2). The studied river section has four consecutive meander bends. The river has a bankfull width of approximately 250 - 270 m (in 2013). The main reason to choose this river reach is that it has a well-developed meandering sand-bed channel. Furthermore, historical and recent changes have been widely studied in this reach (Murshed 1991, CEGIS 2003, 2013, Crosato 2008, IWFM 2011). A further advantage is that much data are available to set up, calibrate, and validate a computer model. Available field data and findings from previous studies are described in the following sections. Additional field data, that were collected to support morphodynamic modelling efforts, are described in Section 4.2.1.

3.3.2 Recent history of morphological changes at study site

Several studies exist in which the historical and recent channel changes in the study area have been investigated. In 2011 the Institute of Water and Flood Management (IWFM) in Bangladesh studied the morphological changes in the study area for selection of the construction site of the then proposed Nagarpur bridge (Latitude 24°2.434' N and Longitude 89°56.778' E). The investigated reach is shown in Figure 3.7 where the location of the bridge is shown by a yellow dot. The study revealed that a cutoff occurred in the period 1989 - 2000, when an old bend way was abandoned. The trace of the abandoned channel can be clearly seen in the satellite images for 2000 onwards. The lateral distance over which the channel shifted between 1989 and 2000 is about 3.2 km. Since 2000, the river restarted meandering with the initially mildly-curved new alignment.

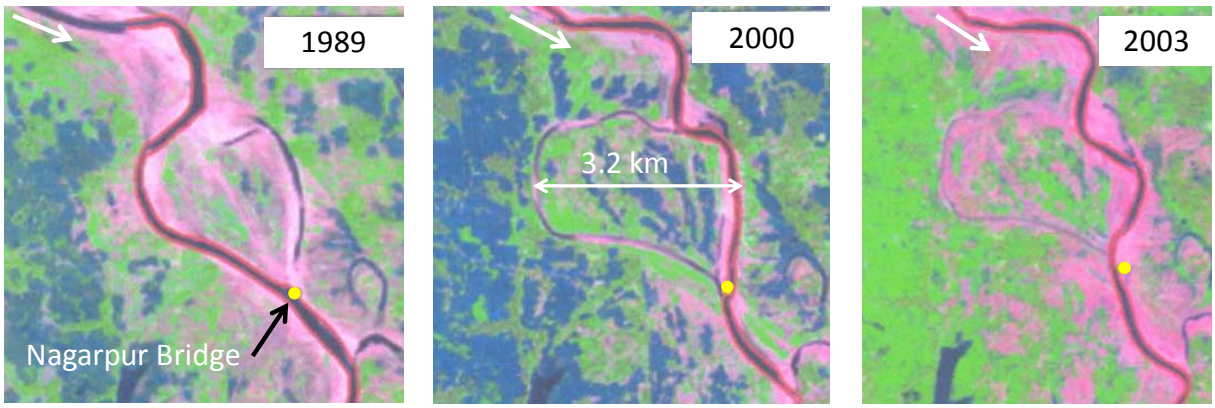

Fig. 3.7 Temporal evolution of a cut-off in the study area during 1989 – 2000. The imagery is a false color composite of Landsat TM data of the study area (adapted from IWFM 2011).

In 2003, the Center for Environmental and Geographic Information Services (CEGIS) in Bangladesh performed a planform analysis of a 24 km reach using satellite images for the

year 1973, 1984 and 2002. The investigated reach encompassed the present study area roughly at the middle. Following CEGIS's methodology, the planform characteristics for the year 2013 were estimated from Google Earth imagery and are shown in Figure 3.8: Figure 3.8(a) shows the temporal evolution of the reach-averaged bankfull channel width, Figure 3.8(b) of the reach-averaged meander wavelength and Figure 3.8(c) of the reach-averaged meander belt width. CEGIS (2003) suggested that the river is adjusting its planform characteristics including the channel width in response to the reduced flow of the river (see Section 3.2.1).

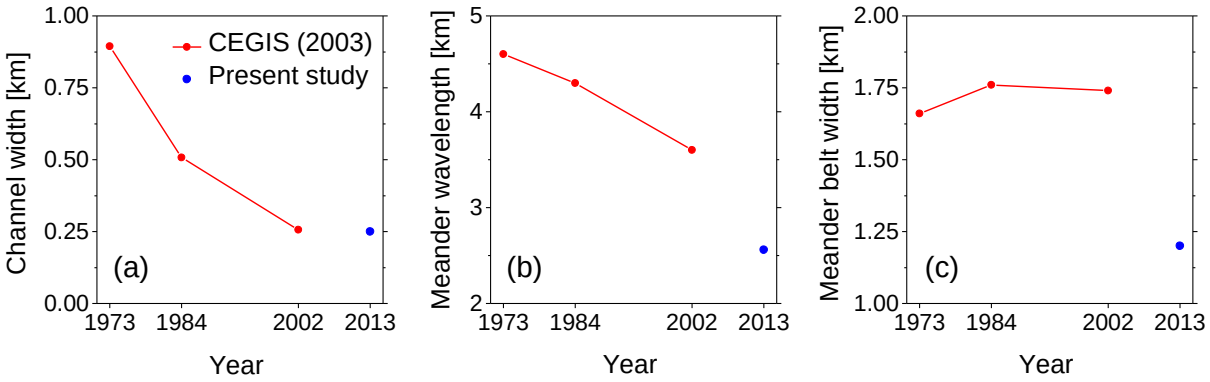

Fig. 3.8 *Historical planform characteristics of the study area (a) reach-averaged bankfull channel width, (b) reach-averaged meander wavelength and (c) reach-averaged meander belt width.*

3.4 Morphological data

3.4.1 Sediment characteristics

The sediment forming the river bed and banks is fine sand, although some silt exists depending on the location. A recent study (in 2014) on sub-soil investigation for the construction of a 520.60 m long Nagarpur Bridge by the Local Government Engineering Department (LGED) in Bangladesh revealed that the sediment ranges between 0.08 mm and 0.13 mm in diameter, and is not cohesive. The median sediment diameter (D_{50}) is approximately 0.1 mm. Figure 3.9 shows the grain size distribution of the bed material at the center of the channel.

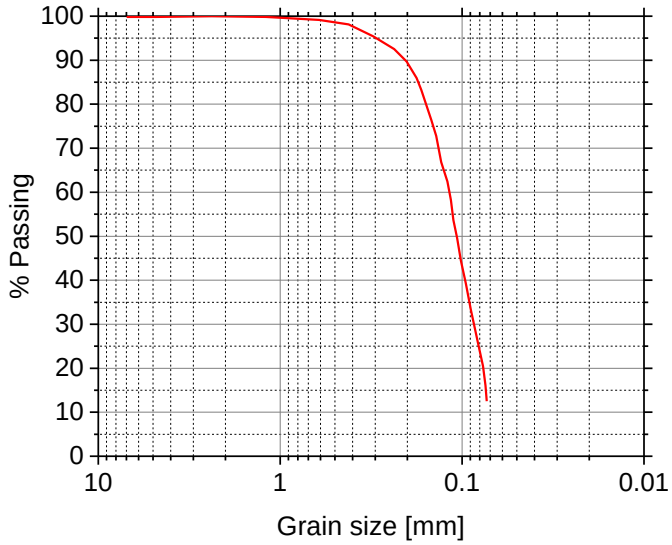

Fig. 3.9 Typical grain size distribution of the Dhaleshwari River at the Nagarpur Bridge site (adapted from LGED 2014).

3.4.2 Sediment rating curve

A large amount of data on the Bengal rivers has been obtained by international research in particular during the River Survey Project (1996), also indicated as FAP24 (Jagers 2003). During the River Survey Project (1996), a sediment rating curve for the Dhaleshwari River was developed based on data measured at Taraghat gauging station (137A) in the period 1971 - 1996. The composition of the sediment is around 89% wash load and the remaining 11% is bed material load (CEGIS 2013). The sediment rating curve for the suspended bed material load is shown in Figure 3.10. It is important to note that, after 1996, various urbanization, irrigation, and other anthropogenic activities have influenced the river sediment load in unknown ways. For instance, the formation of a large sand bar at the south off-take significantly altered the river hydrograph and possibly the sediment load (CEGIS 2013).

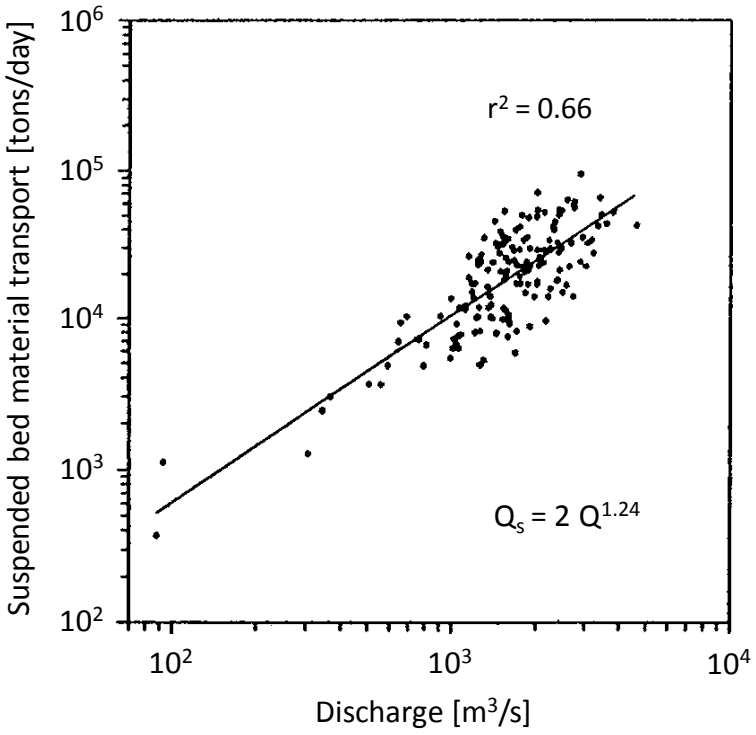

Fig. 3.10 Sediment rating curve for the Dhaleshwari River, constructed based on the measured data at the Taraghat gauging station (137A) (adapted from River Survey Project 1996).

3.4.3 River cross-section geometry

Measurements of discrete cross-sections were provided by the Bangladesh Water Development Board (BWDB). Between Elashin gauging station (68A) and Taraghat Gauging station (137A), the Dhaleshwari River is surveyed by BWDB, mostly in the dry seasons, at eight monitoring locations, among which only two monitoring cross-sections (i.e., fixed transects) are located within the study area. Figure 3.11(a) shows the locations of the cross-sections on the Google Earth imagery at three different time periods. The images in the middle and right panels indicate that the bed-forms within the active channel consist mainly of unvegetated sandy point bars that are submerged for discharges close to bankfull as shown in the image in the left panel. Figure 3.11(b) compares the cross-sectional bed elevation data in 2003, 2013 and 2016. Each cross-section can be divided into an active central region, conveying the ordinary flow discharge, and into two floodplains, flooded by larger discharges. The adjacent flood plains are quite large where the river is free to migrate. The river migrated very actively throughout the period of record. For instance, the observed bank retreat at the downstream monitoring cross-section (CS-2) is about 400 m and bank advance is about 210 m during the 10-year period (2003-2013).

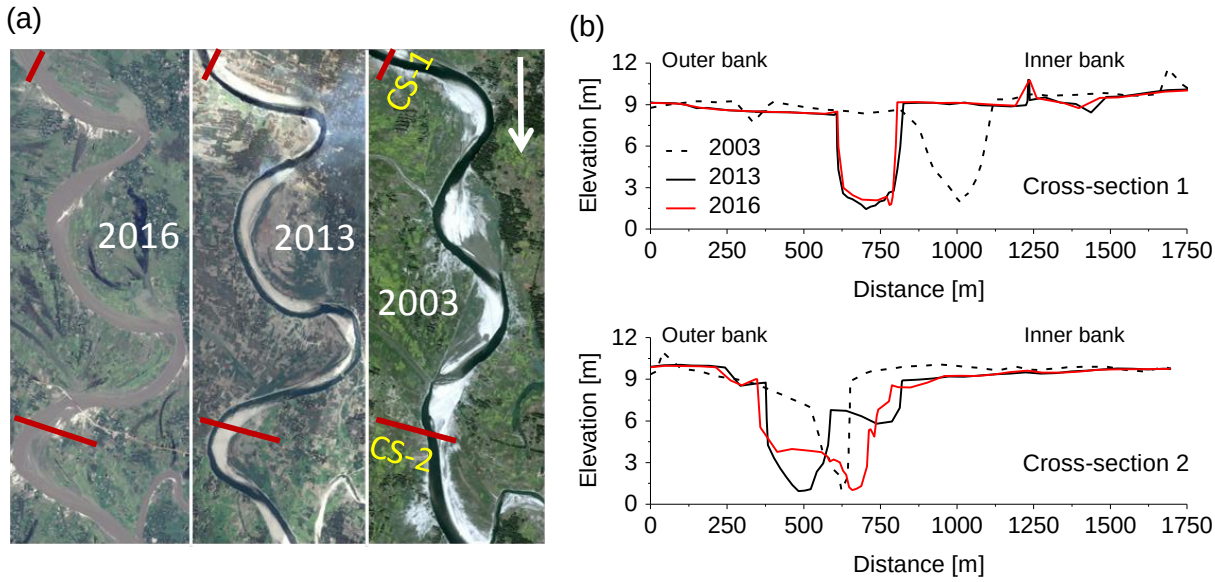

Fig. 3.11 *(a) Planform images (© Google Earth) of the study area and (b) comparison of the river geometries in the time period 2003 - 2016.*

3.5 A review of the previous research in the study area

Murshed (1991) and Crosato (2008) applied the meander migration model "MIANDRAS" to the Dhaleshwari River in the study area in order to assess the capability of the model to reproduce the behavior of real rivers. However, they mistakenly chose discharge data measured at gauging station Jagir (68.5) on the Dhaleshwari branch. Furthermore, the authors assumed the formative (bankfull) discharge to be 1300 $m^3 s^{-1}$ which is far too high for the Dhaleshwari branch after 1967, but in line with the antecedent river regime. Since the mid 1980s, the annual peak flow discharge in this course has never exceeded 280 $m^3 s^{-1}$ (see Section 3.1).

In the model application, Murshed (1991) extracted channel centerline from low-resolution (80 x 80 m) satellite images in 1986, and predicted channel centerline in 1993. Migration coefficients used in the model were also derived from satellite images, but Murshed (1991) was not able to test the validities of the computed planform evolutions due to lack of data. Later, Crosato (2008) extended Murshed's prediction till 2000, and tested their validities by comparing the predictions to the 2005 planimetry. Figure 3.12 shows the predicted river centerlines in 1993 and 2000. The predicted planform in 1993 is closer to the 2005 river configuration than the predicted planform in 2000, demonstrating that "MIANDRAS" overestimated the channel migration significantly. Crosato (2008) ascribed these over predictions to the inflow boundary conditions, and emphasized that the realistic long-term morphological predictions could only be possible by using reliable predictions of the discharge of the Dhaleshwari River.

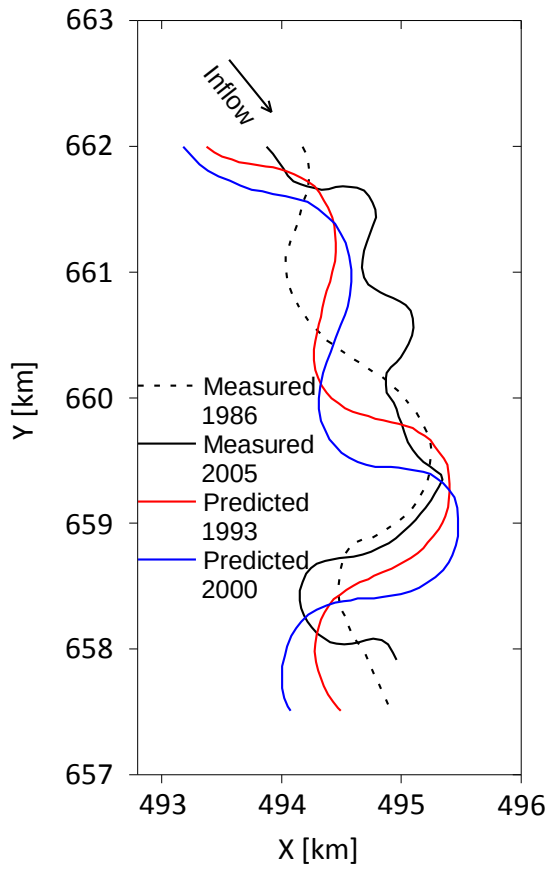

Fig. 3.12 Comparison of river planimetries between observed and predicted by MIANDRAS model (adapted from Crosato 2008).

As outlined in Section 3.2.1.2, the Institute of Water and Flood Management (IWFM) in Bangladesh studied the morphological changes for the site selection of the Nagarpur Bridge. For stability reasons, IWFM (2011) further investigated the risks of bed and bank erosion in a 1.6 km long sinuous river section (that encompasses the bridge site at the middle) by means of numerical model. An in-house developed two-dimensional flow model was applied to simulate the spatial distribution of flow velocities for 50-year design flood scenario. The near-bank velocity and average cross-sectional velocity for both the left and right banks were used to predict the increase in near bank scour depth (and related bank retreat) as a function of this velocity ratio. This modelling approach built on the same theoretical model of Crosato (2008), in which bank migration rate is linearly related to the near-bank excess velocity and excess bank height through empirical erosion coefficients (see Section 2.3.2.3).

To conclude, previous efforts (Murshed 1991, Crosato 2008, IWFM 2011) focused on empirical relations developed with historical data and simple one-dimensional representation of river hydrodynamics, in which the bank erosion process is represented in an idealized, non-mechanistic way. The use of computational models more based on physics is required that could predict the channel planform and the bathymetry to such an extent that the model results could be used in investigating the effects of discharge reduction. This is investigated in the present study in which the state-of-the-art multidimensional hydro and morphodynamic model Delft3D, described in Section 4.1, is used.

3.6 Possible future scenarios of hydro-morphological modifications in the study reach

The prediction of planform changes is important for the site selection of hydraulic structures such as bridges or intakes. Furthermore, for designing bank protection works, it is indispensable to know future planform developments for the safety of structures and lands. As outlined in Section 3.3.2, the Dhaleshwari River in the study area is adjusting its meandering wavelength and other parameters in response to declining flow. This trend indicates that with the decrease in flow volume, the meandering bend can become more sinuous. This in turn increases the risk of outflanking of the approach road of the recently constructed Nagarpur Bridge.

It should be considered that climate change could lead to overall increase in river flow. The Intergovernmental Panel on Climate Change (IPCC) defined climate change as any change in climate over time, whether due to natural variability or as a result of human activity (IPCC 2007). The 4th IPCC Report suggests that temperature rise in South Asia would be similar to the global mean warming, and therefore, South Asia can expect to experience an increase in both average and extreme rainfall during summer monsoon seasons of longer duration. Dasgupta et al. (2015) predicted the climate change effect by developing a hierarchical cascade of three model grids from the Jamuna-Brahmaputra basin to the Greater Dhaka region with decreasing spatial dimensions and increasing grid resolutions to simulate monsoon seasonal flows and water levels in the regional rivers surrounding Dhaka city. They considered the year 2004 as the reference to simulate future scenarios in 2050 because an extreme rainfall event (100-year recurrence interval) occurred in September 2004 (341 mm in 24 hours). The study suggests that average monsoon flow discharge and water levels could increase in the Dhaleshwari River by 13.6 percent and 0.30 m respectively, for the standard IPCC AR4 high-emissions, fossil-fuel intensive (A1FI) scenario in 2050, compared to the 2004 baseline. In general, the changed discharge regime will perhaps influence river morphology. However, it remains largely unknown how climate change will influence the river morphology.

Flow through a distributary mainly depends on the flow of the main river and morphology around the off-take. Because the Dhaleshwari River study reach is located near to the off-take, it is severely conditioned by sediment supply. Sediment sources from the parent river are limited by a large sand-bar deposit at the off-take. A relevant question thus arises on whether the study reach will continue in its planform change trend if no management or restoration strategies are implemented. Restoring the original discharge will have the consequence that meanders will become larger again, but at other locations. Restoring the discharge will not lead to the restoration of the old river course, but the river will change path again. This means that restoring water to the river should be done with knowledge on how the river alignment will change.

4 Methodology

The process-based numerical model Delft3D is described in this chapter (Section 4.1). Following this description, the application of the three-dimensional (3D) model to the case study area (Dhaleshwari River, Bangladesh) is presented (Section 4.2). The 3D model is calibrated against measured three-dimensional flow data, and is used for predicting bed level changes over a one-year period. The influences of sediment-related parameters on the morphological results are investigated. The use of a 3D morphological model is useful for the study, but further analyses are restricted due to computational time. To achieve acceptable computational times and to enlarge the spectrum of investigated scenarios, a 2D morphological model for meander migration is sought (Section 4.3), for which the parameterization of the 3D flow effect is validated against curved flume data (Section 4.3.1). The 2D model is used to simulate bed morphology and meander planform adjustment over a 10-year period under bankfull discharge condition (Section 4.3.2). A sensitivity analysis is carried out to increase the understanding of the impact of various sediment-related parameters on the simulation results. Finally, simulated planform is studied using the parameters which are frequently applied in analogous studies.

4.1 Numerical program Delft3D

4.1.1 Background of Delft3D

The current study applies a process-based numerical morphological model (Delft3D). Delft3D has been developed by Deltares (formerly WL | Delft Hydraulics), and is an open source code (https://oss.deltares.nl/web/delft3d). The modelling suite is divided into several modules assembled around a mutual interface. The flow module Delft3D-Flow is at the core of the modelling system. The standard hydrostatic version of Delft3D-Flow has been used in this study. Delft3D computes two or three dimensional hydrodynamics, sediment transport and bed level changes. Figure 4.1 shows the structure of the Delft3D-FLOW model.

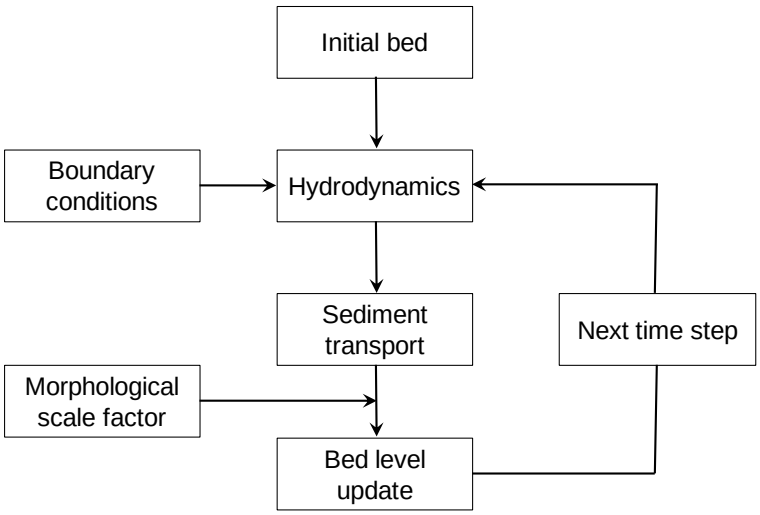

Fig. 4.1 Structure of the Delft3D-FLOW model.

After specifying the initial bathymetry and boundary conditions, the flow module computes water levels and velocities in the model domain for every hydrodynamic time step. Sediment transport is calculated from the flow field. To reduce the computational time of the simulations, the depositional and erosional fluxes to and from the bed are multiplied by a non-dimensional morphological acceleration factor ($MORFAC$), and then the updated bed level is used in the next hydrodynamic time step. This is valid since morphological changes take place over much longer time scales with respect to hydrodynamic changes (Lesser et al. 2004, Roelvink 2006).

All versions of Delft3D have been validated prior to their release using a large number of laboratory flume experiments and exact analytical solutions (Deltares 2014). As Delft3D encompasses the most rigorous theoretical basis for modelling sediment transport and morphological change (Rinaldi et al. 2008, Schuurman et al. 2013), the numerical model has been validated in a wide range of scientific projects for river (e.g., Kasvi et al. 2015, Williams et al. 2016), estuarine (e.g., George et al. 2012, Chu et al. 2013), and coastal systems (e.g., van der Wegen et al. 2011, Dissanayake 2011). The individual modules, which have been applied in this study, are presented in the following sections.

4.1.2 Hydrodynamics

4.1.2.1 3D hydrodynamics

The 3D model employed in Delft3D solves Reynolds Averaged Navier-Stokes' shallow water equations for an incompressible fluid. The governing equations comprise the horizontal momentum equations, the continuity equation, and a turbulence closure model. The vertical momentum equation is reduced to the hydrostatic pressure equation as the vertical accelerations are assumed to be small compared to gravitational acceleration and are not taken into account (Lesser et al. 2004). The closure scheme for turbulence is a k-ε model, in which k is the turbulent kinetic energy and ε is the turbulent dissipation. The equations are solved on an orthogonal curvilinear grid, but for clarity only equations for a Cartesian rectangular grid are given here.

The vertical momentum equation is reduced to the hydrostatic pressure equation. The resulting expression is

$$\frac{\partial P}{\partial \sigma} = \rho g h \tag{4.1}$$

where P is the hydrostatic pressure, σ is the vertical sigma coordinate in which the water column is divided into the same number of vertical grid cells independently of the water depth, ρ is the density of water (kg m^{-3}), g is the gravitational acceleration (m^2 s^{-1}) and h is the water depth (m).

The horizontal momentum equations are

$$\frac{\partial U}{\partial t} + U\frac{\partial U}{\partial x} + V\frac{\partial U}{\partial y} + \frac{\omega}{h}\frac{\partial U}{\partial \sigma} - fV = -\frac{1}{\rho_0}P_x + \frac{1}{h^2}\frac{\partial}{\partial \sigma}\left(\nu_v \frac{\partial U}{\partial \sigma}\right) + \nu_H\left(\frac{\partial^2 U}{\partial x^2} + \frac{\partial^2 U}{\partial y^2}\right) \tag{4.2}$$

$$\frac{\partial V}{\partial t}+U\frac{\partial V}{\partial x}+V\frac{\partial V}{\partial y}+\frac{\omega}{h}\frac{\partial V}{\partial \sigma}+fU=-\frac{1}{\rho_0}P_y+\frac{1}{h^2}\frac{\partial}{\partial \sigma}\left(\nu_v\frac{\partial V}{\partial \sigma}\right)+\nu_H\left(\frac{\partial^2 V}{\partial x^2}+\frac{\partial^2 V}{\partial y^2}\right) \quad (4.3)$$

where x is the downstream coordinate (m), y is the lateral coordinate (m), f is the Coriolis coefficient (s^{-1}), U is the flow velocity in the x direction (m s^{-1}), V is the flow velocity in the y direction (m s^{-1}), ω is the vertical flow velocity relative to the σ-plane (m s^{-1}), ν_H is the horizontal eddy viscosity (m^2 s^{-1}), ν_v is the vertical eddy viscosity (m^2 s^{-1}), ρ_0 is the reference density of water (kg m^{-3}).

The final terms of Equations (4.2) and (4.3) represent the horizontal Reynold's stresses. Assuming a constant density of water, the pressure gradients are calculated as follows:

$$P_x=g\frac{\partial \zeta}{\partial x}+\frac{\partial p}{\rho_0 \partial x} \quad (4.4)$$

$$P_y=g\frac{\partial \zeta}{\partial y}+\frac{\partial p}{\rho_0 \partial y} \quad (4.5)$$

where p is the atmospheric pressure (N m^{-2}), g is the gravitational acceleration (m s^{-2}) and ζ is the water level (m).

The vertical flow velocity W in the z direction is derived from the 3D continuity (mass balance) equation for fluid.

$$\frac{\partial \zeta}{\partial t}+\frac{\partial [hU]}{\partial x}+\frac{\partial [hV]}{\partial y}+\frac{\partial W}{\partial \sigma}=0 \quad (4.6)$$

where t is the time step (s).

In the 3D model, the bed shear stress is calculated using the following formula:

$$\tau_b=\frac{g\rho_0 u_b|u_b|}{C_{3D}^2} \quad (4.7)$$

where τ_b is the bed shear stress (N m^{-2}), u_b is the near-bed flow velocity (m s^{-1}), and C_{3D} is the 3D Chézy coefficient ($m^{1/2}$ s^{-1}) which is calculated as follows:

$$C_{3D}=\frac{\sqrt{g}}{\kappa}\ln\left(1+\frac{\Delta z_b}{2z_0}\right) \quad (4.8)$$

where κ is the von Karman constant (= 0.4), Δz_b is the distance to the computational grid point closest to the bed (m) and z_0 is the bed roughness length (m).

4.1.2.2 2D hydrodynamics with secondary flow parameterization

Following the definition of the σ-coordinate, the water depth is divided into multiple layers in the 3-dimensional computations. As a result, secondary flow, which is important in river bends, is resolved on the vertical grid. This is not possible in the 2D approach because of

depth averaging over the water column. For that reason, in 2D depth-averaged simulations the secondary flow is determined indirectly using a secondary flow model. This leads to an extension to the depth-averaged momentum equations. The hydrodynamics are modelled by applying conservation of momentum (equations 4.9 and 4.10) and conservation of mass (equation 4.11), assuming hydrostatic pressure (Schuurman et al. 2013):

$$\frac{\partial \bar{U}}{\partial t}+\bar{U}\frac{\partial \bar{U}}{\partial x}+\bar{V}\frac{\partial \bar{U}}{\partial y}+g\frac{\partial \zeta}{\partial x}-f\bar{V}+F_{\mathrm{sec},x}=-\frac{1}{\rho_0}P_x+\nu_H\left(\frac{\partial^2 \bar{U}}{\partial x^2}+\frac{\partial^2 \bar{U}}{\partial y^2}\right) \tag{4.9}$$

$$\frac{\partial \bar{V}}{\partial t}+\bar{U}\frac{\partial \bar{V}}{\partial x}+\bar{V}\frac{\partial \bar{V}}{\partial y}+g\frac{\partial \zeta}{\partial y}-f\bar{V}+F_{\mathrm{sec},y}=-\frac{1}{\rho_0}P_y+\nu_H\left(\frac{\partial^2 \bar{V}}{\partial x^2}+\frac{\partial^2 \bar{V}}{\partial y^2}\right) \tag{4.10}$$

$$\frac{\partial \zeta}{\partial t}+\frac{\partial\left[h\bar{U}\right]}{\partial x}+\frac{\partial\left[h\bar{V}\right]}{\partial y}=0 \tag{4.11}$$

where $\bar{U}$ is the depth-averaged velocity component in the x direction (m s^{-1}) and $\bar{V}$ is the depth-averaged velocity component in the y direction (m s^{-1}), $F_{\mathrm{sec},x}$ and $F_{\mathrm{sec},y}$ are the correction terms in order to account the effect of secondary flow on the depth-averaged momentum equations.

The so-called “dispersion terms”, which result from the difference of the depth-averaged velocity and vertical varying velocity, are generally used to model the secondary flow effect in the depth-averaged 2D hydrodynamic model. The correction terms ($F_{\mathrm{sec},x}$ and $F_{\mathrm{sec},y}$ in equations 4.9 and 4.10, respectively) are calculated as follows (Rinaldi et al. 2008, Nabi et al. 2016):

$$F_{\mathrm{sec},x}=\frac{1}{h}\left(-2\frac{\partial \beta h\bar{U}\bar{V}}{\partial x}+\frac{\partial \beta h\left(\bar{U}^2+\bar{V}^2\right)}{\partial y}\right) \tag{4.12}$$

$$F_{\mathrm{sec},y}=\frac{1}{h}\left(2\frac{\partial \beta h\bar{U}\bar{V}}{\partial y}+\frac{\partial \beta h\left(\bar{U}^2+\bar{V}^2\right)}{\partial x}\right) \tag{4.13}$$

The non-dimensional parameter β is given by the following relation:

$$\beta=\beta_c\left(5\alpha-15.6\alpha^2+37.5\alpha^3\right)\frac{h}{R_s} \tag{4.14}$$

in which R_s is the effective radius of streamline curvature (m), β_c is a non-dimensional parameter with values between 0 and 1, and α is a non-dimensional parameter given by

$$\alpha=\min\left(\frac{\sqrt{g}}{\kappa C},\frac{1}{2}\right) \tag{4.15}$$

where C is the Chézy coefficient for 2D model (m$^{1/2}$ s^{-1}).

In the 2D model, the bed shear stress is computed using the following formula:

$$\tau_b = \frac{g\rho_0 u_b |u_b|}{C^2} \tag{4.16}$$

where τ_b is the bed shear stress (N m^{-2}), u_b is the near-bed flow velocity (m s^{-1}) which is determined from the depth-averaged velocity, assuming a logarithmic velocity profile (Kasvi et al. 2015).

The relation between Chézy and Manning's roughness reads:

$$C = \frac{\sqrt[6]{h}}{n} \tag{4.17}$$

where h is the water depth (m) and n is the Manning's roughness coefficient (s m$^{-1/3}$).

An alternating direction implicit (ADI) technique (a finite difference method) is used to solve the momentum and continuity equations. In the ADI method, each time step is split in two stages of half a time step. This scheme implicitly solves the water levels and velocities in the x direction in the first half-step and the y direction terms in the second half-step. A detailed description of the hydrodynamics and numerical scheme of Delft3D can be found in Lesser et al. (2004), and Deltares (2014).

4.1.3 Sediment transport and morphodynamics

Van Rijn approach

For 3D model scenarios, the transport capacity predictor of van Rijn (1993) has been used as this approach has separate expressions for suspended load and bed load transport. The suspended sediment transport is computed by solving the 3D advection-diffusion equation:

$$\frac{\partial c}{\partial t} + \frac{\partial}{\partial x}(Uc) + \frac{\partial}{\partial y}(Vc) + \frac{\partial}{\partial z}\left[(W - w_s)c\right] - \frac{\partial}{\partial x}\left[D_x \frac{\partial c}{\partial x}\right] - \frac{\partial}{\partial y}\left[D_y \frac{\partial c}{\partial y}\right] - \frac{\partial}{\partial z}\left[D_z \frac{\partial c}{\partial z}\right] = 0 \tag{4.18}$$

where w_s is the settling velocity of suspended sediment (m s^{-1}), c is the sediment concentration (kg m^{-3}), D is the sediment diffusivity coefficients in x, y, z directions (m^2 s^{-1}). The horizontal components are user-specified, and the vertical component is taken from the k-ε turbulence closure model used in the hydrodynamic calculation.

The settling velocity of suspended sediment depends on the sediment diameter and is computed as follows:

$$w_s = \begin{cases} \dfrac{(s-1)gD_{50}^2}{18\upsilon_k} & 65\ \mu m < D_{50} \leq 100\ \mu m \\ \dfrac{10\upsilon_k}{D_{50}}\sqrt{1 + \dfrac{0.01(s-1)gD_{50}^3}{\upsilon_k^2}} - 1 & 100\ \mu m < D_{50} \leq 1000\ \mu m \\ 1.1\sqrt{(s-1)gD_{50}} & 1000\ \mu m < D_{50} \end{cases} \tag{4.19}$$

where s is the relative density of sediment (kg m^{-3}), D_{50} is the median sediment diameter (μm) and υ_k is the kinematic viscosity coefficient of water (m^2 s^{-1}).

Bed load is treated below a reference height, and suspended load above it (van Rijn 1993). Suspended sediment is entrained in the water column by imposing a reference concentration at the reference height (van Rijn 2000). The sediment concentration in the reference layer is calculated as follows:

$$c_a = f_{sus} 0.015 \eta \rho_s \frac{D_{50} T_a^{1.5}}{a D_*^{0.3}} \tag{4.20}$$

where c_a is the reference concentration at reference height (kg m^{-3}), f_{sus} is the user-specified calibration factor (default value = 1.0), η is the relative availability of the sediment fraction in the mixing layer (-), ρ_s is the density of sediment particles (kg m^{-3}), and T_a is the dimensionless bed shear stress (-) which characterizes an excess shear stress available to move sediment, D_* is the dimensionless particle diameter (-), and a is the van Rijn's reference height (m).

The exchange of sediment between the bed and the flow is modelled using sink and source terms acting on the near-bed reference layer. The reference layer is entirely above van Rijn's reference height. The source and sink terms determine how much sediment is entering the flow due to upward diffusion from the reference layer and how much sediment is dropping out of the flow due to sediment settling. The resulting expressions are:

$$Source = c_a \left(\frac{D_v}{\Delta z} \right) \tag{4.21}$$

$$Sink = c_{kmx} \left(\frac{D_v}{\Delta z} + w_s \right) \tag{4.22}$$

where c_{kmx} is the concentration of sediment in the reference layer (kg m^{-3}), Δz is the difference in elevation between the centre of the reference layer and van Rijn's reference height (m), and D_v is the vertical sediment mixing coefficient (m^2 s^{-1}) which follows directly from the vertical fluid mixing coefficient calculated by the k-ε turbulence closure model.

Morphodynamic module uses a correction to account for suspended load transport under the reference level. The change in the quantity of bottom sediments caused by the suspended sediment sources and sinks is calculated as:

$$\Delta S_{bed,s}^{(x,y)} = MORFAC \left(Sink - Source \right) \Delta t \tag{4.23}$$

where $\Delta S_{bed,s}^{(x,y)}$ is the change in the bottom sediment mass at grid-cell center (x, y) due to suspended load transport (kg m^{-2}), $MORFAC$ is the user-specified morphological scale factor (-), and Δt is the computational time step (s).

The magnitude of bed load transport is computed by:

$$|S_b| = f_{bed}\, 0.5 \eta \rho_s D_{50} u_*' D_*^{-0.3} T \tag{4.24}$$

where $|S_b|$ is the bed-load transport rate (kg m^{-1} s^{-1}), f_{bed} is the user-specified calibration factor (default value = 1.0), u_*' is the effective bed shear velocity (m s^{-1}), T is the dimensionless bed shear stress (-). u_*' and T are based on the computed velocity in the bottom computational layer.

The direction of the bed load transport is assumed to be equal to the direction of the flow in the bottom computational layer. This results in the following transport components:

$$S_{b,u} = \frac{u_{b,u}}{|u_b|} |S_b| \tag{4.25}$$

$$S_{b,v} = \frac{u_{b,v}}{|u_b|} |S_b| \tag{4.26}$$

where $|u_b|$ is the local near-bed flow velocity magnitude, $u_{b,u}$ and $u_{b,v}$ are the local near-bed flow velocity components.

Engelund-Hansen approach

For 2D model scenarios, the transport capacity predictor of Engelund-Hansen (1967) has been used. The total sediment transport is treated as if it were bed load (van der Wegen et al. 2008). The Engelund-Hansen (1967) sediment transport relation has been used widely in morphodynamic modelling of real rivers (Kasvi et al. 2015, Schuurman et al. 2016). It reads:

$$S_b = S_{bed} + S_{sus} = \frac{0.05 \alpha \bar{U}^5}{\sqrt{g} C \Delta^2 D_{50}} \tag{4.27}$$

where S_b is the total sediment transport per unit width (m^2 s^{-1}), $\bar{U}$ is the depth-averaged flow velocity in the streamline direction (m s^{-1}), Δ is the relative mass density of sediment under water (-), D_{50} is the median sediment diameter (m), and α is a calibration coefficient (O(1)).

Sediment transport is deflected from the depth-averaged flow direction by curvature induced spiral flow. Therefore, the model is parameterized to reproduce physical processes. The spiral flow intensity is computed by the flow module and the effect of spiral flow on the sediment transport direction is parameterized by:

$$\tan(\phi_\tau) = \frac{\bar{V} - \alpha_I \dfrac{\bar{U}}{\sqrt{\bar{U}^2 + \bar{V}^2}} I}{\bar{U} - \alpha_I \dfrac{\bar{V}}{\sqrt{\bar{U}^2 + \bar{V}^2}} I} \tag{4.28}$$

where

$$\alpha_I = \frac{2}{\kappa^2} E_s \left(1 - \frac{1}{2} \frac{\sqrt{g}}{\kappa C} \right) \tag{4.29}$$

where I is the spiral flow intensity (m s^{-2}), ϕ_τ is the angle between downstream and sediment transport direction, C is the Chézy coefficient (m$^{1/2}$ s^{-1}), and E_s is a calibration coefficient to control the spiral flow effect on the bed load transport direction (-).

Adjustment of bed-load transport for bed slope effects

In a two dimensional plane, two bed slope directions exist; a longitudinal slope in the direction of the flow and a transverse slope in the direction perpendicular to the (initial) flow. Both longitudinal bed slope and transverse bed slope influence three-dimensional sediment transport in river bends. Therefore, first, the magnitude of the transport is modified by applying the longitudinal bed slope correction factor (Bagnold 1966). Next, the direction of transport is modified by applying the transverse bed slope correction factor based on the work of Ikeda (1982, 1988) as presented by van Rijn (1993). Bed load transport rates in the x and y directions are then determined from Walstra et al. (2007). The resulting expressions are:

$$S_{b,x} = \alpha_s S'_{b,x} - \alpha_n \alpha_s S'_{b,y} \tag{4.30}$$

$$S_{b,y} = \alpha_s S'_{b,y} + \alpha_n \alpha_s S'_{b,x} \tag{4.31}$$

in which

$$\alpha_s = 1 + \alpha_{bs}\left[\frac{\tan\phi}{\cos\left(\tan^{-1}\psi\right)\left(\tan\phi - \tan\psi\right)} - 1\right] \tag{4.32}$$

$$\alpha_n = \alpha_{bn}\left(\frac{\tau_{b,cr}}{\tau_b}\right)^{0.5} \tan\gamma \tag{4.33}$$

where $S_{b,x}$ and $S_{b,y}$ are the adjusted bed load transport rates in the x and y directions respectively, $S'_{b,x}$ and $S'_{b,y}$ are the un-adjusted bed load transport rates in the x and y directions respectively, α_s is the longitudinal bed slope correction factor, α_n is the transverse bed slope correction factor, ϕ is the angle of repose (= 30° in the simulations), ψ is the longitudinal bed slope, γ is the transverse bed slope, $\tau_{b,cr}$ is the critical bed shear stress, τ_b is the actual bed shear stress, α_{bs} is a user-specified tuning parameter (default value = 1) and α_{bn} is a user-specified tuning parameter (default value = 1.5).

Bed level update

The numerical scheme applies a staggered grid, in which water level points and depth points are collocated in the cell centers, whereas the u and v velocity points are located in the middle of the cell walls. In contrast, the bed load transport vector components described above are computed at the water-level points. In order to ensure numerical stability, the bed load transport vectors are then relocated to velocity points using an upwind computational scheme. The upwind direction is based on the computed directions of the bed-load transport vectors in the water level points (Lesser et al. 2004). Bed load transport components at ve-

locity points are set equal to the component at the upwind water level points. In the example shown in Figure 4.2 the bed load transport component S_{buu} is set equal to $S_{b,x}$ and the component S_{bvv} is set equal to $S_{b,y}$.

The change in bottom sediment due to bed load transport is calculated as follows:

$$\Delta S_{bed}^{(m,n)} = MORFAC \left(\begin{matrix} S_{b,uu}^{(m-1,n)} \Delta y^{(m-1,n)} - S_{b,uu}^{(m,n)} \Delta y^{(m,n)} + \\ S_{b,vv}^{(m,n-1)} \Delta x^{(m,n-1)} - S_{b,vv}^{(m,n)} \Delta x^{(m,n)} \end{matrix} \right) \frac{\Delta t}{A^{(m,n)}} \tag{4.34}$$

where $\Delta S_{bed}^{(m,n)}$ is the change in quantity of bottom sediment at location (m, n) due to bed load transport (kg m^{-2}), $MORFAC$ is the user-specified morphological scale factor (-), Δt is the computational time step (s), $A^{(m,n)}$ is the area of computational cell at location (m, n) (m^2), $S_{b,uu}^{(m,n)}$ and $S_{b,vv}^{(m,n)}$ are the bed load transport vector components in the u and v directions, held at the u and v velocity points respectively (kg m^{-1} s^{-1}), $\Delta x^{(m,n)}$ and $\Delta y^{(m,n)}$ are the widths of cell (m, n) in the x and y directions respectively (m).

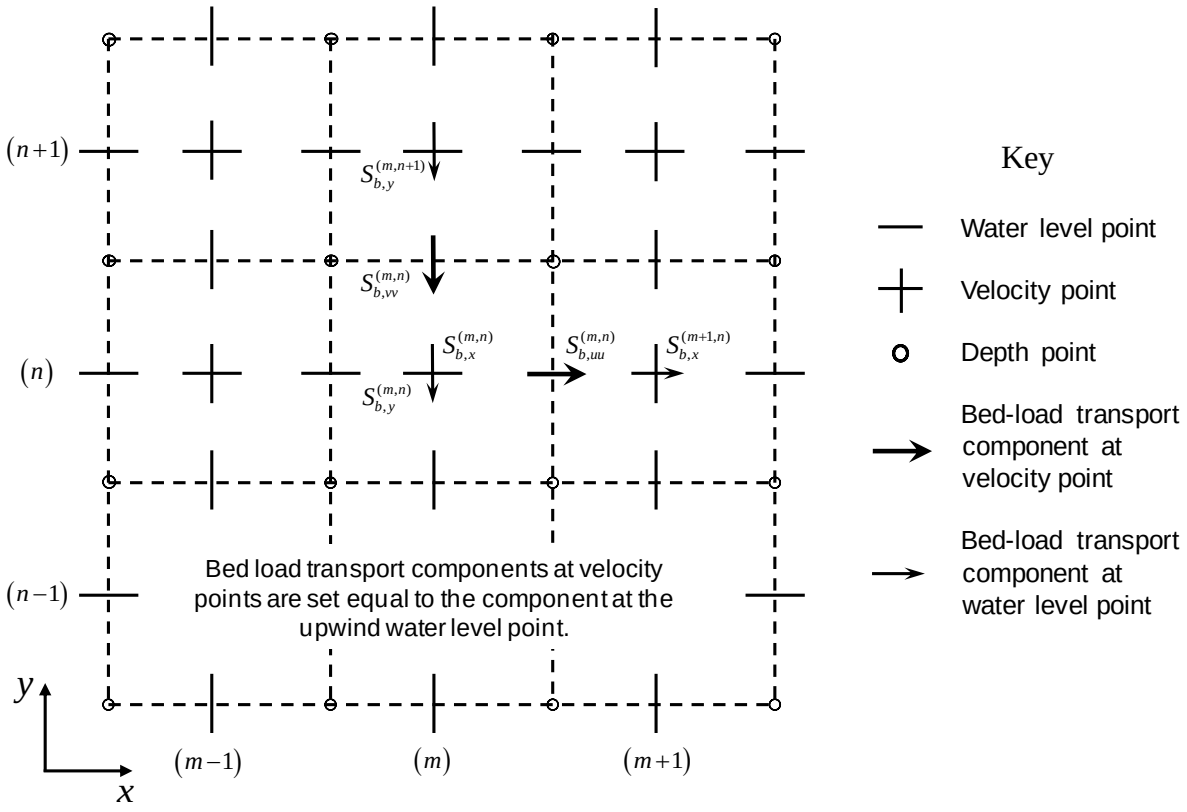

Fig. 4.2 Setting of bed-load transport components at velocity points (adapted from Lesser et al. 2004).

According to the van Rijn approach, the total change in the mass of bed material is the sum of the change due to suspended-load (computed by equation 4.23) and the change due to bed-load (computed by equation 4.34). In the Engelund-Hansen approach, the total change in the mass of bed material is simply calculated by equation 4.34. This change in mass is translated into a bed-level change, and the updated bed level is again used for the following hydrodynamic computation.

Bank erosion scheme

A simplified formulation of bank erosion is implemented in the model so that channel migration can be simulated. This approach is called “dry cell erosion” that allows the partial redistribution of erosion from a wet cell to adjacent dry cells (Lesser et al. 2004, van der Wegen & Roelvink 2008, Deltares 2014, Williams et al. 2016). Bank erosion of a dry grid cell occurs when a neighboring wet grid cell is eroded (see Figure 4.3). The transfer of the total amount of erosion from a wet cell to the adjacent dry cell is specified by a user defined percentage (*ThetSD*). For instance, *ThetSD* equals 1 means that all erosion that would occur in the wet cell is assigned to the adjacent dry cells, which implies that no bed level change of the wet cell takes place. This process continues until the dry grid cell is inundated.

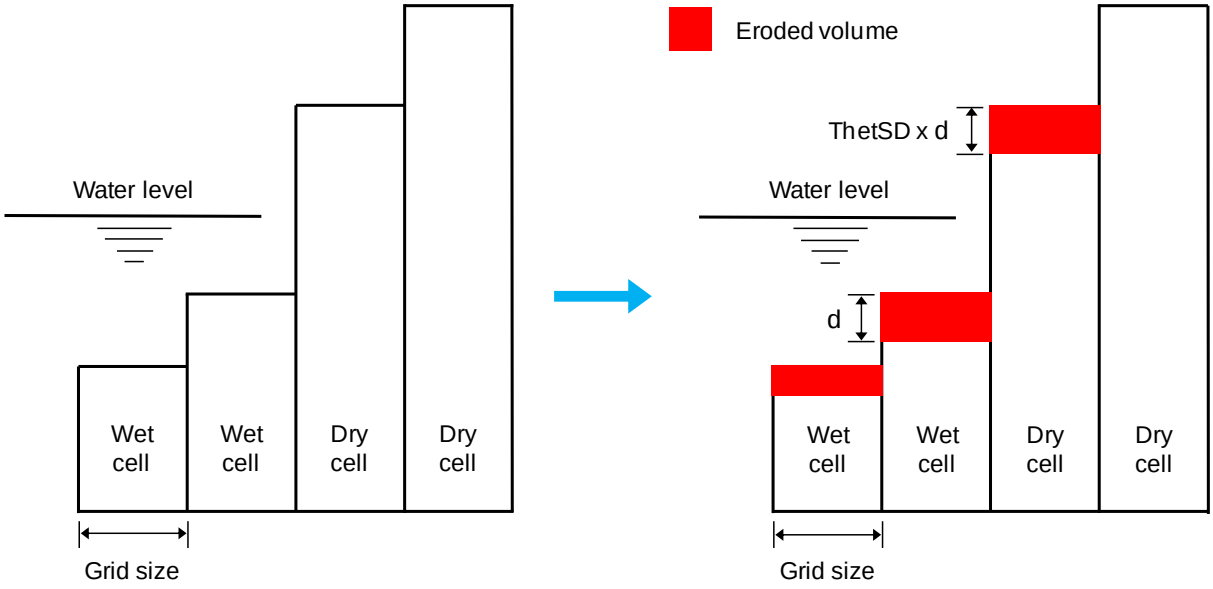

Fig. 4.3 Schematized diagram showing the bank erosion.

4.2 3D morphological modelling

This section presents an application of the 3D numerical model (Delft3D) to the case study area (Dhaleshwari River, Bangladesh). Field data are collected to set up, calibrate and validate the 3D model. The model is calibrated against measured 3D flow data, and is applied to simulate the morphological changes taking place in the study area. To assess model performance the results of a one-year morphodynamic computation are compared with field data. Finally, the influences of sediment-related parameters on the morphological results are evaluated by means of statistical comparison (i.e., Brier Skill Score).

4.2.1 Field campaign and data processing

The 3D modelling imposed high demands on field data. Discharge time-series and sediment grain size distribution are described in the previous chapter (see Section 3.2.3 and Section 3.4.1, respectively). Additional field data, which were collected to set up, calibrate and validate the 3D numerical model, are described in the following sections.

4.2.1.1 Topographic survey

Topographic information was collected at the study site during three separate sampling campaigns. The location of the measurements is shown in Figure 4.4. The first campaign (November - December 2014) included a detailed survey of the channel bathymetry that is essential for 3D morphological modelling. Topographic information was collected at a total of 113 cross-sections, separated by approximately 100 meters. Each cross-section was oriented normal to the channel centerline curvature. Bathymetric data were collected using a boat mounted single-beam echo sounder in conjunction with a Global Positioning System (GPS). The surveyed lines were projected onto the Bangladesh Transverse Mercator (BTM) coordinate system and post-processed in Geographic Information Systems (GIS). Variations in water surface elevation during the topographic data collection period were corrected using water level data from the Elashin gauging station (68A). The survey data yielded a topographic map of the river reach as shown in Figure 4.4. Bed elevation data, which were used to evaluate the predictive capabilities of the numerical model, were collected at 5 cross-sections during the second campaign (December 2015).

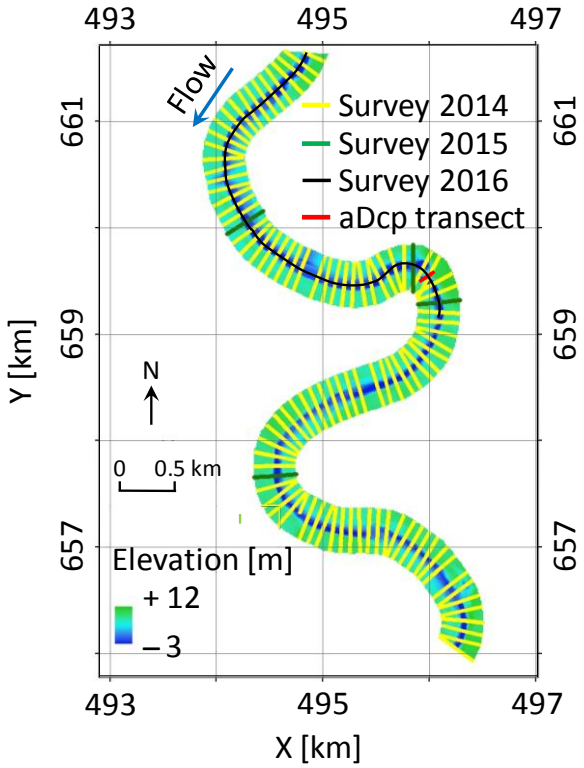

Fig. 4.4 Topographic map of the study area

The third field campaign (18 March 2016) was dedicated to collect bedform information of the studied reach. Repeat bathymetric surveys (~ 4 hours apart) were conducted along a pre-determined line representing the thalweg (see Figure 4.4). The length of the surveyed reach was about 4.4 km. Low-flow conditions (approximately 9 m^3 s^{-1}) prevailed during the day of data acquisition. Longitudinal profiles of bed elevation were recorded using a boat mounted Teledyne Odom Hydrotrac II single-beam echo sounder in conjunction with a differential Global Positioning System (dGPS). The slopes of the free surface were also monitored during this campaign. The bathymetry data were processed and filtered to remove noise, and then, classified into ripples, dunes and bars using the procedure described in Gutierrez et al. (2013). For this purpose, the Bedforms Analysis Toolkit for Multiscale Modelling (Bedforms-ATM, developed by Gutierrez et al. 2013), which is a spline filter and wavelet based open-source MATLAB software to analyze the hierarchies and dimensionality of bed forms, was used. The survey exhibits a wide range of bedform morphologies throughout the meander bend as shown in Figure 4.5 where $h_{1,3}$ represents the height of the first bedform hierarchy (ripples), $h_{2,3}$ shows the height of the second bedform hierarchy (dunes), and $h_{3,3}$ exhibits the bed elevation of the third bedform hierarchy (bars). Dunes of mean height and length of 0.15 and 1 m, respectively, were observed on the river bed in the study reach. Repeated surveys of river bed morphology indicated that due to very low flow discharges in the river, the dunes had not migrated between sequential surveys.

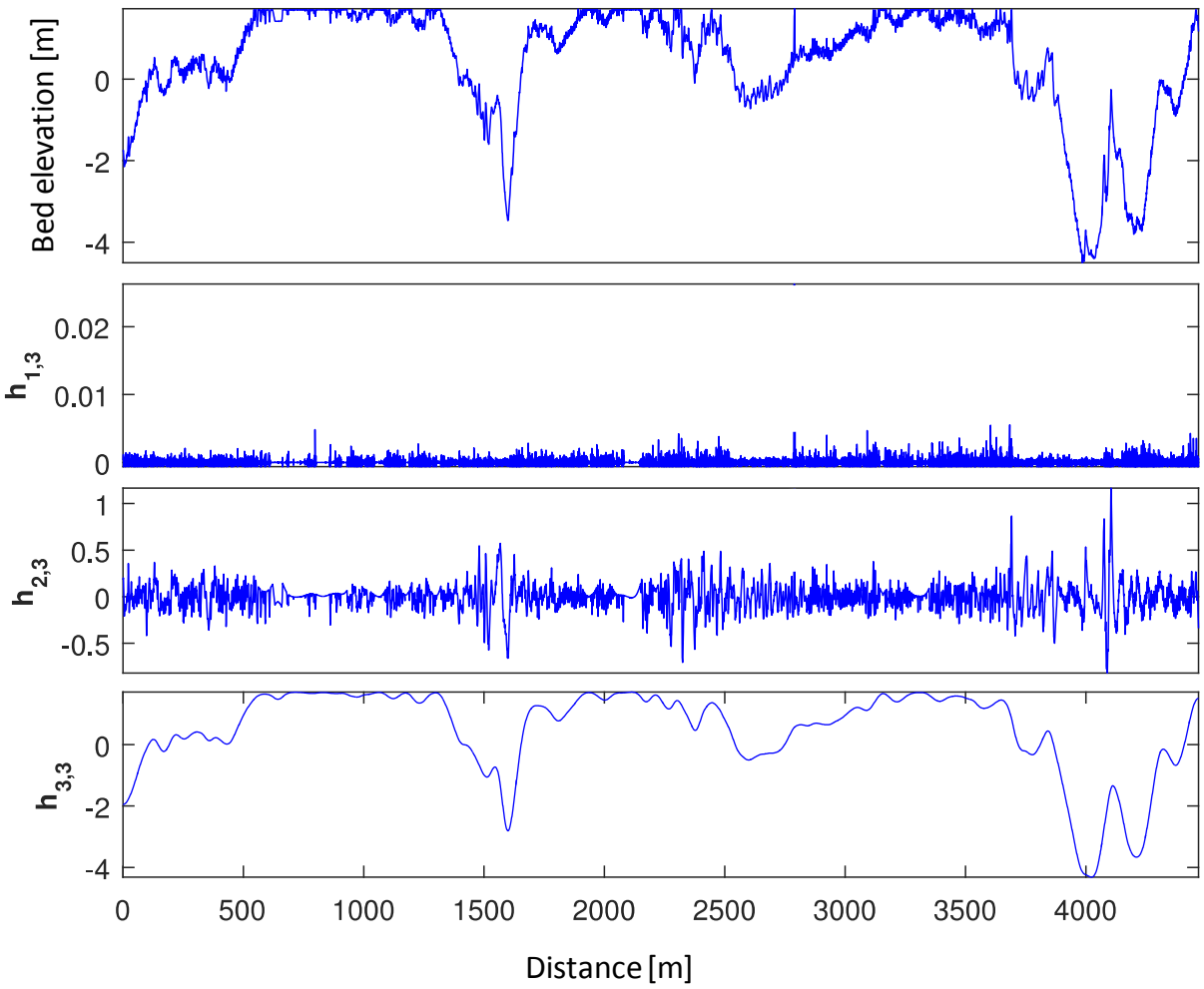

Fig. 4.5 *The hierarchies and dimensionality of bedforms: $h_{1,3}$ represents the first bedform hierarchy (ripples), $h_{2,3}$ represents the second bedform hierarchy (dunes), and $h_{3,3}$ represents the third bedform hierarchy (bars). Bedforms multi-scale discrimination was performed using a spline filter and wavelet-based toolkit Bedforms-ATM (Gutierrez et al. 2013).*

4.2.1.2 3D velocity measurements

Velocity data collection

A boat-mounted Teledyne RDI RiverRay 600 *kHz* acoustic Doppler current profiler (aDcp) was used to measure the three-dimensional flow field at a meander bend section in September 2015 (see Figure 4.6). In principle, the aDcp uses acoustic physics to measure the three-dimensional velocity of flowing water, and subsequently the data can be used to determine flow discharge (Parsons et al. 2013). The aDcp was boat-mounted for the measurement of repeated transects along a cross-section located about 4 km downstream of the upstream boundary (the location of the flow measurements is shown in Figure 4.4). The bottom tracking function of the aDcp was used to monitor the bed elevations, and the aDcp was linked to a Global Positioning System (GPS) to provide both position and boat velocity. The aDcp was configured to measure velocities in 0.5 m bins (size of each depth cell measured). It should be noted that the instrument cannot measure the first 1 m below the water surface and approximately 13% of the depth at the bottom of the channel but extrapolates the flow values

for these unmeasured areas. According to the aDcp measurements, the discharge was 30 $m^3 s^{-1}$ and the corresponding water surface elevation at the downstream end was 6.42 m.

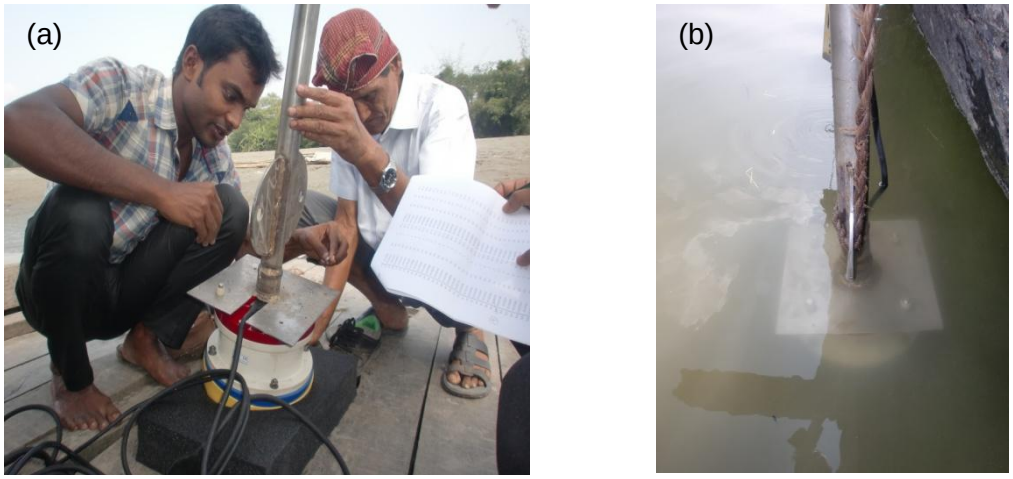

Fig. 4.6 *(a) Setup of aDcp measurements and (b) aDcp mounted to a boat (Photo: Jakaria Pervez).*

Calculation of secondary circulation

Difficulties were encountered with regard to the separation of the primary and secondary components of the flow from the aDcp data because the collected acoustic profiles were not perfectly normal to the mean flow direction. As a result, the rotation of the aDcp data was necessary. For this purpose, the velocity mapping toolbox (VMT), which is an open-source software tool for the post-processing and visualization of aDcp data (Parsons et al. 2013), was used. A major advantage of VMT is that it projects multiple aDcp transects onto a common plane of reference, and averages the data spatially and temporally for visualization of the three-dimensional velocity field within cross-sections (Konsoer et al. 2016). Within VMT, several rotation methods are available and the choice on what method to use is completely determined by the goal of the research. Examples are the studies by Parsons et al. (2013), Bever & MacWilliams (2015), Konsoer et al. (2016) and Engel & Rhoads (2016). Lane et al. (2000) pointed out that zero secondary discharge definition is appropriate for meander bends, as this allows rotation of the whole section. In this case the primary velocity follows such a direction that there is no secondary discharge for the entire section (Lane et al. 2000). Since the study reach is characterized by a series of meander bends, zero secondary discharge definition was used for the rotation of field data.

For the initial data analysis, a horizontal resolution of 0.5 m and vertical resolution of 0.25 m were specified. The acoustic profiles obtained from a single transect yielded a scatter in the measured velocity values and was deemed unacceptable for analysis of the detailed flow structure. In order to obtain representative values of the time-averaged three-dimensional velocities, the measured velocity data from each of the three transects were projected onto a straight-line plane that defines a measurement cross-section, and then averaged and mapped onto the cross-section. The secondary circulation velocities were smoothed using a five-cell horizontal and a four-cell vertical window parameter.

Contour plots of primary velocities with superimposed secondary circulation vectors show the detailed three-dimensional velocity fields at the channel cross-section (see Figure 4.7). The

flow in the channel has a velocity core which is located around the center of the channel thalweg. While looking in the downstream direction, the top layers tend to move towards the left bank (outer bank) as one might expect for such an anticlockwise circulation in a bend.

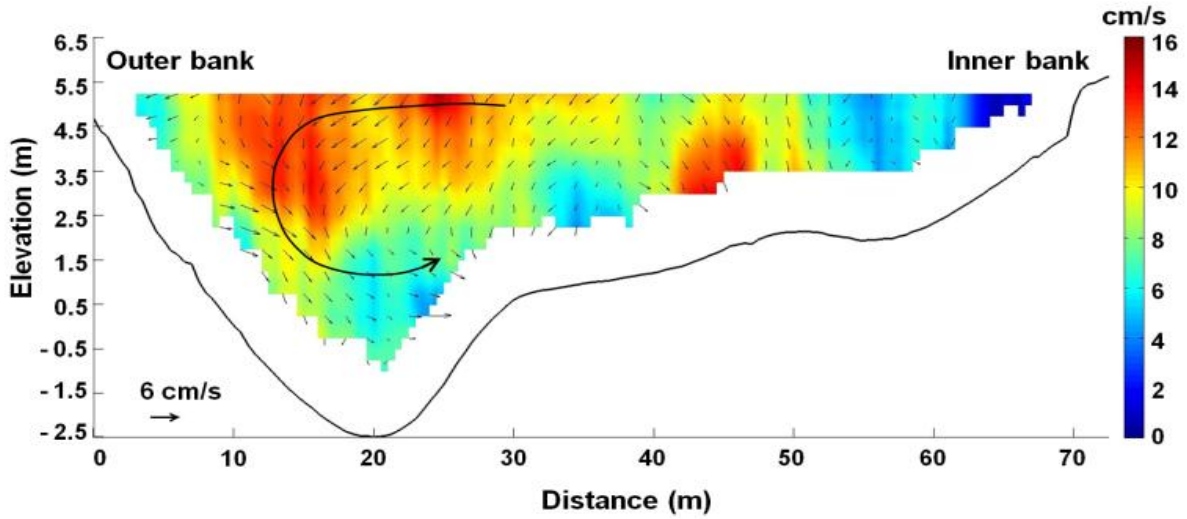

Fig. 4.7 *Cross-sectional contour plots of primary flow and vector representation of secondary flow.*

4.2.2 Model setup

Grid and bathymetry

The results of bathymetric surveys during campaign 1 (November - December 2014) were used to generate a computational digital grid for the 3D morphological model. The grid comprised of 128,000 cells (1600 cells in the longitudinal direction and 80 cells in the transverse direction) in an orthogonal curvilinear grid. The resolution ranged from about 8 m down to about 1 m. The quality of the generated mesh was verified through evaluation of the orthogonality (i.e., cosine value of the angle between the grid lines), aspect ratio (i.e., ratio of grid cell dimensions in longitudinal and transverse direction) and smoothness (i.e., difference between successive grid cell dimensions). All grids satisfied the recommendation for orthogonality < 0.02, aspect ratio < 2, and smoothness < 10%.

The point x, y, z morphological data were projected onto the model grids using triangular interpolation. Ten σ-layers described the vertical grid with increasing resolution towards the bed. Logarithmic layer distribution was used to adequately resolve velocity shear near the bed. As a result, the layers close to the bed had a vertical resolution in the order of tens of centimeters.

4.2.3 Model calibration

A 3D hydrodynamic simulation was performed according to equations 4.1 - 4.8. The acoustic Doppler current profiler (aDcp) data were used for the specification of initial and boundary conditions. The hydraulic boundary conditions were as follows: inflow condition was specified for the upstream and the water level was set at the downstream boundary. The boundaries were located far enough from the area of interest so that small errors in the boundary conditions do not significantly influence the model results. Both the boundary conditions were fixed

during the whole simulation. This implies that these boundary conditions also served as initial conditions for model run. Additionally, a logarithmic velocity profile was prescribed at the inflow boundary.

Since the spatial resolution was much finer at some locations, the smallest grid cells determined the maximum applicable time step. A 6s time step was found to be sufficient enough for the accuracy and stability of the model as evaluated by the Courant criterion. The model started with a real measured bathymetry. Therefore, the model required a spin-up period of 30 minutes for a complete adaptation of the hydrodynamic simulation to the dynamic boundary conditions (Leonardi et al. 2013). A simulation period of 120 minutes was found to be long enough for a disturbance to damp out and for the different parameters to reach their equilibrium values.

The hydrodynamic model needs a specification of the eddy viscosity and diffusivity to resolve the turbulent scales of motion (van der Wegen et al. 2011). In Delft3D the horizontal eddy viscosity is assumed to consist of three parts: sub-grid scale horizontal eddy viscosity, background horizontal eddy viscosity (user-specified), and kinematic viscosity of water (Deltares 2014). Similarly, horizontal eddy diffusivity is assumed to be a superposition of sub-grid scale horizontal eddy diffusivity, background horizontal eddy diffusivity (user-specified), and molecular viscosity of water. The hydrodynamic parameters such as horizontal eddy viscosity and diffusivity to be used in the simulations depend on the flow and the grid size (Hasselaar 2012). For the horizontal, a background value for both the eddy viscosity and diffusivity of 2.25 m^2 s^{-1} were used. The vertical eddy viscosity (and diffusivity) is the maximum of the user-specified background value and the calculated value from the turbulence model (Deltares 2014). In the vertical, the k-ε turbulence closure model was used with a background value for both the eddy viscosity and diffusivity of 10^{-4} m^2 s^{-1}. High values (~ 10^{-4} m^2 s^{-1}) are indicative of strongly coupled flows.

In 3D computations, the bed shear stress is related to the current in the first layer (Sandbach et al. 2012, Mousavi et al. 2012). A higher resolution near the bottom is necessary to adequately resolve the logarithmic profile of the horizontal velocity components in the vertical (Borsje et al. 2011, van der Wegen & Roelvink 2008). Since a logarithmic layer distribution was adopted, the layer thickness, for instance at the deepest locations, varied from 1.8 m at the surface to 0.225 m near the bottom. Following Parsapour-Moghaddam & Rennie (2015), equation 4.8 was applied to compute a 3D Chézy roughness in Delft3D. The bed roughness length (z_0) is related to the effective bed roughness height of Nikuradse (k_s) by $z_0 = k_s / 30$ (Sandbach et al. 2012). The bathymetric profiles show that dunes are the predominant bedform in the Dhaleshwari River and these are evident even at low flow stages (see Figure 4.5). Supposing bedforms are sub-grid and thus captured by the bed roughness parameter, a uniform k_s of 0.15 m was used in the modelling.

Model grid points and bins of the aDcp data were not coincident which made statistical comparison between aDcp data and numerical model results difficult. Therefore, the model was calibrated by visually comparing simulated results and aDcp data. For this purpose, downstream velocities and secondary circulation were extracted from the 3D model at the same location that they were observed. The calibration started with the adjustment of the primary velocity distribution. Next the pattern of the secondary circulation was adjusted so that the

modelled secondary circulation patterns resemble roughly the distribution of those measured, characterized by outward-directed flow near the surface and inward-directed flow near the bed – a sign of secondary circulation. During the calibration process, the sequence of varying the parameter values started with the most sensitive parameter and ended with the least sensitive parameter. Preliminary model runs showed that reasonable results can be obtained by tuning roughness and eddy viscosity. First, the bed roughness was tuned followed by the eddy viscosity.

Figure 4.8 shows the results of the simulation. Although the model does not correctly predict the near-bed velocities near the outer bank, it is fairly accurate in predicting velocities in the upper part of the water column. In summary, the application of a calibrated 3D hydrodynamic numerical model that captures primary and secondary circulation is possible. The agreement between observed and modelled hydrodynamics makes this application a tool to investigate bed level changes in the study area.

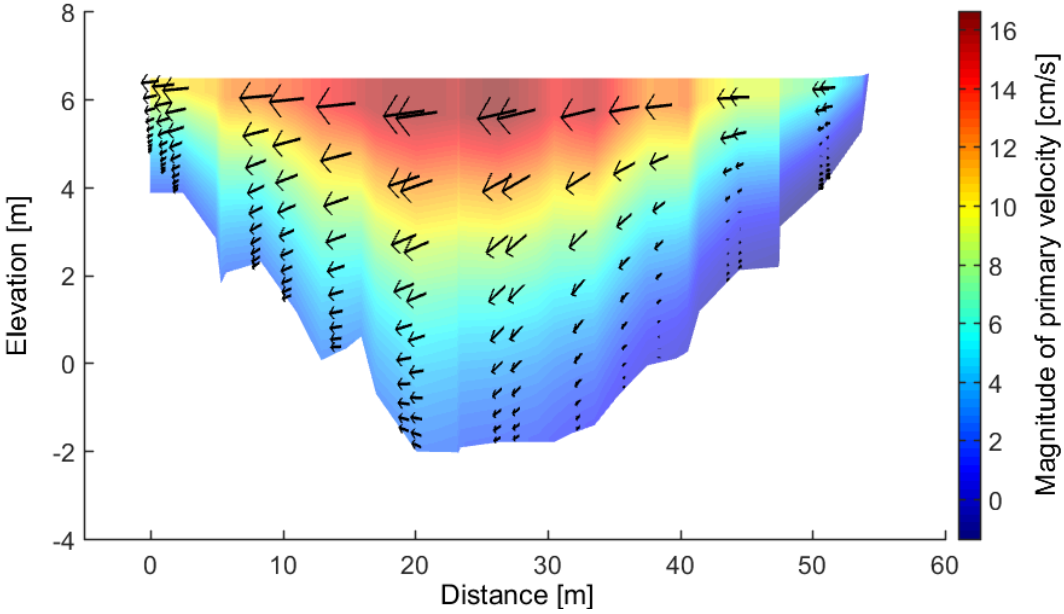

Fig. 4.8 *Secondary circulation (vectors) overlaid on the streamwise velocity (contours) in the same section as observed (Fig. 4.7), but obtained from the model. The cross-section is viewed looking downstream with left bank (outer bank) on the left-hand side.*

4.2.4 Prediction of bed level changes

The bed level was predicted after one year of morphodynamic computation. For this purpose, the model was forced with a combination of discharge and water level boundary conditions. Following the methodology of Huthoff et al. (2010), a simplified discharge hydrograph was constructed from measured discharge time series between 2003 and 2013. The measured data were averaged over intervals of approximately 10 days. Consequently, 36 of these intervals formed a characteristic year. Since there were no gauging stations in the study area, a discharge rating curve at the downstream end of the reach was constructed by performing depth-averaged 2D hydraulic calculations based on the stage-discharge relationship at Taraghat gauging station (137A) (described in Section 4.3.2.2). The synthetic annual hydrograph (also known as “stepped 10-day Q” hydrograph) was set at the upstream and the corresponding water levels were specified for the downstream (see Figure 4.9).

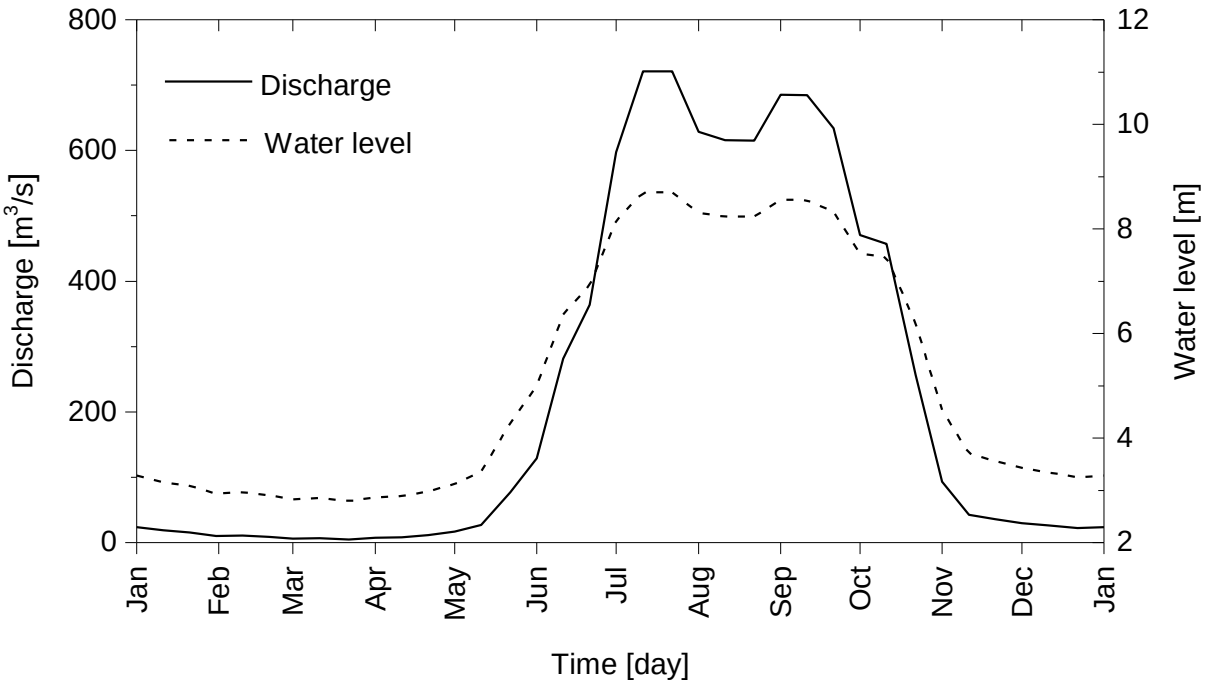

Fig. 4.9 Boundary conditions for the simulations.

The sediment was uniform fine sand (D_{50} = 0.1 mm) with a density of 2,650 kg m^{-3}. The thickness of the bed sediment layer was set to 10 m in order to guarantee enough sediment supply in case of strong local erosion. Van Rijn's formulations were applied for the calculation of suspended and bed load transport (equations 4.18 - 4.26). Sediment transport boundary conditions were in equilibrium. Sediment transport was only calculated above threshold water depths of 0.1 m. The spin-up interval before morphological change was set to 6 hours. The factor for erosion of adjacent dry cells (*ThetSD*) was set to 1 in order to avoid unrealistic scouring in the wet grid cell close to the dry banks. A morphological scale factor (*MORFAC*) of 61 was applied for the acceleration of bed level changes during updates at each hydrodynamic time step. This means that the hydrodynamic run of 6 days is amplified to represent a morphodynamic run of a one year period.

Two test runs were carried out for the period from 1 December 2014, through 1 December 2015. In the first test run, the calibration factors for longitudinal and transverse bed slope effects were set equal to 1 and 1.5 respectively (Delft3D default values). The second run was intended to test the sensitivity of the calibration factors for bed slope effects on the model results, and therefore, longitudinal and transverse bed slope factors were increased respectively from 1 and 1.5 to 10 and 15. Figure 4.10 shows the cross-sectional morphological changes 4.8 km downstream of the upstream boundary, using all parameter settings discussed above.

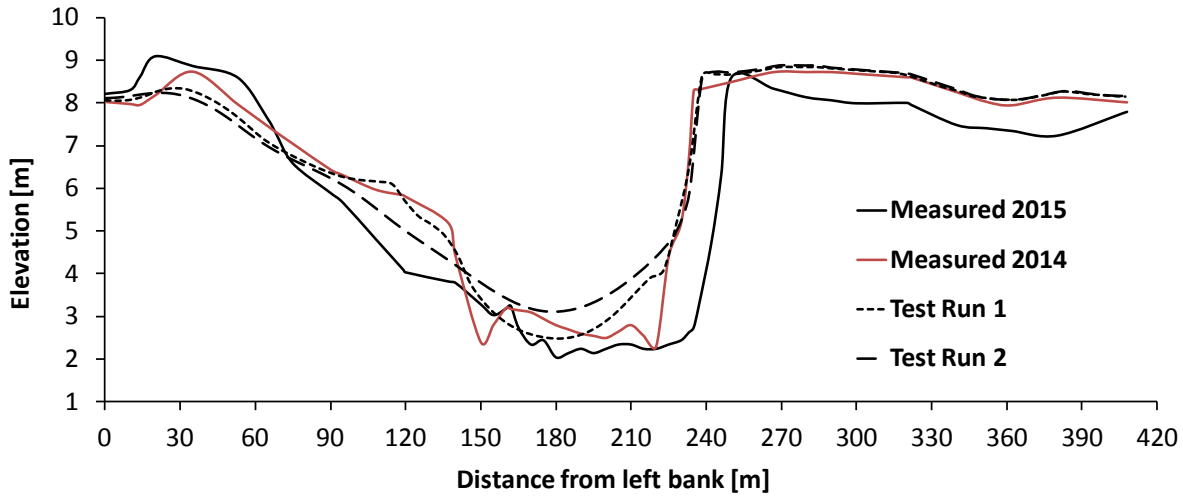

Fig. 4.10 *Measured and computed bed profiles. The cross-section is viewed looking downstream with left bank on the left-hand side.*

4.2.5 Statistical comparison

Although visual comparison of model results to a real bathymetry can be useful to assess model performance, it lacks an objective criterion (van der Wegen et al. 2011). The Brier Skill Score (BSS) is a common approach to determine the accuracy of the prediction compared with a reference case (the initial bathymetry in this case). More explanation of BSS's application in morphodynamic modelling is available in the literature (Walstra et al. 2006, Cronin et al. 2009, Chu et al. 2011, 2013, Dam et al. 2013). Van Rijn et al. (2003) introduced the following relation to compute the BSS for morphological models:

$$BSS = 1 - \frac{\left\langle \left(Y - X\right)^2 \right\rangle}{\left\langle \left(Z_i - X\right)^2 \right\rangle} \tag{4.35}$$

in which, X = computed bed level (m), Y = measured bed level (m), Z_i = initial bed level (m) and the $\langle\ \rangle$ denote the arithmetic mean.

A more comprehensive definition of the BSS is given by Sutherland et al. (2004):

$$BSS = \frac{\alpha_e - \beta_e - \gamma_e + \varepsilon_e}{1 + \varepsilon_e} \tag{4.36}$$

in which

$$\alpha_e = r^2_{Y'X'} \tag{4.37}$$

$$\beta_e = \left(r_{Y'X'} - \frac{\sigma_{Y'}}{\sigma_{X'}} \right)^2 \tag{4.38}$$

$$\gamma_e = \left(\frac{\langle Y' \rangle - \langle X' \rangle}{\sigma_{X'}} \right)^2 \tag{4.39}$$

$$\varepsilon_e = \left(\frac{\langle X' \rangle}{\sigma_{X'}} \right)^2 \tag{4.40}$$

where r = correlation coefficient, σ = standard deviation, $X' = X - Z_i$ and $Y' = Y - Z_i$. The parameter α_e is a measure of bedform phase error and perfect modelling gives α_e = 1. The value β_e is a measure of bedform amplitude error and perfect modelling gives β_e = 0. The parameter γ_e is a measure of an average bed level error and perfect modelling gives γ_e = 0. ε_e is a normalization term that indicates the measurement error.

The BSS classification according to van Rijn et al. (2003) and Sutherland et al. (2004) are shown in the following table.

Tab. 4.1 BSS classification according to van Rijn et al. (2003) and Sutherland et al. (2004).

Classification	$BSS_{van\ Rijn}$	$BSS_{Sutherland}$
Excellent	1.0 – 0.8	1.0 – 0.5
Good	0.8 – 0.6	0.5 – 0.2
Reasonable/Fair	0.6 – 0.3	0.2 – 0.1
Poor	0.3 – 0.0	0.1 – 0.0
Bad	< 0.0	< 0.0

The statistical method Brier Skill Score (*BSS*) (van Rijn et al. 2003, Sutherland et al. 2004) was employed to compare predicted morphologies. The BSS reflects how good the model results are in comparison to the observed change (Dam et al. 2013). Table 4.2 shows decomposition terms (α_e, β_e, γ_e and ε_e) of Sutherland et al. (2004) and the estimated BSS values for the two simulations using both methods.

Tab. 4.2 BSS values for the two test runs according to van Rijn et al. (2003) and Sutherland et al. (2004).

Case	$BSS_{van\ Rijn}$	$BSS_{Sutherland}$				
		α_e	β_e	γ_e	ε_e	BSS
Test Run 1	0.17	0.02	0.04	0.41	0.56	0.17
Test Run 2	0.20	0.11	0.04	0.33	0.56	0.20

The model has a skill score of 0.20 and can be qualified as reasonable/fair according to Sutherland et al. (2004). A BSS of 1 indicates the perfect modelling result, whereas lower values suggest less adequate modelling (Van der Wegen et al. 2008). Therefore, it is meaningful to identify the origin of a score of 0.20 in order to improve the predictions. The decomposition terms in Table 4.2 suggest that the low BSS may be attributed to a weak score of α_e (perfect modelling gives α_e = 1). The parameter α_e is a measure of bedform phase error and the BSS is degraded by a shift in location of the morphologic feature. Another source of er-

ror, to a lesser extent, originates from the high γ_e value (perfect modelling gives γ_s = 0). The parameter γ_e is a measure of an average bed level error and the high γ_e value reduces BSS by deviating the predicted average bed level from the measured.

4.2.6 Discussion

A 3D model generates a complete and detailed picture of the flow field. In many verification studies of morphodynamic models there is often a tendency to focus on the bed evolution only, without providing information on the reliability of secondary flow, mainly because secondary flow data are often lacking (Banda et al. 2016). Furthermore, it is usually preassumed that the model generates necessary secondary flow in meander bends to control sediment transport (Parsapour-Moghaddam & Rennie 2014). In the present study, the 3D model was calibrated against measured three-dimensional flow data at a meander bend, and then the model was used for predicting bed level changes over a one-year period. The simulated morphological changes showed a certain degree of resemblance with the available field data, as evaluated by the Brier Skill Score (see Table 4.2 and Section 4.2.5).

Parameterization of the bed slope effect introduces major uncertainty in predicted bed topography (Leonardi et al. 2013, Kasvi et al. 2015). Two tuning parameters are implemented in Delft3D in order to adjust the bed-load transport for bed-slope effects. Ikeda (1982) suggested a value for transverse bed slope factor of 1.5 based on small-scale experiments, however, other studies documented an increased value from 1.5 to 10 (Van der Wegen et al. 2011) to 50 (Dissanayake 2011) to 80 (Lesser et al. 2004) in order to obtain reasonable results in long-term morphological simulations. In the present study, the statistical comparison (i.e., Brier Skill Score) of the simulations, with and without changing tuning parameters for bed-slope effects on bed-load transport, showed that default parameterization of the bed slope effects led to a lower skill score (BSS = 0.17). Increasing bed slope factor values result in higher BSS score, which indicates that the parameterization of the bed slope effect is necessary for simulating morphological changes in meandering rivers. The results of the simulations are in agreement with the general conclusions made by Schuurman & Kleinhans (2013, 2015). It should be noted that the required computational time prevented further analyses. In fact, the numerical simulation is rather ambitious for application of a full 3D model, as demonstrated by the lack of previous simulations at the scale and degree of complexity of the reach examined in the study. In this respect, 3D numerical model should be evaluated with consideration of the respective computational effort and the gain achieved in the predictability of the model.

4.3 2D morphological modelling

A depth-averaged 2D numerical model, which is implemented in Delft3D, is applied to investigate the morphodynamic processes in the case study area (Dhaleshwari River, Bangladesh). Before the 2D morphological modelling is described, an investigation for the suitability of the depth-averaged 2D approach to model flow in a curved channel in the Leichtweiß-Institute for Hydraulic Engineering and Water Resources (LWI) at the Technische Universität Braunschweig (Germany) is presented (Section 4.3.1). The effect of the three-dimensional flow in a channel bend is parameterized in the 2D approach. Both 2D and 3D models are compared with experimental data acquired in the curved flume. The validated 2D model is then applied to simulate bed topography and meander planform evolution in the case study area (Dhaleshwari River, Bangladesh) over a 10-year period under bankfull discharge condition (Section 4.3.2). A sensitivity analysis is carried out to increase the understanding of the impact of various sediment-related parameters on the simulation results. Finally, simulated planform is studied using planform variables.

4.3.1 Modelling of curved channel flow

Delft3D is implemented to perform 2D and 3D simulations to test the suitability of 2D simulations in comparison to 3D simulations. For this purpose, Delft3D is implemented to simulate flow fields over the flat fixed-bed configuration of a curved flume studied at LWI for which detailed velocity measurements are available. Both 2D and 3D hydrodynamic models are investigated. In addition, taking into account a predicted deformed fixed-bed configuration, 2D and 3D simulation results are compared with each other.

4.3.1.1 Experimental setup

The experimental channel was 2.4 m wide and 26.26 m long with a longitudinal slope of 0.001 m m^{-1}. The banks were vertical and non-erodible. Figure 4.11 shows the schematic view of the double curved S-flume with its dimensions. Zaid (2018) presented detailed 3D flow measurements in the first bend under flat smooth bed conditions. The laboratory experiments were performed with a steady discharge of 0.136 m^3 s^{-1} and the average water depth was 0.1 m. This corresponds to a width-depth ratio of approximately 24, coming close to the conditions of natural meandering streams (Riesterer et al. 2016). Three dimensional flow velocities were measured at 1, 2, 3, 4, and 5 cm above the bed along selected sections of the curved channel using an acoustic Doppler velocimeter (Nortek Vectrino Plus). Detailed information on the experimental setup can be found in the literature (Zaid & Koll 2016).

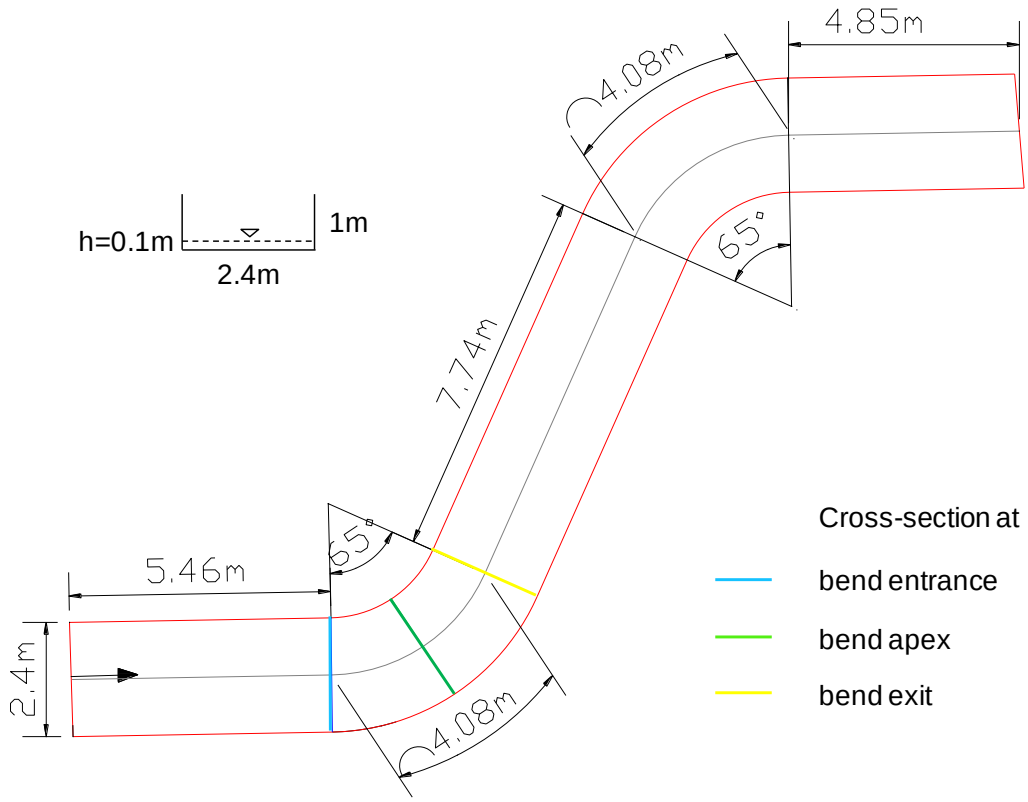

Fig. 4.11 Experimental installation (Zaid & Koll 2016).

4.3.1.2 3D numerical model setup for flat fixed-bed

Grid and bathymetry

In the numerical model a straight inflow section of 2.4 m, a curved section of 65° and a straight outflow section of 3.6 m, as shown in the lower part of Figure 4.11, were implemented with boundary conditions reflecting the experimental setup. The flow domain was defined by an orthogonal curvilinear mesh with a grid size of 0.1 m in the transversal direction and a variable size (0.1 to 0.24 m) in the flow direction. Following the experiments, non-erodible smooth bed and walls were applied. Bathymetry data was projected onto the curvilinear grid, and then linear interpolation was performed to obtain grid-point values. 10 σ-equidistant layers described the vertical grid resolution. The time step of the flow was 0.75 seconds to ensure numerical stability as evaluated by the Courant criterion.

Model calibration

A three-dimensional hydrodynamic simulation was performed according to equations 4.1 - 4.8. The imposed boundary conditions were upstream flow discharge and a constant water level specified for the downstream boundary. The discharge was 0.136 $m^3\ s^{-1}$ and the downstream water depth was 0.1 m. Turbulence closure was achieved by applying a constant background horizontal eddy viscosity (0.008 $m^2\ s^{-1}$) and diffusivity (10 $m^2\ s^{-1}$) (see Section 4.2.3). In the calibration process, for optimizing the agreement between measured and modelled streamwise velocities along the centerline of the flume, Manning's roughness n value was adjusted to 0.008 $s\ m^{-1/3}$, which corresponds to the flat smooth bed conditions. Figure 4.12 shows that the model computes logarithmic velocity profiles in the vertical direction reasonably well.

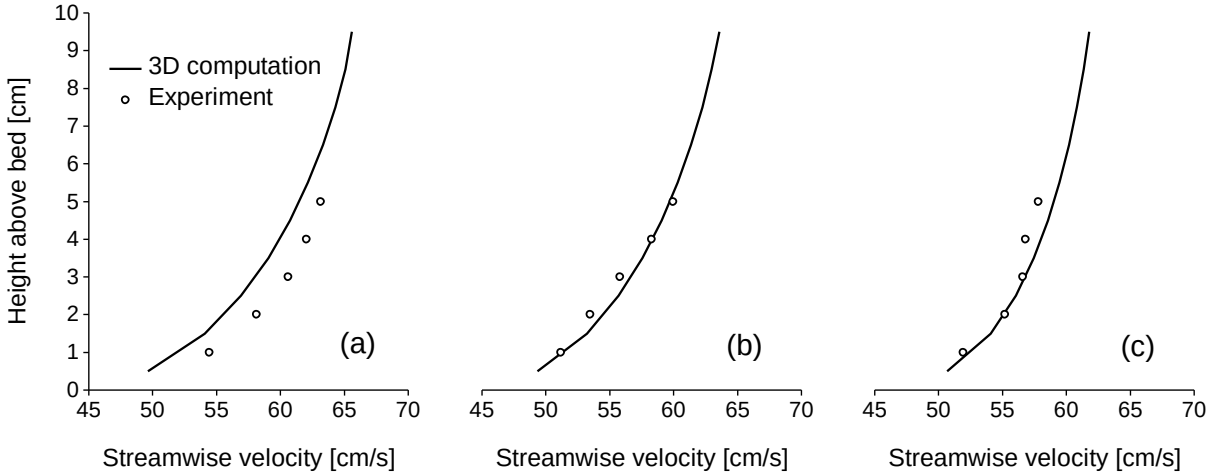

Fig. 4.12 Comparison of computed and measured velocities along the centerline of the flume at (a) bend entrance, (b) bend apex and (c) bend exit.

4.3.1.3 2D numerical model setup for flat fixed-bed

The 3D calibrated model, developed in the previous section, was run in depth-averaged 2D mode (equations 4.9 - 4.17). It should be noted that no further calibration was performed by varying bed roughness. Instead, a parameterization for secondary flow, which is the characteristic for curved channels, was used. The so-called “dispersion terms”, which result from the difference of the depth-averaged velocity and vertical varying velocity, were used to model the secondary flow effect in the depth-averaged 2D hydrodynamic model. For this purpose, secondary flow correction factor (β_c in equation 4.14) was adjusted to 1.

4.3.1.4 Comparison of 3D and 2D simulation results for flat fixed-bed

Comparison of depth-averaged streamwise velocity

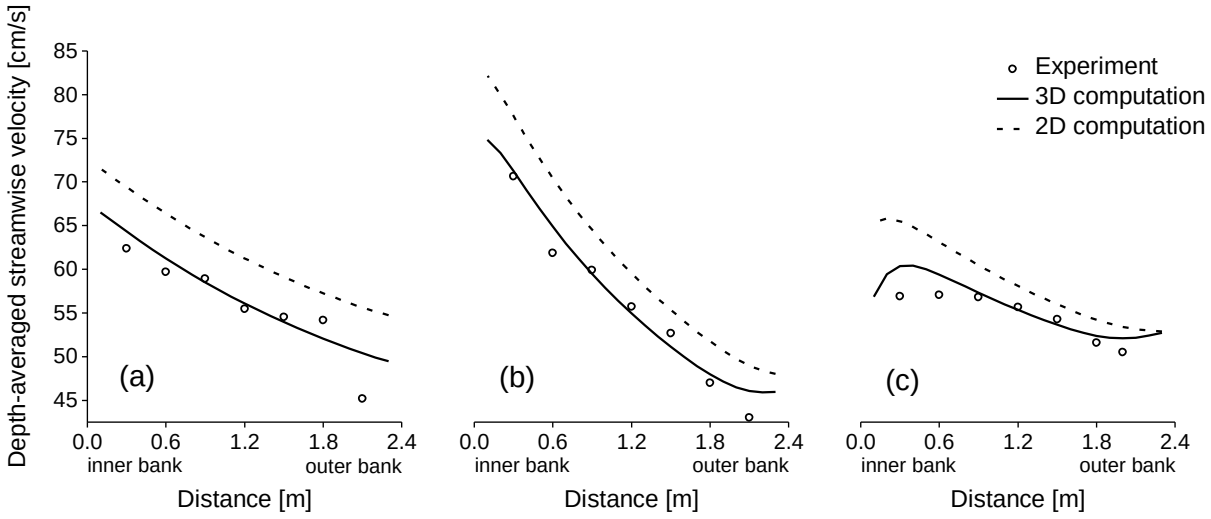

Fig. 4.13 Comparison of experimental values of depth-averaged streamwise velocity with 3D and 2D simulations at (a) bend entrance, (b) bend apex and (c) bend exit.

Figure 4.13 (a, b, c) indicates that both 3D and 2D computations show a similar tendency, that means, larger velocity near the inner bank region and smaller velocity near the outer

bank region. The results show that depth-averaged streamwise velocities are well reproduced by both 3D and 2D computations and the difference is less than 8%.

Comparison of bed shear stress

Within the experiment, the “experimental” pattern of the bed shear stress was estimated by fitting a log law to the measured near-bed velocity profile (Whiting & Dietrich 1990). As expected, the highest bed shear stresses were found near the inner bank around the bend apex. The comparison between numerical simulations and experimental data shows that boundary shear stresses, which are the most important agent affecting morphological changes, are well simulated with a 2D implementation of the numerical model.

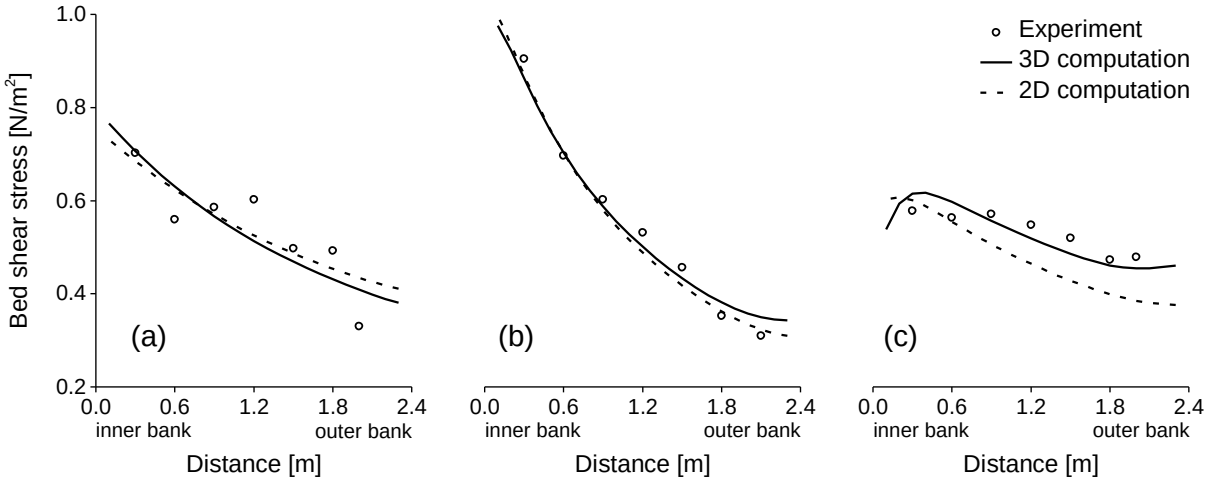

Fig. 4.14 *Comparison of experimental values of bed shear stress with 3D and 2D simulations at (a) bend entrance, (b) bend apex and (c) bend exit. The experimental values of the bed shear stress were estimated by fitting a log law to the measured near-bed velocity profile (Whiting & Dietrich 1990).*

4.3.1.5 Numerical model setup for deformed fixed-bed

The laboratory open-channel bend, reported in the previous section, does not represent open-channel bends found in the nature because of its flat-smooth bed configuration. There is no experimental data in the flume with movable bed. To obtain a deformed bed, the 3D calibrated model was run under mobile bed conditions, and fixed channel walls were applied by default. The median diameter of the bed sediment was 0.2 mm. At the inflow boundary, the amount of sediment inflow was equal to the local sediment transport capacity. Sediment transport was predicted by the van Rijn approach (equations 4.18 - 4.26). Computation of morphodynamics included the necessary bed slope effects on morphology (equations 4.30 - 4.34) and were performed until equilibrium conditions were achieved where the rate of bed level change with time was statistically constant. Secondary flow induced by channel curvature was found to strongly influence the bend morphology. Starting from a flat bed, a bed topography with a scour at the inner bank region and deposition at the outer bank region formed. The predicted bed topography is shown in Figure 4.15(a). The bed level changes of a typical cross-section at the bend apex is shown in Figure 4.15(b) in which the main channel shifted towards the inner bank as the sand bar developed progressively at the outer bank.

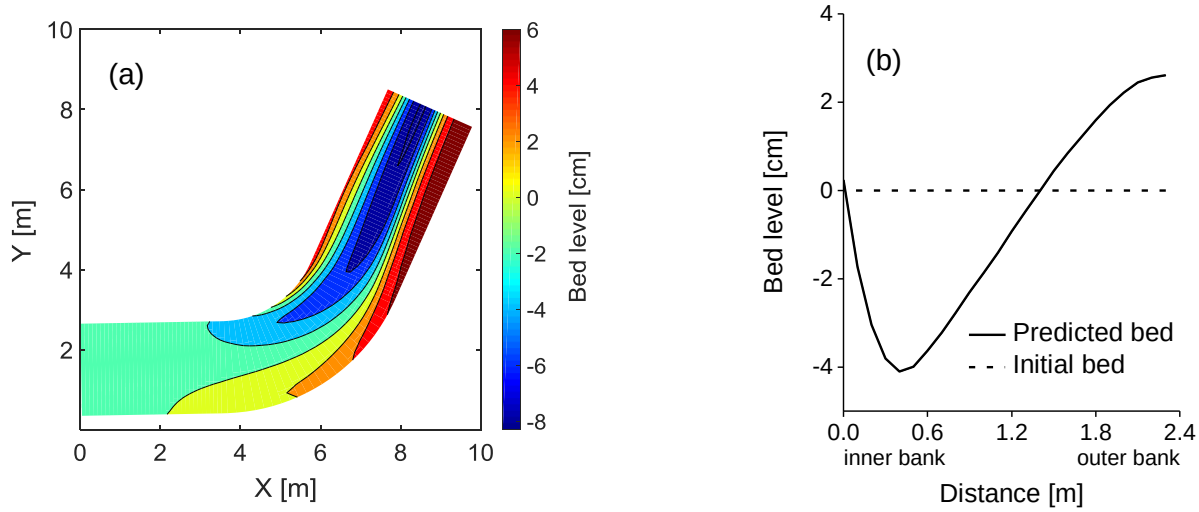

Fig. 4.15 *(a) Predicted bed topography and (b) predicted bed changes of a typical cross-section at the bend apex as shown in Figure 4.11.*

The predicted deformed bed, as shown in Figure 4.15(a), was fixed for the subsequent runs. The same simulations as in the previous section were repeated taking into account the deformed fixed-bed.

4.3.1.6 Comparison of 3D and 2D simulation results for deformed fixed-bed

Comparison of depth-averaged streamwise velocity

The comparison of depth-averaged streamwise velocity between 3D and 2D computations for the deformed fixed-bed is shown in Figure 4.16. It is interesting to note that the difference between 3D and 2D model results became smaller than the results under flat fixed-bed conditions, now remaining below 6%.

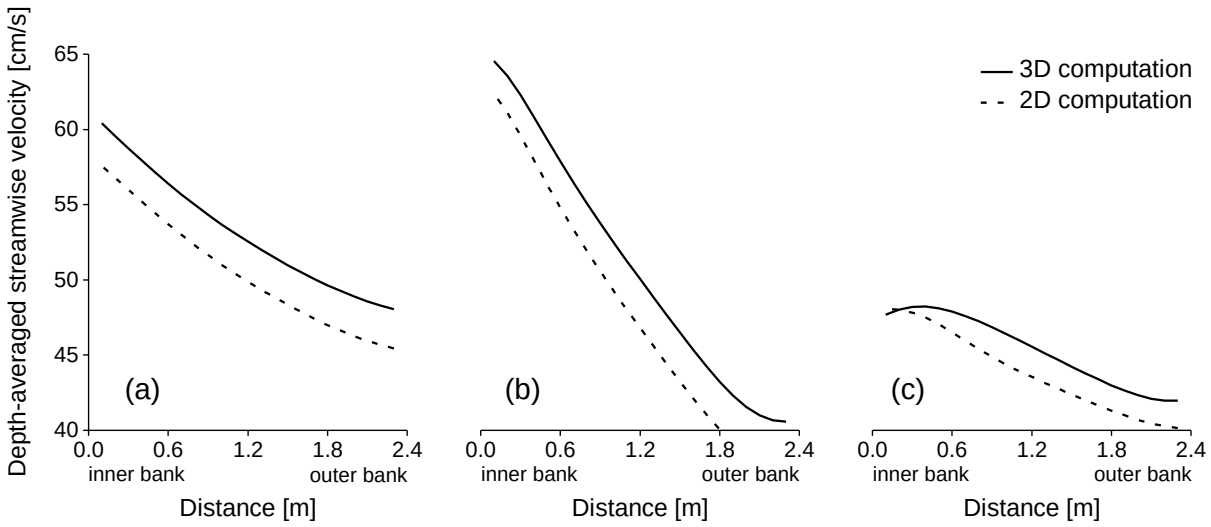

Fig. 4.16 *Comparison of depth-averaged streamwise velocity between 3D and 2D simulations at (a) bend entrance, (b) bend apex and (c) bend exit.*

Comparison of bed shear stress

The comparison of bed shear stress between the 3D and 2D models for the deformed fixed-bed is shown in Figure 4.17. The three-dimensional computation resulted in slightly larger bed shear stress values compared with the depth-averaged computation. The average

differences between the 3D and 2D model results were 0.05, 0.07 and 0.08 N m^{-2} at the bend entrance, bend apex and bend exit, respectively.

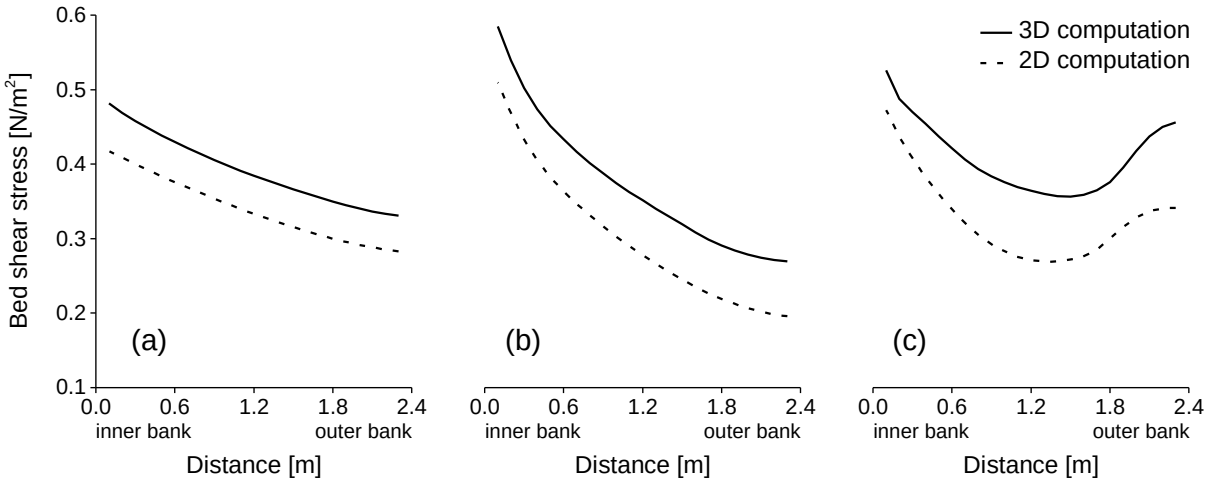

Fig. 4.17 Comparison of bed shear stress values between 3D and 2D simulations at (a) bend entrance, (b) bend apex and (c) bend exit.

The analysis of the spatial distribution of bed shear stress was carried out by the difference model, in which the bed shear stress contours represent the difference between the bed shear stress distribution predicted by 3D and 2D computations (see Figure 4.18). As depicted in the plan view of the bed shear stress distribution, overall agreement is good under a flat fixed-bed as well as a deformed fixed-bed conditions. The results indicate that the qualitative behaviour of bed shear stress is essentially unchanged. No important differences were found between 2D and 3D computations in both cases.

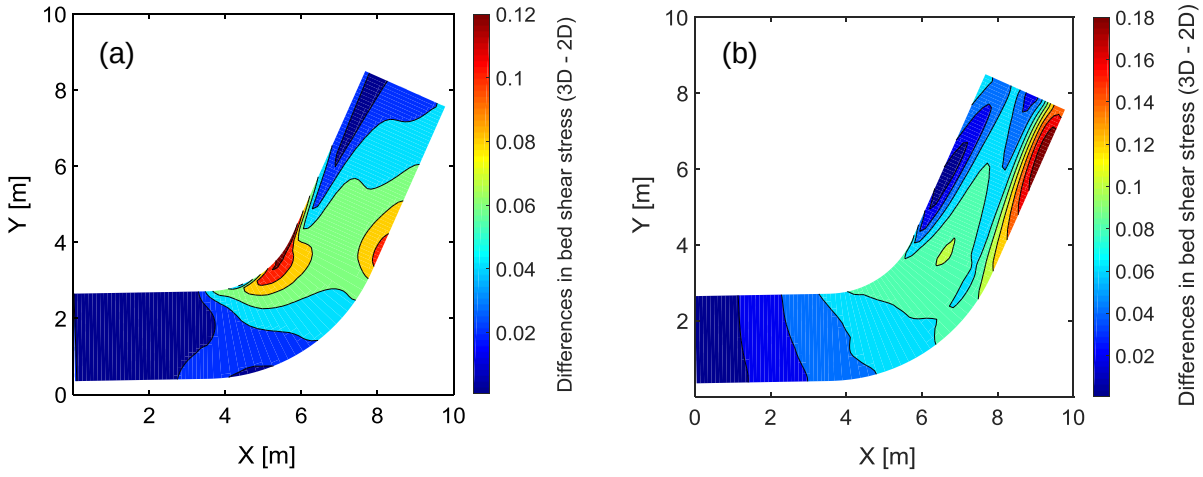

Fig. 4.18 Plan view of the bed shear stress distribution by the difference model (a) flat fixed-bed and (b) deformed fixed-bed.

4.3.1.7 Suitability of depth-averaged 2D simulations

The hydrodynamic module of the numerical model Delft3D was implemented to perform 2D and 3D simulations. The effect of spiral flow was parameterized in the 2D model by means of a secondary flow model (equations 4.9 – 4.17). Both 2D and 3D models were investigated, using both flat fixed-bed and deformed fixed-bed conditions. The two models were compared with experimental data in a flat-bed curved flume. The results of the simulations show that

depth-averaged streamwise velocities were well reproduced by both 2D and 3D computations. Boundary shear stresses, which are the most important agent affecting morphological changes, were also well simulated with a 2D implementation of the numerical model. The differences between 2D and 3D results with deformed fixed-bed were more or less similar to the differences between 2D and 3D results with flat fixed-bed.

The analysis of the simulation results further reveals that a depth-averaged 2D hydrodynamic model with an appropriate parameterization of secondary flow effect (i.e., secondary flow correction) leads to reasonable predictions of the velocities and bed shear stresses in curved channels. The results of the simulations are in agreement with those reported in the literature (Hsieh & Yang 2003, Qin et al. 2016, Guan et al. 2016, Riesterer et al. 2016). The simulation results are strongly relevant for practical purposes, because a 2D simulation has less complexity that reduces simulation time to a large extent in comparison to a 3D simulation. Since this flume experiment involved a fixed-width channel, it should be noted that these results relate only to changes made to the flow sub-model. Therefore, the findings of this study should be tested in natural scenerios under different hydrodynamic and morphodynamic regimes.

4.3.2 2D modelling of river morphological changes

An application of the depth-averaged 2D morphological model to the case study (Dhaleshwari River, Bangladesh) is presented. In the depth-averaged 2D model, the parameterization of the secondary flow is based on the results of the curved laboratory flume case study (see Section 4.3.1). The present case study is an important supplement to the fixed-width flat-bed curved flume experiments presented in the previous section, because the studied reach has undergone a sequence of channel evolution that includes bank erosion and planform changes, providing an opportunity to evaluate these aspects of the numerical model. The objective is to demonstrate that a 2D numerical model of a deformable meandering channel can simulate the long-term evolution of river planform and bed morphology. An advantage in using a 2D model is that the computational time is at least an order of magnitude shorter than a fully 3D model. This section describes the depth-averaged 2D model schematization, calibration and validation. A sensitivity analysis is carried out to increase the understanding of the impact of various user-specified parameters on the simulation results. Finally, simulated planform is studied using the parameters which are frequently applied in analogous studies.

4.3.2.1 Model setup

The depth-averaged 2D model was preferred because the Dhaleshwari River is relatively wide and shallow, and the flow field is mainly developed in the horizontal direction. Furthermore, with appropriate parameterization, the effects of secondary flow and bed slope effects on bed-load transport can also be incorporated into the depth-averaged 2D model (see Section 4.3.2.3).

Grid

The modelled reach was 51.5 km long and stretched from Elashin gauging station (68A) to Taraghat gauging station (137A) (see Figure 3.2). The channel banklines were digitized from a satellite image, dated to June 2003 (source: Google Earth). The delineation of the active banks followed the criteria used in the analysis of the bankfull width (see Section 3.3.2). The digitized lines were projected onto the Bangladesh Transverse Mercator (BTM) coordinate system and post-processed in Geographic Information Systems (GIS). Floodplains were added on each side of the channel in the study area (from river kilometer 21.44 to river kilometer 29.64) (see Figure 4.19). The width of the floodplains was 700 m on both sides of the channel. This floodplain barely needs to be broad enough for the migrating river not to reach the outer edge of the domain, as this would result in very deep channels resting up against the boundary (Vested et al. 2014). It should be emphasized that the only purpose of the 51.5 km long model was to generate the hydraulic boundary conditions for a shorter model (described in Section 4.3.2.3) that merely represents the study area.

Once the geometry had been defined, the computational mesh was constructed independently in a curvilinear coordinate system as the meandering planform is best described in the curvilinear coordinate. The advantage of this approach is that the grid cells follow the natural curved geometry of the river. However, the complex planimetric channel shape required the use of variable cell sizes. Grid schematizations were in general a trade-off between the processes to be modelled and computational time. The geometry of the main

channel was discretized into 831 cells in the streamwise direction and 10 cells in the transverse direction. The average length of the grid cells was 60 m. The width of the cells was about 27 m so that the bankfull channel width becomes 270 m. Each floodplain was discretized into 140 cells in the streamwise direction and 25 cells in the transverse direction. On average, cells were between 1 m and 180 m in length and 28 m in width. The resolution varied between 6 m in the inner concave boundary area and 78 m in the convex boundary area. This scale of resolution was selected to be neither too coarse to capture features such as bars, nor too fine that computational time is too high.

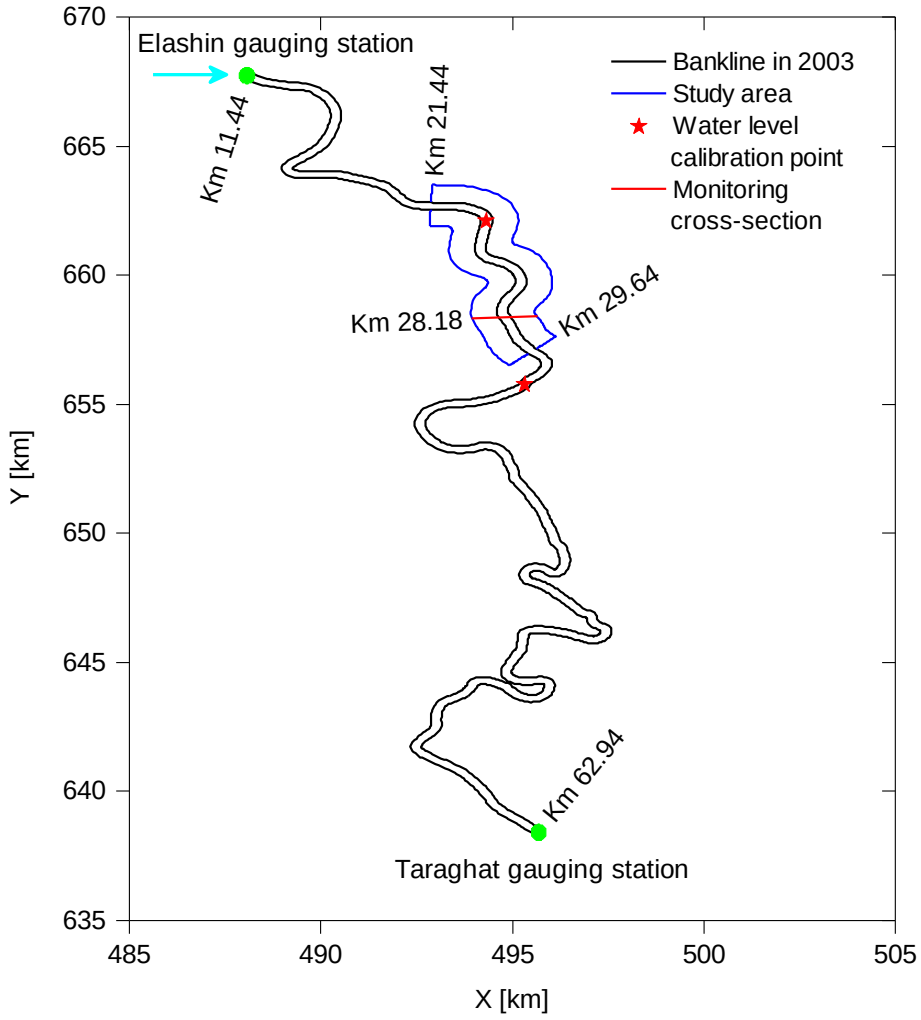

Fig. 4.19 Map of the study area.

The quality of the final grid was determined by its orthogonality, smoothness and aspect ratio. The grids were orthogonalized as much as possible in an automated procedure minimizing deviations from orthogonality of adjacent cell midpoints. Difference between successive grid cell dimensions (referred to as smoothness) was less than 10% in the main channel and 25% in the floodplains. Ratio of grid cell dimensions in longitudinal and transverse direction (referred to aspect ratio) was kept around 2 in the main channel, as the flow was predominantly in streamwise direction.

Bathymetry

The underlying model bathymetry was an approximation of the river topography as it was based on measurements of discrete cross-sections provided by the Bangladesh Water Development Board (see Section 3.4.3). The reach was surveyed at eight cross-sections during April 2003. Topographic information was projected onto the curvilinear grid, and then linear interpolation was performed to obtain grid-point values. This resulted in the initial digital elevation model (DEM), with less distinct gradients in pool and riffle morphology. Despite the lack of detailed bathymetric information, the DEM was considered suitable for the application as the spatial-temporal scales were relatively large (51.5 km and 10 years, respectively). Furthermore, local differences between the real and the modelled bathymetry have relatively small influence on meander morphology in longer-time scales, as pointed out in other morphological modelling applications (e.g., Ziliani et al. 2013).

4.3.2.2 Hydrodynamic calibration

A depth-averaged 2D hydrodynamic simulation was performed according to equations 4.9 - 4.17. The imposed boundary conditions were upstream flow discharge and a constant water level specified for the downstream boundary. The discharge was 615 m^3 s^{-1} and the downstream water level was 6.42 m. To consider the effects of secondary currents in bends, secondary flow correction factor (β_c in equation 4.14) was set to 1. Turbulence closure was achieved by applying the default values of horizontal eddy viscosity (1 m^2 s^{-1}) and diffusivity (10 m^2 s^{-1}). The time step was 30 seconds to ensure numerical stability as evaluated by the Courant criterion. In the calibration process, the water level record in the middle of the reach was used to calibrate the hydrodynamic model. For optimizing the agreement between water surface elevations predicted by the model and those measured in the field, Manning's roughness n value was adjusted to 0.054 s $m^{-1/3}$. The average difference between predicted and observed water surface elevations was 0.06 m. It is important to remark that the relatively large extent of the model domain guarantees the absence of boundary effects in the study area. Figure 4.20 shows the comparison between measured water levels and predicted water surface elevation for the calibrated Manning's n value, and hence this value was adopted for the subsequent runs. Since there were no gauging stations in the study area, a discharge rating curve at the downstream end of the reach (river kilometer 29.64) was constructed by performing hydraulic calculations based on the stage-discharge relationship at Taraghat gauging station (river kilometer 62.94) (see Figure 4.19).

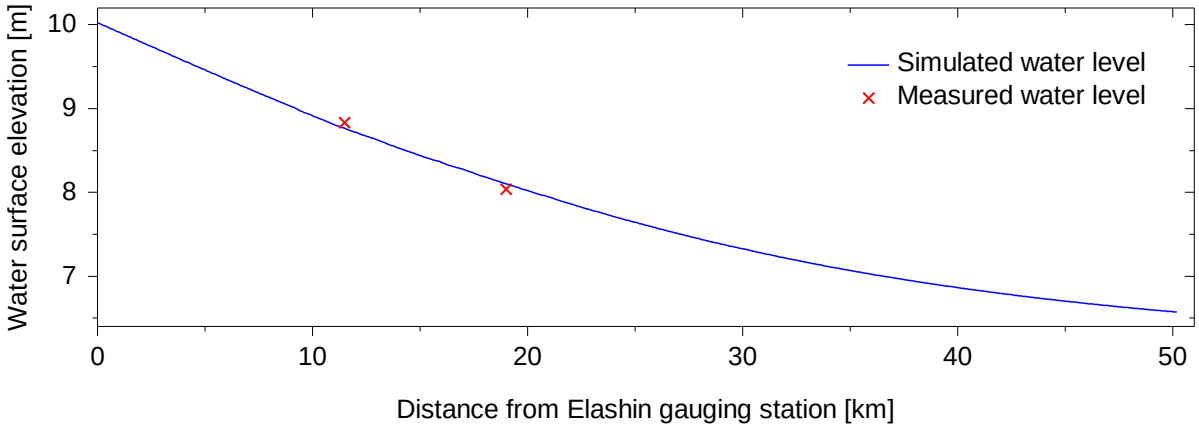

Fig. 4.20 Comparison between measured and predicted water levels.

4.3.2.3 Morphodynamic calibration

Modelling of sediment transport in a natural river is a challenging task due to scarcity of reliable field data. Moreover, a high degree of empiricism is inherent in sediment transport models (Villaret et al. 2013). A 8.2 km long river section including floodplains was used to demonstrate the morphodynamic calibration and validation of the model. This reach is 10 km downstream from the Elashin gauging station (68A) and between river kilometers 21.44 and 29.64 (see Figure 4.19). Twenty-eight simulations were run under fixed bed conditions by varying flow discharge in the range 35 - 980 m^3 s^{-1}, in which discharge was varied by 35 m^3 s^{-1}. For all simulations, discharge was specified at the upstream boundary and a corresponding water surface elevation was set at the downstream boundary. As mentioned in the previous section, in the absence of measured data, the model used a predicted stage-discharge relationship at the downstream boundary.

The sediment was assumed to be composed of uniform sand (D_{50} = 0.1 mm) with a mass density of 2650 kg m^{-3} and a porosity of 0.40. The same sediment characteristics were imposed over the entire model domain. Sediment transport was calculated above a threshold water depth (0.05 m). Grid cells with smaller water depth were considered inactive. The sediment transport rate in each grid cell was assumed to be equal to the local sediment transport capacity, computed by the Engelund-Hansen (1967) total load transport formula (equation 4.27). The sediment input at the upstream boundary was calculated at transport capacity. The bed composition at the upstream boundary was adjusted as a means of adjusting the sediment-feeding rate. Although sediment transport was not actually measured in the study reach, a comparison of results could be made considering the sediment rating curve for the Dhaleshwari River which was developed based on data measured at the Taraghat gauging station (137A) in the period 1971 - 1996 (see Section 3.4.2).

Figure 4.21 shows a comparison of results in a relatively straight river reach near the downstream boundary of the study area. The results from the simulations are the consequence of application of the aforementioned sediment transport capacity predictor combined with the hydraulic model and bed material data. It appeared that the Engelund-Hansen (1967) sediment transport formula over-estimated the measured transport rate on average by a factor 1.8. This may be considered as acceptable, considering the limitation in using an out-of-date rating curve.

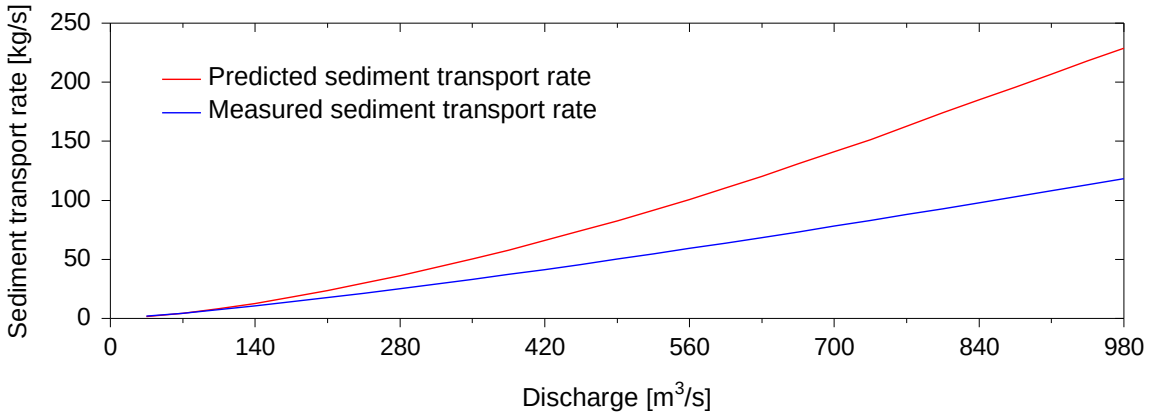

Fig. 4.21 Comparison between measured and predicted sediment transport rate.

Verhaar et al. (2008), Kasvi et al. (2015) and Guan et al. (2016) suggested that the best test for the accuracy of the sediment transport rate would be through comparison against a morphological survey of a river. To this end, the model was used to reproduce the morphological changes taking place over 10 years. This time scale was selected as it is a long period and the processes were dominated by natural evolution. The simulations started with the 2003 DEM. The model was run under mobile bed conditions for the bankfull discharge, assuming that the unsteady forcing on the river is morphologically equivalent to bankfull discharge (Schuurman et al. 2013, 2016, Bolla Pittaluga et al. 2014). The bankfull discharge was characterized by a stage corresponding to the elevation of the floodplains at the end of the reach, and equaled to 700 m^3 s^{-1}. The bankfull discharge is a good test because the entire channel was wetted.

The duration of bankfull discharge in a calendar year was necessary for the computational tests. A “stepped 10-day Q” hydrograph was constructed based on the discharge time series measured at Taraghat gauging station (137A) for the period 1979 – 2013 (see Section 3.2.2 and Figure 3.4). Discharge values less than 100 m^3 s^{-1} were excluded from the analysis, as these low flows would not lead to any morphological changes in the study area. The duration of bankfull discharge in a year was estimated to 204 days. This means that the model assumed that the annual morphological changes occur in 204 days.

The model was run for a spin-up interval of 6 hours in order to achieve a fully developed hydrodynamic state before allowing morphological changes in the bottom. At the start of the simulation, the thickness of the underlayer was 10 m in order to guarantee enough sediment supply in case of locally strong erosion. The bed level change is the result of sediment transport, secondary flow effect on bed-load transport direction, bed slope effects, bank erosion, and mass conservation in the bed. A cross-section in the more active portion of the eroding reach was selected for simulation. The cross-section, located at river kilometer 28.18 (see Figure 4.19), was deemed representative of the reach as a whole because the retreat observed at this section closely matched the mean rate of actively eroding reach. Cross-sectional measurement data in 2013 were exploited to calibrate the morphodynamic model. First, since sediment transport is proportional to the Engelund-Hansen formula, sediment transport was scaled up by 180% (α = 1.8 in equation 4.27). The magnitude was then subjected to the spiral flow. To correct the sediment transport direction, the calibration factor for spiral flow effect on bed load transport direction (E_s) was adjusted to 1.5. Second, the sedi-

ment transport rates were corrected for the sloping bed according to equations 4.30 - 4.33. The factor for transverse bed slope effects (α_{bn}) was tuned to 15.5. Third, since bank erosion algorithm is based on the distribution of the erosion between the source wet cell and the adjacent dry cell, a factor for erosion of adjacent dry cells was set to 1. This implies that all erosion that would occur in the wet cell is assigned to the adjacent dry cells. Preliminary tests runs (not shown here) suggested that the resulting morphology is relatively insensitive to the bank erosion percentage. Finally, to reduce computational time, a morphological scale factor ($MORFAC$ in equation 4.34) of 10 was used for bed level change. The effect of the chosen $MORFAC$ is that the 204 days of flow results in a morphological change representing 10 years. The equation of conservation of channel bed sediment was then solved to compute the bed level changes.

Figure 4.22 shows the results of the simulation, in which Figure 4.22(a) shows the predicted bed topography and river alignment in 2013 and Figure 4.22(b) shows the thalweg alignment. Notably, lateral channel migration increased the channel bend amplitude and channel length. As the bend amplitude increased, more of the meander bend migration was in the downstream direction, leading to the development of a more sinuous meandering thalweg as becomes visible from Figure 4.22(b). This phenomenon is similar to that observed in laboratory experiments (Friedkin 1945, Ackers & Charlton 1970, Schumm & Khan 1972, Schumm et al. 1987, Braudrick et al. 2009, Visconti et al. 2010, van Dijk 2013) and numerical modelling (Olsen 2003, Duan & Julien 2005, 2010, Rüther & Olsen 2007, Crosato & Saleh 2010, Asahi et al. 2013, Nicholas 2013, van Dijk et al. 2014, Schuurman et al. 2016, van de Lageweg et al. 2016).

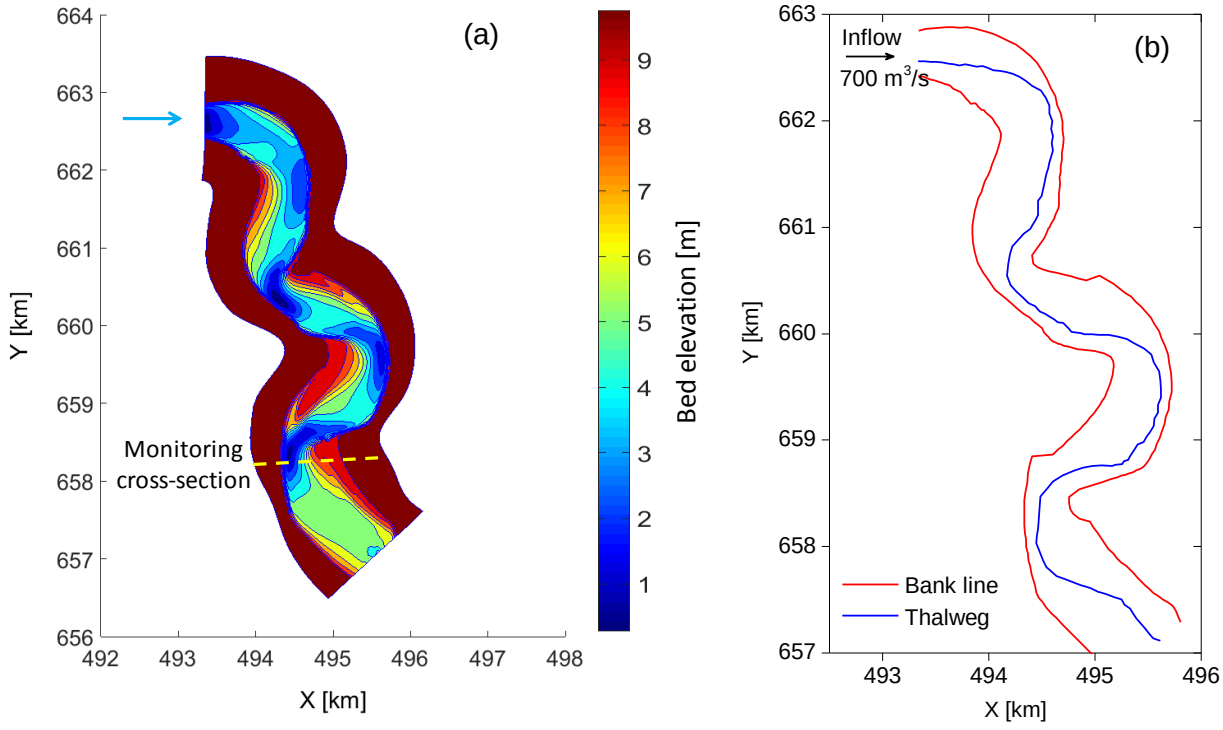

Fig. 4.22 (a) Simulated bed topography and (b) simulated bank lines and thalweg.

Figure 4.23 shows that modelled and measured bed level changes over the 10-year period generally compare rather well at the monitoring cross-section (see Figure 4.19). The modelled cross-section is asymmetric in shape with gently sloping inner banks, a deep thalweg

near the outer bank, and near vertical outer bank. The observed bank retreat of about 400 m and bank advance of about 210 m are accurately reproduced by the model. The predicted inner bank is, however, about 0.65 m shallower than measurements indicate. The reason is that the bankfull discharge, which was characterized by a stage corresponding to the elevation of the floodplains at the downstream end, became sub-bankfull flow as soon as the hydrodynamic adaptation took place with respect to the changing morpholgy. A similar outcome has been reported in recent studies that have highlighted how a formative discharge in a channel with fixed (non-erodible) banks differs from that of a channel with erodible banks (Bolla Pittaluga et al. 2014). In contrast, Braudrick et al. (2009) observed overbank flow in an experimental meandering channel although the flow was intended to be at bankfull stage.

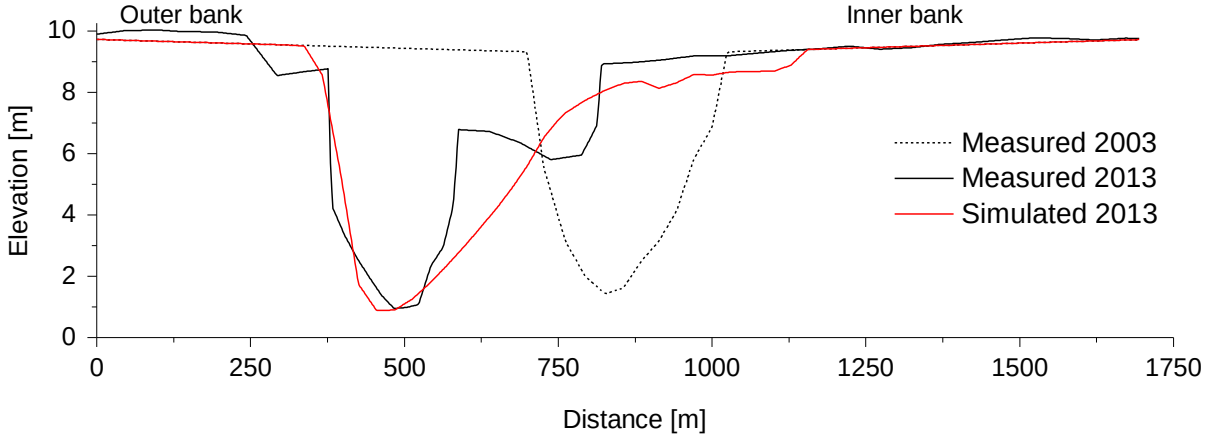

Fig. 4.23 *Comparison of observed and simulated bed topography in April 2013 at the monitoring cross-section (CS-2) as shown in Figure 3.11(a).*

Investigating the results in some more details reveals that the difference of the maximum scour depths is 0.07 m, which is reasonable. The results of the simulation further show that there are some discrepancies in terms of depth in erosion and deposition near the inner bank region. Indeed, the model has shown a tendency to underpredict transverse slopes. In order to compare the measured and modelled bed changes, a statistical analysis was undertaken using the Brier Skill Score (*BSS*) (see Section 4.2.5). A BSS score of 0.93 was achieved, which is classified as an excellent comparison by both van Rijn (2003) and Sutherland et al. (2004). This provides reasonable confidence in the predictive capability of the calibrated model.

4.3.2.4 Model validation

Following the successful model hindcast for the decade (2003 – 2013), a validation run was also conducted for a period of 3 years (April 2013 – April 2016). Visual comparison between observed and simulated evolution of thalweg in 2014 suggests that the model is able to resolve the presence of pool-bar topographies along the channel, although prediction has deviations of comparable magnitude (see Figure 4.24).

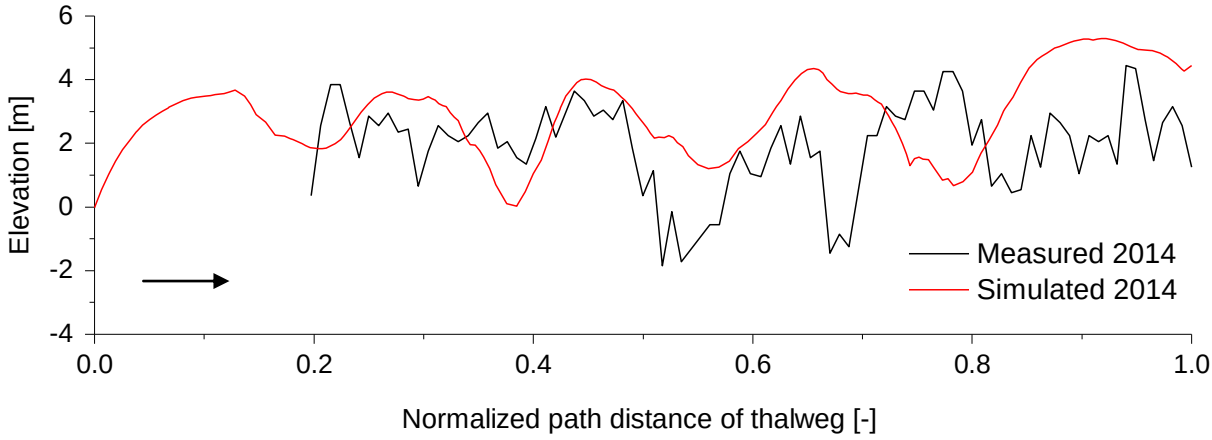

Fig. 4.24 Comparison of observed and simulated evolution of thalweg in December 2014.

Concerning the maximum scour depth and deposition levels at the monitoring cross-section, the difference between the predicted bathymetry and the measured values do not seem to change with time (see Figure 4.25). A BSS score of 0.89 was achieved, which implies that the prediction error does not increase in time. Particularly against this background, this validation attests adequate model skill for the purpose of this study.

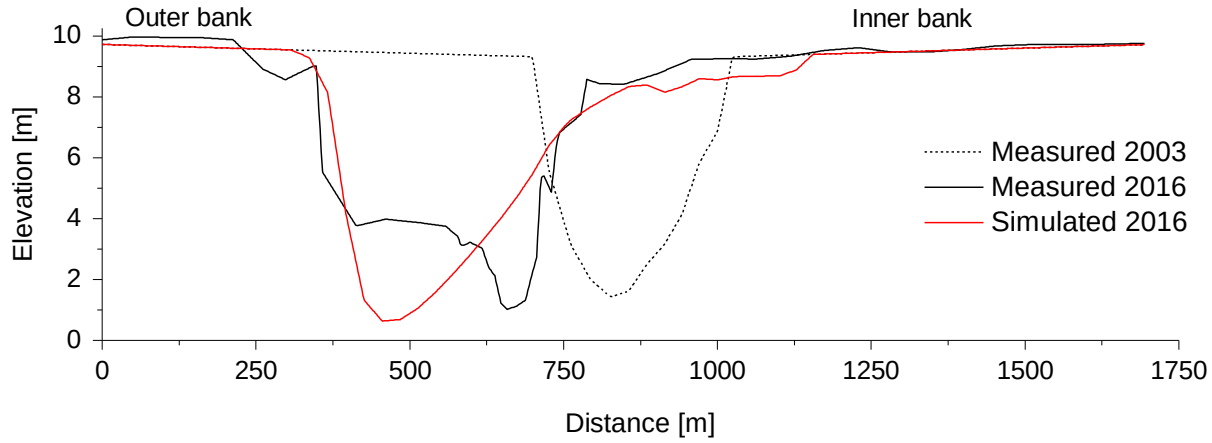

Fig. 4.25 Comparison of observed and simulated bed topography in April 2016 at the monitoring cross-section (CS-2) as shown in Figure 3.11(a).

4.3.2.5 Sensitivity analysis

A sensitivity analysis was carried out to increase the understanding of the impact of various user-specified parameters on the simulation results. First, the model was run with default parameters. In other runs, only one parameter deviated from the default run supposing that the change in each parameter would lead to a modification of river morphology. This approach was adopted so that the results could be easily interpreted and used to guide parameterizations for other Delft3D models used in the following chapters.

Variables for sensitivity analysis

A sensitivity analysis was performed to assess the effects of Manning's roughness coefficient (n), spiral flow effect on bed-load transport direction (E_s), transverse bed slope effect (α_{bn}), median grain size (D_{50}), and porosity in the predictive ability of the model. The parameters of Experiment E 0 were the default parameters, which were used in all other runs;

only the parameter under examination deviated from the default run. Table 4.3 describes how parameters were varied from those defined for the reference (calibrated) model.

Tab. 4.3 Model runs of the sensitivity analysis

Experiment No.	Manning's roughness parameter (*n*) (s $m^{-1/3}$)	Spiral flow calibration coefficient (E_s) (-)	Transverse bed slope factor (α_{bn}) (-)	Median grain size (D_{50}) (mm)	Porosity (-)
E 0	0.054	1.5	15.5	0.1	0.4
E 1a	0.044	1.5	15.5	0.1	0.4
E 1b	0.064	1.5	15.5	0.1	0.4
E 2a	0.054	0	15.5	0.1	0.4
E 2b	0.054	1	15.5	0.1	0.4
E 2c	0.054	2	15.5	0.1	0.4
E 3a	0.054	1.5	5	0.1	0.4
E 3b	0.054	1.5	10	0.1	0.4
E 3c	0.054	1.5	20	0.1	0.4
E 4a	0.054	1.5	15.5	0.08	0.4
E 4b	0.054	1.5	15.5	0.09	0.4
E 4c	0.054	1.5	15.5	0.11	0.4
E 4d	0.054	1.5	15.5	0.12	0.4
E 4e	0.054	1.5	15.5	0.1	0.36
E 4f	0.054	1.5	15.5	0.1	0.44

Results of *the* sensitivity analysis

Direct evaluation of model sensitivity is restricted in scope because observed data are scarce and only available at the locations of monitoring cross-sections as shown in Figure 3.11(a). The digital elevation model of difference (DoD) is a common approach in morphological modelling that allows for an objective and quantitative comparison between model runs (Plüß & Kösters 2014, Williams et al. 2016). For this purpose, a digital elevation model of difference (DoD) was built by subtracting the initial (2003) and simulated (2013) bed topographies for each of the model runs. The spatial distribution of net erosion and deposition was plotted so that the DoDs could be qualitatively compared. Furthermore, in order to compare quantitatively, the erosion and deposition volumes and sediment budgets were calculated for each of these model runs. Table 4.4 shows predicted volumetric changes of erosion/deposition for bed roughness (Experiment 1), spiral flow effect on bed-load transport direction (Experiment 2), transverse bed slope effect (Experiment 3), and bed composition (Experiment 4) sensitivity tests. A further set of evaluation was conducted using measured data at the loca-

tions of monitoring cross-section (CS-2) as shown in Figure 3.11(a). In addition, Brier Skill Score (*BSS*) was computed at the monitoring cross-section.

Tab. 4.4 Predicted volumes of morphological changes and Brier Skill Scores for different runs.

Experiment No.	Volumetric changes between the initial (2003) and simulated (2013) geometries					Brier Skill Score (BSS)
	Erosion (m^3)	% Change from reference	Deposition (m^3)	% Change from reference	Net (m^3)	
E 0	9559064		11979453		2420388	0.93
E 1a	6976584	27	9593633	20	2617049	0.82
E 1b	3109384	67	19871965	-66	16762582	0.89
E 2a	3025752	68	15780832	-32	19379631	-0.03
E 2b	6689226	30	13100732	-9	6411506	0.32
E 2c	12175698	-27	11712124	2	463574	0.67
E 3a	17286794	-81	5386879	55	11899915	0.70
E 3b	11841425	-24	9609451	20	2231974	0.90
E 3c	7770532	19	14009242	-17	6238710	0.46
E 4a	10254955	-7	12075453	-1	1820499	0.92
E 4b	9886746	-3	12022827	0	2136081	0.92
E 4c	9289323	3	11882283	1	2592960	0.93
E 4d	9055345	5	11822148	1	2766803	0.93
E 4e	9360477	2	11920456	0.5	2559979	0.93
E 4f	9770228	-2	12016043	-0.3	2245815	0.92

Experiment 0: reference run

The model was run with default parameters, that is, a constant Manning's roughness (0.054 s $m^{-1/3}$), spiral flow effect on bed-load transport direction (1.5), transverse bed slope effect (15.5), a uniform sediment grain size (D_{50} = 0.1 mm), and porosity (0.40).

Experiment 1: bed roughness

Bed roughness is often tuned to fit a measured water surface slope. The model was calibrated with a uniform Manning's n value (0.054 s $m^{-1/3}$) which was recomputed to Chézy bed roughness (equation 4.17). The Manning's roughness value was kept constant in the model, but the Chézy coefficient varied with flow depth (Lotsari et al. 2014). It should be noted that the objective of the sensitivity tests was to explore the effects of Manning's n value on the simulation results rather than the choice of empirical roughness functions. In order to analyze the effect of the Manning's n value on the morphological results, the default value was changed to 0.044 s $m^{-1/3}$ and 0.064 s $m^{-1/3}$.

Figure 4.26(a) shows DoDs for the bed roughness sensitivity experiments. Low roughness value (E 1a) resulted in decreasing erosion and deposition volumes by 27% and 20% respectively, compared to the reference simulation (E 0). High roughness value (E 1b) resulted in decreasing erosion volumes by 67% and increasing deposition volumes by 66%. The results indicate that the Manning's roughness has significant effects on the modelled bed morphology. These findings are in line with the recent study by Guan et al. (2016). Figure 4.26(b) compares observed and predicted bed levels for simulations with different roughness values. Low roughness value (E 1a) caused under-prediction of lateral erosion, whereas high roughness value (E 1b) caused deeper scour near the outer bank. In the former case, the BSS score decreased to 0.82, whereas in the latter case BSS was 0.89.

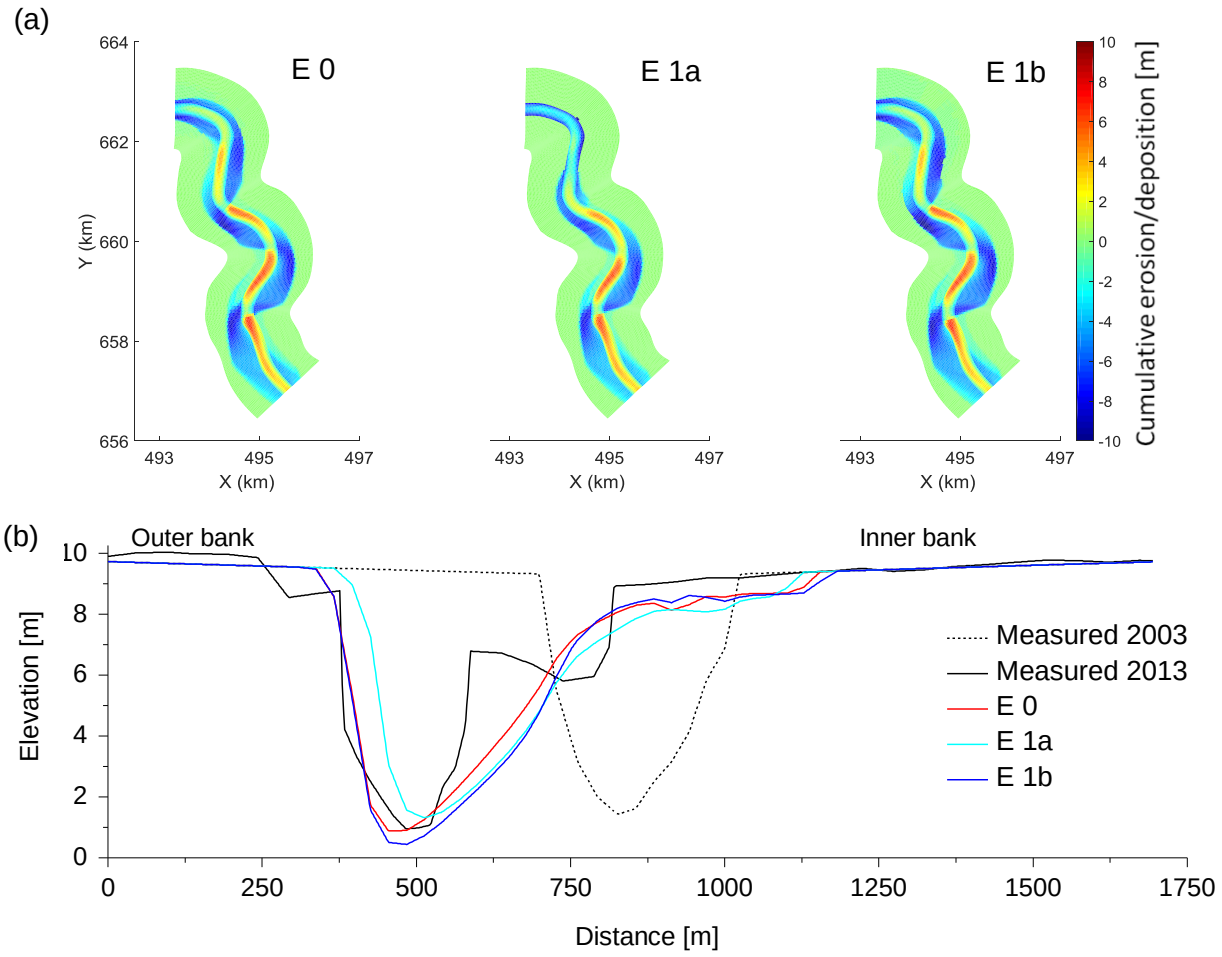

Fig. 4.26 *(a) The simulated spatial distribution of net bed erosion and deposition for the three parameterizations of Manning's roughness and (b) comparison of observed and simulated bed topography in April 2013 at the monitoring cross-section (CS-2) as shown in Figure 3.11(a).*

Experiment 2: effect of spiral motion on bed-load transport direction

In this experiment, sensitivity to E_s, which is an user-specified coefficient to control the effect of spiral motion on bed-load transport, was tested. Although E_s can be used as a calibration parameter, previous studies limited its value to 1 for investigating the impact of including or excluding the secondary flow effects on bed-load transport (e.g., Kasvi et al. 2015). Experiment 2a used a null value of E_s which implies that the effect of the spiral flow was not included in the bed-load transport direction (Deltares 2014, Nabi et al. 2016). Consequently, this

resulted in a relatively straight channel, as shown in Figure 4.27(a). A comparison between DoDs shows that incorporating the spiral flow effect on bed-load transport direction (E 2b) roughly doubled the erosion volume and reduced the deposition volume by approximately one-sixth. The simulation with E_s value of 2 increased the erosion volume by approximately one-quarter and decreased the deposition volume by 2%, compared to the reference simulation (E 0).

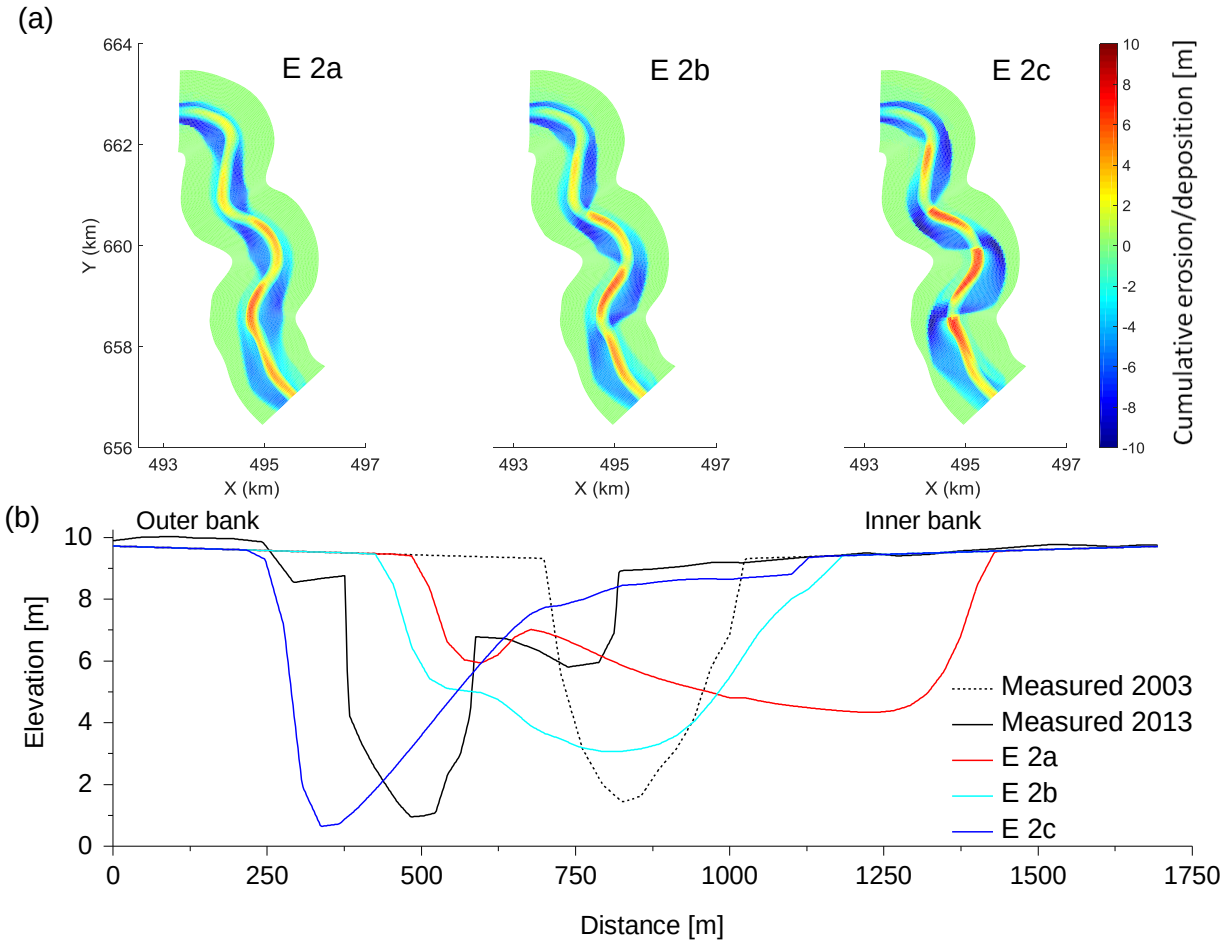

Fig. 4.27 *(a) The simulated spatial distribution of net bed erosion and deposition for the three parameterizations of spiral flow effect on bed-load transport direction and (b) comparison of observed and simulated bed topography in April 2013 at the monitoring cross-section (CS-2) as shown in Figure 3.11(a).*

Figure 4.27(b) compares the measured and predicted bed levels for different values of E_s. The simulation with no spiral flow effect caused an unusual amount of bank erosion in the inner curve of river bend, indicating lateral channel shifting in the wrong direction. As a result, the predicted cross-sectional shape is considerably different from the observed shape, leading to a negative BSS-value. A higher value of E_s led to a channel migration more laterally towards the outer bank, which demonstrates that the parameterization for the spiral flow effect on bed-load transport is of crucial importance in a depth-averaged simulation.

Experiment 3: sensitivity to transverse bed slope effect

The curved shape of the channel and the transverse bed slope of the point bar induce a certain three-dimensional flow field, which in turn controls the sediment transport. Accurate numerical predictions of the sediment transport, therefore, depend critically on the accurate

modelling of transverse bed slope. However, an exact parameterization of the transverse bed slope effect can only be achieved by calibration (Schuurman & Kleinhans 2013, 2015, Schuurman et al. 2013, 2016). The suggested value is 1.5 (Deltares 2014). In order to obtain reasonable results in long-term morphological simulations, this value has been increased from 1.5 to 10 (van der Wegen et al. 2011) to 80 (Lesser et al. 2004). The importance of the parameterizaion for the transverse bed slope effect (α_{bn}) was investigated for three different values: 5, 10, and 20.

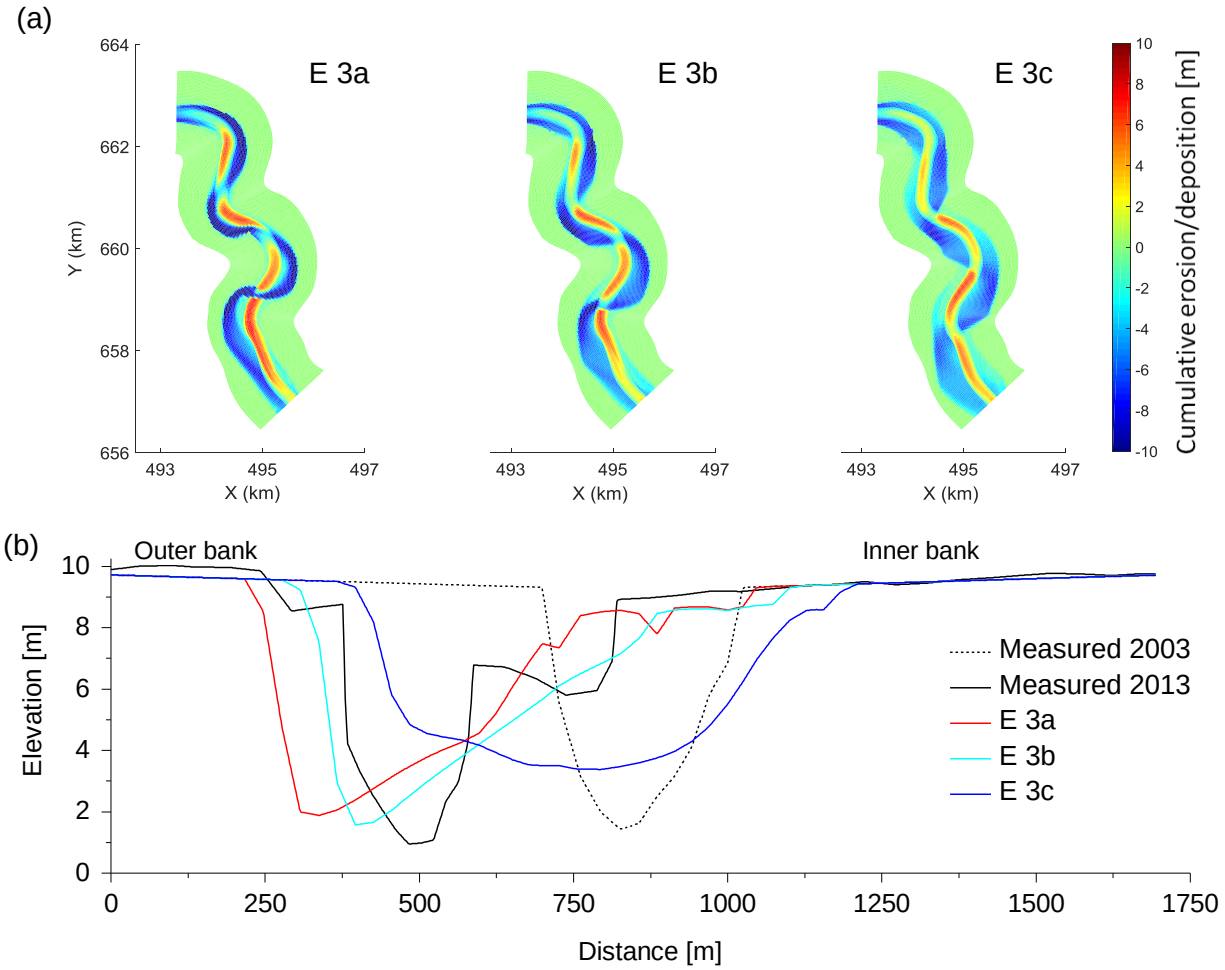

Fig. 4.28 *(a) The simulated spatial distribution of net bed erosion and deposition for the three parameterizations of effect of transverse bed slope and (b) comparison of observed and simulated bed topography in April 2013 at the monitoring cross-section (CS-2) as shown in Figure 3.11(a).*

The transverse bed slope effect parameterization showed a notable effect on the morphological results (see Figure 4.28(a)). A comparison between DoDs shows that the simulation with a α_{bn} value of 5 (simulation E 3a) increased the erosion volume by 81% and decreased the deposition volume by 55%, compared to the reference simulation (E 0). High value of α_{bn} (simulation E 3c) reduced the erosion volume by approximately one-fifth and increased the deposition volume by approximately one-sixth. Figure 4.28(b) compares the measured and predicted bed levels for different values of α_{bn}. A higher value of α_{bn} flattened the cross-sectional profile resulting in a shallower and wider channel, leading to a poor *BSS*-value.

This observation is in line with the results of the previous studies in lowland sand-bed streams (e.g., Kasvi et al. 2015, Schuurman et al. 2016).

Experiment 4: sensitivity to grain size and porosity

A well modelled bed composition is crucial for the modelling of the bed morphology. The sensitivity of the numerical model to grain size and porosity was investigated to examine how much these parameters control the morphological results.

Grain size parameterization is considered to be an uncertainty factor as morphological results depend on the prediction of sediment transport, which in turn depends on the choice of the median grain size (Bolla Pittaluga et al. 2014, Guan et al. 2015, 2016). The real-world grain size distribution is spatially varying and the sediment consists mostly of fine sand (see Section 3.4.1). The median grain size was varied by ±10% and ±20% around the default value (D_{50} = 0.1 mm). Figure 4.29(a) shows that both erosion and deposition area are influenced slightly by the grain size parameterization (simulations E 4a to E 4d). The net bed erosion and deposition volumes for the four runs are also found to be similar with a difference smaller than 7%. Furthermore, it is evident from Figure 4.29(b) that all runs predict the similar erosion and deposition depths with a slight difference. A change in grain size parameterization with respect to the default value hardly affects the model skill. This contradicts the general conclusions by Kasvi et al. (2015) and Guan et al. (2016), who suggested that the grain size parameterization is crucial for the modelling of the bed morphology. The reason causing these small differences is that median grain size variation was very low (0.08 mm to 0.12 mm). Apparently, increasing model complexity by introducing multiple sand fractions would not necessarily lead to better model performance. For this reason, bed sediment sorting mechanisms and spatial distribution of bed sediments can be safely excluded from further experiments in the present study.

Morphological changes are computed from residual sediment mass transport, which are then converted into bed level changes using the user-specified porosity (Püß & Kosters 2014). In addition to the grain size parameterization, sensitivity to porosity (simulations E 4e and E 4f) was tested. The porosity was changed by ±10% around the default value (0.4). Figure 4.29(a) shows that both erosion and deposition area are not influenced by the prosity of sediments (simulations E 4e and E 4f). Figure 4.29(b) compares the measured and predicted bed levels for different values of porosity (simulations E 4e and E 4f). No important differences in predicted bed elevation were found between simulation E 4e and simulation E 4f. It was found that a change in porosity with respect to the default value hardly affects the model skill.

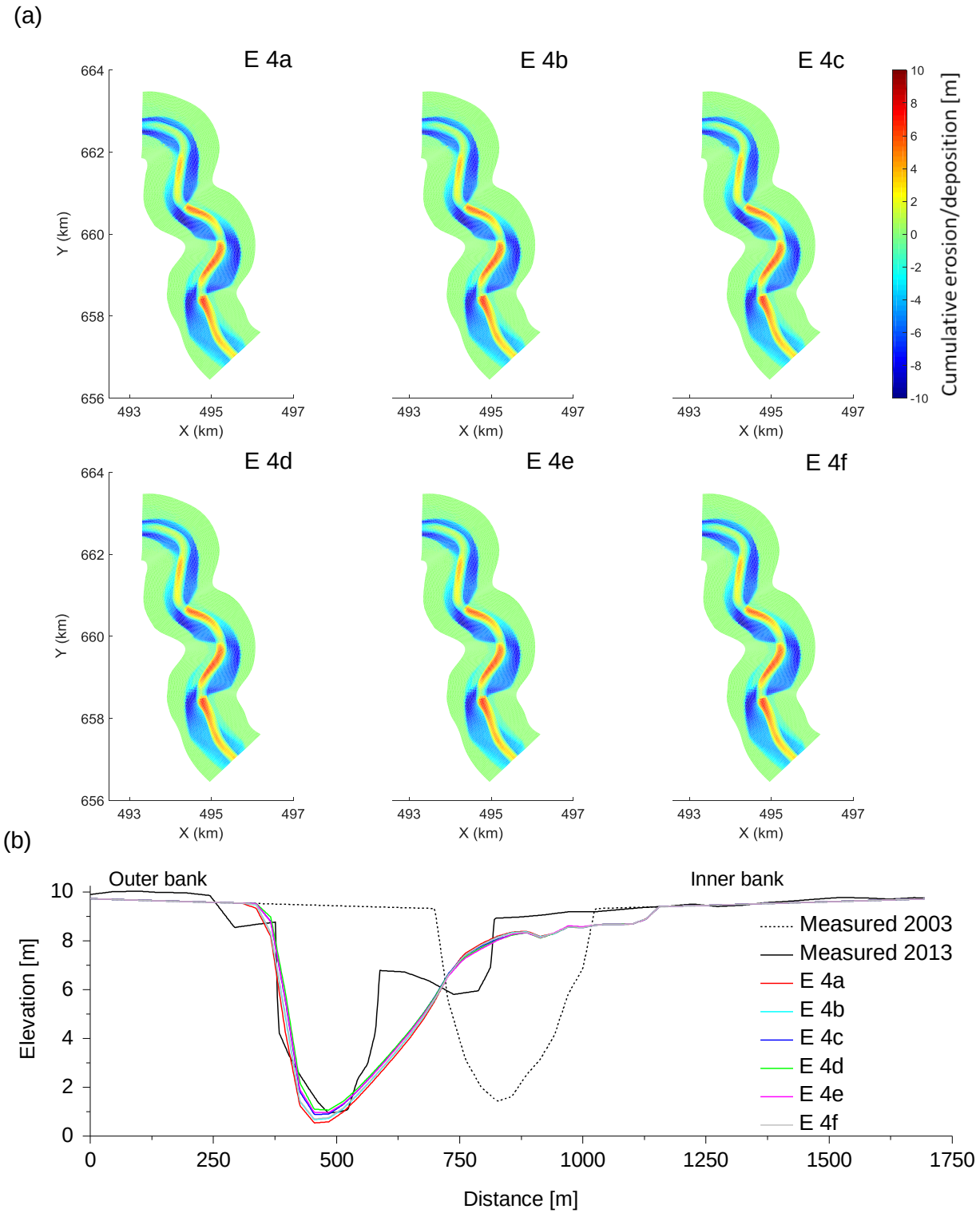

Fig. 4.29 *(a) The simulated spatial distribution of net bed erosion and deposition for the four parameterizations of grain size and for the two parameterizations of porosity and (b) comparison of observed and simulated bed topography in April 2013 at the monitoring cross-section (CS-2) as shown in Figure 3.11(a).*

4.3.2.6 Planform geometry

For the investigation of the planform evolution, the simulated planform was studied using the parameters which are frequently applied in analogous studies (see Section 2.2.6.1).

Method for analysis

For ease of analysis of the planform geometry, it was desirable to represent the shape and position of the channel as a single curve in two-dimensional space. Meander planform parameters can be quantified in multiple ways (Crosato 2008, Schuurman et al. 2015, Konsoer et al. 2016), e.g., by the thalweg (line of lowest height) or by the channel centerline of the river. The shape of a meandering channel is best represented by the position of the thalweg, because this closely corresponds to the position of a bend's outer bank, and maximizes the channel's radius of curvature regardless of stage. On the other hand, in the case of obtaining a channel's centerline, which is defined as the midpoints of a series of line segments connecting corresponding points on the left and right bank, it requires careful selection of left- and right-bank point pairs which might not be straightforward. Furthermore, this method is particularly subjective when the transverse bed slope predicted by the model is somewhat too shallow.

Following the methodology of Schuurman et al. (2016), planform statistics were computed considering the thalweg. This choice was motivated by the fact that the channel's thalweg is independent of the modelled bankfull width and can be found directly by applying a suitable operation to the digital elevation model using a Matlab script. The upstream 1 km of the total 8.2 km long reach was not considered to eliminate boundary effects. The meander pattern was quantified by four parameters (meander belt width, meander wavelength, radius of curvature and channel bankfull width) and the relationships between these parameters. The procedure for determining the parameters is described in the following.

Determination of meander belt width, meander length and meander wavelength

The Delft3D computational grid in the horizontal plane is fixed. This means that the grid itself remains stationary but that the flow domain is adapted in each morphological time step throughout the simulation due to bed level changes resulting from sediment transport. Consequently, the thalweg alignment (line of lowest height) elongates and the spacing between consecutive cross-sections changes. Because of non-equidistant cross-section spacing, the thalweg shifting introduces a spurious oscillation into the thalweg alignment (see Figure 4.30).

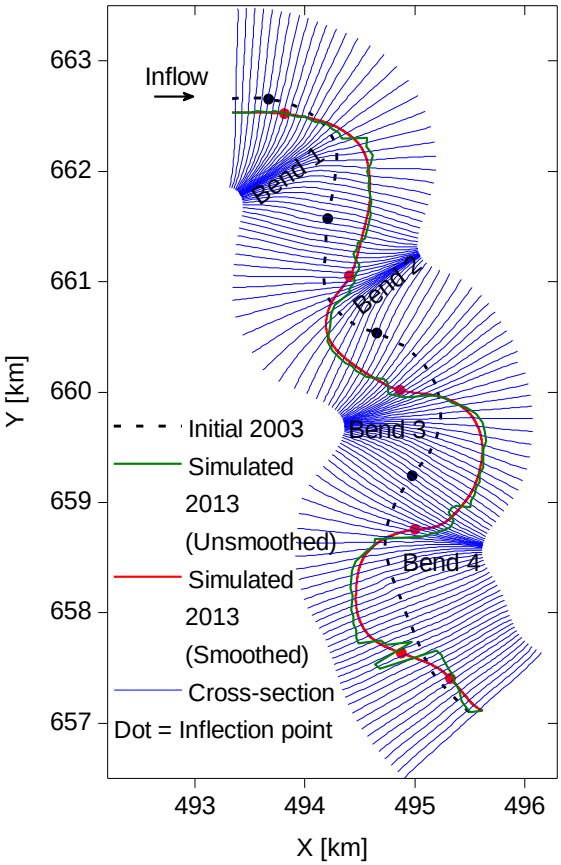

Fig. 4.30 Delineation of meander bends.

For investigating planform behavior, the thalweg was extracted from the model results in 2013, and then smoothed by means of cubic spline interpolation using an in-house developed Matlab script (Meander Analysis Toolbox, developed by S. Niewerth in the Leichtweiß-Institute for Hydraulic Engineering and Water Resources). For this purpose, a curvature series of equally-spaced points along the thalweg was calculated using the Matlab script and then moving average techniques were applied for smoothing noisy x, y coordinate data as suggested by Motta et al. (2012). A 4th-degree polynomial filter with averaging windows of three nodes was employed. The smoothed thalweg was splitted at each inflection point where a change in the direction of curvature occurs. Accordingly, four meander bends were defined by the location of inflection point. Each bend or loop was numbered for ease of location and discussion (see Figure 4.30). Following Williams (1986), a single wavelength was assigned to each meander bend. The meander belt width M_B (i.e., shortest distance between tangents drawn outside of the meanders), meander length L (i.e., curvilinear distance between the end points of a complete meandering wave cycle) and meander wavelength λ (i.e., straight line distance between the end points of a complete meandering wave cycle) are reported in Figure 4.31.

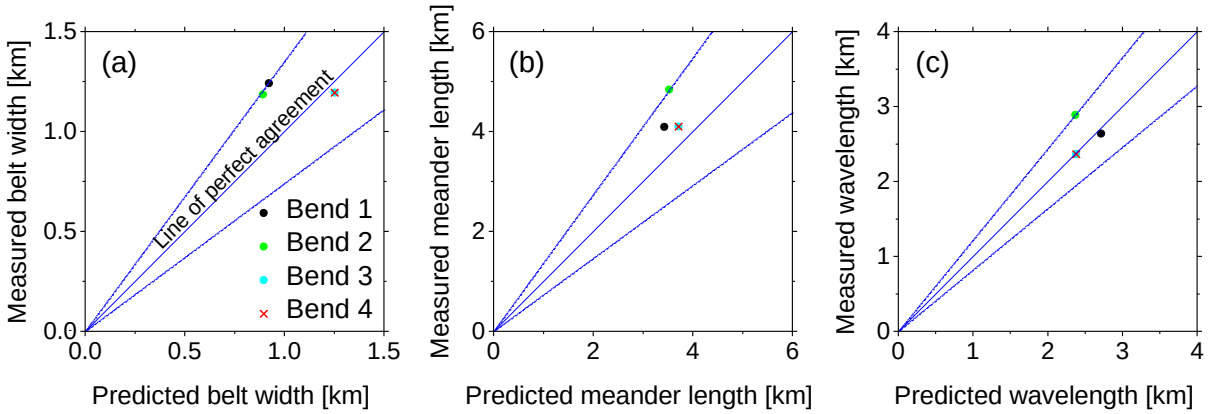

Fig. 4.31 *Comparison of model results and observations (a) meander belt width M_B (the dashed lines show the 27% error boundaries), (b) meander length L (the dashed lines show the 26% error boundaries) and (c) meander wavelength λ (the dashed lines show the 18% error boundaries).*

The comparison of the model results with the observations in 2013 shows that the maximum differences for M_B, L and λ are 27%, 26% and 18%, respectively. Statistical analysis of model predictions with respect to the observations yielded a RMSE of 0.22 km for M_B, 0.78 km for L and 0.26 km for λ. The analysis of the results shows that the model predicts the parameter λ more correctly than the other parameters.

Determination of radius of curvature

The radius of a best-fit circle for a meander bend is commonly used to determine the radius of curvature (Magdaleno & Fernández-Yuste 2011), although several other morphological studies used the average value to represent the radius of curvature (R) for a bend (Schuurman et al. 2016, Konsoer et al. 2016). The present study used the best-fit circle method in which circles of known radius were superimposed on a meander bend, and the circle that best seemed to fit the channel thalweg around the bend was chosen to obtain the parameter R. Although somewhat subjective, this method allows for an objective and quantitative comparison between model results and observations. Following the methodology of Magdaleno & Fernández-Yuste (2011), straight and quasi-straight sub-reaches were not taken into account in considering a best-fit circle for a meander bend. Figure 4.32(a) shows the best-fit circles with their estimated R values. Figure 4.32(b) shows the comparison of model results and observations. The comparison of model results and observations shows that the maximum difference for radius of curvature is 400 m. The difference, expressed as RMSE, between predicted and observed R values is 261 m.

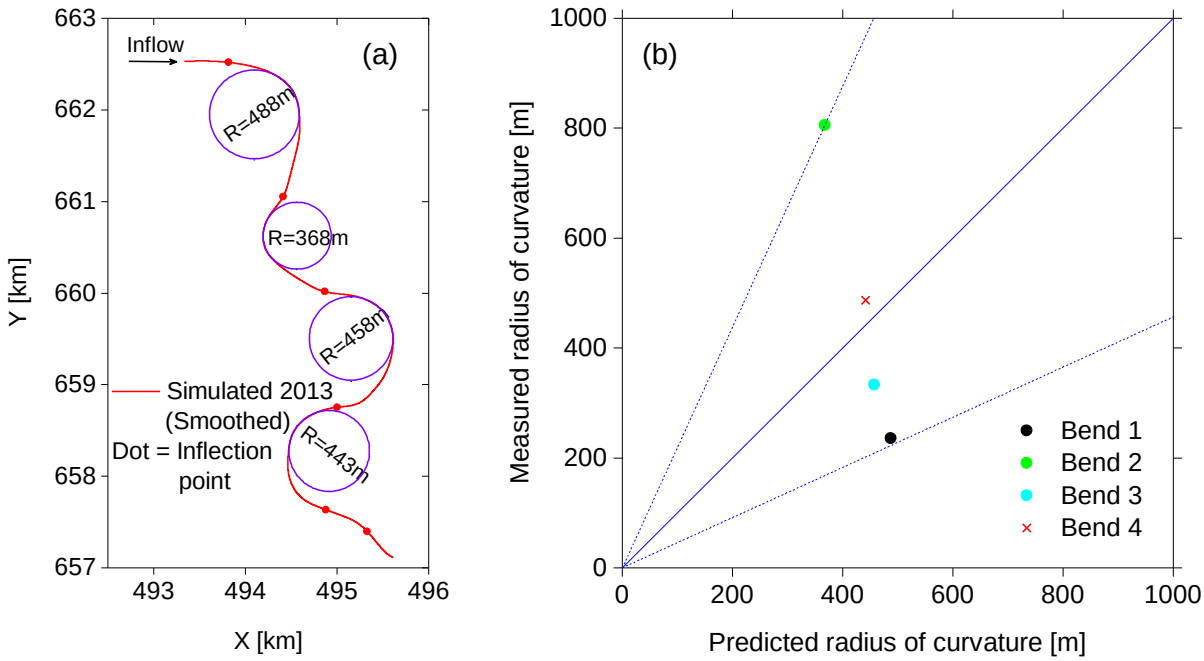

Fig. 4.32 *(a) Determination of radius of curvature R and (b) comparison of model results and observations (the dashed lines show the 54% error boundaries).*

Determination of channel bankfull width

In the numerical simulation, the boundary of the flow domain is no longer fixed and it changes in time. As a result, the cross-sections, which were orthogonal to the streamwise direction at the beginning of the simulation, skewed during the meander simulation as shown in Figure 4.30. This is an obstacle to any reasonable determination of channel width. The Meander Analysis Toolbox (MAT) facilitated the rotation of the cross-sections like a hinge on the smoothed thalweg. Local depth values were projected onto the (rotated) cross-sections by linear interpolation. Channel widths were obtained from these cross-sections assuming a constant floodplain elevation of 8.29 m which corresponds to the water surface elevation at the downstream boundary at the end of the simulation. Since the simulated channel width varies along the channel (see Figure 4.33(a)), the mean width for a bend was obtained by averaging the computed values at different cross-sections within a bend. Figure 4.33(b) plots a comparison of model results and observations, indicating that the modelled channel bankfull width is significantly higher than real value.

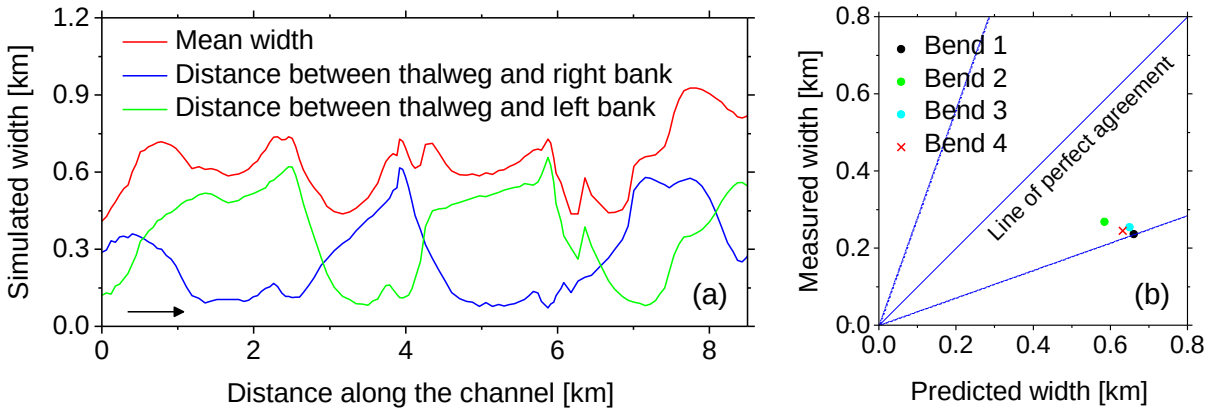

Fig. 4.33 *(a) Width variation along the channel and (b) comparison of model results and observations for the bend-averaged channel width (the dashed lines show the 65% error boundaries).*

The present computations underestimated point bar height and transverse bed slopes. The model results require a few comments. Firstly, it should be noted that the simplified formulation of bank erosion implemented in the model allows the partial redistribution of erosion from a wet cell to adjacent dry cells (see Figure 4.3 and Section 4.1.3); however, this approach promotes erosion even in straight reaches. Secondly, due to a lack of formulations for the bank accretion process, the 2D model resulted in unrealistic river widening. The transverse bed slope predicted by the model is somewhat too shallow in relation to the field data. Underprediction of the transverse side slope implies that the model predicts an unrealistically high cross-stream sediment flux across the point bar near the inner bank that is directed toward the outer bank. This results in the bar extending too far across the channel, which in turn results in a larger bankfull channel width than the measured one. The cause of an inability to accurately estimate the sediment flux vector might be an inherent problem with the sediment transport model, because the sediment transport requires the input of a range of numerical and physical parameters (as outlined in Section 4.1.2.3) that eventually control the sediment movement.

Recent studies showed a major influence of the transverse bed slope effect on bed topography in meandering rivers (Kasvi et al. 2015, Schuurman et al. 2016). The transverse bed slope effect calculates the sediment transport deflection by the direct effect of gravity on particles moving on the transverse slope, and therefore, the bed slope effect is implemented in all process-based morphological models (e.g., Delft3D, Mike21C, Telemac, CCHE2D, Nays2D) and even in linearized meander models (e.g, Ikeda et al. 1981, Crosato 2008). However, an exact parameterization of the transverse bed slope effect can only be achieved by calibration. With calibration the parameter values that produce the best fit between model predictions and observations are sought. Accurate numerical predictions of the sediment transport, therefore, depend critically on the accurate modelling of the transverse bed slope effect.

Analytical approximation of transverse bed slope

There is clearly an increasing need for independent checks to be made of modelled results. Struiskma et al. (1985) developed an analytical model for predicting the bed deformation in curved channels (equations 2.2 – 2.4). At the apex of bend 4, the transverse bed slope was

computed by using the analytical model. The transverse bed slope predicted by the analytical model is about 8%, whereas the slope computed by the numerical model is 2.67%. The transverse bed slope magnitude of the analytical model is three times larger than that of the numerical model. Comparison between the transverse bed slopes predicted by the analytical model and field data is not practical, because the analytical model was developed based on fixed-width curved flume experiments.

Relationships between the planform parameters and channel width

Regression relationships between planform parameters and channel width are reported in the literature (see Table 2.1), in which channel width serves as a scale indicator and meander features (i.e., meander-belt width, meander wavelength, radius of curvature) as dependent variables. Normalizing the planform parameters by channel width allows for a scale-independent comparison of results with prior studies. For this purpose, meander geometry was also evaluated by normalizing the meander features by the channel width. Figure 4.34 plots a comparison of model results and observations, indicating that the modelled planform parameters normalized by channel width are significantly smaller than observed values.

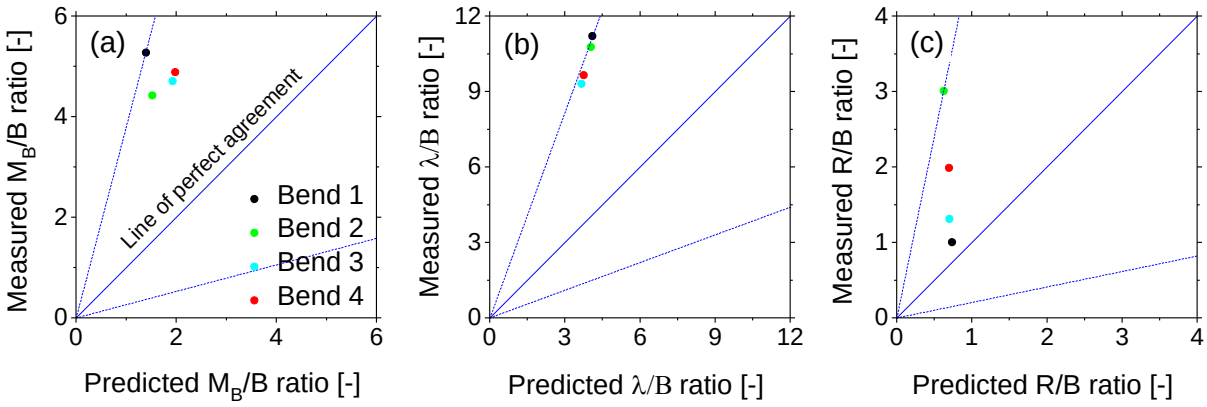

Fig. 4.34 *Comparison of model results and observations (a) meander belt width to channel width ratio M_B/B (the dashed lines show the 74% error boundaries), (b) meander wavelength to channel width ratio λ/B (the dashed lines show the 63% error boundaries) and (c) radius of curvature to channel width ratio R/B (the dashed lines show the 80% error boundaries).*

It is more useful to identify the causes of deviations and to formulate recommendations for the subsequent analyses of planform geometries in the study area. When the model results are normalized by channel width derived from field data, relationships between planform parameters and channel width lies within an acceptable limit (see Figure 4.35). As expected, M_B/B ratio ranges from 3 to 6, λ/B ratio ranges from 9 to 12, and R/B ratio ranges from 1.3 to 2, which coincides with other studies (e.g., Leopold & Wolman 1960, Zeller 1967, Hickin & Nanson 1984, Williams 1986, Julien 2002, Magdaleno & Fernandez-Yuste 2011). This implies that the modelled channel width was poorly predicted in comparison to other parameters. It seems meaningful to normalize planform parameters by channel width derived from field data rather than simulation results. This recommendation is reasonable for the present river, in which inner bank deposition keeps pace with outer bank erosion resulting in an almost-constant width especially after the year 2000, as shown in Figure 3.8(a). The main ad-

vantage of this approach is that presenting the results in this format would allow river managers a greater insight into probable river corridor widths and inform decisions on development within likely erosion areas as well as potential river restoration designs.

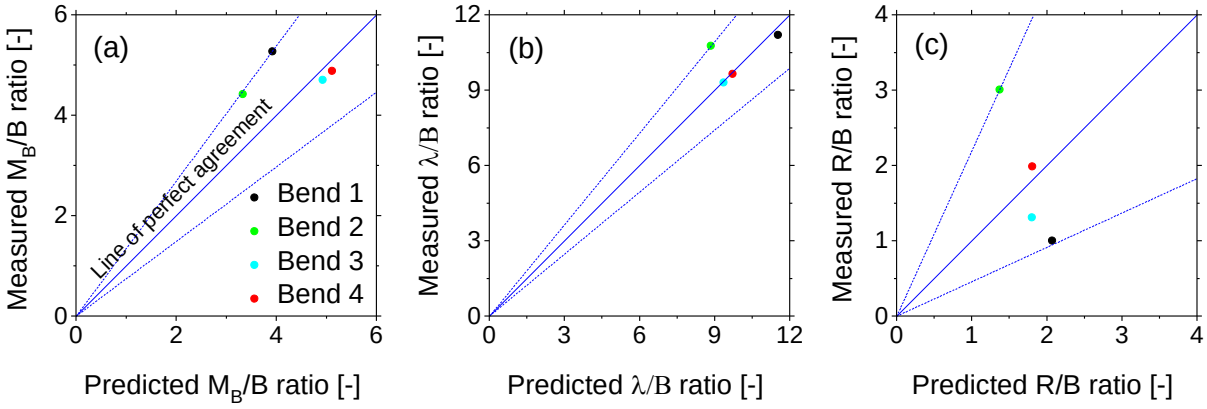

Fig. 4.35 *Comparison of model results normalized by measured channel width and observations (a) meander belt width to channel width ratio M_B/B (the dashed lines show the 25% error boundaries), (b) meander wavelength to channel width ratio λ/B (the dashed lines show the 18% error boundaries) and (c) radius of curvature to channel width ratio R/B (the dashed lines show the 54% error boundaries).*

4.3.2.7 Migration behavior

Temporal evolution

Figure 4.36(a) represents an overview of the simulated pattern formation after 2, 4, 6, 8, and 10 years, demonstrating that most bank erosion and planform shift occurred within the first two years period, with negligible rates of bank retreat subsequently. The bends always grow with time, but migration rates were fastest during initial bend development at the beginning of the simulation. The initial direction of channel migration was in the lateral direction, across the floodplain. Lateral channel migration increased the channel bend amplitude and channel length. As the bend amplitude increased, most of the meander bend migration was in the downstream direction. This process occurred first in the approach bend (i.e. bend 1) through redirection of the approaching flow and triggered a cascade of morphological changes, eventually propagating in the entire reach. This observation is consistent with observations by Whiting & Dietrich (1993) and da Silva (1995) in various sine-generated laboratory meanders and by Blanckaert (2010) in a single-bend laboratory flume, and with numerical results (e.g., Duan & Julien 2010, Asahi et al. 2013). A comparison of the predicted thalweg alignment in 2013 and the available thalweg information for the same year is plotted in Figure 4.36(b). The model results correspond well to the observations, considering the limitation in using a fixed upstream end. Indeed, the upstream end has to be fixed in place implying that this has to be a fixed place in reality too. As a substitute, it has to be placed so far upstream of the reach of interest that its fixation does not influence the results. Due to the long computational times, the model's upstream boundary could not be extended; this means that all physical processes, such as river bank erosion, were poorly resolved in the bends close to the inlet.

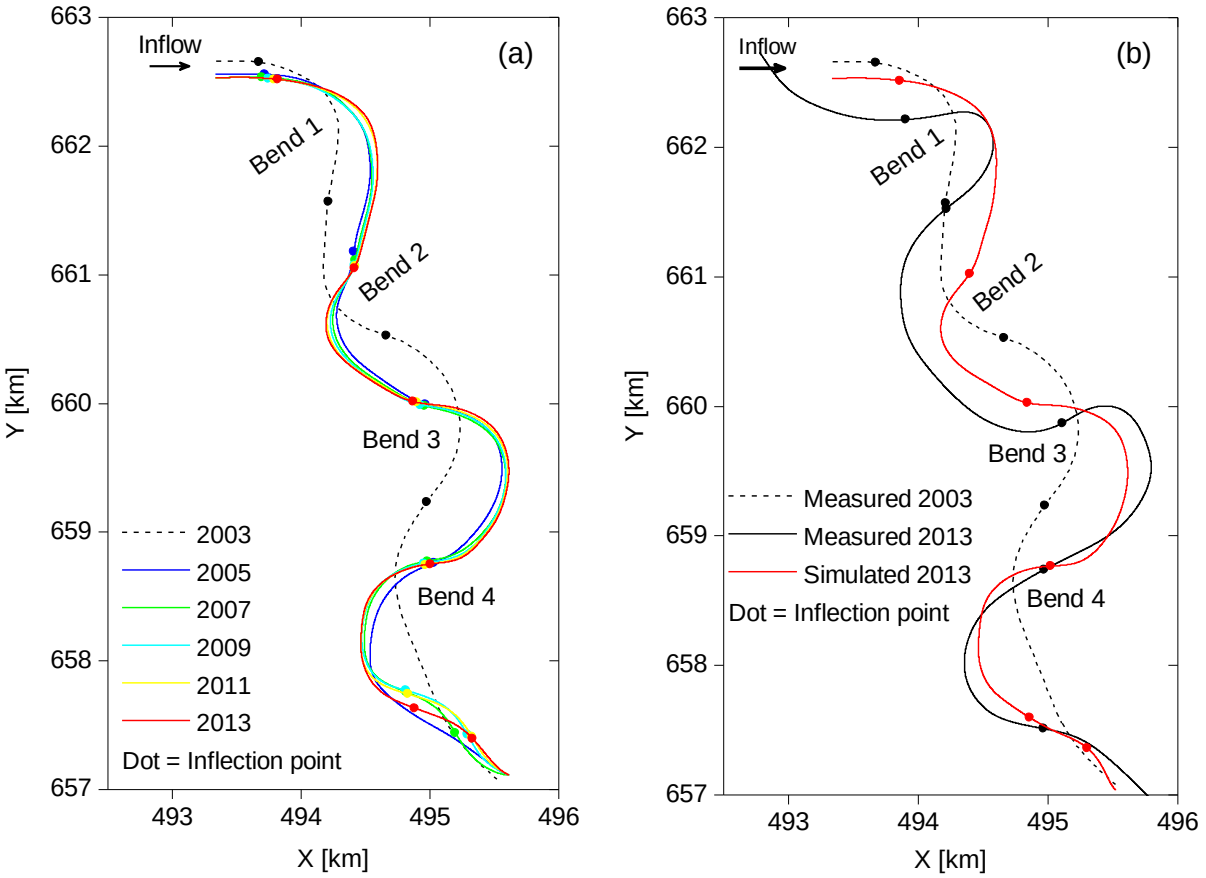

Fig. 4.36 *(a) Temporal changes in plan forms of simulated channel and (b) comparison of modelled and measured planform in 2013.*

Migration metrics

Migration was computed as the distance the channel moved perpendicular to the channel thalweg (see Figure 4.37(a)). Channel migration was quantified in terms of both maximal bank retreat and channel activity (or floodplain area loss). Maximal bank retreat refers to a single location along the reach, whereas channel activity (or floodplain area loss) is computed as the total bank retreat along the entire reach divided by the product of initial thalweg length and elapsed time, as shown in Figure 4.37(b) (Magdaleno & Fernández-Yuste 2011). Simulation results suggest that the maximum migration rate is about 1.7 times the spatially averaged migration rates for the study reach. Table 4.5 shows that maximal bank retreat was underpredicted by about 6%, whereas channel activity (or floodplain area loss) was overestimated by about 7%.

Tab. 4.5 *Maximal bank retreat and channel activity.*

Maximal bank retreat (m)		Channel activity (m/year)	
Measured	Simulated	Measured	Simulated
557	522	28.4	30.5

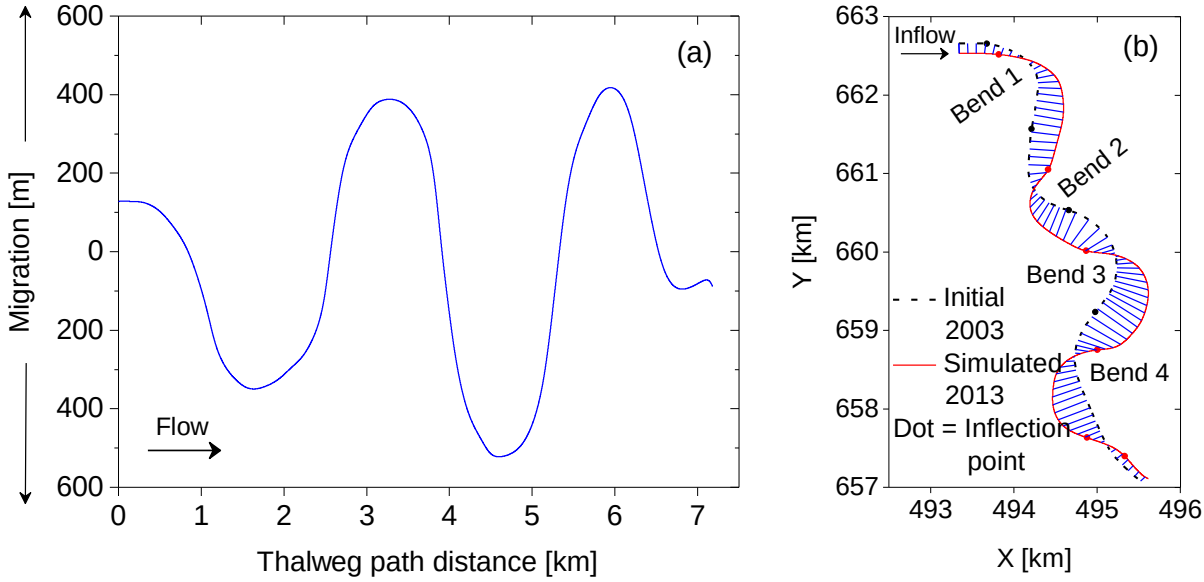

Fig. 4.37 *(a) Simulated migration as a function of thalweg path distance and (b) procedure for estimating channel activity (channel activity is quantified as the shaded area divided by the product of initial thalweg length and elapsed time).*

4.3.2.8 Discussion

1D meander migration models are incapable of representing bed topography changes across the width due to lack of information with regard to the transverse flow field. Consequently, numerical models of increasing complexity have been developed in the past three decades (see Section 2.4.2), and their validities have also been tested using small scale laboratory experiments (e.g., Olsen 2003, Duan & Julien 2005, 2010, Rüther & Olsen 2007, Asahi et al. 2013). A number of authors have attempted to reproduce a meandering channel evolved from a simple, flat-bedded initial condition to a more complex bar-pool morphology (e.g., Crosato & Saleh 2010, Nicholas 2013, Nicholas et al. 2013, Schuurman et al. 2015, van de Lageweg et al. 2016). Comparatively few attempts have been made to simulate meander evolution in a real river using process-based numerical models, because field datasets for model validation covering typical morphological time-scales of years to decades are scarce. Using surveyed river bathymetry within a short meandering reach, several researchers have modelled patterns of erosion and deposition over short time periods comprising single or few flood events in a year (e.g, Lotsari et al. 2013, Kasvi et al. 2015, Guan et al. 2016). Given the lack of previous research into process-based morphodynamic modelling of a sand-bed meandering river over decadal time scales, the current study tests whether a numerical model is able to reproduce bed morphology and planform characteristics of a freely meandering river. Since the long-term morphological evolution could only be studied by two-dimensional models because of computational costs, a depth-averaged 2D morphodynamic model, which includes the necessary parameterization of three-dimensional flow effects and transverse bed slope effects on morphology, was applied to the case study area (Dhaleshwari River, Bangladesh). The simulation results showed that the chosen set of boundary conditions and physics in the numerical model is sufficient to reproduce morphological characteristics such as scour depth, bank erosion and pool-riffle morphology, even though the model failed to reproduce bankfull channel width to some extent (see Figure 4.22 and 4.23). Regarding the planimetric evolution, the model predicted correctly the locations and patterns of bank migra-

tion evident from observed data (see Figure 4.36). The overall agreement is reasonable, even though large discrepancy is locally observed, particularly in the bends close to the inlet boundary. The differences between model results and field observations can partly be explained by the fact that the simulation was carried out under bankfull discharge condition whereas natural meandering channels rarely experience steady hydrological and sediment supply regimes over a decade. The planform statistics confirmed that the model results are realistic and are in accordance with statistical studies in the literature (e.g., Leopold & Wolman 1960, Zeller 1967, Williams 1986, Julien 2002), provided that the channel width derived from field data has been used as the scale indicator for the normalization of planform parameters (see Figure 4.35). The results suggest that a 2D modelling approach can capture the natural dynamics of meandering rivers, in terms of both the evolution of bed topography and channel planform.

The results of the study revealed that the poor prediction of the channel bankfull width is an artifact of the numerical model's limitations in representing the transverse bed slope (see section 4.3.2.6). The tendency of the model to underpredict the transverse bed slope is probably not caused by the bend-flow sub-model as the secondary flow parameterization used in the depth-averaged 2D computations was validated against curved flume data (see Section 4.3.1.3). This points out to a limitation with the sediment-related parameters. The depth-averaged 2D model showed marginal sensitivity to sediment grain size and porosity, but showed more sensitivity to bed roughness, spiral flow effect on bed-load transport direction and transverse bed slope effect (see Section 4.3.2.5). The results are in agreement with the general conclusions by Mosselman (1998), Kleinhans et al. (2008), Schuurman et al. (2015) and Guan et al. (2016), but contradict to Kasvi et al. (2015) who argued that a depth-averaged 2D model could predict the feature of erosion and deposition reasonably well in a natural meandering bend without the inclusion of a secondary flow parameterization due to the major role of main flows. The results of the sensitivity tests in the present study showed that exclusion of the parameterized effect of spiral flow on sediment transport (E_s) resulted in a relatively straight channel, and a higher value of E_s led to a channel migration more laterally towards the outer bank (see Figure 4.27). Sensitivity tests suggest that spiral flow effect on bed-load transport direction (E_s) and transverse bed slope effect (α_{bn}) had large influence on the morphological results. The results further showed that spiral flow effect on bed-load transport direction (E_s) leads to correct representation of location of bar-pool topographies whereas transverse bed slope effect parameterization (α_{bn}) leads to formation of transverse bed slope (see Section 4.3.2.5).

Many river modelling studies have applied constant discharge, assuming a steady discharge gives similar yearly morphodynamics to the real hydrograph. In numerical models, both constant discharge and variable discharge have been applied with variable results. Schuurman et al. (2016), Nikolas et al. (2013) and others argued that discharge variation in the form of an annual hydrograph hardly affects long-term river morphology. On the other hand, Crosato & Saleh (2010), Asahi et al. (2013) and Kaless et al. (2015) state that higher flows favor outer bank erosion and lower flows favor inner bank deposition. Kikillus et al. (2016) pointed out that the order of the occurence of the flood events has influence on the bed change predictions. Nevertheless, the results from the present study reveal that schematization of

the varying discharge of a river into a single discharge to describe the morphological parameters of a river is possible. However, there is a need to test the capacity of the developed 2D model to simulate meander evolution under different boundary conditions.

5 Constant discharge scenarios

The aim of this chapter is to apply the depth-averaged 2D model (presented in Section 4.3.2) in a series of numerical experiments for the investigation of the effects of different discharge magnitudes on channel morphology and planform adjustment in the study area. To focus on how river discharge affects the river planform and bed morphology, discharge boundary conditions were varied by a constant discharge (equal to 10% of the bankfull discharge). In the simulations, discharge was maintained constant following similar simplified approaches presented in Schuurman et al. (2013, 2015). In these approaches, it is assumed that a constant discharge corresponds to the dominant or effective discharge integrating all the morphodynamic work done over a yearly hydrograph. All the major parameters of meander planform are selected for their relevance to an explanation of the observed planform changes in the studied reach.

5.1 Constant river discharge

The river discharge was prescribed by constant values of 700, 630, 570, 490, and 420 $m^3 s^{-1}$. A discharge magnitude of 420 $m^3 s^{-1}$ roughly corresponds to the mean annual discharge (Q_{ma}). Smaller discharges were not considered as they would produce a comparable morphology over longer time at the expense of increasing simulation time. It is worth noticing that 700 $m^3 s^{-1}$ represents bankfull discharge (Q_{bf}) for the study area (see Section 4.3.2.3). Higher discharges than bankfull were not used for two reasons. First, they are assumed to poorly affect the river channel morphology because of their short duration (Paarlberg et al. 2015). Second, higher discharges may result in a braided river network in the simulations even though the overbank flow is usually shallow as compared to the main channel flow (van Dijk et al. 2014, Schuurman et al. 2016).

For a comparison of the chosen constant river discharge scenarios at a same evolution stage, the duration of flow discharge in a year is needed for each model so that all models have equal input of flow volume (Jefferson 1902). The estimation of the duration of each discharge in a calendar year followed the criteria used in the analysis of the duration of bankfull flow discharge described in Section 4.3.2.3. Table 5.1 summarizes the estimated duration of flow in a year for each discharge magnitude.

Tab. 5.1 Estimated annual duration of flow for each discharge

Discharge ($m^3 s^{-1}$)	% of the bankfull discharge (Q_{bf})	Duration of flow discharge in a year (day)
700	100	203
630	90	227
560	80	255
490	70	291
420	60	339

5.2 Model setup

The used grid covers 8.2 km of the river section including floodplains. The 2003 digital elevation model (DEM), as described in Section 4.3.2.1, was used as the initial bathymetry for simulation. For all simulations, discharge was specified at the upstream boundary and a corresponding water surface elevation was set at the downstream boundary. In the absence of measured water level data, the simulation used a predicted stage-discharge relationship at the downstream boundary which was based on hydraulic calculations using measured data at Taraghat gauging station (137A) (see Figure 3.2). The bed and banks were assumed to be erodible and were composed of the same fine sand. The sediment transport was computed by the Engelund & Hansen (1967) total load transport formula. At the inflow boundary, the input of sediment was kept equal to the local sediment transport capacity. A dry cell erosion approach was considered by transferring erosion in the wet grid cell to the closest adjacent dry grid cells so that channel migration and sand movement can be simulated. A morphological acceleration factor ($MORFAC$) of 10 was selected based on several trial simulations which were undertaken with incremental $MORFAC$s to determine the highest $MORFAC$ value that can be used safely for a given simulation.

Two series of simulations were performed (series A and B). The parameters of Run A0 were the default parameters, that is, constant Manning's roughness (0.054 s $m^{-1/3}$), spiral flow effect on bed-load transport direction (1.5), transverse bed slope effect (15.5), a uniform sediment grain size (D_{50} = 0.1 mm), and porosity (0.40). All other runs in series A were based on the same parameters. Series B, which also includes the reference simulation (Run A0), represents simulations for a calibrated situation to interpret field observations. Calibration was required for only two coefficients; spiral flow effect on bed-load transport direction (E_s) and transverse bed slope effect (α_{bn}), which were identified as the parameters that exert the most influence over channel morphology (see Section 4.3.2.5). Table 5.2 describes how parameters were varied in series B from those defined for the reference simulation (Run A0).

Tab. 5.2 Description of the test runs

Series	Run	Discharge (m^3 s^{-1})	Spiral flow effect on bedload transport direction (E_s)	Transverse bed slope effect (α_{bn})
Series A	A0	700	1.50	15.5
	A1	630	1.50	15.5
	A2	560	1.50	15.5
	A3	490	1.50	15.5
	A4	420	1.50	15.5
Series B	A0	700	1.50	15.5
	B1	630	1.60	15.5
	B2	560	1.70	16.5
	B3	490	1.75	17
	B4	420	1.85	16

5.3 Results

5.3.1 Bed topography change

The comparison of the transverse bed profiles of the measured and computed data is presented in Figure 5.1 where Figure 5.1(a) shows the results of the simulations for series A and Figure 5.1(b) for series B. Both figures indicate that the maximum deposition occurred near the inner bank, and the maximum scour depth took place near the outer bank. The profile shape and the extent of accretion and erosion varied with the discharge variations. Decreasing the discharge led to the flattening of the transversal profile near the inner bank. The differences between the observed and simulated bed profiles reduce with increased river discharge, indicating the dominant role of a high river discharge in controlling sediment transport and morphodynamic development. The direct comparison of Figures 5.1(a) and 5.1(b) reveals that the main differences between series A and series B are found in the outer bank region as the series B simulations result in a more pronounced bank retreat than the series A simulations.

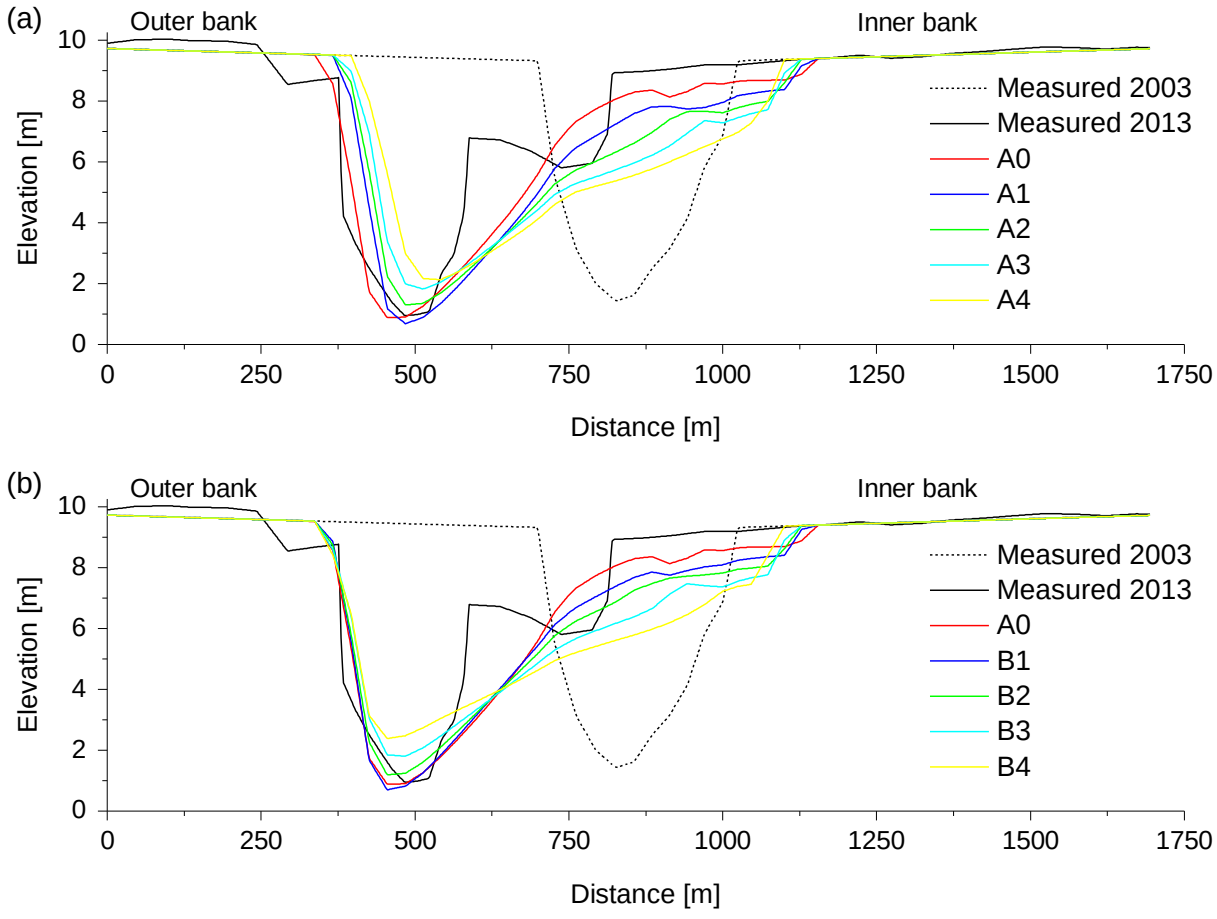

Fig. 5.1 *Comparison of observed and simulated bed topography in April 2013 at the monitoring cross-section (CS-2) as shown in Figure 3.11(a): (a) series A and (b) series B.*

In order to compare the measured and modelled bed changes, a statistical analysis was undertaken using the Brier Skill Score (*BSS*) (see Section 4.2.5). The BSS-values of series A and series B are compared in Figure 5.2 dependent on the discharge. The BSS-values of series B simulations slightly decrease with discharge. In contrast, the BSS-values of series A simulations, in which the parameters of Run A0 were used “as it is” in all runs, gradually de-

crease with the decreasing discharge, demonstrating that a morphodynamic model calibrated with bankfull discharge does not remain valid for all sub-bankfull discharges. This highlights the significance of model calibration for each specific discharge conditions.

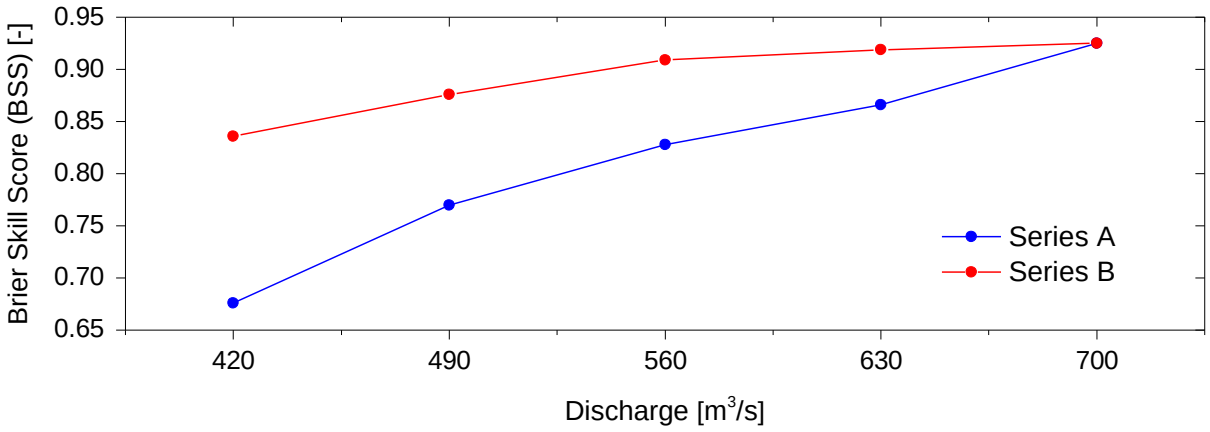

Fig. 5.2 The Brier Skill Score (BSS) of the predicted profiles for various values of flow discharge.

5.3.2 Relation between E_s and flow discharge

The results of the series B simulations suggest the need to further examine the influence of the variability of the input (calibration) parameters on the morphological simulations. The combination of the coefficients affecting the spiral flow intensity due to curvature (E_s) and transverse bed slope (α_{bn}) provided the best match between the predicted and measured bed topographies. These coefficients are uncertain (Nicholas 2013, Schuurman et al. 2013, Kasvi et al. 2015) and based on small scale flume experiments (Ikeda 1982, Struiksma et al. 1985, Talmon et al. 1995, Wiesemann et al. 2006), and therefore, were adjusted during model calibration. As outlined in Section 2.3.3, E_s is linearly related to the spiral flow parameter, and also linearly affects the transverse bed slope (equations 2.2 and 2.3). For ease of calibration, previous studies have kept E_s constant and tuned α_{bn} during calibration (e.g., Schuurman et al. 2015). Empirically the E_s parameter would be unity, which means a mild curvature in the river bends. However, during migration river bends change their curvature, and the hydrodynamics of sharp bends differs to some extent from bends with mild curvature. Increasing the value of E_s leads to an increase of the effects of curvature on the flow field, which in turn enhances the erosive potential near the outer bank as becomes visible from Figure 5.1(b). The plot of E_s as a function of discharge demonstrates that E_s is linearly related to discharge magnitude (see Figure 5.3). As expected, the higher the discharge, the smaller the value of E_s.

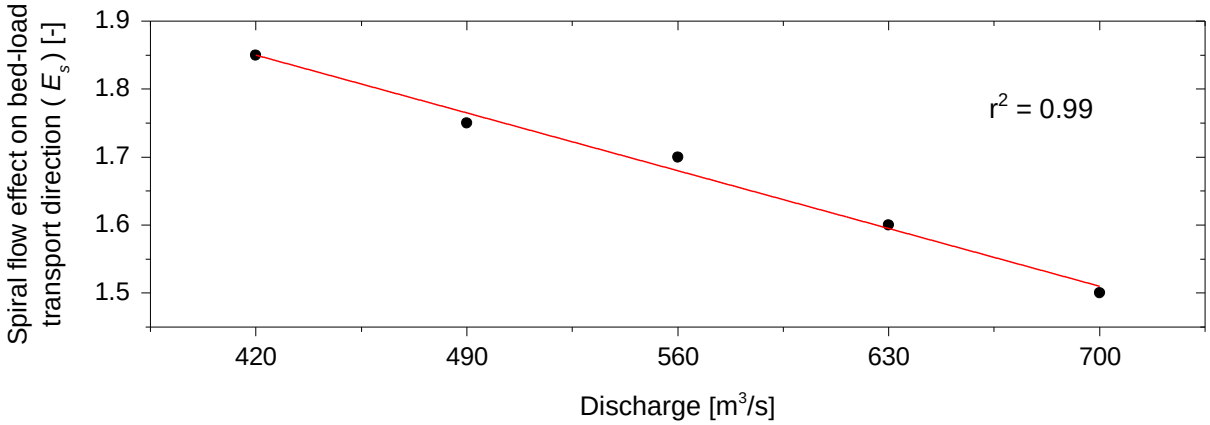

Fig. 5.3 *The E_s parameter as a function of discharge (Series B).*

5.3.3 Description of formative discharge

As outlined in Section 4.3.2.6, the meander geometry analysis was carried out under the implicit assumption that the bankfull flow (Q_{bf}) is dominant or channel-forming discharge. Recent numerical studies for natural rivers with fixed (non-erodible) wall suggest that the channel forming discharge, which controls the river bed morphology, is typically less than Q_{bf} (Frascati & Lanzoni 2013, Bolla Pittaluga et al. 2014, Lanzoni et al. 2014). The channel-forming discharge in meandering rivers with erodible floodplains can best be illustrated by means of an example. For this purpose, twenty-eight simulations were run under mobile bed conditions by varying flow discharge in the range 35 - 980 m^3 s^{-1}, in which discharge was varied by 35 m^3 s^{-1}. The parameters of Run A0 were used “as it is” in all runs (see Section 5.2).

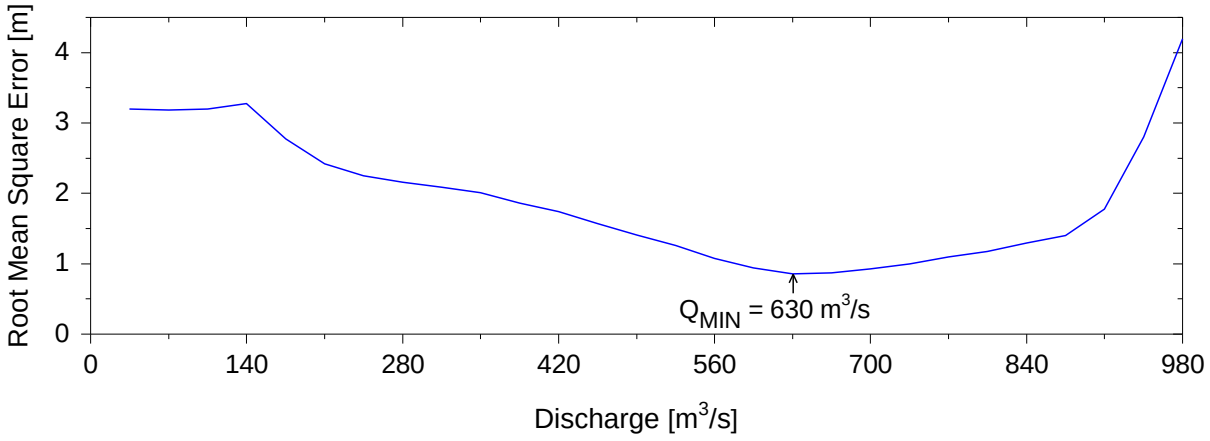

Fig. 5.4 *The Root Mean Square Error (RMSE) of the predicted profiles for various values of flow discharge. The monitoring cross-section (CS-2) is shown in Figure 3.11(a).*

The model-based predictions of bed morphology at the monitoring cross-section (CS-2 as shown in Figure 3.11(a)) were compared with field observations by means of the Root Mean Square Error (RMSE) for various values of the flow discharge. Figure 5.4 shows that minimum error is attained for a flow discharge of 630 m^3 s^{-1}. This indicates that, in the presence of erodible floodplains, the river bed morphology is determined by discharges of moderate intensity rather than by Q_{bf}. It is interesting to note that the estimated channel-forming discharge is close to the characteristic effective discharge (628 m^3 s^{-1}, see Table 3.1) which is

based on observed flow records and sediment transport measurements for the period 1996 – 2016.

5.3.4 Planform geometry

5.3.4.1 Relationships between the planform parameters and channel width

Planform geometry variables such as meander belt width (M_B), meander wavelength (λ) and radius of curvature (R) were estimated following the methodology described in Section 4.3.2.6. These variables were normalized by the channel width (B) derived from field data rather than simulation results as the modelled channel width was poorly predicted in comparison to other parameters. Relationships between M_B, λ, R and B were determined to indicate their interdependence and to reflect the degree of meander regularity for different constant discharge scenarios.

Figure 5.5 shows a comparison of model results and observations for series A and B. The subplots in the figure show that the better agreement is found in case of simulations in series B. Investigating the results in some more details reveals that, in both series, model results with bankfull discharge (Run A0) show scatter planform statistics, whereas results with sub-bankfull discharges (Run A1 - A4, Run B1 - B4) show regular planform statistics. The subtle yet significant differences between model results with bankfull discharge and sub-bankfull discharges indicate an occurrence in meandering planform change trends in response to changing discharge regimes.

The examination of the relationships among planform geometry variables reveals that meander belt width to channel width ratio (M_B/B) ranges from 4 to 6, meander wavelength to channel width ratio (λ/B) ranges from 8 to 12, and radius of curvature to channel width ratio (R/B) ranges from 1.4 to 2.4. M_B/B and λ/B ratios are in agreement with those reported in the literature (e.g., Zeller 1967, Williams 1986, Julien 2002). However, the range of the R/B ratio is lower than the range ($2< R/B <3$) commonly reported in the literature (e.g., Hickin & Nanson 1984). A further discussion is provided in Section 5.3.6.3.

(a)

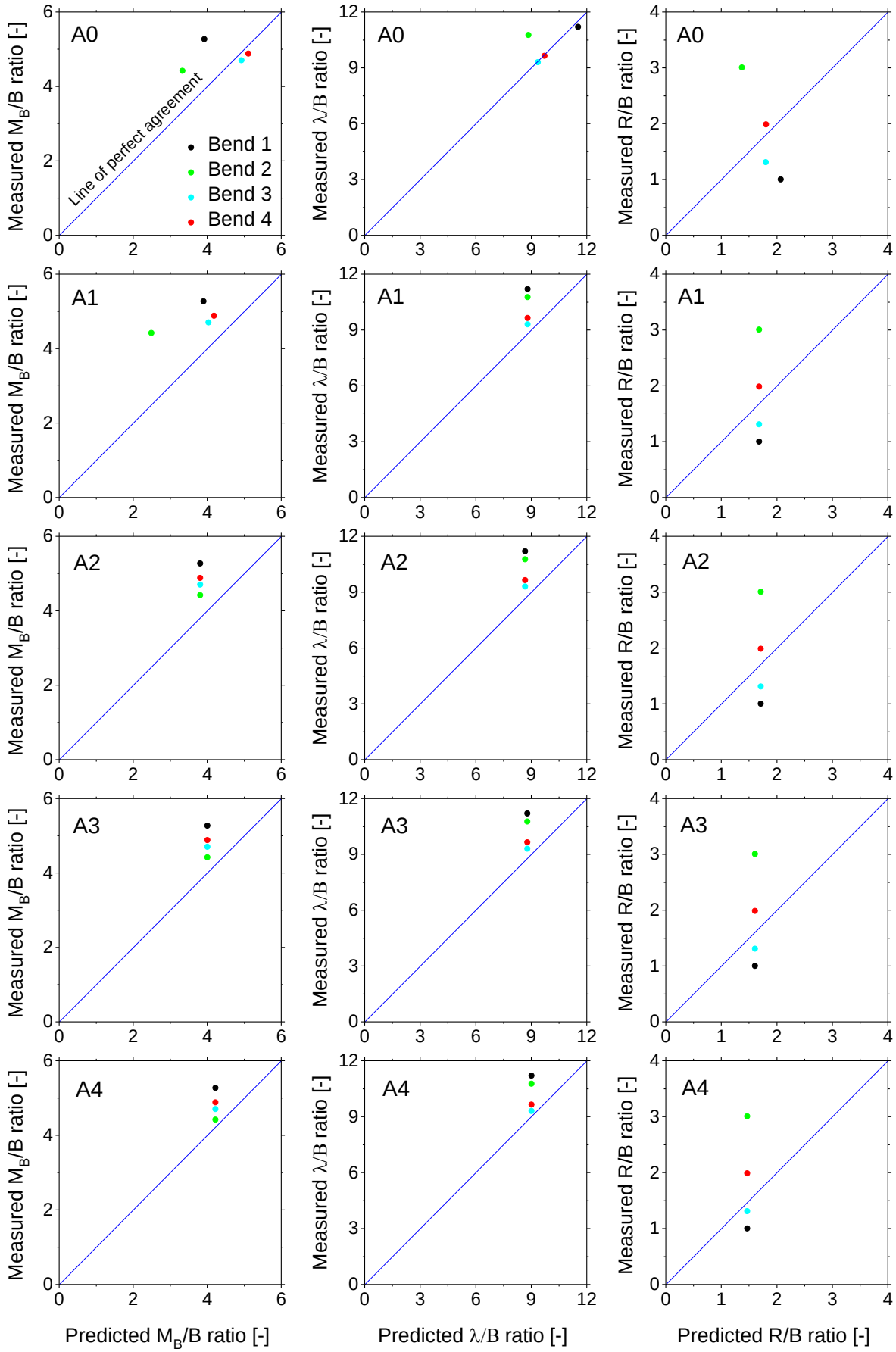
A0
A1
A2
A3
A4
Line of perfect agreement
Bend 1
Bend 2
Bend 3
Bend 4
Measured M_B/B ratio [-]
Measured λ/B ratio [-]
Measured R/B ratio [-]
Predicted M_B/B ratio [-]
Predicted λ/B ratio [-]
Predicted R/B ratio [-]

(b)

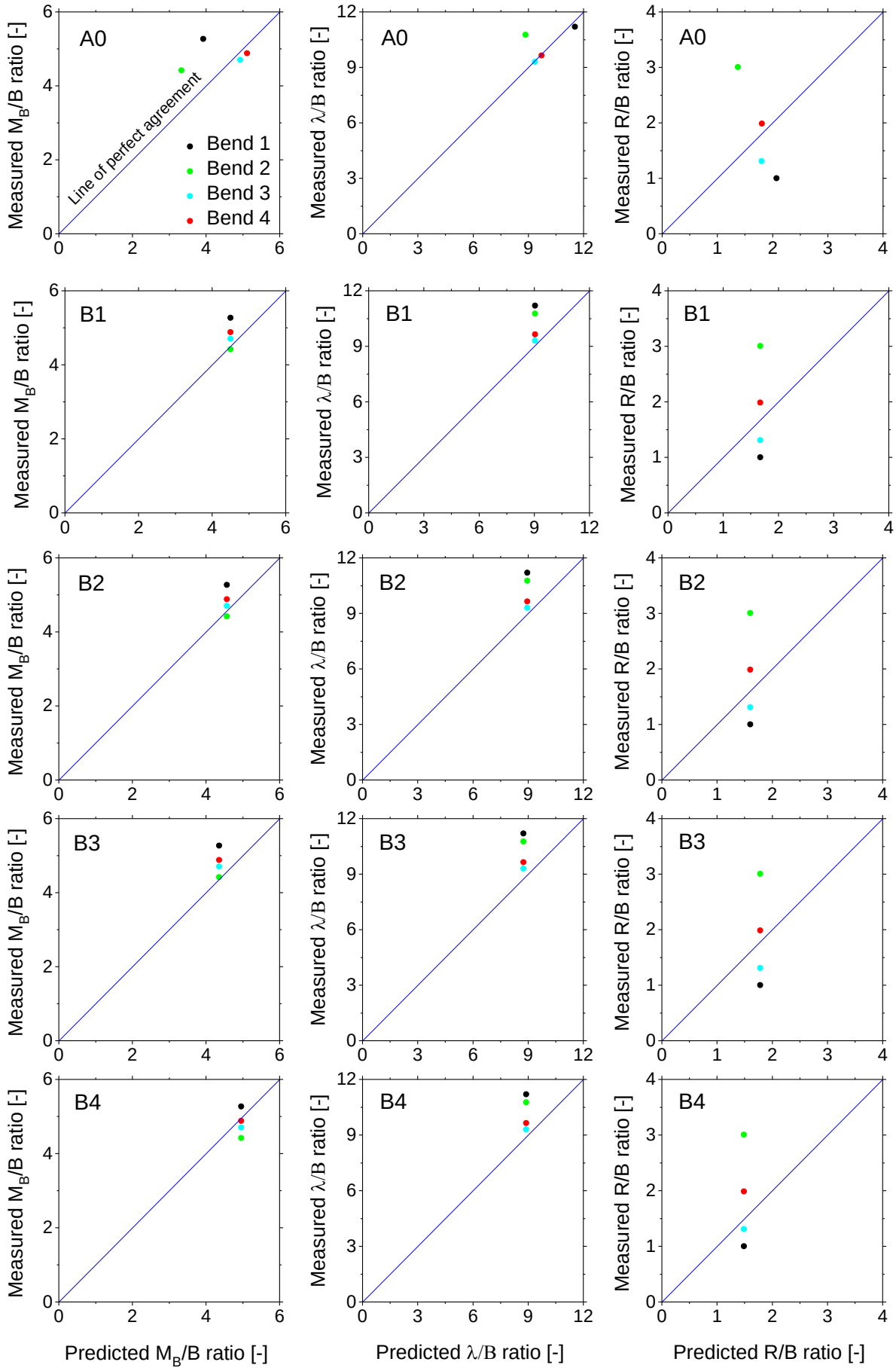

Fig. 5.5 Comparison of model results and observations (a) series A and (b) series B.

5.3.4.2 Relationships between meander wavelength and discharge

In order to investigate the link between meander wavelength (λ) and discharge (Q), the reach-averaged λ is plotted against Q in Figure 5.6, as meandering planform is best described by the wavelength (Leopold & Wolman 1960). A power regression function was applied to the results of the series B simulations in order to model the relationship between λ and Q. The algebraic manipulation of the power regression equation yields the following relation:

$$\lambda = 104\sqrt{Q} \tag{5.1}$$

where λ and Q are in meters and cubic meters per second, respectively.

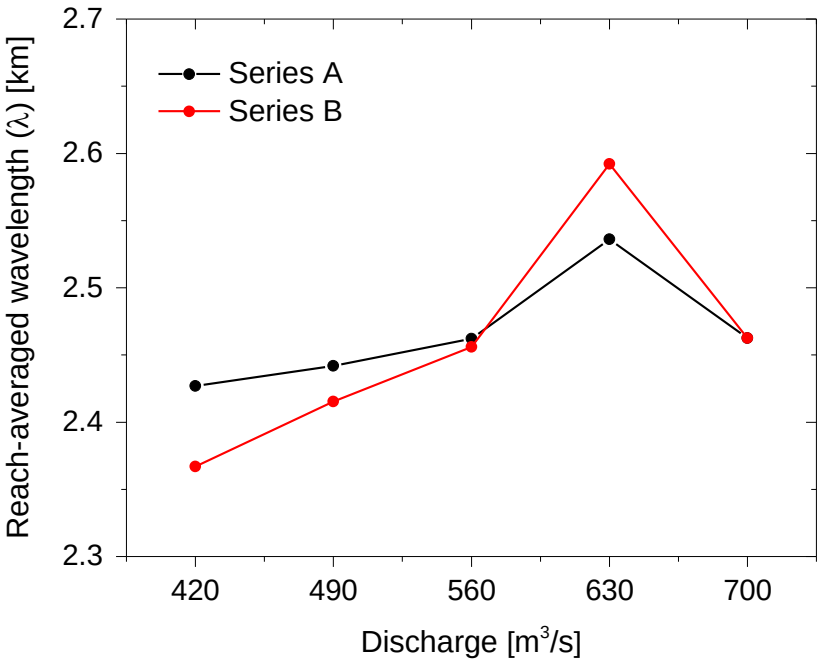

Fig. 5.6 Reach-averaged meander wavelength as a function of discharge.

In both series A and series B, a peak value of λ lies between 560 and 700 $m^3 s^{-1}$. To be more specific, the peak value is found at a discharge somewhat close to 630 $m^3 s^{-1}$. It is interesting to note that this discharge magnitude is equal to the formative discharge (see Section 5.3.3) and also close to the characteristic effective discharge for the period 1996 – 2016 (628 $m^3 s^{-1}$, see Table 3.1).

5.3.5 Meandering pattern

Figure 5.7 presents an overview of the pattern formation after morphodynamic computations of a 10 year period in both series A and series B. As expected, the higher the discharge, the higher are the changes of the planimetric configuration. Notably, lateral channel migration increased the channel bend amplitude and channel length. As the bend amplitude increased, more of the meander bend migration was in the downstream direction. This observation is in agreement with the experimental work by Friedkin (1945), who showed that the size of bends becomes greater with increase in discharge (Visconti et al. 2010, van Dijk 2013). A compari-

son of the predicted thalweg alignment in 2013 and the available thalweg information for the same year shows that closer agreement is found in the downstream part of the river reach.

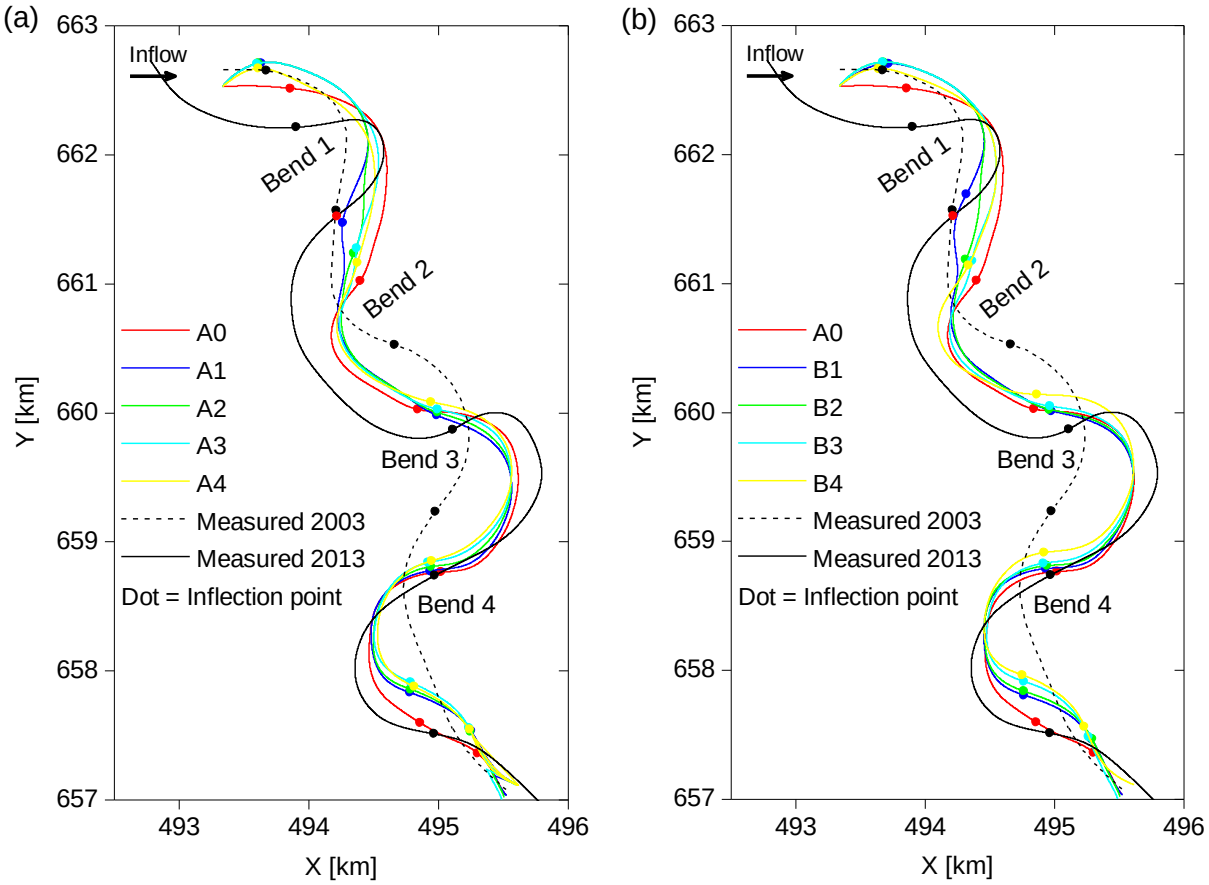

Fig. 5.7 Simulated planform (a) series A and (b) series B.

5.3.6 Migration characteristics

5.3.6.1 Maximal bank retreat

For each of the constant discharge scenarios, channel migration was quantified in terms of maximal bank retreat following the procedure described in Section 4.3.2.7. The migrated distance perpendicular to the thalweg (in 2003) was computed over the 10-year period at each meter interval on the 2003 thalweg alignment. Figure 5.8(a) shows that, in general, meander bends appear to migrate downstream as a coherent waveform. The higher the discharge, the higher the migration in the downstream direction. Figure 5.8(b) shows that, for both series A and series B, maximal bank retreat increases with discharge. This can be best explained by stream power which is expressed as a product of unit weight of water, discharge and water-surface slope. For a sand bed river, like the Dhaleshwari River, higher discharge has higher stream power as the water-surface slope is very mild. Stream power represents the energy of the river to move sediment (Bagnold 1966). Therefore, the greater its value, the greater will be the rate of sediment transport, which is the case in the present numerical tests. This result supports the findings of Nanson & Hickin (1986) and Nicoll & Hickin (2010).

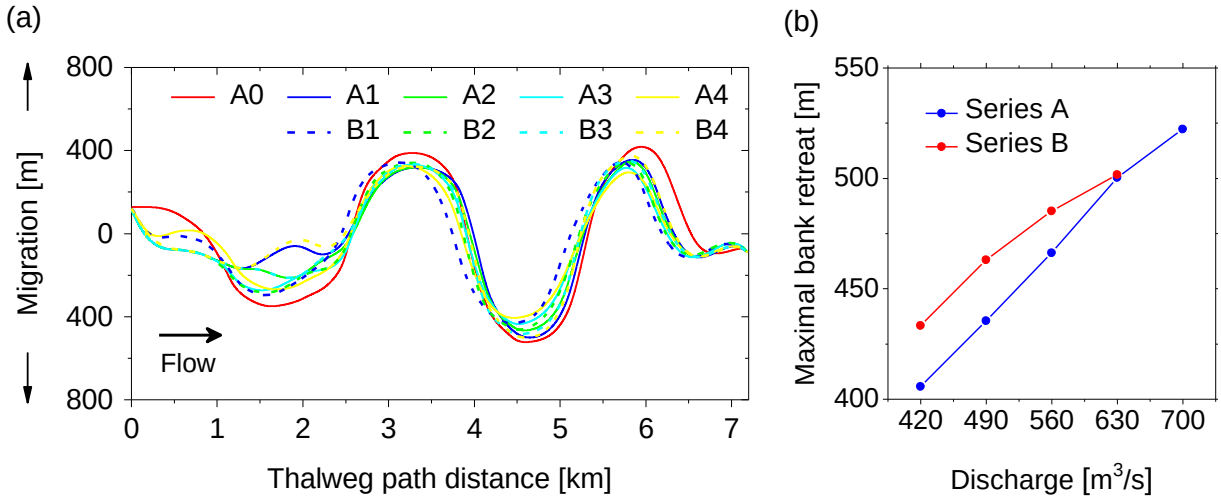

Fig. 5.8 *(a) Simulated migration along thalweg alignment and (b) maximal bank retreat as a function of discharge.*

Stream power (W m^{-1}) is defined as the rate of energy dissipation (or loss) against the bed and banks of a stream per unit downstream length (Bagnold 1966). The stream power values of series A and series B are compared in Figure 5.9(a). Series B, in which model parameters were tuned to mimic the natural channel migration at the outer bank of the monitoring cross-section as shown in Figure 5.1(b), reports higher stream power. This enhanced stream power is the result of higher water level gradient at the end of simulations as explained by the plot of water surface slope versus discharge in Figure 5.9(b). It should be noted that the plot shows a discontinuity at bankfull flow due to the fact that bankfull discharge became sub-bankfull flow as soon as the hydrodynamic adaptation took place with respect to the changing morphology (see Section 4.3.2.3), which resulted in a higher water level gradient at the end of simulation.

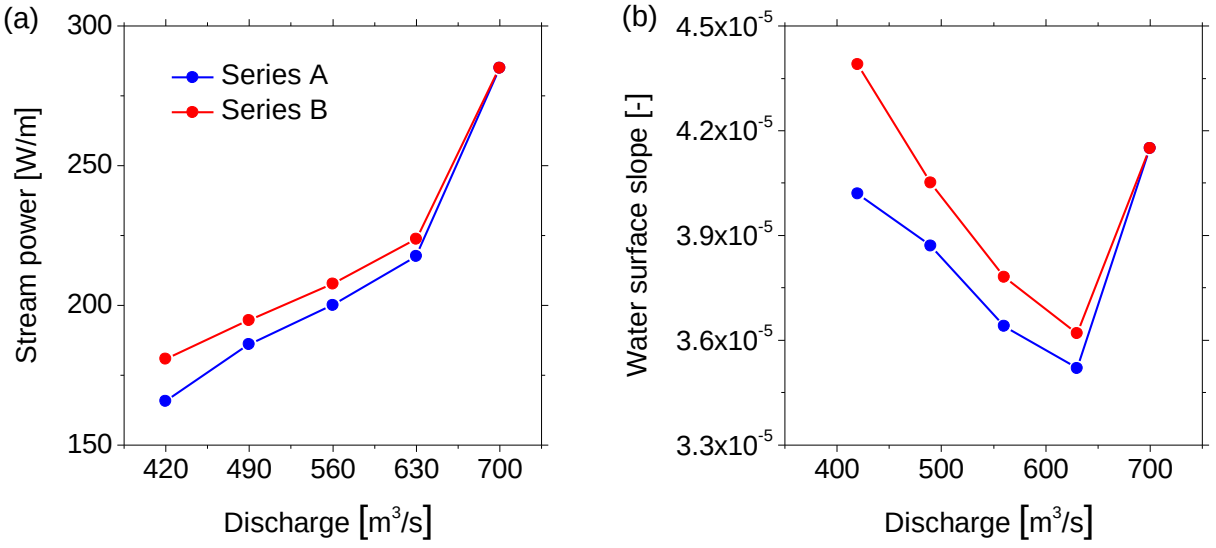

Fig. 5.9 *(a) Relationship between stream power and discharge and (b) plot of water surface slope versus discharge.*

5.3.6.2 Channel activity

The examination of the meander migration pattern over the 10-year simulation period reveals that the river meanders generally tend to translate downstream as a coherent waveform (see Figure 5.7). More importantly, the higher the flow discharge, the higher the migration in the

downstream direction. To investigate further the influence of discharge on river morphology, the migration rate in terms of channel activity was examined for the entire study reach. For each of the constant discharge scenarios, the estimation of channel activity followed the procedure described in Section 4.3.2.7. The channel migration, computed at each meter interval of the initial channel thalweg, was summarized for all bends in the study reach and then divided by the product of the initial thalweg length and the number of years, in order to obtain a reach-averaged annual migration rate. Figure 5.10 plots the channel activity as a function of discharge for both series A and series B. No significant tendencies were found that increase or decrease in value across a range of sub-bankfull discharge scenarios. The plot shows the maximum channel activity at 700 m^3 s^{-1} which was intended to be at bankfull stage, but was found sub-bankfull flow at the end of the simulation (see Section 4.3.2.3).

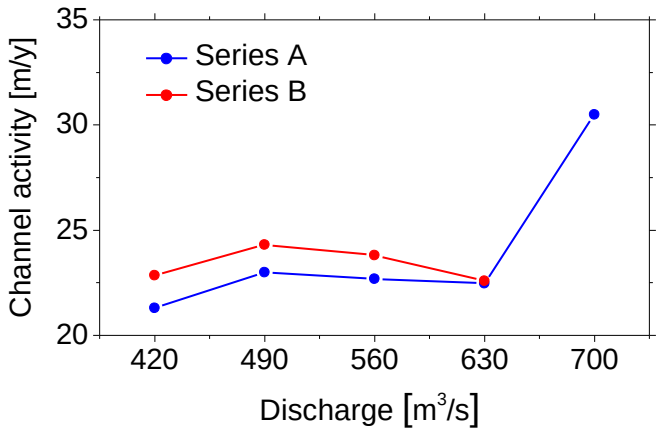

Fig. 5.10 Relationship between channel activity and discharge.

5.3.6.3 Relationship between bend migration rate and bend radius of curvature

It has been shown that the maximum lateral erosion rate for a meander bend occurs when the ratio of radius of curvature (R) to channel width (B) is in the range of about 2 to 3. In fact, Hickin & Nanson (1984) observed that the maximum bend migration rates occur at approximately R/B = 2.5 if migration rates and R/B are averaged over an appreciable portion of the bends. This result is based on the study of several sand-bed rivers in Canada. Other researchers used local instead of bend-averaged values and found that the maximum migration rates occur at R/B = 1.5 – 2.0 (e.g., Hooke 1997). Figure 5.11 plots the ratio of radius of curvature to channel width (R/B) as the independent variable and ratio of yearly meander migration rate to river channel width as the dependent variable. Considerable scatter remains in the data. The envelope curve of the relationship between migration rate and bend radius, both divided by channel width, has the same shape as reported in the literature (e.g., Hickin & Nanson 1984, Crosato 2009, Blanckaert 2011). The results indicate that the local channel migration rate increases with increasing bend sharpness until it reaches a maximum at a certain critical value (R/B = 1.7) of the bend sharpness. Beyond this critical value, the migration rate decreases if bend sharpness increases. The values of R/B corresponding to the peak resulted in good agreement with the field observations in freely meandering rivers (e.g., Hooke 1997).

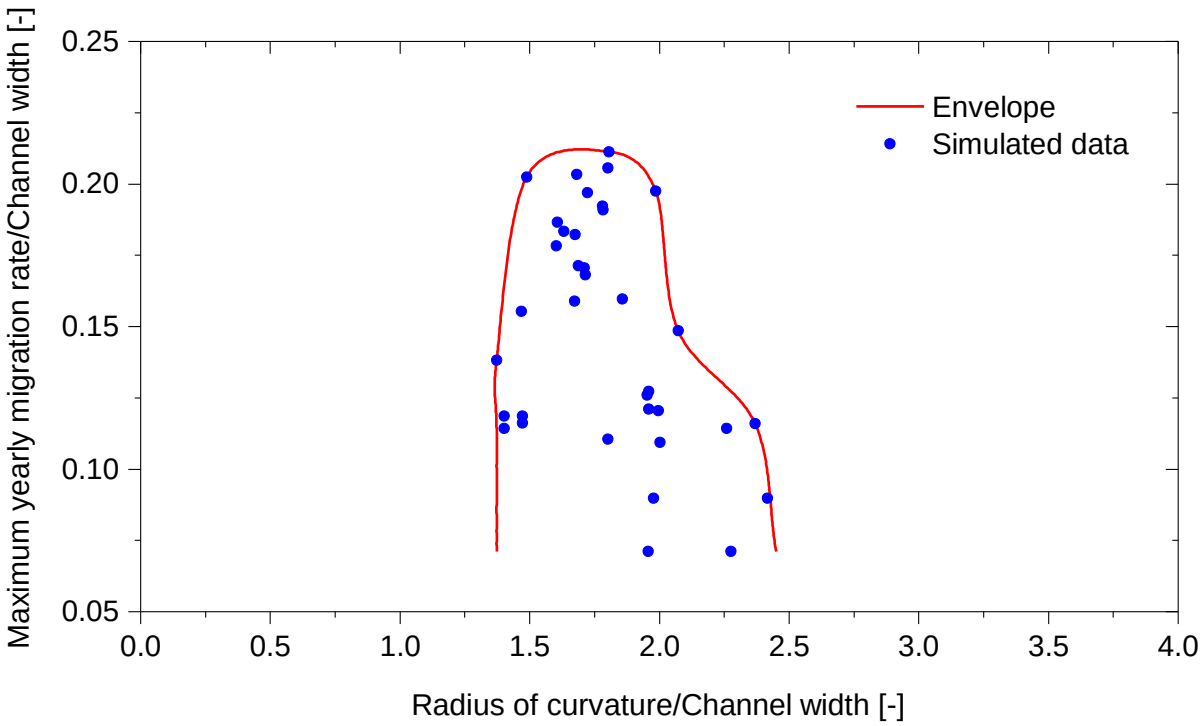

Fig. 5.11 *Local migration rates as a function of the local curvature ratio (R/B) for the simulation results (series A and series B).*

5.4 Discussion

The discussion is based on answers to questions.

How does river discharge influence the parameterization controlling the spiral flow effect on bed-load transport?

In practice, numerical morphodynamic models are based on various assumptions and simplifications, and therefore, have uncertainty in their parameterizations. Kleinhans et al. (2008), Schuurman et al. (2015) and others reported that the coefficients affecting the spiral flow intensity due to curvature (E_s) and transverse bed slope (α_{bn}) play a similar role in influencing model behavior, since both are, in effect, controlling the sediment transport. For ease of calibration, the previous studies have chosen to keep E_s equal to unity as this value is based on laboratory experiments in mildly curved bends and to tune α_{bn} during calibration using the available information of the bed topography (e.g., Vested et al. 2014, Schuurman 2015, Kasvi et al. 2015, Williams et al. 2016). It should be noted that during migration river bends change their curvature, and the hydrodynamics of sharp bends differs to some extent from bends with mild curvature. Crosato (2011), based on a personal communication with Struiksma, suggested that E_s should have a value between 0.4 and 1.2 in the case studies of real rivers. However, this assumption remains untested (Zerfu et al. 2015). The results of the simulations in the present study show that, when a model calibrated with bankfull discharge is used for the simulations with sub-bankfull discharges (series A, see Section 5.3.1), the Brier Skill Scores (*BSS*) of the predictions gradually decrease with the decreasing discharge (see Figure 5.2). This means that a morphodynamic model calibrated with bankfull discharge does not remain valid for all sub-bankfull discharge conditions, demonstrating the signifi-

cance of model calibration for each specific discharge. Investigating the relation between the calibration parameter E_s and the flow discharge reveals that the higher the discharge, the smaller are the E_s coefficient, and a linear relationship is apparent (see Figure 5.3). Further work would be useful in confirming the relationship between E_s and discharge magnitude, as it has not been previously reported. Nevertheless, this finding is useful in selecting appropriate parameter values for use in numerical tests with controlled discharge scenarios.

How does river discharge influence the meander wavelength in a meandering reach?

In numerical models, the upstream boundary condition is important since the input of water and sediment is what forces the system. The water inflow can be a hydrograph, or a ''dominant'' discharge which somehow integrates the effects of the natural hydrological regime. In order to test theories for wavelength, which is the most widely used geometric property of meanders, numerical simulations were carried out assuming constant discharge to be the dominant discharge. The analysis of the simulation results reveals that the meander wavelength is proportional to the square root of discharge (equation 5.1). The results are in line with the classical experimental results reported in Friedkin (1945), in which increase of meander dimensions with discharge has been observed. A physical explanation of an observed relationship between meander wavelength and discharge is that stream energy, which is represented by discharge, is in proportion to meander wavelength. It should be noted that factors controlling meander geometry other than discharge, such as water-surface slope, may be ignored in a mild-sloped river. It is interesting to note that the results of the study are also consistent with empirical equations that relate meander wavelength to dominant discharge (Inglis 1949, Leopold & Wolman 1957, Dury 1964, Carlston 1965, Schumm 1967, 1977, Ackers & Charlton 1970, Mackey 1993). However, the coefficient of best-fit equation, among researchers, depends upon which they select as a typical value of dominant discharge.

How to estimate the dominant discharge in a freely meandering river?

The dominant discharge is generally used as a preliminary guide for restoration design, or field evaluation of hydrologic conditions (Leopold & Wolman 1960, Goodwin 2004, Doyle et al. 2007). Morphodynamic river models generally use bankfull (or channel-forming) discharge as a representative flow rate for simulations of long-term channel response, such as evolution of meandering channels (e.g., Schuurman et al. 2016). Bolla Pittaluga et al. (2014) and Lanzoni et al. (2014) applied one-dimensional models to the Magra River (Italy) and to the Po River (Italy) respectively, and suggested that the river bed morphology is controlled by moderate discharges in the presence of fixed (non-erodible) walls. Similar results were obtained by Frascati & Lanzoni (2013), who used a two-dimensional analytical linearized model to the Po River in Italy. The above mentioned studies reported that the dominant or channel-forming discharge lies between the mean annual discharge (Q_{ma}) and the bankfull discharge (Q_{bf}) for natural rivers with fixed (non-erodible) wall. Numerical tests in the present study indicate that, in the presence of erodible floodplains, the river bed morphology is determined by a discharge of moderate intensity between Q_{ma} and Q_{bf}. It has been found that a discharge magnitude of 630 $m^3 s^{-1}$ provides least Root Mean Squared Error (RMSE) of the simulated bed topography. This value is close to the characteristic effective discharge (628 $m^3 s^{-1}$, see Table 3.1) which is based on observed flow records and sediment transport

measurements for the period 1996 – 2016. It should be noted that the flow regime not only influences channel cross-sectional shape, but also affects meander geometry. By means of numerical simulations, it has been shown how river discharge affects the reach-averaged meander wavelength (λ) in a specific meandering reach. The dominant discharge can be defined by the maximum value of the wavelength-discharge curve. The advantage of this novel method is that this simulation approach accounts for site-specific hydro-morphological and sediment characteristics. When the reach-averaged meander wavelength was plotted against discharge magnitude, a peak value in meander wavelength was found in the range between 560 and 700 $m^3 s^{-1}$, in particular, at a discharge close to 630 $m^3 s^{-1}$. Although the above mentioned three methods are based on different approaches, the computed characteristic channel-forming discharges are surprisingly similar. Therefore, it can be concluded that a discharge magnitude of about 630 $m^3 s^{-1}$ (90% of the bankfull discharge) best describes the dominant discharge of the Dhaleshwari River. The results of this study can be extrapolated to other meandering rivers with similar climatic and physical characteristics.

Which statistics must be considered for predicting migration rate in practice?

The parameters, which are frequently applied in analogous studies, are meander belt width, meander wavelength and radius of curvature. According to, among others, Magdaleno & Fernández-Yuste (2011) and van de Wiel & Darby (2004), geomorphic activity parameters (maximal bank retreat and channel activity) should be used as they provide complementary information to the planform parameters. The analysis of simulation results reveals that each discharge scenario has a different impact on planform parameters. Investigating the results in some more detail reveals that the maximal bank retreat is highly affected and the channel activity is less affected. It should be noted the maximal bank retreat refers to a single location along the reach, whereas the channel activity refers to the total floodplain area loss, summarizing the total bank retreat along the entire reach (see Section 4.3.2.7).

Hickin & Nanson (1984) showed a functional relationship between rate of migration and radius of curvature - both in non-dimensional form. The form of their relation has been verified by many other researchers subsequently (Crosato 2009, Nicoll & Hickin 2010). Although a general shape of the relation is now accepted, Hickin & Nanson's (1984) tool for application to a particular river is limited unless site specific data on observed rates of bend shifting are available for calibration purposes. Furthermore, there is no guarantee that the meander migration rate indicated by an envelope curve based on the past behavior of a river could not be exceeded in future. In light of the limitations of existing empirically-based analyses, it is argued that a process-based simulation approach could be useful as an alternative means of analyzing and predicting meander bend migration. The results of the simulations reveal that maximum migration rates occur at R/B = 1.6 – 1.8 (critical value = 1.7), which is slightly lower compared to R/B = 2 – 3 that is generally reported as being typical for freely meandering rivers (Hickin & Nanson 1984, Williams 1986) (see Figure 5.11). This difference can partly be explained by the fact that the previous studies used bend-averaged instead of local values of migration rates and R/B. These findings have important implications for the prediction of river response to changes in regime. As an illustration, for a given value of R/B for a bend in question, the probability of annual maximum migration rate per width that a certain amount of migration will occur can be estimated.

6 Effect of discharge variation

River discharge is rarely constant - it can vary rapidly, sometimes over a large range. Climate change could result in higher discharges, enhancing sediment transport and meander dynamics. It could also result in more and longer periods of drought with lower river discharge. All these issues require an investigation tool enabling the prediction of the river morphology in the longer time scales (decades to centuries). For this purpose, the final set of simulations focused on undertaking a comparison of model predictions and observed data with discharge variations in the form of an annual hydrograph. The simulation results are expected to be envelopes of the possible outcomes from computations with steady discharge scenarios as described in the previous chapter.

6.1 Hydrograph modelling approach

A hydrograph is a time history of the discharge and serves as the input parameter for the hydraulic models. To allow for the historic discharge data to be used, a simplified and real hydrograph, respectively, were considered.

6.1.1 Simplified hydrograph

Simplified discharge hydrographs are widely used to simulate interactions between flow, sediment transport, and morphology (Mosselman 1998, Crosato & Saleh 2010, Asahi et al. 2013). An important task in long-term morphological modelling is, therefore, the schematizations of the river flow that has worked through in the continual development of a river reach. To study the meander morphology in the study area, a simplified discharge hydrograph (also known as “stepped 10-day Q” hydrograph) was constructed from measured discharge time series between 2003 and 2013 (see Section 4.2.4). The suitability of this schematization is discussed by Huthoff et al. (2010). For the long-term morphological modelling, a description of the inter-annual variability of the water discharges was specified in terms of a repeated annual hydrograph (also known as “cyclic flow”), as shown in Figure 6.1. When water discharge is expressed as an input hydrograph, its evolution in the downstream direction should be considered. However, in a relatively short reach of the sand-bed river with no major tributaries in the study area, the variation of the hydrograph was neglected.

In the simplified hydrograph, the seasonal variability in a hydrological year is conserved, but the extreme flood peaks are missing. This can be explained, for instance, by means of a “stepped 10-day Q” hydrograph, in which the measured discharge data are averaged over intervals of approximately 10 days over the period of record so that 36 of these intervals form a characteristic year (Huthoff et al. 2010). Consequently, the peak discharge in this simplified hydrograph takes the value of an ordinary flood that is slightly above the bankfull discharge (Q_{bf}) (see Figure 6.1).

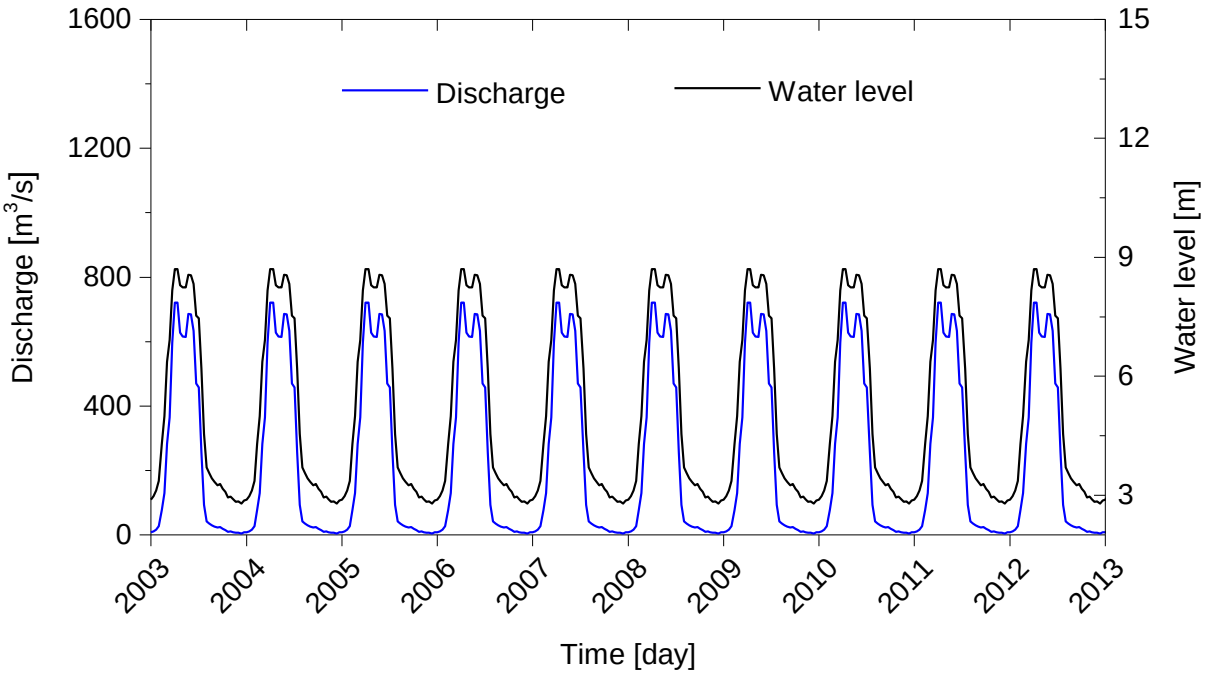

Fig. 6.1 Simplified hydrograph.

6.1.2 Real hydrograph

A real hydrograph represents a series of intensive flood events that includes both ordinary floods and high floods. The morphological changes in the study area are the result of historically different distribution of the river flow (CEGIS 2013). In order to simulate the historic morphological changes, continuous time-series of daily discharges for the period 2003 – 2013 (see Figure 3.4) were taken into account. Figure 6.2 shows that the period includes four major flood events with peak daily mean discharges of 1500 $m^3 s^{-1}$ (in 2003), 1185 $m^3 s^{-1}$ (in 2004), 1199 $m^3 s^{-1}$ (in 2008), and 1097 $m^3 s^{-1}$ (in 2010). The recurrence interval of these floods varied between 1.5 and 3 years. A brief period of acute shortage of formative discharges less than bankfull, for example, 502 $m^3 s^{-1}$ (in 2006), 538 $m^3 s^{-1}$ (in 2009), and 599 $m^3 s^{-1}$ (in 2011), also exists. Particularly against this background, the selected data are assumed to be representative to account for typical high- and low- forcing conditions.

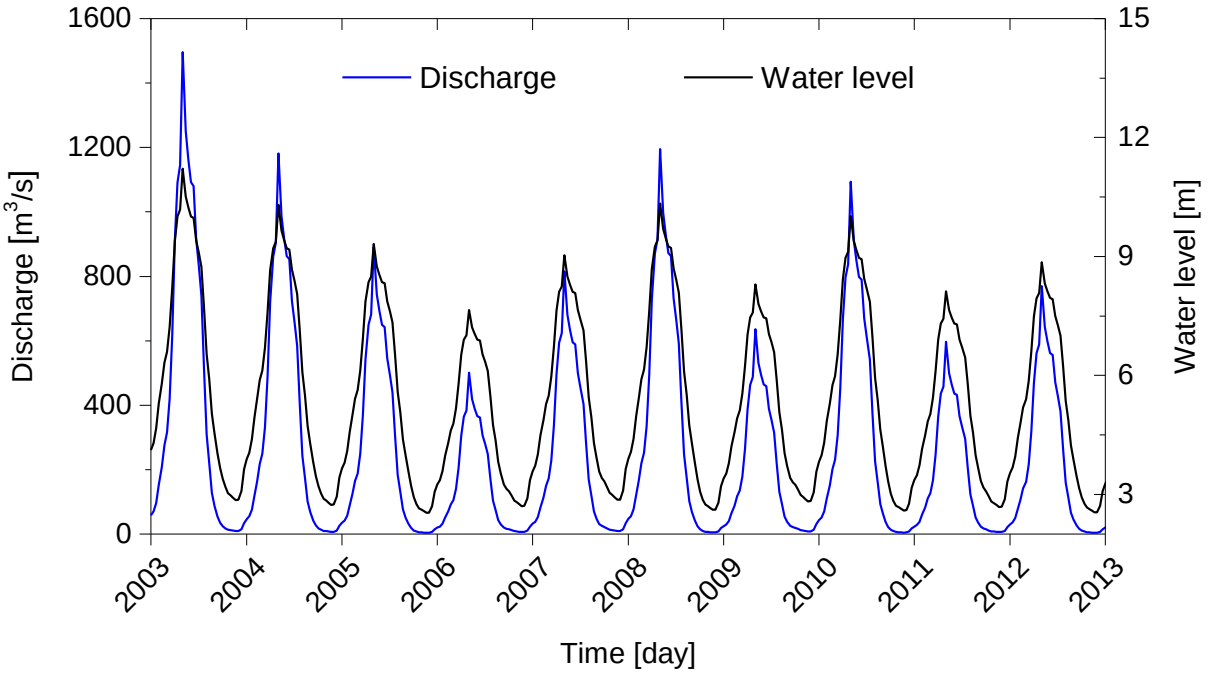

Fig. 6.2 Real hydrograph.

6.2 Model setup

The used domain, grid and bathymetry are similar to the one used in Section 5.2. For all simulations, the input hydrograph was specified at the upstream boundary and a corresponding time-series water surface elevation was set at the downstream boundary. In the absence of measured water level data, the simulation used a predicted stage-discharge relationship at the downstream boundary which is based on hydraulic calculations using measured data at Taraghat gauging station (station 137A in Figure 3.2).

The 10-year time period, from 2003 to 2013, was selected for model calibration. The entire model was given a uniform bottom roughness (Manning's coefficient = 0.054 s $m^{-1/3}$), which is the result of the calibration of the water level presented in Figure 4.20. The morphodynamic calibration strategy is similar to the one described in Section 4.3.2.3. A uniform sediment (D_{50} = 0.1 mm) was assumed, with unlimited supply from the bed. The sediment transport was predicted by the Engelund & Hansen (1967) total load transport formula. By comparing channel morphological changes at the monitoring cross-section (CS-2) as shown in Figure 3.11(b) and calculated by the model, sediment transport was scaled up by 180% (α = 1.8 in equation 4.27). To correct the sediment transport direction, the calibration factor for spiral flow effect on bed-load transport direction (E_s) and transverse bed slope effects (α_{bn}) were adjusted to 1.7 and 16, respectively. A dry cell erosion approach was considered by transferring erosion in the wet grid cell to the closest adjacent dry grid cells so that channel migration and sand movement can be simulated. The choice of $MORFAC$ = 10 allowed the simulations to stay with acceptable computation times (equation 2.12).

6.3 Results

6.3.1 Bed topography change

In case of hydrograph simulations, the river was modelled in analogy to a (dynamic) sediment-fed flume. That is, the inflow rates of water as well as the sediment inflow rates were continually changing as the sediment transport at the upstream boundary was calculated at transport capacity. The response of the bed-load transport rate to fluctuating flow discharge caused fluctuating bed elevations. This result is similar to that reported by Viparelli et al. (2011) and Wong & Parker (2006), although they used the constant sediment-feeding rate in their physical and numerical experiments. The final river alignment and bed topography are shown in Figure 6.3 where Figure 6.3(a) shows the results of the simplified hydrograph simulations and Figure 6.3(b) for the real hydrograph simulations. Both figures indicate that hydrograph simulations predict correctly the locations and patterns of bank migration evident from observed data (see Figure 3.11(a)). The resulting channel features show that the location of pools and riffles are very similar to those described by the model in Figure 4.22(a), in which the flow discharge was held constant. However, the riffles in varying discharge conditions tended to be much deeper than that of bankfull discharge condition. These results contradict the findings of Kleinhans et al. (2008) who concluded that model with constant discharge or feeding it with the discharge record would not result in very different large-scale meander morphology.

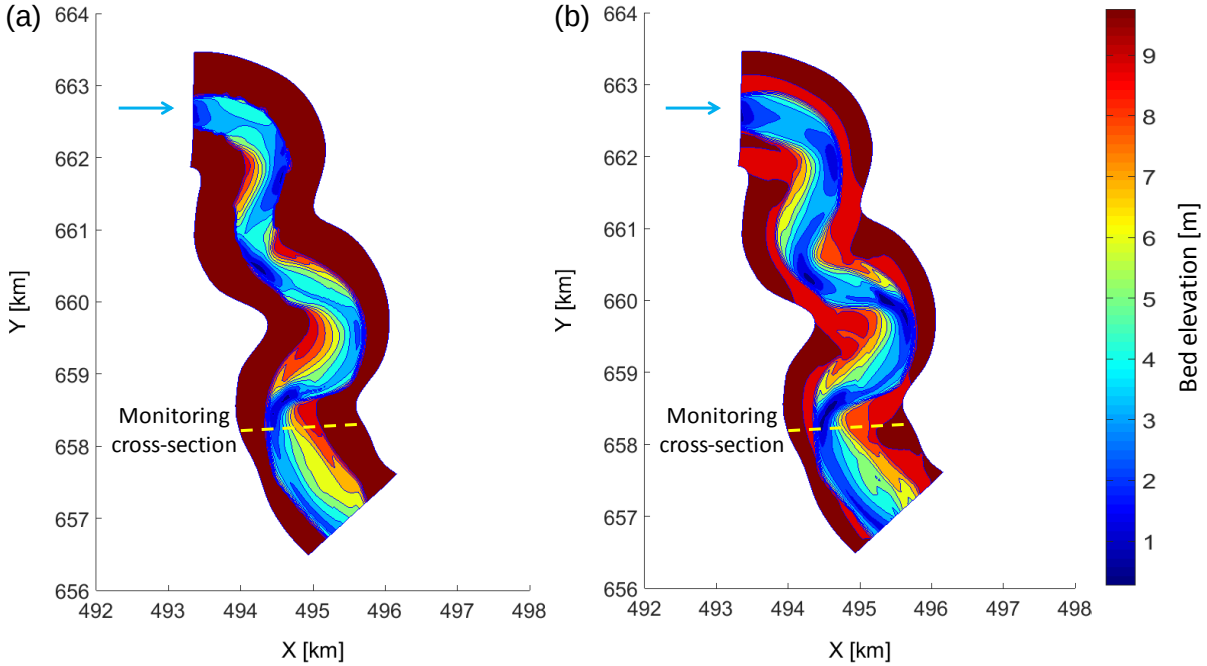

Fig. 6.3 Simulated bed topography in April 2013 (a) simplified hydrograph and (b) real hydrograph.

The direct comparison of Figures 6.3(a) and 6.3(b) reveals that the main morphological differences between the simplified and real hydrograph scenarios are found on the floodplain as the real hydrograph simulation results in a more pronounced erosion than the simplified hydrograph simulation. During over-bank flow conditions in the real hydrograph simulation, a local influx of sediment to the river channel caused erosion of the floodplain surface, which in

turn led to a slightly higher channel width than that of the simplified hydrograph simulation (see Figure 6.4).

The comparison of the transverse bed profiles of the measured and computed data is presented in Figure 6.4. The results indicate that, in both the simplified and real hydrograph simulations, the maximum deposition occurred near the inner bank, and the maximum scour depth took place near the outer bank. The direct comparison of simplified hydrograph and real hydrograph reveals that the main differences between these two simulations are found at the outer bank region as the simplified hydrograph simulation results in a more pronounced bank retreat than the real hydrograph simulation. In order to compare the measured and modelled bed changes, a statistical analysis was undertaken using the Brier Skill Score (*BSS*) (see Section 4.2.5). The skill scores obtained for simplified and real hydrograph simulations are 0.91 and 0.90, respectively, which can be classified as an excellent comparison by both van Rijn (2003) and Sutherland et al. (2004).

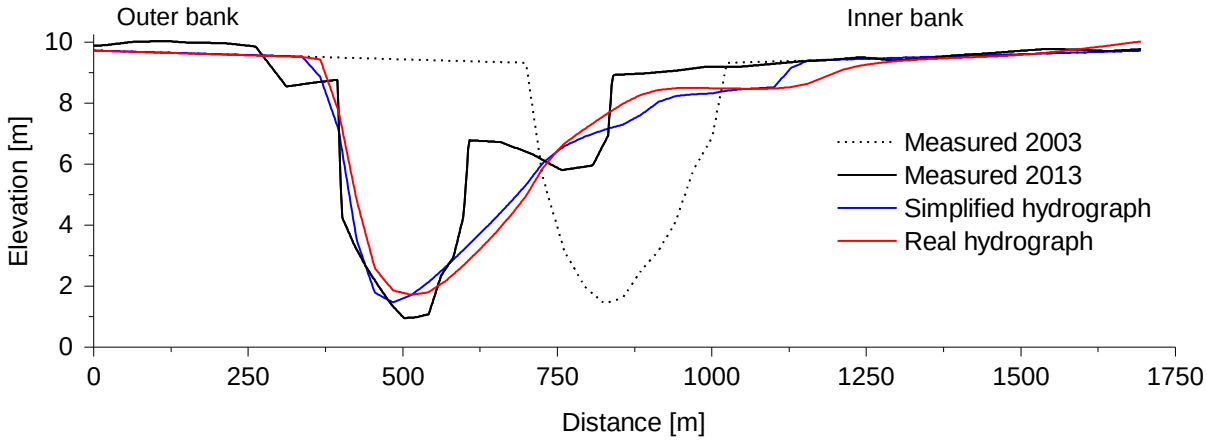

Fig. 6.4 *Comparison of observed and simulated bed topography in April 2013 at the monitoring cross-section (CS-2) as shown in Figure 3.11(a).*

6.3.2 Effect of morphological scale factor (*MORFAC*)

This section deals with the investigation of the effects of morphological scale factor (*MORFAC*) on the morphological results and how to interpret a simplified hydrograph in the prediction calculation. For large spatial-temporal scales (8.2 km and 10 years, respectively), the computational effort becomes large. For example, using a desktop computer with a moderate specification (Intel Core i7 3.50 GHz processor, 32 GB of RAM, Windows 7 ×64), the depth-averaged 2D model needs about 80 hours. In order to reduce computational costs, the *MORFAC* approach was used (equation 2.12).

Lesser et al. (2004), Roelvink (2006) and others pointed out that prediction error increases with the increase of the acceleration factor. So far, there is no selection criterion for the priori determination of the highest *MORFAC* that can be used in a given situation (Ranasinghe et al. 2011, Wilmink 2015, Williams et al. 2016). It depends on the time-varying boundary conditions and physical characteristics of a study area (Dissanayake 2011, Deltares 2014). A number of simulations were carried out for a 10-year morphological period by varying different model settings (*MORFAC*, number of cycles of the simplified hydrograph). Table 6.1 shows how parameters were varied in the numerical tests. The simplified hydrograph is cy-

cled in the simulations MF1CF and MF10CF, whereas simulations MF1 and MF10 consider a single cycle of hydrograph in the computations. Simulation MF10 takes into account a one-year hydrograph, whereas simulation MF1 uses a (hypothetical) hydrograph stretched over a whole 10-year period.

Tab. 6.1 Description of the test runs

Run	$\Sigma\Delta t_{hydro}$	$MORFAC$	Cycle of simplified hydrograph in the prediction calculation
MF1CF	10 years	1	10 cycles of the hydrograph equivalent to 10 years of hydrodynamic time.
MF10CF	1 year	10	10 cycles of the hydrograph compressed to 1 year of hydrodynamic time.
MF1	10 years	1	1 cycle of the hydrograph stretched to 10 years of hydrodynamic time.
MF10	1 year	10	1 cycle of the hydrograph equivalent to 1 year of hydrodynamic time.

The comparison of the transverse bed profiles of the measured and computed data is presented in Figure 6.5. The visual comparison suggests that, when the simplified hydrograph is cycled, both simulations MF1CF and MF10CF develop the closest match to the field data. In the former case, 10 year hydrodynamic simulation with a $MORFAC$ = 1 represents 10 years of morphodynamic evolution, whereas in the later case, 1 year hydrodynamic simulation (i.e., compressed, see Table 6.1) with a $MORFAC$ = 10 represents 10 years of morphodynamic evolution. Furthermore, the results show that different values for the $MORFAC$ result in similar behavior of the profile with only (very) small differences. On the other hand, both simulations MF1 and MF10 predict more pronounced bank retreat and significantly less scour depths near the outer bank region. Results of these simulations also suggest that different values for the $MORFAC$ result in similar behavior of the bed profile with only minor differences.

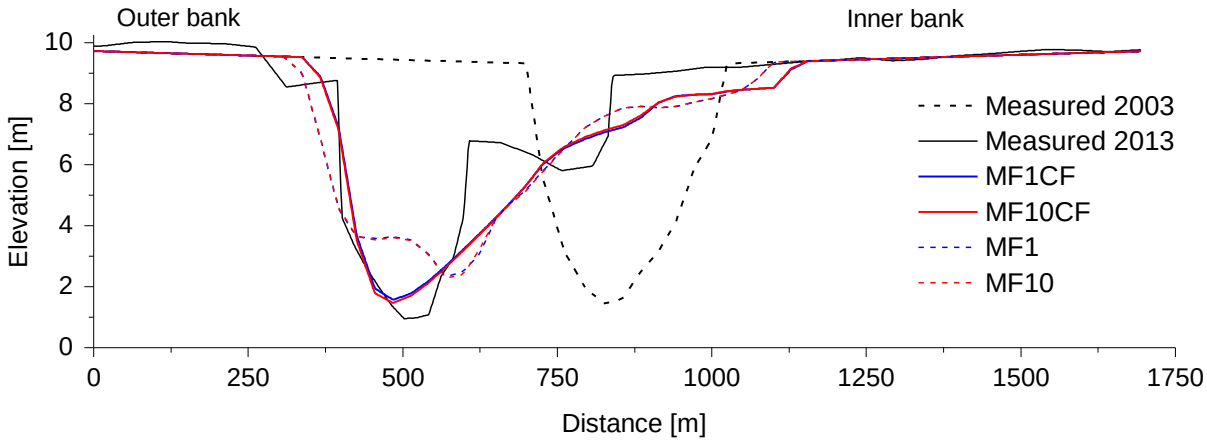

Fig. 6.5 Comparison of observed and simulated bed topography in April 2013 at the monitoring cross-section (CS-2) as shown in Figure 3.11(a).

In order to compare the measured and modelled bed changes, a statistical analysis was undertaken using the Brier Skill Score (*BSS*) (see Section 4.2.5). The statistical comparison (see Table 6.2) suggests that the integrated bed level update over the morphological period of 10 years is quantitatively similar for the tested range of $MORFAC$s. Furthermore, the results of the analysis show that it is important to consider the cycled or repeated annual hydrograph in order to investigate morphological changes for river applications. It can be concluded that flow inputs (i.e., time-varying boundary conditions) should be compressed by reducing their duration rather than the number of cycles. This result is in contrast to the findings of Williams et al. (2016), who simulated a gravel-bed braided river (Waimakariri River, New Zeland) and suggested that flow inputs can easily be reduced by reducing the number of cycles.

Tab. 6.2 Brier Skill Score (BSS) of the test runs

Run	BSS
MF1CF	0.91
MF10CF	0.91
MF1	0.88
MF10	0.88

6.3.3 Meandering pattern

Figure 6.6 represents an overview of the pattern formation in both simplified and real hydrograph simulations after morphodynamic computations of a 10 year period. As time progressed, the meandering amplitude and channel length increased. As the bend amplitude increased, more of the meander bend migration was in the downstream direction. The results of the simulations are in agreement with the experimental results reported in the literature (Friedkin 1945, Ackers & Charlton 1970, Schumm & Khan 1972, Schumm et al. 1987, Braudrick et al. 2009, Visconti et al. 2010, van Dijk 2013). The simulated meandering patterns are very similar to those described by the model in Figure 5.7, which demonstrates that the present results are envelopes of the possible outcomes from the computations with steady discharge conditions as suggested by Mosselman (1998). Investigating the results in some more detail reveals that hydrograph simulations produce a more realistic pattern of meander planform evolution that is consistent with the observed pattern in the study area. The results of these simulations also emphasize the importance of discharge variability in morphodynamic simulations and are in agreement with the results from similar studies in the literature (Larsen et al. 2006, Gautier et al. 2007, Crosato & Saleh 2010, Nicholas et al. 2013, Asahi et al. 2013, van Dijk et al. 2014, Schwendel et al. 2015).

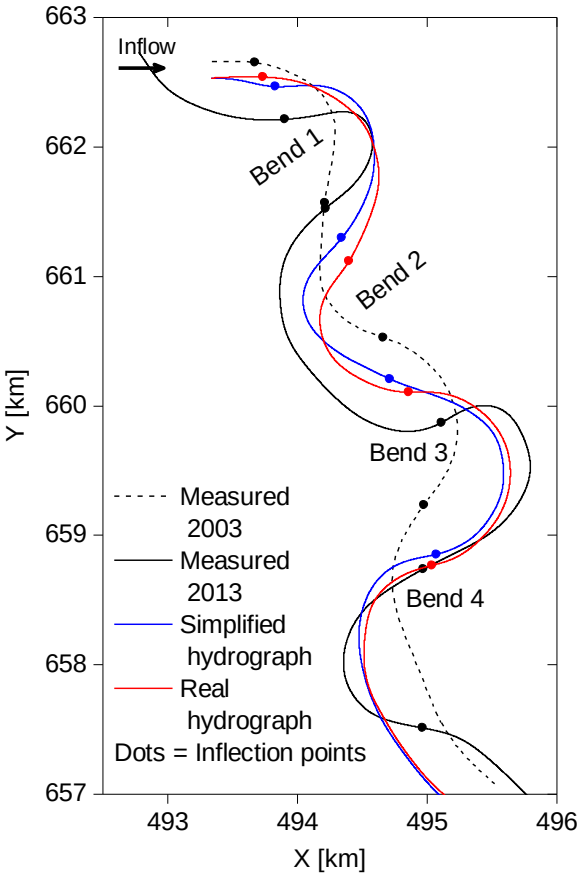

Fig. 6.6 Simulated planform.

6.3.4 Planform geometry

6.3.4.1 Relationships between the planform parameters and channel width

Planform geometry variables such as meander belt width (M_B), meander wavelength (λ) and radius of curvature (R) were estimated following the methodology described in Section 4.3.2.6. In order to generalize the results, these variables were normalized by the channel width derived from field data. The reason for not using the predicted channel width in the normalization is that the poor prediction of channel width is an artifact of the numerical model's limitations in representing the transverse bed slope (see Section 4.3.2.6).

Figure 6.7(a) plots a comparison of model results and observations for simplified hydrograph where the dashed lines show the 16% error boundaries for meander belt width and channel width ratio (M_B/B), the 31% error boundaries for meander wavelength and channel width ratio (λ/B), and the 54% error boundaries for radius of curvature and channel width ratio (R/B), respectively. The computed mean values of M_B/B, λ/B and R/B are 4.95, 11.85 and 1.81, respectively. Figure 6.7(b) plots a comparison of model results and observations for real hydrograph where the dashed lines show the 23% error boundaries for M_B/B, the 29% error boundaries for λ/B, and the 48% error boundaries for R/B, respectively. The computed mean values of M_B/B, λ/B and R/B are 4.46, 11.80 and 1.96, respectively.

The reach-averaged observed values of M_B/B, λ/B and R/B are 4.82, 10.23 and 1.82, respectively. It is to be noted that reach-averaged M_B/B and R/B values are well reproduced by both simplified and real hydrograph computations and the difference is less than 8% compared to the observed data. The difference for reach-averaged λ/B is about 16%. This difference can be ascribed to the subjectivity involved in delineating the wavelength end points from the simulated planforms (see Section 4.3.2.6). In quantitative terms, the overall agreement is reasonable. To summarize, realistic discharge variation had a relatively small effect on the long-term meander pattern, demonstrated by the reach-averaged planform statistics that fluctuated around the steady statistics of the simplified hydrograph simulation.

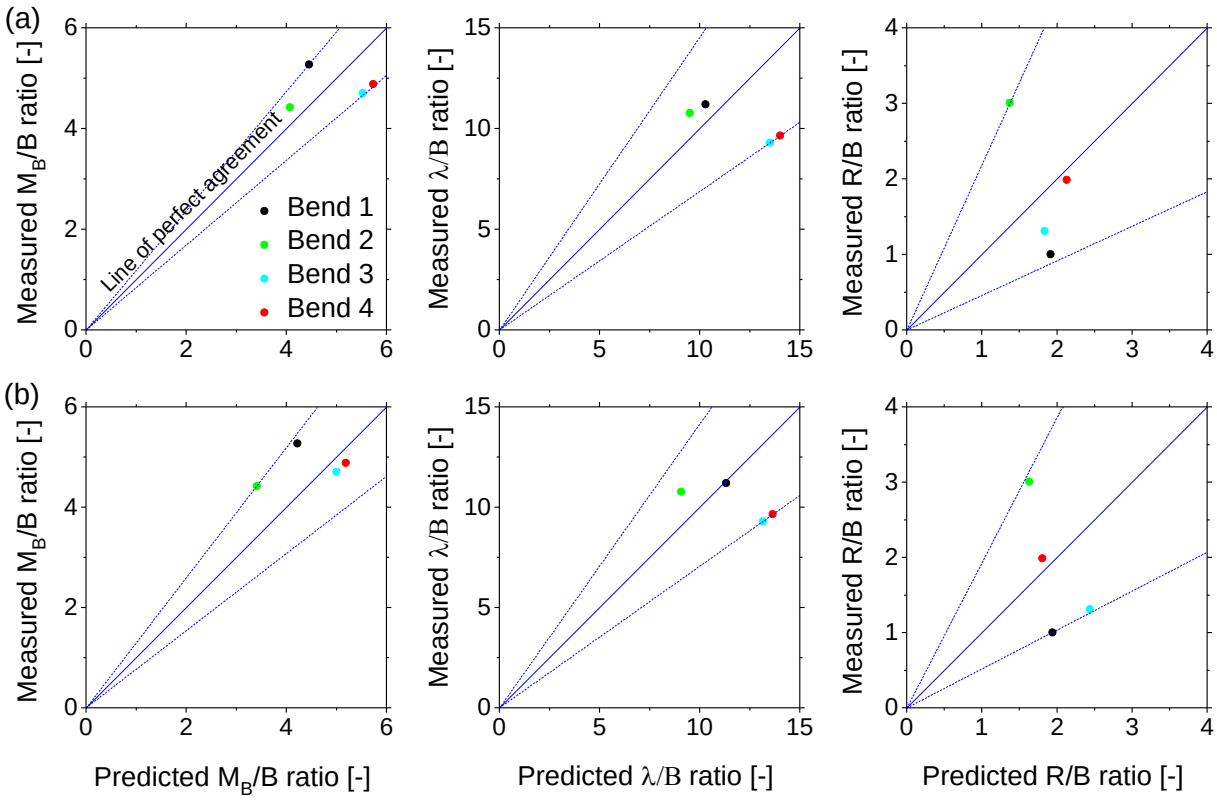

Fig. 6.7 *Comparison of model results and observations (a) simplified hydrograph and (b) real hydrograph.*

6.3.4.2 Comparison with earlier empirical equations

The only complete model of a river is the river itself where the boundary conditions include both ordinary floods and high floods. Inflow boundary conditions based on the real hydrograph incorporated the full range of discharge magnitudes and durations recorded at the Taraghat gauging station (137A) during the 10-year period. In contrast, the simplified hydrograph does not represent the historical time series of streamflow. Rather consecutive identical floods are repeated (see Figure 6.1). Therefore, in this section, the results of simplified hydrograph computations were excluded from the comparisons with prior studies. Based on the results of real hydrograph computations, the following relationships among reach-averaged planform parameters and channel width have been derived:

$$M_B \approx 4.5B \tag{6.1}$$

$$\lambda = 11.8B \tag{6.2}$$

$$R \approx 2B \tag{6.3}$$

where meander belt width (M_B), meander wavelength (λ), radius of curvature (R), and channel width (B) are in meters.

Traditionally, statistical studies of meandering channel evolution have been based on old maps (Jefferson 1902), and later, aerial photography (Leopold & Wolman 1957). The above relationships in equations 6.1 to 6.3 allow for a comparison of results with prior studies (see Table 2.1). Regression relationships for meander belt width versus channel width, both in meters, are: $M_B \approx 17.6B$ (Jefferson 1902), $M_B = 7.9B$ (Leopold & Wolman 1960) $M_B = 9.1B$ (O'Boyle 1981) and $M_B = 6B$ (Williams 1986). The apparent lack of agreement with Jefferson (1902) is mainly due to the meander belt width delineation. He defined meander belt width as the distance between tangents drawn outside of a series of meanders on the planform, whereas others used lateral distance between tangential lines of two successive meander bends.

The meander wavelength and channel width ratios (λ/B) of Jefferson (1902) at 12.6, Inglis (1949) at 12.1, Leopold & Wolman (1960) at 11.6, O'Boyle (1981) at 11.6 are close to the present numerical results (λ/B = 11.8 in equation 6.2). The ratio of radius of curvature to channel width (R/B) has a mean value in the range of 2 to 3 ($R/B \approx 2$ in equation 6.3), which is in accordance with earlier empirical relationships (e.g., Leopold & Wolman 1960, Young 1974, O'Boyle 1981, Hickin & Nanson 1984, Williams 1986). Bagnold (1960) and Hickin & Nanson (1984) indicated that the migration is largely reduced or even stopped for values outside the range of 2 to 3. Present result ($R/B \approx 2$) implies that the river is actively migrating in the studied reach.

6.3.4.3 Meandering channel response to altered flow regime

How the wavelength of alluvial meandering rivers varies with the sequence of floods is unknown. In order to investigate the meandering channel response to altered high- and low-floods, flood-driven changes were evaluated by examining a time series of meander wavelength. For the sake of simplicity, annual mean discharges were considered as floods last 4 to 6 months in the tropical monsoon climate (see Section 3.2.1) over which most geomorphological works are carried out. Reach-averaged meander wavelength was estimated at the end of the falling limb of hydrograph. Figure 6.8 plots annual mean discharge histogram and reach-averaged meander wavelength for each year. A key observation is that larger floods favor enlargement of meander wavelength and smaller floods favor shortening of meander wavelength during the first 50% of the simulation period. It is interesting to note that this tendency is similar to that reported in Section 5.3.4.2 where the meander wavelength increases with the discharge magnitude. These observations are also in consistent with those made in previous experimental studies (Friedkin 1945, Visconti et al. 2010, van Dijk 2013) and in statistical regression analysis of Inglis (1949), Leopold & Wolman (1957), Dury (1964), Carlston (1965), Ackers & Charlton (1970), Schumm (1967, 1977), and Mackey

(1993). However, after the first 5-year period, the meander wavelength becomes nearly unresponsive regardless of changes in flood magnitudes.

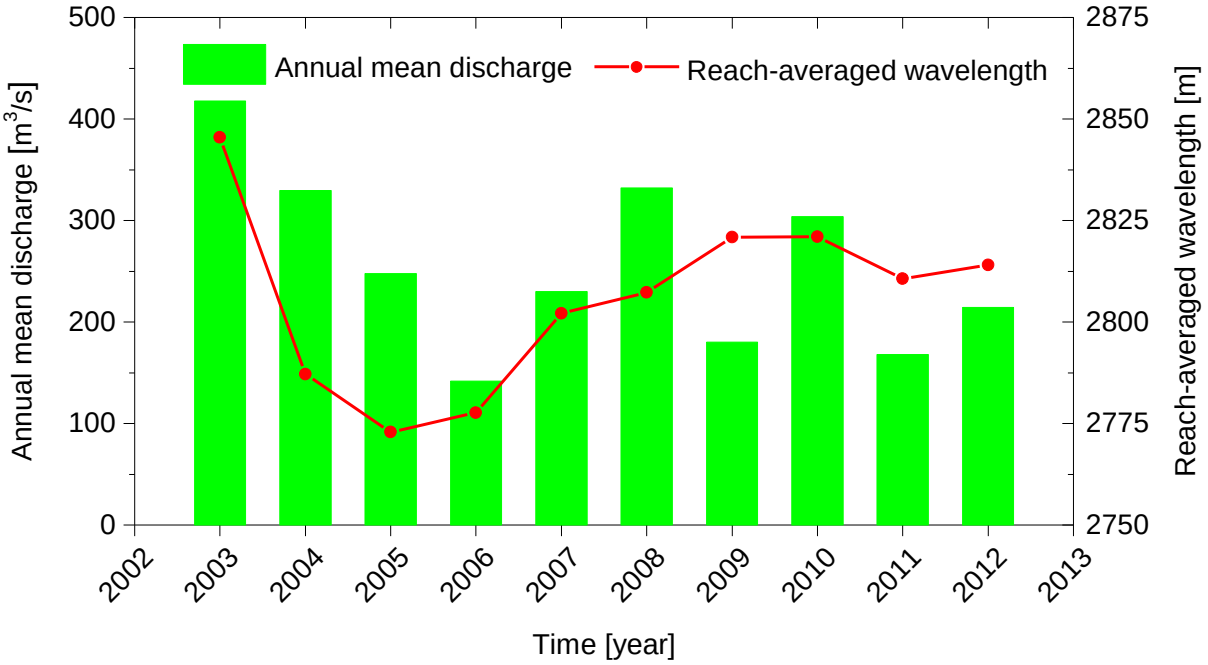

Fig. 6.8 Annual mean discharge histogram and reach-averaged meander wavelength.

6.4 Prediction of future planimetric evolution

The statistical trend analyses of the historic hydrologic data indicate that discharge series are characterized by a negative trend, suggesting a possible future water resources scarcity (see Figure 3.6). The alteration of natural flow regimes may also occur due to climate change or management strategies (such as augmentation of dry season flows). The computer model developed in the previous section can be used as a tool for predicting future channel alignments taking into account different hydrologic scenarios.

6.4.1 Scenario of simulations

The effect of hydrologic conditions was investigated by applying three discharge scenarios: reference simulation (Run No CC), climate change scenario (Run CC) and climate change with augmentation scenario (Run CC+A). The simulations were undertaken for 47 years starting from the initial bathymetry in 2003. The various future river channel simulation approaches, which are based on the prediction of future discharge scenarios, are described below.

6.4.1.1 Reference simulation

The reference simulation (Run No CC) does not take into account future climate change. Rather, it implicitly assumes that the observed monotonic trend in the past will continue into the future. For extrapolating river discharges into the future (2017-2050), a statistical moment-based Matlab script (Hydro Fit Curve, see Section 3.2.3) was used. In this method, the statistical mean of the hydrograph was calculated from the data series of the last recent years (2003-2016). The standard deviation and the mean maximum discharges for each year were computed, and then the maximum discharges were extrapolated by generating normal

random numbers. The width of the distribution was narrowed by tuning standard deviation. 0.5 standard deviations resulted in a pattern of fluctuation in time series similar to the pattern of fluctuation in the period 2003-2016.

6.4.1.2 Climate change scenario

The climate change (Run CC) scenario is a “what if” scenario in which the impact of climate change on the river discharge is superimposed onto the reference discharge scenario (Run No CC). Dasgupta et al. (2015) suggested that average monsoon flow discharge could increase in the Dhaleshwari River by 13.6 %, for the standard IPCC AR4 high-emissions, fossil-fuel intensive (A1FI) scenario in 2050, compared to the 2004 baseline (see Section 3.6). Based on this study, for simplicity, a linear increase in discharge was assumed, and was added to the reference discharge scenario for the future (2017-2050).

6.4.1.3 Climate change with augmentation scenario

The climate change with augmentation (Run CC+A) scenario stems from the climate change discharge scenario that encompasses the dry season flow augmentation. The Institute of Water Modelling (IWM) in Bangladesh investigated various options for augmenting low flows in the rivers surrounding capital Dhaka (IWM 2004). The study examined that the Dhaleshwari south off-take could be an option for the diversion of flow from the Jamuna River. Henan (2015) recommended an off-take flow of 300 $m^3 s^{-1}$ to satisfy the demands for water quality, navigation and irrigation. Later, because of unfavorable morphology at the south off-take of the Dhaleshwari River and the very active channel shifting in the meandering reaches downstream of the off-take, the “Dhaleshwari south off-take” option had not been selected as the ideal option. From the engineering point of view, it would be interesting to investigate a “what if” augmentation scenario under the future climate change (2017-2050).

6.4.2 Results of different scenarios

Figure 6.9 shows the simulated planform pattern for different scenarios in 2050, in which channel alignments are represented by the thalweg of the channel. Results of the simulations suggest that different discharge scenario results in similar behavior of the thalweg profile with only minor differences.

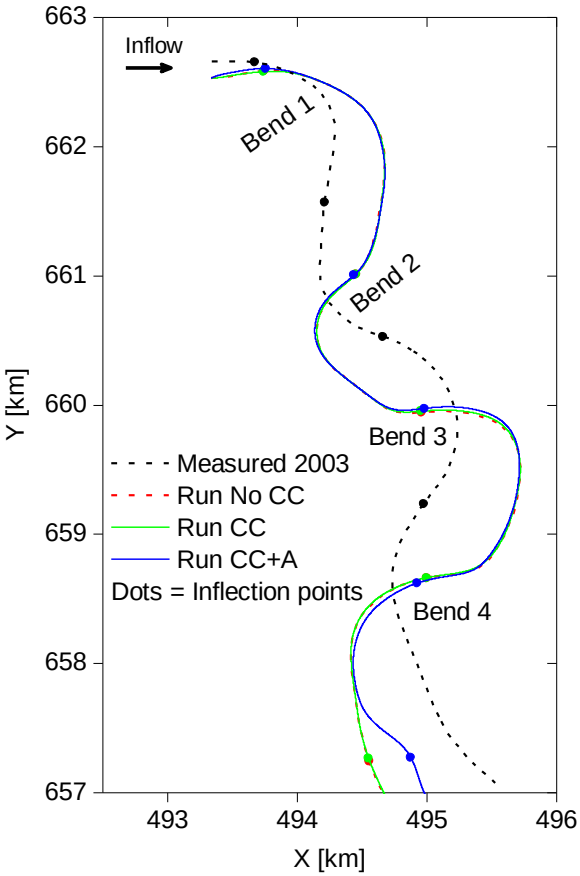

Fig. 6.9 Predicted thalweg profile in 2050 for different scenarios.

For each scenario, three planform parameters were calculated: meander belt width (M_B), meander wavelength (λ) and radius of curvature (R). In order to generalize the results, these parameters were normalized by the present channel width observed in the field, based on the assumption that meanders tend to maintain roughly constant bankfull widths during evolution (Leopold & Wolman 1960, Crosato 2008). A comparison of the planform statistics between the three simulations is shown in Figure 6.10 where Figure 6.10(a) shows the results for meander belt width and channel width ratio (M_B/B), Figure 6.10(b) for meander wavelength and channel width ratio (λ/B) and Figure 6.10(c) for radius of curvature and channel width ratio (R/B).

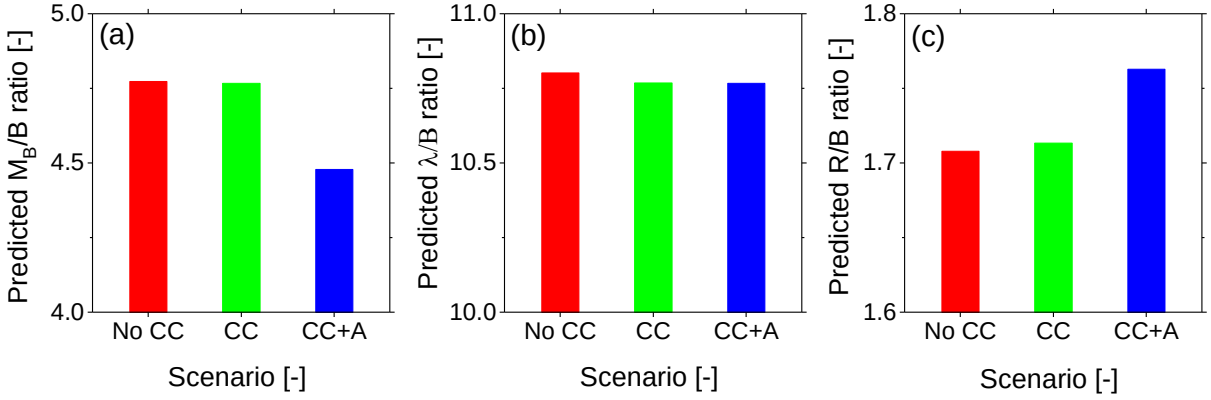

Fig. 6.10 Predicted planform parameters in 2050 for different scenarios.

The analysis of the simulation results reveals that the climate change scenario (Run CC) causes (very) small changes in the reach-averaged M_B/B, λ/B and R/B values in comparison to the reference simulation (Run No CC). The simulation results further reveal that, in case of climate change with augmentation scenario (Run CC+A), no significant tendencies to increase or decrease are found in the parameter λ/B, but the reach-averaged M_B/B might decrease by 6.5% and the reach-averaged R/B might increase by 3.2%, with respect to the reference scenario (Run No CC).

6.5 Discussion

The discussion is based on answers to questions.

How can the morphological scale factor ($MORFAC$) approach be used under an imposed cyclic hydrograph?

Morphological change typically occurs on a longer time scale than corresponding changes in flow. The $MORFAC$ approach is a technique to bridge the gap between hydrodynamic and morphological timescales (Lesser et al. 2004, Roelvink 2006). In order to reduce computational costs for long term applications, the $MORFAC$ approach is commonly used. The results of the simulations under an imposed cyclic hydrograph show that different value for the morphological scale factor ($MORFAC$) result in similar behavior of the bed profile with only (very) small differences for the tested range of $MORFAC$s (see Section 6.3.2). This finding is in good agreement with the literature (Kleinhans et al. 2008, Nicholas et al. 2013, Schuurman et al. 2015). Williams et al. (2016) suggested that, in case of cyclic flow (i.e., repeated annual hydrograph), flow inputs can easily be reduced by reducing the number of cycles. In the present study, however, resulting morphologies were found very sensitive to the cycle of simplified hydrograph in the prediction calculation. The main result of this study is that flow inputs can be compressed by reducing their duration rather than the number of cycles. This result is in contrast to the findings of Williams et al. (2016) which can partly be explained by the fact that their simulation experiments were based on a gravel-bed braided river geometry (the Waimakariri River in New Zeland) which is somewhat differing from the current research geometry.

How does the meander wavelength response to altered high- and low- floods in a meandering reach?

In the constant “dominant” discharge scenarios, it has been observed that the meander wavelength increases with the constant discharge magnitude (see Section 5.3.4.2). The aforementioned research addresses the question as whether or not meander wavelength undergo cyclic elongation or shortening due to natural variability in river discharges. In order to investigate the meandering channel response to altered high- and low- floods, a simulation was conducted using time-varying discharge record as a realistic boundary condition. The results of the simulation reveal that larger floods favor enlargement of meander wavelength and smaller floods favor shortening of meander wavelength during the first 50% of the simulation period. This observation is in agreement with the experimental work by Friedkin (1945), who showed that the size of bends becomes greater with increase in discharge. It is interesting to note that this tendency is similar to that observed in the constant discharge scenarios

where the meander wavelength increases with the discharge magnitude (see Section 5.3.4.2). However, after the first 5-year period, the meander wavelength becomes nearly unresponsive regardless of changes in flood magnitudes.

What is the impact of different hydrologic scenarios on the future river planform?

The impact of different hydrologic conditions on the river planimetric evolution in 2050 was investigated by applying three discharge scenarios: reference simulation (Run No CC), climate change scenario (Run CC) and climate change with augmentation scenario (Run CC+A). The results indicate that anticipated climate change scenario (Run CC) will have no important influence on the reach-averaged planform parameters, with respect to the reference scenario (Run No CC) (see Figure 6.10). This means that, despite the discharge increase by 0.4% per year after 2016 due to climate change, the meander planform parameters would not deviate much from the forecasted future conditions without climate change. The results further reveal that, in case of climate change with augmentation scenario (Run CC+A), the river may experience minor changes in planform variables, with respect to the reference scenario (Run No CC). These differences can be ascribed to the magnitude and duration of dry season flow. In case of Run No CC and Run CC, for a large part of the year (about 5 to 6 months), the discharge and water level were too low to transport the sediment, whereas in Run CC+A, the discharge never dropped below 300 $m^3 s^{-1}$ which is higher than the threshold discharge (approximately 105 $m^3 s^{-1}$, see Figure 5.4) that drives changes in channel morphology. Despite the continuous bed-load transport throughout the year driven by the dry season flow augmentation, the resulting planform variables exhibited minor changes from the reference scenario (see Figure 6.10). From the perspective of river management, the above results confirm that if the dry season flow augmentation plan is implemented, the river should reach conditions that are not too far from the forecasted future conditions without climate change, and consequently, remarkable and unexpected changes in river planform should not occur. The results of this study can be extrapolated to other freely meandering rivers in the Brahmaputra-Jamuna basin with similar climatic and physical characteristics.

7 Conclusions and recommendations

The main objective of the present thesis was to explore the capacity of a process-based numerical model to simulate the adaption of both planform dynamics and bed topography to changed discharge regimes. In order to achieve the main objective, six specific research questions were formulated, and the following conclusions are reached by elaborating these questions. Recommendations are given for aspects needing further investigations.

7.1 Conclusions

This section addresses the individual research questions formulated in Section 2.7.

Research question 1: Which morphological features of meandering rivers can be simulated using a process-based numerical model?

A specific reach in the Dhaleshwari River (Bangladesh) was taken as a case study as it provided data for model validation to explore the capability of the open-source code Delft3D for the simulation of morphological development. Both two-dimensional (2D) and three-dimensional (3D) modelling approaches were applied. The 3D model was used for predicting bed level changes over a one-year period and the results showed a certain degree of resemblance with the available field data, but the required computational time restricted further analyses. To achieve acceptable computational times and to enlarge the spectrum of investigated scenarios, a 2D morphological model for meander migration was subsequently applied (Section 4.3), for which the parameterization of the 3D flow effect was validated against curved flume data (Section 4.3.1). The model was then used to simulate bed morphology and meander planform adjustment in the study area over a 10-year period, under both bankfull (Section 4.3.2) and varying discharge (Chapter 6) conditions. The results showed that the 2D model was able to reproduce morphological characteristics such as scour depth, bank erosion and pool-riffle morphology, even though the model showed some deficiencies to reproduce bankfull channel width. The problem of the prediction of channel width was an artifact of the numerical model's limitations in representing the transverse bed slope. Regarding the planimetric evolution, the simulated pattern based on the bankfull discharge scenario appeared to deviate somewhat from the observed pattern in the study area (see Section 4.3.2.7), whereas simulations with varying discharge produced a more realistic planform pattern (see Section 6.3.3). The planform parameters (i.e., meander belt width, meander wavelength and radius of curvature) confirmed that the model results are realistic and are in agreement with statistical studies reported in the literature (e.g., Leopold & Wolman 1960, Hickin & Nanson 1984, Williams 1986, Julien 2002). The results further suggest that the time-varying discharge scenario is important for the prediction of bed topography and meander planform (see Section 6.3.4.2).

Research question 2: How does the input of sediment-related parameters affect the modeled morphodynamics?

The models' sensitivity to various user-defined parameters (roughness, secondary flow effect on sediment transport, transverse bed slope effect, grain size, porosity) was analyzed. The simulation of bed level changes by three-dimensional (3D) modelling was linked with the

question of how sensitive the model predictions to bed slope effects were. The statistical comparison (i.e., Brier Skill Score) of the simulations showed that parameterization of the bed slope effect introduced uncertainty in predicted topography, even though the model was calibrated with three-dimensional flow data (see Section 4.2.5). Using the depth-averaged 2D model, extensive sensitivity tests were performed to identify the key processes and most sensitive input parameters (see Section 4.3.2.5). The model showed marginal sensitivity to sediment grain size and porosity. The three most sensitive parameters were the bed roughness, the spiral flow effect on bed-load transport direction (E_s) and the parameter for the transverse bed slope effect (α_{bn}). Although the parameters E_s and α_{bn} played a similar role in influencing model behavior (channel migration laterally towards the outer bank), the parameter E_s led to correct representation of the location of pool-riffle morphology whereas α_{bn} led to formation of transverse bed slope. The results revealed that increasing the value of E_s enhanced the erosive potential near the outer bank. The relation between the calibration parameter E_s and the flow discharge revealed that the higher the discharge, the smaller was the E_s coefficient, and a linear relationship was apparent (see Figure 5.3). Further work will be useful to confirm the relationship between E_s and discharge magnitude, as such a relationship has not been previously reported.

Research question 3: How can the morphological scale factor ($MORFAC$) approach be used under an imposed cyclic hydrograph?

Hydrodynamic forcing due to varying river discharges is usually a short-term process with time scales ranging from hours to seasons whereas the morphological development of a river is examined on a timescale from seasons up to decades. Input reduction is imperative to long-term morphodynamic simulations to achieve acceptable computational times. Lesser et al. (2004) and Roelvink (2006) recommended the morphological acceleration technique ($MORFAC$) to bridge the gap between hydrodynamic and morphological timescales. In the present study, the applicability of the $MORFAC$ approach under a cycled annual hydrograph was studied using the depth-averaged 2D model (Chapter 6). The results of the simulations show that different values of $MORFAC$ result in similar behavior of the bed profile with only (very) small differences for the tested range of $MORFAC$s (see Section 6.3.2). This demonstrates that the flow inputs can be compressed by reducing their duration by using the $MORFAC$ approach. The results are in line with the previous studies (e.g., Kleinhans et al. 2008, Nicholas et al. 2013, Schuurman et al. 2015), but contradict the general conclusions by Williams et al. (2016) who suggested that, in case of cyclic hydrograph, flow inputs can easily be reduced by reducing the number of cycles. In the present study, however, resulting morphologies were found to be sensitive to the cycle of simplified hydrograph in the prediction calculation. Therefore, it can be concluded that, using a morphological scale factor ($MORFAC$), flow inputs can be compressed by reducing their duration without the need to change the order of hydrographs.

Research question 4: How does river discharge influence the meander wavelength in a meandering reach?

Empirical equations that relate meander wavelength to dominant discharge (e.g., Inglis 1949, Leopold & Wolman 1957, Dury 1964) are based on data from different reaches in the same river or different streams. To date, it has not been reported how river discharge affects meander wavelength in a specific meandering reach. In order to investigate the link between meander wavelength and discharge, numerical simulations were carried out assuming constant discharge to be the dominant discharge (Chapter 5). Discharge boundary conditions were varied from bankfull discharge to mean annual discharge by a constant discharge (equal to 10% of the bankfull discharge). The results of the simulations showed that the meander wavelength is proportional to the square root of discharge (see Section 5.3.4.2). The next step was to test whether or not meander wavelength undergoes cyclic elongation or shortening due to natural variability in river discharges. In order to investigate the meandering channel response to altered high- and low- floods, a simulation was conducted using time-varying discharge records as a realistic boundary condition (Chapter 6). The results showed that larger floods favor enlargement of meander wavelength and smaller floods favor shortening of meander wavelength during the first 50% of the simulation period (see Section 6.3.4.3). It is interesting to note that this tendency is similar to that found in the constant discharge scenarios where the meander wavelength increases with the discharge magnitude (see Section 5.3.4.2). The results also revealed that the meander wavelength becomes nearly unresponsive to altered high- and low- floods after the first 5-year period regardless of changes in flood magnitudes.

Research question 5: How to estimate the dominant discharge in a freely meandering river?

Dominant discharge is the most important parameter for river restoration or engineering design. Frascati & Lanzoni (2013), Lanzoni et al. (2014) and Bolla Pittaluga et al. (2014) described the application of numerical models to predict dominant (or channel-forming) discharge for a natural river with fixed (non-erodible) walls. The current research focused on a freely meandering reach of the Dhaleshwari River in Bangladesh (Chapter 5). The numerical tests confirmed that, in the presence of erodible floodplains, the dominant or channel forming discharge lies in between the mean annual discharge and the bankfull discharge. The results showed that a discharge magnitude of 630 $m^3 s^{-1}$ provides least Root Mean Squared Error (RMSE) of the simulated bed topography (see Section 5.3.3). This value is close to the characteristic effective discharge (628 $m^3 s^{-1}$) which was based on sediment discharge rating equation and theoretical flow frequency distributions (see Section 3.2.4). For the calculation of the dominant discharge, a new approach has been proposed. By means of numerical simulations, it was shown how river discharge affects the meander wavelength (see Section 5.3.4.2). The dominant discharge can be defined by the maximum value of the wavelength-discharge curve as the flow regime not only influences channel cross-sectional shape, but also affects meander geometry. The peak value in the wavelength-discharge curve was found in the range between 560 and 700 $m^3 s^{-1}$, in particular, at a discharge close to 630 $m^3 s^{-1}$, which coincides with the channel-forming discharge and the effective discharge. The advantage of this novel method is that this simulation approach accounts for site-specific hydro-morphological and sediment characteristics. Nevertheless, it can be concluded that a

discharge magnitude of about 630 $m^3 s^{-1}$ (90% of the bankfull discharge) best describes the dominant discharge of the Dhaleshwari River. The results of this study can be extrapolated to other freely meandering rivers with similar climatic and physical characteristics.

Research question 6: Can a process-based numerical model be used to assess the impact of hydrologic scenarios on the future river planform?

A depth-averaged 2D numerical model was applied to the Dhaleshwari River case study for predicting future channel planform (Chapter 6). The effect of hydrologic conditions on the river planform was investigated by applying three discharge scenarios: reference simulation (Run No CC), climate change scenario (Run CC) and climate change with augmentation scenario (Run CC+A). To assess the impacts of hydrologic scenarios, different scenarios were compared to the reference scenario (Run No CC), which reflects the hydrological situation for the year 2050 (see Section 6.4.2). The results showed that the anticipated climate change scenario (Run CC) will have no important influence on the planform changes in the study area. In response to the dry season flow augmentation (Run CC+A), the river may experience minor changes in the planform variables. From the perspective of river management, the above results confirm that if the dry season flow augmentation plan is implemented, the river should reach conditions that are not too far from the forecasted future conditions without climate change, and consequently, remarkable and unexpected changes in river planform should not occur. The results of this study attest that a numerical model can be used as a tool for predicting future river planimetric evolution.

7.2 Recommendations and future outlook

The main idea of this research was originally triggered by the gap that most state-of-the-art numerical models have been applied on laboratory scale or hypothetical rivers, and to a lesser extent on real rivers, and were able to model bed morphology or meander planform, but not both. In the present study, both the bed morphology and meander planform reproduction were tested in a real case study. Key challenges for predicting meandering river morphodynamics are identified. Recommendations, along with some open questions that still require further research, are described as follows:

- The study reveals that the fixed computational grid in the horizontal plane is an obstacle to any reasonable determination of meander planform parameters (see Section 4.3.2.6). In each morphological time step, the grid itself remains stationary but the flow domain adapts to bed level changes resulting from sediment transport. As a result, the cross-sections, which were orthogonal to the streamwise direction at the beginning of the simulation, are found skewed during the meander simulation, which necessitates the re-orthogonalization of the grid for the investigation for simulated planform. Unfortunately, no such adaptive grids are presently available in Delft3D. Future research should therefore focus on the development of adaptive grids to be used in modelling real rivers morphodynamics.

- In the present study, meander planform variables were normalized by the channel bankfull width derived from the field data rather than the model results. It was found that the poor prediction of channel width is an artifact of the numerical model's limita-

tions in representing the transverse bed slope (see Section 4.3.2.6). The parameterization of transverse bed slope effects, which is implemented in all process-based morphological models and is not unique to the model used in this study, is based on small-scale flume experiments (Ikeda 1982, Struiksma et al. 1985, Talmon et al. 1995). As by today, an exact parameterization of the transverse bed slope effect can only be achieved by calibration. More research needs to be performed to develop a reliable and physics-based method to quantify transverse bed slope effects. In the reach-scale field investigations, this issue cannot be properly resolved in the absence of more field data.

- It should be noted that the reality is more complex than the numerical models and that the models are less than perfect expressions of reality. In regard to channel shifting, the results of model application were highly encouraging, even though bank erosion was simplistically implemented in the model by specifying the distribution of the total amount of erosion from a wet cell to the adjacent dry cell by a user-specified percentage (ThetSD) (see Figure 4.3). A physics-based method combining the fluvial shear erosion and gravitational mass failure processes would be useful to gain more insight in the historical and future morphological evolution in meandering rivers.

- The opposite process of bank erosion, which is bank accretion, is a fundamental process leading to the channel width formation in meandering rivers. The depth-averaged 2D model used in this study lacks a bank accretion formulation, which makes it inappropriate for prediction of the channel width evolution (see Section 4.3.2.6). The processes by which inner bank deposition keeps pace with outer bank erosion are still not well understood. Even though the results of the simulations for the observed morphological changes in the studied reach are strongly relevant, this issue could not be resolved due to the poor prediction of channel bankfull width (see Section 6.3.1). Nevertheless, the results of this study provide a valuable base for continuing this line of research.

- The present study focused on discharge as an important factor in the morphological evolution in a sand-bed meandering reach. Other important factors such as bank accretion, bed sediment sorting, vegetation encroachment on point bars, and consolidation of sediment were ignored in the modelling. Furthermore, the current depth-averaged 2D model did not distinguish between bed-load and suspended load since a total sediment transport formula was used (see Section 4.1.3). Since most of the bed material load in the sand-bed river is transported in suspension (see Section 3.4.2), additional numerical experiments are required to clarify the role of graded sediment and sediment transport in suspension.

- Sediment supply from upstream and bank erosion control channel geometry in sand-bed meandering rivers with erodible banks. The present study was using sediment inflow rate at transport capacity, and the numerical simulations with varying discharge boundary conditions showed that the response of the bed-load transport rate to fluctuating flow discharge caused fluctuating bed elevations (see Section 6.3.1). An open

question is therefore whether it is possible to establish a clear association between the two sources (sediment supply from the upstream and bank erosion).

- In a depth-averaged 2D simulation, the coefficient controlling the spiral flow effect on bed-load transport direction (E_s) is of crucial importance to correctly model morphological behavior, particularly in river bends (see Section 4.3.2.5). The present study revealed that the higher the flow discharge, the smaller is the E_s coefficient, and a linear relationship is apparent (see Figure 5.3). Further research would be useful to confirm the relationship between E_s and discharge magnitude, as such a relationship has not been previously reported.

- The effect of hydrologic conditions on the river planimetric evolution was investigated by applying three discharge scenarios for the year 2050 (see Section 6.4.2). Unfortunately, it is impossible to test the accuracy of the predictions, as no measurements are available. However, the model can be used in a probabilistic framework for assessment using Monte Carlo simulations, which make it possible to consider a range of values of key parameters. Using confidence levels, the future extent of river planimetric evolution can be predicted. Presenting the results in this format would allow river managers a greater insight into the possible future channel locations.

8 References

Ackers, P., and Charlton, F.G. (1970): Meander geometry arising from varying flows. J. of Hydrol., Vol. 11, 230-252.

Asahi, K., Shimizu, Y., Nelson, J., and Parker, G. (2013): Numerical simulation of river meandering with self-evolving banks. J. Geophys. Res. Earth Surf., Vol. 118, 2208-2229, DOI:10.1002/jgrf.20150.

Bagnold, R.A. (1966): An approach to the sediment transport problem from general physics. U.S. Geol. Surv. Prof. Pap., 422-J, 37 p.

Bagnold, R.A. (1960): Some aspects on the shape of river meanders. U.S. Geol. Surv. Prof. Pap., 282-E, 135-144.

Banda, M.S., Dittrich, A., and Pervez, J. (2016): Morphodynamic modelling of a meandering sand bed river using Delft3D. River Sedimentation: Proc. of the 13th Intern. Symp. on River Sedimentation. September 19-22, 2016, Stuttgart, Germany.

Banda, M.S., and Egashira, S. (2016): Migration characteristics of a meandering river: The Madhumati River, Bangladesh. Sustainable Hydraul. in the Era of Global Change: Proc. of the 4th IAHR Europe Congress, July 27-29, 2016, Liege, Belgium.

Bates, R.E. (1939): Geomorphic history of the Kickapoo region, Wisconsin. Geol. Soc. America Bull., Vol. 50, 819-880.

Bathurst, J.C., Hey, R.D., and Thorne, C.R. (1979): Secondary flow and shear stress at river bends. J. Hydraul. Eng., Vol. 105, No. 10, 1277-1295.

Bernard, R.S. (1993): STREMR: Numerical model for depth-averaged incompressible flow. Technical report: REMR-HY-11, U.S. Army Engineer Waterways Experiment Station, Vicksburg, Mississippi, USA.

Bever, A.J., and MacWilliams, M.L. (2015): Factors influencing the calculation of periodic secondary circulation in a tidal river: numerical modelling of the lower Sacramento River, USA. Hydrol. Proc., DOI:10.1002/hyp.10690.

Biedenharn, D.S., Thorne, C.R., Soar, P.J., Hey, R.D., and Watson, C.C. (2001): Effective discharge calculation guide. Intern. J. Sediment Res., Vol. 16, No. 4, 445-459.

Blanckaert, K. (2011): Hydrodynamic processes in sharply-curved river bends and their morphological implications. J. Geophys. Res., Vol. 116, F01003, DOI:10.1029/2010JF001806.

Bogoni, M., Putti, M., and Lanzoni, S. (2017): Modeling meander morphodynamics over self-formed heterogeneous floodplains. Water Resour. Res., Vol. 53, 5137-5157, DOI:10.1002/2017WR020726.

Bolla Pittaluga, M., Luchi, R., and Seminara, G. (2014): On the equilibrium profile of river beds. J. Geophys. Res. Earth Surf., Vol. 119, 317-332, DOI:10.1002/2013JF002806.

Borsje, B.W., Roos, P.C., Kranenburg, W.M., and Hulscher, S.J.M.H. (2011): Modelling sand-wave formation in a numerical shallow water model. In RCEM 2011, 7th IAHR Symp. on River, Coastal and Estuarine Morphodynamics, Beijing, China.

Braudrick, C.A., Dietrich, W.E., Leverich, G.T., and Sklar, L.S. (2009): Experimental evidence for the conditions necessary to sustain meandering in coarse bedded rivers. Proc. Natl. Acad. Sci. U.S.A., Vol. 106, No. 40, 16936-16941, DOI:10.1073/pnas.0909417106.

Bridge, J.S. (2003): Rivers and floodplains: Forms, processes and sedimentary record. Blackwell Publishing, Oxford, UK, 504 p.

BWDB (2011): Assessment of Old Brahmaputra and Dhaleshwari River and its trend. Processing and Flood Forecasting Circle, Bangladesh Water Development Board (BWDB), Dhaka, Bangladesh.

Carlston, C.W. (1965): The relation of free meander geometry to stream discharge and its geomorphic implications. American J. Sc., Vol. 263, 864-885.

Cea, L., and Vázquez-Cendón, M.E. (2007): Depth averaged turbulence models and source terms. Numerical modelling of Hydrodynamics for water resources: Proc. of the Conf. on Numerical Modelling of Hydrodyn. Sys., 18-21 June 2007, Zaragoza, Spain.

CEGIS (2013): Report on the Dhaleshwari River under the study on 'Morphological analysis of various rivers in support of RTW Hydro-technical investigation on major rivers'. Draft report, December 2013, Center for Environmental and Geographic Information Services (CEGIS), Dhaka, Bangladesh.

CEGIS (2003): Planform analysis of the Dhaleshwari River in connection with the Elasin bridge project. July 2003, Center for Environmental and Geographic Information Services (CEGIS), Dhaka, Bangladesh.

Chang, H.H. (1988): On the cause of river meandering. In White, W.R., editor, Intern. Conf. on River Regime, New York, John Wiley & Sons, 83-93.

Chu, K., Winter, C., Hebbeln, D., and Schulz, M. (2013): Improvement of morphodynamic modelling of tidal channel migration by nudging. Coast. Eng., Vol. 77, 1-13, DOI: 10.1016/j.coastaleng.2013.02.004.

Chu, K., Winter, C., Hebbeln, D., and Schulz, M. (2011): Optimization scheme for coastal morphodynamic model. J. Coast. Res., Vol. 64, 736-740.

Cronin, K.C., Devoy, R.J.D., and Gault, J. (2009): The value of different modelling approaches to investigate estuarine morphodynamics. J. Coast. Res., Vol. 56, 932-936.

Crosato, A., Desta, F.B. Cornelisse, J., Schuurman, F., and Uijttewaal W.S.J. (2012): Experimental and numerical findings on the long-term evolution of migrating alternate bars in alluvial channels. Water Resour. Res., Vol. 48, W06524, DOI:10.1029/2011WR011320.

Crosato, A., and Saleh, M.S. (2010): Numerical study on the effects of floodplain vegetation on river planform style. Earth Surf. Proc. Land., Vol. 36, 711-720.

Crosato, A. (2009): Physical explanations of variations in river meander migration rates from model comparison. Earth Surf. Proc. Land., Vol. 34, No. 15, 2078-2086.

Crosato, A. (2008): Analysis and modelling of river meandering. PhD thesis, TU Delft, the Netherlands, IOS Press, ISBN 978-1-58603-915-8.

Crosato, A. (1989): Meander migration prediction. Excerpta, G.N.I., Vol. 4, 169-198, Publisher Libreria Progetto, Padova, Italy.

Darby, S.E., Alabyan, A.M., and Van de Wiel, M.J. (2002): Numerical simulation of bank erosion and channel migration in meandering rivers. Water Resour. Res., Vol. 38, No. 9, 1163, DOI:10.1029/2001WR000602.

Dam, G., Van der Wegen, M., and Roelvink, J.A. (2013): Long-term performance of process-based models in estuaries. Proc. Coast. Dyn. Conf., Archachon, France.

Dasgupta, S., Zaman, A., Roy, S., Huq, M., Jahan, S., and Nishat, A. (2015): Urban flooding of Greater Dhaka in a changing climate: Building local resilience to disaster risk. Directions in development. Washington, DC: World Bank. DOI:10.1596/978-1-4648-0710-7. License: Creative Commons Attribution CC BY 3.0 IGO.

De Vries, M. (1993): Use of models for river problems. Studies and reports on Hydrology, Vol. 51, United Nations Educational, ISBN-13: 978-9231028618.

Deltares (2014): Delft3D-FLOW, User manual: Simulation of multi-dimensional hydrodynamic flows and transport phenomena, including sediments. Version: 3.15, Revision: 36498, 24 October 2014. Available at: http://oss.deltares.nl/web/delft3d/manuals.

Dey, S. (2014): Fluvial hydrodynamics, hydrodynamic and sediment transport phenomena. Springer Publisher, 2014.

Dietrich, W.E., and Whiting, P. (1989): Boundary shear stress and sediment transport in river meanders of sand and gravel. In River Meandering, Ikeda S., Parker G. (eds), American Geophys. Uni., Washington, USA, 1-50.

Dissanayake, P.K. (2011): Modelling morphological response of large tidal inlet systems to sea level rise. PhD thesis, UNESCO-IHE, Delft.

Dittrich, A., and Huppmann, O. (2013): Morphodynamics of the Rhine river between the weirs Märkt and Breisach. Leichtweiß-Institute for Hydraulic Engineering and Water Resources, Mitteilungen, Heft 158/13.

Doyle, M.W., Shields, D., Boyd, K.F., Skidmore, P.B., and Dominick, D. (2007): Channel-forming discharge selection in river restoration design. J. Hydraul. Eng., Vol. 133, No. 7, 831-837, DOI:10.1061/(ASCE)0733-9429(2007)133:7(831).

Duan, J.G., and Julien, P.Y. (2010): Numerical simulation of meandering evolution. J. Hydrol., Vol. 391, No. 1/2, 34-46.

Duan, J.G., and Julien, P.Y. (2005): Numerical simulation of the inception of meandering channel. Earth Surf. Proc. Land., Vol. 30, 1093-1110.

Duran, R., Beevers, L., Crosato, A., and Wright, N.G. (2009): Bank retreat study of a meandering river reach case study: River Irwell. In Proc. of the 7th Intern. Symp. of Ecohydraulics, Concepción, Chile, ISBN 978-981-08-2100-5.

Dury, G.H. (1976): Discharge prediction, present and former, from channel dimensions. J. Hydrol., Vol. 30, 219-245.

Dury, G.H. (1964): Principles of underfit streams. U.S. Geol. Surv. Prof. Pap., Vol. 452-A, Washington, DC.

Egozi, R., and Ashmore, P. (2009): Experimental analysis of braided channel pattern response to increased discharge, J. Geophys. Res., Vol. 114, F02012, DOI:10.1029/2008JF001099.

Einstein, H.A. (1950): The bed-load function for sediment transportation in open-channel flows. U.S. Dept. of Agriculture, Soil Conservation Service, Tech. Bull., No. 1026.

Engel, F.L., and Rhoads, B.L. (2016): Three-dimensional flow structure and patterns of bed shear stress in an evolving compound meander bend. Earth Surf. Proc. Land., Vol. 41, 1211-1226, DOI:10.1002/esp.3895.

Engelund, F., and Hansen, E. (1967): A monograph on sediment transport in alluvial streams. Tech. Univ. of Denmark, Technisk Forlag, Copenhagen, Denmark.

Fargue, L. (1868): Etude sur la correlation entre la configuration du lit et la profondeur d'eau dans les rivières a fond mobile. Annales des Ponts et Chaussées, Vol. 38, 34-92.

Fatichi, S. (2011): MATLAB code for the Mann-Kendall non-parametric trend test modified to account for autocorrelations. Available at http://www.mathworks.com/matlabcentral/fileexchange/25533-mann-kendall-modified-test [Verified 24 November 2017].

Ferro, V., and Porto, P. (2012): Identifying a dominant discharge for natural rivers in southern Italy. Geomorphology, Vol. 139, 313-321.

Frascati, A., and Lanzoni, S. (2013): A mathematical model for meandering rivers with varying width. J. Geophys. Res. Earth Surf., Vol. 118, No. 3, 1641-1657. DOI:10.1002/jgrf.20084.

Friedkin, J.F. (1945): A laboratory study of meandering of alluvial rivers. U.S. Waterways Experiment Station, Vicksburg.

Frostick, L.E., McLelland, S.J., and Mercer, T.G. (2011): Users guide to physical modelling and experimentation: Experience of the HYDRALAB network. Taylor & Francis (IAHR Design Manual). https://books.google.at/books?id=R-eMQXU85HAC. ISBN 9780415609128.

Gao, Y. (2017): Dealing with missing data in hydrology - Data analysis of discharge and groundwater time-series in Northeast Germany. PhD thesis, Freie Universität Berlin, Germany.

Gaurav, K., Tandon, S., Devauchelle, O., Sinha, R., and Métivier, F. (2017): A single width-discharge regime relationship for individual threads of braided and meandering rivers from the Himalayan Foreland. Geomorphology, Vol. 295, 126-133.

Gautier, E., Brunstein, D., Vauchel, P., Roulet, M., Fuertes, O., Guyot, J.L., Darozzes, J., and Bourrel, L. (2007): Temporal relations between meander deformation, water discharge and sediment fluxes in the floodplain of the Rio Beni (Bolivian Amazonia). Earth Surf. Proc. Land., Vol. 32, 230-248.

George, D.A., Gelfenbaum, G., and Stevens, A.W. (2012): Modeling the hydrodynamic and morphologic response of an estuary restoration. Estuaries and Coasts, DOI:10.1007/s12237-012-9541-8.

Goodwin, P. (2004): Analytical solutions for estimating effective discharge. J. Hydraul. Eng., Vol. 130, 729-738.

Guan, M., Wright, N.G., Sleigh, P.A., Ahilan, S., and Lamb, R. (2016): Physical complexity to model morphological changes at a natural channel bend. Water Resour. Res., DOI:10.1002/2015WR017917.

Guan, M., Wright, N.G., Sleigh, P.A., and Carrivick, J.L. (2015): Assessment of hydro-morphodynamic modelling and geomorphological impacts of a sediment-charged jökulhlaup, at Sólheimajökull, Iceland. J. Hydrol., Vol. 530, 336-349.

Gutierrez, R.R., Abad, J.D., Parsons, D.R., and Best, J.L. (2013): Discrimination of bed form scales using robust spline filters and wavelet transforms: Methods and application to synthetic signals and bed forms of the Ro Parana, Argentina. J. Geophys. Res. Earth Surf., Vol. 118, No. 3, 1400-1418, DOI:10.1002/jgrf.20102.

Hager, W.H. (2003): Fargue, founder of experimental river engineering. J. Hydraul. Res., Vol. 41, No. 3, 227-233.

Hasegawa, K. (1989): Universal bank erosion coefficient for meandering rivers. J. Hydraul. Eng., Vol. 115, No. 6, 744-765.

Hasselaar, R.W. (2012): Development of a generic automated instrument for the calibration of morphodynamic Delft3D model applications. MSc thesis, TU Delft.

Henan (2015): Feasibility study on Buriganga River restoration project. Vol. 1, Final report, Henan Water & Power Engineering Consulting Co. Ltd. with DUCT Engineering Ltd. from Bangladesh, December 2015.

Hickin, E.J., and Nanson, G.C. (1984): Lateral migration rates of river bends. J. Hydraul. Eng., Vol. 110, No. 11, 1557-1567.

Hooke, J.M. (2008): Temporal variations in fluvial processes on an active meandering river over a 20-year period. Geomorphology, Vol. 100, No. 1, 3-13.

Hooke, J.M. (2007): Complexity, self-organization and variation in behavior in meandering rivers. Geomorphology, Vol. 91, 236-258.

Howard, A.D. (1992): Modelling channel migration and floodplain development in meandering streams. In Lowland Floodplain Rivers, Carling P.A., Petts G.E. (eds.), John Wiley & Sons: Chichester, 1-42.

Howett, J. (2017): Meander belt delineation: Developing a predictive model for meander belt width. MSc thesis, Electronic thesis and dissertation repository, 4915. https://ir.lib. uwo. ca/etd/4915.

Hsieh, T.Y., and Yang, J.C. (2003): Investigation on the suitability of two dimensional depth averaged models for bend flow simulation. J. Hydraul. Eng., Vol. 129, No. 8, 597-612.

Huthoff, F., van Vuren, S., Barneveld, H.J., and Scheel, F. (2010): On the importance of discharge variability in the morphodynamic modelling of rivers. River Flow 2010, Proc. of the Intern. Conf. on Fluvial Hydraulics, Braunschweig, Germany, 985-991.

Hydralab+ (2016): Critical review of challenges for representing climate change in physical models. Deliverable 8.I, Editor: McLelland S., van de Lageweg W., Baynes E., 181 p.

Ikeda, S. (1988): Lateral bed load transport on side slopes. In: Civil Engineering Practice 2, Technomic Publishing Company, USA.

Ikeda, S. (1982): Lateral bed-load transport on side slopes. J. Hydraul. Div., Vol. 108, No. 11, 1369-1373.

Ikeda, S., Parker, G., and Sawai, K. (1981): Bend theory of river meanders. Part 1: Linear development. J. Fluid Mech., Vol. 112, 363-377.

Inglis, C.C. (1949): The behavior and control of rivers and canals. Research Publication No. 13, Central Water-power Irrigation and Navigation Research Station, Poona, India.

IWFM (2011): Hydrological and morphological study and environmental impact assessment (EIA) of proposed 500m RCC bridge over the Dhaleshwari River at Nagarpur upazila of Tangail district. Draft final report, April 2011, Institute of Water and Flood Management (IWFM), BUET, Dhaka, Bangladesh.

IWM (2004): Feasibility and mathematical model study of approaching and investigating strategy for rehabilitating the Buriganga-Turag-Shitalakhya river system and augmentation of dry season flow in the Buriganga River. Final report, August 2004, Institute of Water Modelling, Dhaka, Bangladesh.

Jagers, H.R.A. (2003): Modelling planform changes of braided rivers. PhD thesis, University of Twente, the Netherlands.

Jefferson, M.S.W. (1902): Limiting width of meander belts. Nat. Geogr. Mag., Vol. 13, 373-384.

Johannesson, H., and Parker, G. (1989): Linear theory of river meanders. In Ikeda S. and Parker G., (Eds.), River Meandering, American Geophys. Union, Washington, D.C.

Johannesson, H., and Parker, G. (1987): Theory of river meanders. Project report no. 278, St. Anthony Falls Hydraul. Lab., University of Minnesota, 147 p.

Johannesson, H., and Parker, G. (1985): Computer simulated migration of meandering rivers in Minnesota. Project report no. 242, St. Anthony Falls Hydraul. Lab., University of Minnesota, p. 73.

Julien, P.Y. (2002): River Mechanics. Cambridge University Press, 434 p.

Julien, Y. (1985): Planform geometry of meandering alluvial channels. Report CER84-85PYJ5, Dept. of Civil Eng., Colorado State University, Colorado, 49 p.

Kahya, E., and Kalayci, S. (2004): Trend analysis of streamflow in Turkey. J. Hydrol., Vol. 289, 128-144, DOI:10.1016/j.jhydrol.2003.11.006.

Kaless, G., Mao, L., Moretto, J., Picco, L., and Lenzi, M.A. (2015): The response of a gravel-bed river planform configuration to flow variations and bed reworking: a modelling study. Hydrol. Proc., Vol. 29, 3812-3828, DOI:10.1002/hyp.10504.

Kalkwijk, J.T., and De Vriend, H.J. (1980): Computation of the flow in shallow river bends. J. Hydraul. Res., Vol. 18, No. 4, 327-342, DOI:10.1080/00221688009499539.

Kasvi, E., Laamanen, L., Lotsari, E., and Alho, P. (2017): Flow patterns and morphological changes in a sandy meander bend during a flood-spatially and temporally intensive ADCP measurement approach. Water, Vol. 9, No. 106, DOI:10.3390/w9020106.

Kasvi, E., Alho, P., Lotsari, E., Wang, Y., Kukko, A., Hyyppä, H., and Hyyppä, J. (2015): Two-dimensional and three-dimensional computational models in hydrodynamic and morphodynamic reconstructions of a river bend: sensitivity and functionality. Hydrol. Proc., Vol. 29, No. 6, 1604-1629, DOI:10.1002/hyp.10277.

Kasvi, E., Vaaja, M., Alho, P., Hyyppä, H., Hyyppä, J., Kaartinen, H., and Kukko, A. (2013): Morphological changes on meander point bars associated with flow structure at different discharges. Earth Surf. Proc. Land., Vol. 38, 577-590.

Kendall, M.G. (1975): Rank correlation methods. 4th ed., Charles Griffin, London.

Kikillus, A., Seitz, L., Haun, S., and Wieprecht, S. (2016): Long-term numerical investigations of the effects of training structures in a river reach with ongoing river bed deepening. River Sedimentation: Proc. of the 13th Intern. Symp. on River Sedimentation, September 19-22, 2016, Stuttgart, Germany.

Kiss, T., and Sipos, G. (2007): Braid-scale channel geometry changes in a sand-bedded river: significance of low stages, Geomorphology, Vol. 84, 209-221, DOI:10.1016/j.geomorph.2006.01.041.

Kleinhans, M.G., Jagers, H.R.A., Mosselman, E., and Sloff, C.J. (2008): Bifurcation dynamics and avulsion duration in meandering rivers by one-dimensional and three-dimensional models, Water Resour. Res., 44, W085454, FOI:10.1029/2007WR005912.

Knighton, A.D., and Nanson, G.C. (1993): Anastomosis and the continuum of channel pattern. Earth Surf. Proc. Land., Vol. 18, 613-625.

Konsoer, K.M., Rhoads, B.L., Best, J.L., Langendoen, E.J., Abad, J.D., Parsons, D.R., and Garcia, M.H. (2016): Three-dimensional flow structure and bed morphology in large elongate meander loops with different outer bank roughness characteristics. Water Resour. Res., Vol. 52, No. 12, 9621-9641, DOI:10.1002/2016WR019040.

Lacey, G.G. (1930): Stable channels in alluvium. In: Minutes of the proceedings of the institution of civil engineers, Thomas Telford-ICE Virtual Library, Vol. 229, 259-292.

Lagasse, P.F., Spitz, W.J., Zevenbergen, L.W., and Zachmann, D.W. (2004): Handbook for predicting stream meander migration. Transportation Research Board, Washington, DC. ISBN 978-0-309-08814-5.

Lane, S.N., Bradbrook, K.F., Richards, K.S., Biron, P.M. and Roy, A.G. (2000): Secondary circulation cells in river channel confluences: measurement artefacts or coherent flow structures? Hydrol. Proc., Vol. 14, 2047-2071.

Lanzoni, S., Luchi, R., and Bolla Pittaluga, M. (2014): Modelling the morphodynamic equilibrium of an intermediate reach of the Po River (Italy). Adv. Water Resour., Vol. 81, 95-102, DOI:10.1016/j.advwatres.2014.11.004.

Larsen, E.W., Fremier, A.K., and Girvetz, E.H. (2006): Modeling the effects of variable annual flow on river channel meander migration patterns, Sacramento River, California, USA. J. American Water Resour. Assoc., Paper No. 04231.

Legleiter, C.J., Harrison, L.R., and Dunne, T. (2011): Effect of point bar development on the local force balance governing flow in a simple, meandering gravel bed river, J. Geophys. Res., Vol. 116, No. F1, F01005, DOI:10.1029/2010JF001838.

Leonardi, N., Canestrelli, A., Sun, T., and Fagherazzi, S. (2013): Effect of tides on mouth bar morphology and hydrodynamics. J. Geophys. Res.: Oceans, Vol. 118, No. 9, 4169-4183.

Leopold, L.B., and Maddock, T.J. (1953): Hydraulic geometry of stream channels and some physiographic implications. U.S. Geol. Surv. Prof. Pap., Vol. 252, 55 p.

Leopold, L.B., and Wolman, M.G. (1960): River meanders. Geol. Soc. of America Bull., Vol. 71, No. 6, 769-794.

Leopold, L.B., and Wolman, M.G. (1957): River channel patterns: Braided, meandering, and straight. Geol. Surv. Prof. Pap., 282 B, Physiographic and Hydraulic Studies of Rivers, U.S. Dept. of the Interior, U.S. Gov. Print. Off., Washington, DC.

Leopold, L.B., Wolman, M.G., and Miller, J.P. (1964): Fluvial processes in geomorphology. W.H. Freeman and Co., San Francisco, U.S.A.

Lesser, G.R., Roelvink, J.A., Kester, J.A.T.M.V., and Stelling, G.S. (2004): Development and validation of a three-dimensional morphological model. Coast. Eng., Vol. 51, 883-915, DOI:10.1016/j.coastaleng.2004.07.014, 2004.

LGED (2014): Report on the subsoil investigation for the construction of 520.60m bridge over the Dhaleshwari River on Nagarpur-Mirzapur via Mokna upazila road under Tangail district. December 2014, Local Government Engineering Department (LGED), Dhaka, Bangladesh.

Lien, H.C., Hsieh, T.Y., Yang, J.C., and Yeh, K.C. (1999): Bend-flow simulation using 2D depth-averaged model. J. Hydraul. Eng., Vol. 125, No. 10, 1097-1108.

Lindley, E.S. (1919): Regime channels. Proceedings, Punjab Engineering Congress, Vol. 7, 63 p.

Lotsari, E., Thorndycraft, V. and Alho, P. (2015): Prospects and challenges of simulating river channel response to future climate change. In: Progress in Physical Geography, http://hdl.handle.net/10138/224861.

Lotsari, E., Wainwright, D., Corner, G.D., Alho, P., and Käyhkö, J. (2013): Surveyed and modelled one-year morphodynamics in the braided lower Tana River. Hydrol. Proc., Vol. 28, No. 4, 2685-2716.

Mackey, S.D. (1993): Theoretical modeling of alluvial architecture. PhD thesis, State University of New York, Bringhamton, USA.

Magdaleno, F., and Fernández-Yuste, J. (2011): Meander dynamics in a changing river corridor. Geomorphology, Vol. 130, 197-207.

Mann, H.B. (1945): Non-parametric test against trend. Econometrica, Vol. 13, No. 3, 245-259, DOI:10.2307/1907187.

Métivier, F., Lajeunesse, E., and Devauchelle, O. (2017): Laboratory rivers: Lacey's law, threshold theory, and channel stability. Earth Surf. Dyn., Vol. 5, No. 1, 187-198, DOI: 10.5194/esurf-5-187-2017.

Mosselman, E. (1998): Morphological modelling of rivers with erodible banks. Hydrol. Proc., Vol. 12, No. 8, 1357-1370.

Motta, D., Abad, J.D., Langendoen, E.J., and Garcia, M.H. (2012a): A simplified 2D model for meander migration with physically-based bank evolution. Geomorphology, Vol. 163, 10-25.

Motta, D., Abad, J.D., Langendoen, E.J., and García, M.H., (2012b): The effects of floodplain soil heterogeneity on meander planform shape. Water Resour. Res., V. 48, 17 p., DOI: 10.1029/2011WR011601.

Mousavi, A., Mehrnahad, A.R., and Pirestani, M.R. (2012): 3-dimensional numerical model and laboratory for flow and bed deformation around a T-shaped spur dike in a 90° bend. Sixth Intern. Conf. on Scour and Erosion (ICSE6), August 27-31, 2012, Paris.

Murshed, K.G. (1991): Effect of bank erosion products on meander migration. MSc thesis No. H.H. 82, UNESCO-IHE, Delft, the Netherlands.

Muste, M., Aberle, A., Admiraal, D., Ettema, R., Garcia, M.H., Lyn, D., Nikora, V., and Rennie, C. (2017): Experimental hydraulics: Methods, instrumentation, data processing and management. Volume II: Instrumentation and measurement techniques - CRC press book, ISBN 9781138027534 - CAT# K25651, 906 p.

Nabi, M., Ottevanger, W., and Giri, S. (2016): Computational modelling of secondary flow on unstructured grids. River Sedimentation: Proc. of the 13th Intern. Symp. on River Sedimentation, September 19-22, 2016, Stuttgart, Germany.

Nanson, G.C., Hickin, E.J. (1986): A statistical analysis of bank erosion and channel migration in western Canada. Geol. Soc. of America Bull., Vol. 97, 497-504.

Nash, J.E., and Sutcliffe, J.V. (1970): River flow forecasting through conceptual models, Part I - A discussion of principles. J. Hydrol., Vol. 10, No. 3, 282-290, DOI:10.1016/0022-1694(70)90255-6.

Navier, C.L.M.H. (1823): Mem Acad. R. Sci. Paris, Vol. 6, 389-416.

NHC (2016): Flood and riverbank erosion risk management investment program (FRERMIP): Project-1, Technical note no. 7, Water resources preparation and baseline. March 2016, Northwest Hydraulic Consultants (NHC), Dhaka, Bangladesh.

Nicholas, A.P. (2013): Modelling the continuum of river channel patterns. Earth Surf. Proc. Land., Vol. 38, 1187-1196, DOI:10.1002/esp.3431.

Nicholas, A.P., Ashworth, P.J., Smith, G.H.S., and Sandbach, S.D. (2013): Numerical simulation of bar and island morphodynamics in anabranching megarivers. J. Geophys. Res., Vol. 118, 2019-2044, DOI:10.1002/jgrf.20132.

Nicoll, T.J., and Hickin, E.J. (2010): Planform geometry and channel migration of confined meandering rivers on the Canadian prairies. Geomorphology, Vol. 116, 37-47, DOI: 10.1016/j.geomorph.2009.10.005.

O'Boyle, J.M. (1981): Relationships between the morphometric parameters of meander planform in south County Down. Irish Geography, Vol. 14, No. 1, 65-74.

Olsen, N.R.B. (2003): 3D CFD Modelling of a self-forming meandering channel. J. Hydraul. Eng., Vol. 129. No. 5, 366-372.

Parsapour-Moghaddam, P., and Rennie, C.D. (2017): Hydrostatic versus nonhydrostatic hydrodynamic modelling of secondary flow in a tortuously meandering river: Application of Delft3D. River Research and Applications, Vol. 33, No. 9, 1400-1410.

Parsapour-Moghaddam, P., and Rennie, C.D. (2015): ADCP validation of 3D morphodynamic modelling in clay-bed meandering rivers. E-proceedings of the 36th IAHR World Congress, 28 June - 3 July 2015, the Hague.

Parsapour-Moghaddam, P., and Rennie, C.D. (2014): Morphodynamic modelling of a tortuous meandering clay bed river using Delft3D: Stillwater Creek, Ottawa. River Flow 2014, Proc. of the Intern. Conf. on Fluvial Hydraulics, Lausanne, Switzerland, 1163-1171.

Parsons, D.R., Jackson, P.R., Czuba, J.A., Engel, F.L., Rhoads, B.L., Oberg, K.A., Best, J.L., Mueller, D.S., Johnson, K.K., and Riley, J.D. (2013): Velocity mapping toolbox (VMT): a processing and visualization suite for moving-vessel ADCP measurements. Earth Surf. Proc. Land., Vol. 38, 1244-1260.

Peakall, J., and Warburton, J. (1996): Surface tension in small hydraulic river models - the significance of the Weber number. J. Hydrol., New Zealand, Vol. 35, No. 2, 199-212.

Peakall, J., Ashworth, P.J., and Best, J.L. (1996): Physical modelling in fluvial geomorphology: Principles, applications and unresolved issues. In: Rhoads B.L., Thorn C.E. (Eds.) The Scientific Nature of Geomorphology, John Wiley & Sons, Chichester, 221-254.

Plüß, A., and Kösters, F. (2014): Morphodynamic modelling for the entire German Bight: an initial study on model sensitivity and uncertainty. Adv. Geosci., Vol. 39, 61-68. DOI: 10.5194/adgeo-39-61-2014.

Posner, A.J., and Duan, J.G. (2012): Simulating river meandering processes using stochastic bank erosion coefficient. Geomorphology, 163-164: 26-36.

Radecki-Pawlik, A. (2015): Why do we need bankfull and dominant discharges? In: Rowinski P., Radecki-Pawlik A. (eds.). Rivers – Physical, Fluvial and Environmental Processes. Series: GeoPlanet: Earth and Planetary Sciences, Springer, Switzerland, 497-518.

Rahman, M.M., Mahmud, F., and Uddin, M.N. (2012): Effect of sand bars on failure of bank protection work along large sand bed braided river. Sixth Intern. Conf. on Scour and Erosion (ICSE6), August 27-31, 2012, Paris.

Ranasinghe, R., Swinkels, C., Luijendijk, A., Roelvink, D.J.A., Bosboom, J., Stive, M., and Walstra, D. (2011): Morphodynamic upscaling with the MORFAC approach: Dependencies and sensitivities. Coast. Eng., Vol. 58, 806-811. DOI:10.1016/j.coastal eng. 2011.03.010.

Riesterer, J., Wenka, T., Brudy-Zippelius, T., and Nestmann, F. (2016): Bed load transport modelling of a secondary flow influenced curved channel with 2D and 3D numerical models. J. Appl. Water Eng. Res., Vol. 4, No. 1, 54-66, DOI:10.1080/23249676.2016. 1163649.

Rinaldi, M., Mengoni, B., Luppi, L., and Darby, S.E. (2008): Numerical simulation of hydrodynamics and bank erosion in a river bend. Water Resour. Res., AGU, Vol. 44, W09428, DOI:10.1029/2008WR007008.

River Survey Project (1996): Special report No. 18: Sediment rating curves and balances. October 1996, Water Resources Planning Organization (WARPO), Dhaka, Bangladesh.

Rodi, W. (2017): Turbulence modeling and simulation in hydraulics: A historical review. J. Hydraul. Eng., Vol. 143, DOI:10.1061/(ASCE)HY.1943-7900.0001288.

Rodi, W. (1980): Turbulence models and their applications in hydraulics: A state of the art review. Book publication of IAHR, Delft, the Netherlands.

Rodriguez, J.F., Bombardelli, F.A., Garcia, M.H., Frothingham, K.M., Rhoads, B.L., and Abad, J.D. (2004): High-resolution numerical simulation of flow through a highly sinuous river reach. Water Resour. Management, Vol. 18, No. 3, 177-199.

Roelvink, J.A. (2006): Coastal morphodynamic evolution techniques. Coast. Eng., Vol. 53, 277-287, DOI:10.1016/j.coastaleng.2005.10.015.

Rozovskii, I.L. (1957): Flow of water in bends of open channels. Kiev: Academy of Sciences of Ukrainian SSR. Kiev, 1957, Israel Program for Scientific Translations, Jerusalem, 1961.

Rüther, N., Jacobsen, J., Olsen, N.R.B., and Vatne, G. (2010): Prediction of the threedimensional flow field and bed shear stresses in a regulated river in mid-Norway. Hydrol. Res., Vol. 41, No. 2, 145-152.

Rüther, N., and Olsen, N.R.B. (2007): Modelling free-forming meander evolution in a laboratory channel using three-dimensional computational fluid dynamics. Geomorphology, Vol. 89, 308-319.

Sandbach, S., Lane, S., Hardy, R., Amsler, M., Ashworth, P., Best, J., Nicholas, A., Orfeo, O., Parsons, D., Reesink, A., and Szupiany, R. (2012): Application of a roughness-length representation to parameterize energy loss in 3-D numerical simulations of large rivers. Water Resour. Res., Vol. 48, W12501, DOI:10.1029/2011WR011284.

Sarker, M.H., Akter, J., and Ruknul, F.M. (2011): River bank protection measures in the Brahmaputra-Jamuna River: Bangladesh Experience. International seminar on 'River, Society and Sustainable Development', Dibrugarh University, India.

Schumm, S.A. (1977): The fluvial system. The Blackburn Press, Caldwell, New Jersey, USA, 338 p.

Schumm, S.A. (1967): Meander wavelength of alluvial rivers. In: Science, Vol. 157, No. 3796, 1549-1550, DOI:10.1126/science.157.3796.1549.

Schumm, S.A., and Khan, H.R. (1972): Experimental study of channel patterns. Geol. Soc. of America Bull., Vol. 83, 1755-1770.

Schumm, S.A., Mosley, M.P., and Weaver, W.E. (1987): Experimental fluvial geomorphology. John Wiley & Sons, New York, 413 p., ISBN 0-471-83077-1.

Schuurman, F. (2015): Bar and channel evolution in meandering and braiding rivers using physics-based modelling. PhD thesis, Utrecht University, ISBN: 978-90-6266-391-0.

Schuurman, F., Kleinhans, M.G., and Middelkoop, H. (2016): Network response to disturbances in large sand-bed braided rivers. Earth Surf. Dyn., Vol. 4, 25-45.

Schuurman, F., Shimizu, Y., Iwasaki, T., and Kleinhans, M.G. (2016): Dynamic meandering in response to upstream perturbations and floodplain formation. Geomorphology, Vol. 253, 94-109, DOI:10.1016/j.geomorph.2015.05.039

Schuurman, F., and Kleinhans, M.G. (2015): Bar dynamics and bifurcation evolution in a modelled braided sand-bed river. Earth Surf. Proc. Land., Vol. 40, 1318-1333, DOI: 10.1002/esp.3722.

Schuurman, F., Marra, W.A., and Kleinhans, M.G. (2013): Physics-based modelling of large braided sand-bed rivers: bar pattern formation, dynamics, and sensitivity. J. Geophys. Res., Vol. 118, 2509-2527, DOI:10.1002/2013JF002896.

Schuurman, F., and Kleinhans, M.G. (2013): Major bed slope effects affecting all river morphodynamics models. 10th Intern. Conf. Fluv. Sedimentology, Utrecht University Repository. https://dspace.library.uu.nl/handle/1874/310248.

Schuurman, F., and Kleinhans, M.G. (2011): Self-formed braided bar pattern in a numerical model. In: Proc. of the 7th IAHR Conf. on River, Estuarine and Coastal Morphodynamics, Beijing, China, 1647-1657.

Schwendel, A.C., Nicholas, A.P., Aalto, R.E., Sambrook, S.G.H., and Buckley, S. (2015): Interaction between meander dynamics and floodplain heterogeneity in a large tropical sand-bed river: The Rio Beni, Bolivian Amazon. Earth Surf. Proc. Land. DOI:10.1002/esp.3777.

Sen, P.K. (1968): Estimates of the regression coefficient based on Kendall's Tau. J. American Stat. Assoc., Vol. 63, 1379-1389.

Shahjahan, M. (1970): Factors controlling the geometry of fluvial meanders. Bull. Intern. Assoc. Sci. Hydrol., Vol. 15, No. 3, 13-24.

Shukry, A. (1950): Flow around bends in an open flume. Transactions of the American Society of Civil Engineers, Vol. 115, No. 1, 751-779.

Singh, V.P. (2003): On the theory of hydraulic geometry. Intern. J. Sediment Res., Vol. 18, No. 3, 196-218.

Soar, P.J., and Thorne, C.R. (2001): Channel restoration design for meandering rivers. ERDC/CHL CR-01-1, Vicksburg, MS: U.S. Army Engineer Research and Development Center.

Stokes, G.G. (1845): Trans. Camb. Phil. Soc., Vol. 8, 287-305.

Struiksma, N., Olesen, K.W., Flokstra, C., and De Vriend, H.J. (1985): Bed deformation in curved alluvial channels. J. Hydraul. Res., Vol. 23, No. 1, 57-79.

Sukhodolov, A., Blettler, M., Zhang, J., Suhodolova, T., and Nützmann, G. (2015): A study of flow dynamics and implications for benthic fauna in a meander bend of a lowland river. J. Hydraul. Res., Vol. 53, No. 4, 488-504.

Sun, T., Meakin, P., Jøssang, T., and Schwarz, K. (1996): A simulation model for meandering rivers. Water Res. Res., Vol. 32, No. 9, 2937-2954.

Sutherland, J., Peet, A.H., and Soulsby, R.L. (2004): Evaluating the performance of morphological models. Vol. 51, 917-939, Coast. Eng., DOI:10.1016/j.coastaleng.2004.07.015.

Talmon, A.M., Struiksma, N., and Van Mierlo, M. (1995): Laboratory measurements of the direction of sediment transport on transverse alluvial-bed slopes. J. Hydraul. Res., Vol. 33, No. 4, 495-517.

Thorne, C.R. (1982): Processes and mechanisms of river bank erosion. In: Gravel-Bed Rivers, R.D. Hey, J.C. Bathurst and C.R. Thorne, (Eds.), John Wiley and Sons, Chichester, England, 227-272.

van Dijk, W.M. (2013): Meandering rivers: Feedbacks between channel dynamics, floodplain and vegetation. PhD thesis, University of Utrecht, 206 p.

van Dijk, W.M., Schuurman, F., van de Lageweg, W.I., and Kleinhans, M.G. (2014): Bifurcation instability and chute cutoff development in meandering gravel-bed rivers. Geomorphology, Vol. 213, 277-291.

van de Lageweg, W.I., Van Dijk, W.C., Box, D., and Kleinhans, M.G. (2016): Archimetrics : a quantitative tool to predict three-dimensional meander belt sand-body heterogeneity. Depositional Record, Vol. 2, No. 1, 22-46. DOI:10.1002/dep2.12.

Van der Wegen, M., Jaffe, B.E., and Roelvink, J.A. (2011): Process-based morphodynamic hindcast of decadal deposition patterns in San Pablo Bay, California, 1856-1887. J. Geophys. Res., Vol. 116, F02008, DOI:10.1029/2009JF001614.

Van der Wegen, M., and Roelvink, J.A. (2008): Long-term morphodynamic evolution of a tidal embayment using a two-dimensional, process-based model. J. Geophys. Res., Vol. 113, C03016, DOI:10.1029/2006JC003983.

van de Wiel, M.J., and Darby, S.E. (2004): Numerical modelling of bed topography and bank erosion along tree-lined meandering rivers. In: Bennett S.J. and Simon A. (eds.) Riparian Vegetation and Fluvial Geomorphology. American Geophysical Union, Washington, DC, Vol. 8, 267-282.

van Rijn, L.C. (2000): General view on sediment transport by currents and waves. Rep. Z2899, Delft Hydraulics, Delft, the Netherlands.

van Rijn, L.C. (1993): Principles of sediment transport in rivers, estuaries and coastal seas. Aqua Publications, Amsterdam.

van Rijn, L.C. (1984a): Sediment transport: Part I: Bed load transport. J. Hydraul. Div., Vol. 110, No. 10, 1431-1456.

van Rijn, L.C. (1984b): Sediment transport: Part II: Suspended load transport. J. Hydraul. Div., Vol. 110, No. 11, 1613-1641.

van Rijn, L.C., Walstra, D.J.R., Grasmeijer, B., Sutherland, J., Pan, S., and Sierra, J.P. (2003): The predictability of cross-shore bed evolution of sandy beaches at the time scale of storms and seasons using process-based profile models. Coast. Eng., Vol. 47, 295-327.

Vargas-Luna, A. (2016). Role of vegetation on river bank accretion. PhD thesis, TU Delft, DOI:10.4233/uuid:286c36e8-3cac-403c9d0a-72a5232c5093.

Vasquez, J.A., Millar, R.G. and Steffler, P.M. (2005): Vertically-averaged and moment of momentum model for alluvial bend morphology. River, Coastal and Estuarine Morphodynamics: RCEM 2005 – Parker & García (eds.) 2006 Taylor & Francis Group, London, ISBN 0 415 39270 5.

Verhaar, P.M., Biron, P.M., Ferguson, R.I., and Hoey, T.B. (2008): A modified morphodynamic model for investigating the response of rivers to short-term climate change. Geomorphology, Vol. 101, No. 4, 674-682.

Vested, H., Tjerry, S., Christensen, B., and Dubinski, I.M. (2014): Numerical simulation of estuarine and river morphology. Intern. Conf. on Small Scale Morphological Evolution of Coastal, Estuarine and River Systems, At Nantes, 6-7 October 2014.

Villaret, C., Hervouet, J.M., Kopmann, R., Merkel, U., and Davies, A.G. (2013): Morphodynamic modelling using the Telemac finite-element system. Comput. Geosci., Vol. 53, No. 4, 105-113, DOI:10.1016/j.cageo.2011.10.004.

Viparelli, E., Gaeuman, D., Wilcock, P., and Parker, G. (2011): A model to predict the evolution of a gravel bed river under an imposed cyclic hydrograph and its application to the Trinity River. Water Resour. Res., Vol. 47, W02533, DOI:10.1029/2010WR009164.

Visconti, F., Camporeale, C., and Ridolfi, L. (2010): Role of discharge variability on pseudomeandering channel morphodynamics: results from laboratory experiments. J. Geophys. Res., Vol. 115, F04042, DOI:10.1029/2010JF001742.

Walstra, D.J.R., van Rijn, L.C., van Ormondt, M. Brière, C., and Talmon, A.M. (2007): The effects of bed slope and wave skewness on sediment transport and morphology. Proc. of Coastal Sediments, ASCE, New Orleans, USA, DOI:10.1061/40926(239)11.

Walstra, D., Ruggiero, P., Lesser, G., and Gelfenbaum, G. (2006): Modelling nearshore morphological evolution at seasonal scale. Proc. 5th Coast. Dyn. Intern. Conf., Barcelona, DOI:10.1061/40855(214)45.

Wang, Z., and Dittrich A. (1992): A study on problems in suspended sediment transportation. Proc. of the 2nd Intern. Conf. on Hydraulic and Environmental Modelling of Coastal, es-

tuarine and River Waters. Editor: Falconer, R.A., Shiono, K., Matthew, R.G., University of Cambridge, Vol. 2, 467-478.

Weisscher, S.A.H., Baar, A.W., Uijttewaal, W.S.J., and Kleinhans, M.G. (2017): The effect of transverse bed slope and sediment mobility on bend sorting. Book of abstracts, NCR days, February 1-3, 2017.

Whiting, P.J., and Dietrich, W.E. (1990): Boundary shear stress and roughness over mobile alluvial beds, J. Hydraul. Eng., Vol. 116, No. 12, 1495-1511.

Wiesemann, J.U., Mewis, P., and Zanke, U.C.E. (2006): Downslope transport (transverse sediment transport). 3rd Chinese-German joint symp. Coast. Ocean Eng., Vol. 1, 1-16, 2006.

Williams, G.P. (1986): River meanders and channel size. J. Hydrol., Vol. 88, 147-164.

Williams, G.P. (1978): Bankfull discharge of rivers. Water Resour. Res., Vol. 14, No. 6, 1141-1154.

Williams, R.D., Measures, R., Hicks, D.M., and Brasington, J. (2016): Assessment of a numerical model to reproduce event-scale erosion and deposition distributions in a braided river. Water Resour. Res., Vol. 52, 6621-6642, DOI:10.1002/2015WR018491.

Wilmink, R.J.A. (2015): Accelerated morphological modelling: a schematized case study into the medium and long term morphological acceleration techniques Morfac and Mormerge. MSc thesis, University of Twente, the Netherlands, http://essay.utwente.nl/67609/

Wolman, M.G., and Miller, J.P. (1960): Magnitude and frequency of forces in geomorphic processes. J. Geol., Vol. 68, No. 1, 54-74.

Wong, M., and Parker, G. (2006): One-dimensional modelling of bed evolution in a gravel bed river subject to a cycled flood hydrograph. J. Geophys. Res., Vol. 111, F03018, DOI:10.1029/2006JF000478.

Wu W. (2007): Computational river dynamics. Taylor & Francis, UK, 494 p.

Wu, W., and Wang, S. (2004): Depth-averaged 2D calculation of flow and sediment transport in curved channels. Intern. J. Sed. Res., Vol. 19, No. 4, 241-257.

Yalin, M.S. (1971): Theory of hydraulic models. Macmillan, London, 266.

Yossef, M., Jagers, H.R.A., Vuren, S., and Sieben, J. (2008): Innovative techniques in modelling large-scale river morphology. Int. Conf. on Fluvial Hydraulics, River Flow 2008, Cesme, Izmir, Turkey, 1065-1074.

Young, R.W. (1974): The meandering valleys of the Shoalhaven river system: a study of stream adjustment to structure and changed hydrologic regimen. PhD thesis, University of Sydney, Australia.

Zaid, B.A. (2018): Development of design guidelines for shallow groynes. PhD thesis, Universitätsbibliothek Braunschweig, DOI:10.24355/dbbs.084-201804100941.

Zaid, B.A., and Koll, Ka. (2016): Experimental investigation of the location of a shallow groyne for bank protection. Int. Conf. on Fluvial Hydraulics, River Flow 2016, Saint Louis, USA, Edited by Constantinescu, Garcia & Hanes, Taylor & Francis Group, London, ISBN 978-1-138-02913-2, 1286-1292.

Zeller, J. (1967): Meandering channels in Switzerland. In: Proc. of the Symp. on River Morphology, Intern. Assoc. Sci. Hydrol., Vol. 75., 174-186.

Ziliani, L., Surian, N., Coulthard, T.J., and Tarantola, S. (2013): Reduced-complexity modeling of braided rivers: Assessing model performance by sensitivity analysis, calibration, and validation. J. Geophys. Res. Earth Surf., Vol. 118, 2243-2262.

Zolezzi, G., Luchi, R., and Tubino, M. (2012): Modelling morphodynamic processes in meandering rivers with spatial width variations. Rev. Geophys., Vol. 50, RG4005, DOI:10. 1029/2012RG000392.